UNIVERSITY OF CALGARY

Investigation of Non-Thermal Enhanced Oil Recovery Techniques for Heavy Oil Production

by

Glen Brook

A THESIS

SUBMITTED TO THE FACULTY OF GRADUATE STUDIES

IN PARTIAL FULFILMENT OF THE REQUIREMENTS FOR THE

DEGREE OF MASTER OF SCIENCE

DEPARTMENT OF CHEMICAL AND PETROLEUM ENGINEERING

CALGARY, ALBERTA

AUGUST, 1999

© Glen Brook 1999

National Library of Canada
Acquisitions and Bibliographic Services
395 Wellington Street
Ottawa ON K1A 0N4
Canada

Bibliothèque nationale du Canada
Acquisitions et services bibliographiques
395, rue Wellington
Ottawa ON K1A 0N4
Canada

Your file Votre référence

Our file Notre référence

The author has granted a non-exclusive licence allowing the National Library of Canada to reproduce, loan, distribute or sell copies of this thesis in microform, paper or electronic formats.

The author retains ownership of the copyright in this thesis. Neither the thesis nor substantial extracts from it may be printed or otherwise reproduced without the author's permission.

L'auteur a accordé une licence non exclusive permettant à la Bibliothèque nationale du Canada de reproduire, prêter, distribuer ou vendre des copies de cette thèse sous la forme de microfiche/film, de reproduction sur papier ou sur format électronique.

L'auteur conserve la propriété du droit d'auteur qui protège cette thèse. Ni la thèse ni des extraits substantiels de celle-ci ne doivent être imprimés ou autrement reproduits sans son autorisation.

0-612-48367-3

Canada

Abstract

Experiments have been performed on physical models with rectangular geometry and multiple wells used as injectors and producers. Primary production of heavy oil, along with water, gas and aqueous polymer solution displacements of heavy oil have been performed using the models. Optimized water flooding followed by polymer flooding was found to be a very effective strategy. Visualization of some of the experiments has been performed using X-ray CT scanning and gamma nuclear imaging systems. Experiments have been history matched using numerical simulation in order to evaluate unknown characteristics of the experiments, such as relative permeability curves. Simulations were performed to evaluate experimental results at the field level. The simulations revealed a number of issues that need to be resolved before application of the investigated techniques are likely to be successful. A number of recommendations for future research to help resolve these issues have been presented.

Acknowledgements

I would like to thank my supervisor Dr. Apostolos Kantzas for his guidance and support during my studies. I am very grateful for the help given to me by Dan Marentette and Kevin Allsopp in the laboratory. Kelly Hamilton's assistance with the imaging portion of the work was greatly appreciated. I would also like to thank Michael Aikman for helping me with the simulation portion of the study. As well, I would like to thank the following people for the help they have lent me over the course of my work: Dr. Konstantin Mirotchnik, Michael Benedek, Natalia Mirotchnik, Derek Verhegge, and my fellow graduate students. This study would not have been possible without the financial support of the Alberta Department of Energy. I would like to thank Mr. Bill Good, our liaison with the Alberta Department of Energy for his support and for showing a genuine interest in the project.

Dedicated to My Parents,

Rick and Rosemary.

TABLE OF CONTENTS

Approval Page ii
Abstract iii
Acknowledgements iv
Dedication v
Table of Contents vi
List of Tables viii
List of Figures ix
List of Symbols xiv

CHAPTER ONE: INTRODUCTION 1

CHAPTER TWO: LITERATURE REVIEW 4
2.1 Primary Production 4
2.2 Water Flooding 11
2.3 Enhanced Recovery 13

CHAPTER THREE: DESCRIPTION OF APPARATUS AND PROCEDUCRES 28
3.1 Ambient Conditions Physical Models 28
3.1.1 Description 28
3.1.2 Saturation Procedure 29
3.1.3 Production Set-up 30
3.2 Reservoir Conditions Physical Models 31
3.2.1 Description 31
3.2.2 Saturation Procedure 33
3.2.3 Production Set-up 34
3.2.4 Modifications for Sand Production 35
3.3 Live Oil Generation Apparatus 36
3.4 Aluminum Core Holder 36
3.5 Visualization Equipment 37
3.5.1 Gamma Ray Camera 37
3.5.2 X-Ray CT Scanner 38
3.6 Porosity and Permeability Measurements 38
3.7 Measurement of Liquid Properties 40

CHAPTER FOUR: EXPERIMENTAL RESULTS AND DISCUSSION 41
4.1 Experiment #1 44
4.2 Experiment #2 52
4.3 Experiment #3 56
4.4 Experiment #4 60
4.5 Experiment #5 63
4.6 Experiment #6 68
4.7 Experiment #7 72
4.8 Experiment #8 76
4.9 Experiment #9 80

CHAPTER FIVE: SIMULATION RESULTS AND DISCUSSION 124
5.1 Experiment #5 124
5.2 Experiment #6 132
5.3 Experiment #1 134
5.4 Reservoir Models 136
5.5 Field Scale Simulations 136

CAPTER SIX: CONCLUSIONS AND RECOMMENDATIONS 165

REFERNCES 170

List of Tables

Table 4.1: Summary of Experiments Performed 44
Table 4.2: Conditions of Ambient Model #1 After Saturation, Experiment #1 45
Table 4.3: Conditions of Ambient Model #2 After Saturation, Experiment #2 52
Table 4.4: Conditions of Reservoir Model #1 After Saturation, Experiment #3 56
Table 4.5: Conditions of Reservoir Model #2 After Saturation, Experiment #4 61
Table 4.6: Conditions of Ambient Model #2 After Saturation, Experiment #5 64
Table 4.7: Conditions of Ambient Model #1 After Saturation, Experiment #6 69
Table 4.8: Conditions of Aluminum Core Holder After Saturation, Experiment #7 72
Table 4.9: Conditions of Reservoir Model #1 After Saturation, Experiment #8 76
Table 4.10 Conditions of Reservoir Model #2 After Saturation, Experiment #9 80

List of Figures

Figure 3.1: Picture of Ambient Model #1 28
Figure 3.2: Well Configuration of Ambient Models 29
Figure 3.3: Production Set Up of Ambient Models 31
Figure 3.4: Top View of Reservoir Model #1 32
Figure 3.5: Top View of Reservoir Model #2 33
Figure 3.6: Production Set Up for Reservoir Models 35
Figure 3.7: Set Up for Permeability Measurements 39
Figure 4.1: Permeability vs. Overburden 83
Figure 4.2: Permeability vs. Overburden 83
Figure 4.3: Cumulative Production First Production Cycle Experiment #1 84
Figure 4.4: Water Cut First Production Cycle Experiment #1 84
Figure 4.5: Cumulative Production Second Production Cycle Experiment #1 85
Figure 4.6: Water Cut Second Production Cycle Experiment #1 85
Figure 4.7: Polymer Solution Viscosity vs. Shear Rate 86
Figure 4.8: Cumulative Production Tenth Production Cycle Experiment #1 86
Figure 4.9: Water Cut Tenth Production Cycle Experiment #1 87
Figure 4.10: Cumulative Production Eleventh Production Cycle Experiment #1 87
Figure 4.11: Water Cut Eleventh Production Cycle Experiment #1 88
Figure 4.12: Cumulative Oil Production and Water Cut Experiment #1 88
Figure 4.13: Cumulative Production First Production Cycle Experiment #2 89
Figure 4.14: Water Cut First Production Cycle Experiment #2 89
Figure 4.15: Cumulative Production Sixth Production Cycle Experiment #2 90
Figure 4.16: Water Cut Sixth Production Cycle Experiment #2 90
Figure 4.17: Cumulative Oil Production and Water Cut Experiment #2 91
Figure 4.18: Cumulative Production First Production Cycle Experiment #3 91
Figure 4.19: Gas Oil Ratio Primary Production Experiment #3 92
Figure 4.20: Cumulative Production Second Production Cycle Experiment #3 92
Figure 4.21: Water Cut and GOR Second Production Cycle Experiment #3 93
Figure 4.22: Cumulative Production Third Production Cycle Experiment #3 93

Figure 4.23: Water Cut and GOR Third Production Cycle Experiment #3 94
Figure 4.24: Cumulative Production Seventh Production Cycle Experiment #3 94
Figure 4.25: Water Cut and GOR Seventh Production Cycle Experiment #3 95
Figure 4.26: Cumulative Production Eighth Production Cycle Experiment #3 95
Figure 4.27: Water Cut and GOR Eighth Production Cycle Experiment #3 96
Figure 4.28: Cumulative Oil Production and Water Cut Experiment #3 96
Figure 4.29: GOR Experiment #3 97
Figure 4.30: Cumulative Production First Production Cycle Experiment #4 97
Figure 4.31: GOR and Water Cut First Production Cycle Experiment #4 98
Figure 4.32: Cumulative Production Second Production Cycle Experiment #4 98
Figure 4.33: Water Cut and GOR Second Production Cycle Experiment #4 99
Figure 4.34: Cumulative Production Third Production Cycle Experiment #4 99
Figure 4.35: Water Cut and GOR Third Production Cycle Experiment #4 100
Figure 4.36: Cumulative Production Sixth Production Cycle Experiment #4 100
Figure 4.37: Water Cut and GOR Sixth Production Cycle Experiment #4 101
Figure 4.38: Cumulative Oil Production and Water Cut Experiment #4 101
Figure 4.39: GOR Experiment #4 102
Figure 4.40: Cumulative Production First Production Cycle Experiment #5 102
Figure 4.41: Water Cut First Production Cycle Experiment #5 103
Figure 4.42: Image of Ambient Model #2 After First Water Flood 103
Figure 4.43: Cumulative Production Second Production Cycle Experiment #5 104
Figure 4.44: Water Cut Second Production Cycle Experiment #5 104
Figure 4.45: Image of Ambient Model #2 After Second Water Flood 105
Figure 4.46: Cumulative Production Third Production Cycle Experiment #5 105
Figure 4.47: Water Cut Third Production Cycle Experiment #5 106
Figure 4.48: Image of Ambient Model #2 at 4.5 hours into Polymer Food 106
Figure 4.49: Cumulative Oil Production and Water Cut Experiment #5 107
Figure 4.50: Cumulative Production First Production Cycle Experiment #6 107
Figure 4.51: Water Cut First Production Cycle Experiment #6 108
Figure 4.52: Image of Ambient Model #1 After First Water Flood 108
Figure 4.53: Polymer Solution Viscosity vs. Shear Rate 109

Figure 4.54: Cumulative Production Second Production Cycle Experiment #6 109
Figure 4.55: Water Cut Second Production Cycle Experiment #6 110
Figure 4.56: Image of Ambient Model #1 5 hour into Polymer Flood 110
Figure 4.57: Cumulative Oil Production and Water Cut Experiment #6 111
Figure 4.58: Cumulative Production First Production Cycle Experiment #7 111
Figure 4.59: Water Cut First Production Cycle Experiment #7 112
Figure 4.60: Cumulative Production Second Production Experiment #7 112
Figure 4.61: Water Cut Second Production Cycle Experiment #7 113
Figure 4.62: Saturation vs. Time Second Production Cycle Experiment #7 113
Figure 4.63: Images of Aluminum Core Holder During Polymer Flood at 75 mm 114
Figure 4.64: Cumulative Oil Production and Water Cut Experiment #7 115
Figure 4.65: Cumulative Production First Production Cycle Experiment #8 115
Figure 4.66: Cumulative Production Second Production Cycle Experiment #8 116
Figure 4.67: Water Cut Second Production Cycle Experiment #8 116
Figure 4.68: Cumulative Production Fourth Production Cycle Experiment #8 117
Figure 4.69: Water Cut Fourth Production Cycle Experiment #8 117
Figure 4.70: X-ray Image of Reservoir Model 31 After Experiment #8 118
Figure 4.71: Porosities of Sand Pack After Experiment #8 118
Figure 4.72: Cumulative Oil Production and Water Cut Experiment #8 119
Figure 4.73: Cumulative Production First Production Cycle Experiment #9 119
Figure 4.74: Cumulative Production Second Production Cycle Experiment #9 120
Figure 4.75: Water Cut Second Production Cycle Experiment #9 120
Figure 4.76: Cumulative Production Third Production Cycle Experiment #9 121
Figure 4.77: Water Cut Third Production Cycle Experiment #9 121
Figure 4.78: Cumulative Production Fourth Production Cycle Experiment #9 122
Figure 4.79: Water Cut Fourth Production Cycle Experiment #9 122
Figure 4.80: Cumulative Oil Production and Water Cut Experiment #9 123
Figure 5.1: Simulation Grid for Experiment #5 145
Figure 5.2: Cumulative Production, Experiment #5 Water Floods 145
Figure 5.3: Relative Permeability Curves From Simulation of Experiment #5 146
Figure 5.4: Water Cut, Experiment #5 Water Floods 146

Figure 5.5: Cumulative Oil Production, Experiment #5 Water Floods 147
Figure 5.6: Water Saturations After Sim. of First Water Flood Exp. #5, Areal View ...147
Figure 5.7: Water Saturations After Sim. of First Water Flood Exp. #5, Profile View ..148
Figure 5.8: Cumulative Production, Experiment #5 148
Figure 5.9: Water Cut, Experiment #5 149
Figure 5.10: Cumulative Oil Production, Experiment #5 149
Figure 5.11: Water Saturations 4.5 hours into Polymer Flood Exp. #5, Areal View 150
Figure 5.12: Cumulative Production, Experiment #6, Water Flood 150
Figure 5.13: Water Cut, Experiment #6, Water Flood 151
Figure 5.14: Cumulative Oil Production, Experiment #6, Water Flood 151
Figure 5.15: Relative Permeability Curves From Simulation of Experiment #6 152
Figure 5.16: Water Saturation After Simulation of Water Flood Exp #6 Areal View 152
Figure 5.17: Cumulative Production, Experiment #6 153
Figure 5.18: Water Cut, Experiment #6 153
Figure 5.19: Cumulative Production, Experiment #1, Water Floods and Gas Floods ...154
Figure 5.20: Relative Permeability Curves From Simulation of Experiment #1 154
Figure 5.21: Cumulative Production, Experiment #1 155
Figure 5.22: Water Cut, Experiment #1 155
Figure 5.23: Simulation Grid for Field Scale Simulation 156
Figure 5.24: Oil/Water Relative Perm. Curves used for Field Scale Simulations 156
Figure 5.25: Gas/Water Relative Perm. Curves used for Field Scale Simulations 157
Figure 5.26: Cumulative Oil Production and Water Cut, Field Model Water Flood 157
Figure 5.27: Production Rates, Field Model Water Flood 158
Figure 5.28: Water Saturations After Simulation Water Flood, Profile View 158
Figure 5.29: Water Saturations After Simulation Water Flood, Areal View 159
Figure 5.30: Cum. Prod. and Water Cut, ALCOFLOOD 935 Injected at 13 years 159
Figure 5.31: Production Rates, ALCOFLOOD 935 Injected at 13 years 160
Figure 5.32: Water Saturations , 13 years into Sim. Polymer Flood, Areal View 160
Figure 5.33: Water Saturations , 13 years into Sim. Polymer Flood, Profile View 161
Figure 5.34: Cum. Prod. and Water Cut, ALCOFLOOD 1275A Injected at 13 years ..161
Figure 5.35: Production Rates, ALCOFLOOD 1275A injected at 13 years 162

Figure 5.36: Cum. Prod. and Water Cut, ALCOFLOOD 1275A Injected at 6 years 162
Figure 5.37: Production Rates, ALCOFLOOD 1275A Injected at 6 years 163
Figure 5.38: Cum. Prod. and Water Cut, 1275A Injected at 13 years, Reduced Slug ...163
Figure 5.39: Production Rates, 1275A Injected at 13 years, Reduced Slug 164

List of Symbols

a	radioactive counts per pixel
a_o	radioactive counts per pixel at t=0
a_b	radioactive counts per pixel for baseline
A_c	area under capillary pressure curve
b	width of porous media (m)
b	constant, equation 4.12
C	concentration of radioactivity (mCi/L)
C_b	concentration of radioactivity for baseline (mCi/L)
$CT_{measured}$	average CT number measured for core slice
$CT_{100\% brine}$	average CT number of core slice saturated 100 % with brine
$CT_{100\% oil}$	average CT number of core slice saturated 100 % with oil
f_w	fractional flow of water (fraction)
g	gravity constant (m/s^2)
GOR	gas oil ratio
H	proportional constant for power law (cP·s)
h	height of porous media (m)
I_{sr}	stability number
k_o	oil relative permeability (m^2)
k_w	water relative permeability (m^2)
k_{rwo}	water relative permeability at residual oil (m^2)
k_{ocw}	oil relative permeability at connate water (m^2)
M	mobility ratio
N_{ca}	capillary number
N_g	gravity number
n	exponential constant for power law
OOIP	original oil in place
P	pressure (MPa)
S_o	oil saturation (fraction)
S_{or}	residual oil saturation (fraction)
S_w	water saturation (fraction)

S_{wc}	connate water saturation (fraction)
t	seconds (s)
T	temperature (Kelvins)
v	superficial velocity (m/s)
α	angle of deviation from vertical (°)
$\Delta\rho$	density difference between water and oil (kg/m^3)
μ	viscosity (mPa·s or cP)
μ_a	apparent polymer solution viscosity (mPa·s or cP)
μ_w	water viscosity (mPa·s or cP)
μ_o	oil viscosity (mPa·s or cP)
ν	interstitial velocity (m/s)
λ	time constant (1/s)
σ_e	pseudo interfacial tension (mN/m or dyne/cm)
σ_{ow}	oil water interfacial tension (mN/m or dyne/cm)
ϕ	porosity (fraction)

CHAPTER ONE: INTRODUCTION

Western Canada possesses a large number of heavy oil fields. However, the high viscosity of the oil makes it difficult to recover. With the decline of conventional oil reserves, successful recovery of this resource becomes more important. Since heavy oil prices are lower than conventional oil, it is more sensitive to oil price fluctuations. Any successful recovery method must be able to operate under these tighter margins.

Under primary production only about 10 % of the original oil in place (OOIP) in a heavy oil reservoir can be recovered. As a result, there is still a large quantity of oil remaining in the reservoir after primary production with a great deal of potential if a low cost method of recovering this oil is available.

The majority of enhanced recovery techniques employed for recovering heavy oil are thermal in nature. Such thermal techniques include Cyclic Steam Stimulation, Steam Flooding, SAGD and In-situ Combustion. These recovery techniques have been successful in certain areas where they have been employed. However, they are not suitable for all areas. Moreover, there are environmental concerns associated with thermal recovery techniques. Many harmful emissions are produced as a result of steam generation and from burning heavy oil in the case of in-situ combustion. There are many reservoirs that have a thickness of 5 m or less. In such reservoirs, thermal recovery techniques involving steam are not economic due to excessive heat losses to the overburden and underburdern. For these fields, non-thermal recovery techniques are required.

This study involved investigation of non-thermal heavy oil recovery techniques. The objective was to investigate both certain techniques and a combination of techniques to help develop a strategy for low cost recovery of the remaining heavy oil in a reservoir after primary production. The study incorporates all stages of recovery, not just enhanced recovery. Techniques that have been successful in the past for recovering conventional oil were used in the investigation. These techniques included water

flooding, immiscible gas flooding and polymer flooding. New polymer products were investigated for the polymer flooding aspect of the study. These products were less expensive than many of the existing products on the market.

As well, experiments were performed to determine if the production of sand during primary production would have an effect on subsequent recovery techniques. The effects of sand production on subsequent recovery are currently unknown.

Experimental work and numerical reservoir simulation were used as part of the study. For the experimental work, physical models were used to evaluate the recovery techniques. The performance of the different recovery techniques could be compared to each other and could be evaluated. Four physical models with rectangular geometry and multiple wells were used along with a cylindrical core holder. The presence of multiple wells allowed for modification of the flood pattern used in the experiments.

Visualization of some experiments was performed using a gamma ray camera system and X-ray CT scanning. This provided further insight into the mechanisms involved in the various recovery techniques.

Numerical reservoir simulation was used to supplement the experimental results. The experiments were history matched with the simulator. The success of the history matches were used to evaluate the capability of the simulator to match heavy oil displacements. The ability of the numerical simulation to account for the highly unstable nature of heavy oil displacements is uncertain. These history matches also allowed for the determination of some unknown characteristics of the floods performed, such as relative permeability curves. Once these unknown characteristics were determined, simulations were performed to estimate the potential performance of the recovery techniques on a field scale.

The results from both the experimental work and the simulation have provided insight into some of the issues involved in the use of water flooding, gas flooding and polymer

flooding for the recovery of heavy oil. These results should also provide a good basis for further research in this area.

In the next chapter a literature review is presented to provide a background on the current situation of heavy oil in Western Canada. This is followed by a description of the experimental apparatus and procedures used in this study. The results of the experimental work and their implications for heavy oil recovery are presented. A description of the numerical simulation portion of the study along with results obtained from this work is presented. Finally, the conclusions of the study are summarized along with recommendations for future work.

CHAPTER TWO: LITERATURE REVIEW

2.1 Primary Production

Production rates of many heavy oil reservoirs in Western Canada have been observed to be significantly higher than rates predicted by classical radial flow models (Smith, 1988; Loughead and Saltuklaroglu, 1992). The high production rates of heavy oil have been accompanied by production of large amounts of sand. As well, wellhead samples of the produced heavy oil have been observed to be in the form of a stable oil continuous foam (Sarma and Maini, 1992). This enhanced production has been termed "Cold Production" due to the lack of thermal stimulation required to achieve these production rates. There has been much research conducted on "foamy oil" flow and sand production in an attempt to understand the mechanisms involved in Cold Production.

Smith (1988) proposed a model for predicting heavy oil primary production in the Lloydminster region where anomalously good production had been observed. The model included the simultaneous flow of oil and gas as microbubbles. The flowing mixture had a viscosity that was intermediate between that of the heavy oil and the gas. His model also included mechanisms for sand production that resulted in permeability enhancement in the form of either a near well bore cavity or possibly wormholes. He states that the production of sand would lead to a reduction of the in-situ stress leaving the formation more susceptible to fracture. Smith (1988) believes this would explain the sudden failure of many injection schemes attempted in this area.

Islam and Chakma (1990) investigated the flow of microbubbles in heavy oil with a series of flow test using capillary tubes and unconsolidated cores. The microbubbles in their experiment were generated artificially by injecting the gas into the oil through a sintered metal cap. They observed a smaller pressure drop across the core when gas was present in the form of microbubbles than when the gas was a continuous phase. They also observed that the presence of asphaltenes in the oil resulted in slower dissolution of gas from the oil.

According to Loughead and Saltuklaroglu (1992), sand production results in high permeability and porosity channels that improve inflow performance. They observed high negative skin values when injectivity and build up tests were performed on wells that had produced large amounts of sand. They also believed that high critical gas saturations, of about 25 – 35 %, existed in heavy oil reservoirs. At gas saturations below these critical values, the gas exists as microbubbles in the oil and does not impede the flow of oil in the porous medium. As well, they believed that sand production would result in an increase in the formation compressibility that would negatively impact secondary displacement processes.

Sarma and Maini (1992) conducted steady state experiments with heavy oil in unconsolidated sand packs to investigate the effect of "foamy oil" flow. They found a decrease in the mobility of the oil due to the nucleation of microbubbles in the oil, contradicting the findings of Islam and Chakma (1990). However, they believed that the formation of an oil continuous foam would improve oil recovery by not allowing the formation of a continuous gas phase and therefore providing sustained pressure maintenance.

Maini *et al* (1993) found the critical gas saturation in solution gas drive experiments to be very high (about 40 %). They believed that an oil continuous foam exists in the porous media until the gas saturation becomes larger than the critical gas saturation. Again, they found a decrease in the oil mobility due to the presence of microbubbles.

Shen and Batycky (1996) re-interpreted the results of Maini *et al* (1993) to show that there was an increase in the oil mobility due to microbubble nucleation. They stated that when the initial live oil viscosity was used to calculate the expected mobility of the oil there was indeed a reduction in the average mobility in the sand pack. However, when the measured pressure profile was compared to that calculated using the initial live oil viscosity it was found that the measured pressure gradient was less than the calculated one away from the outlet. Matching the pressure gradient in this region of the sand pack required a 10 % to 40 % increase in the oil mobility. Approaching the outlet, the

measured pressure gradient was greater than the calculated one. Their explanation for the local mobility enhancement was that the nucleation of microbubbles at the oil interfaces (oil/sand and oil/water) lubricated the flow of the oil. Near the outlet the increasing gas saturation and entrapment of bubbles caused a decrease in the oil mobility.

Kraus *et al* (1993) presented a model for simulating foamy oil behaviour. In their model, the conventional PVT properties used for black oil simulation are adjusted to account for kinetic effects. The high viscosity of the oil causes the gas to be entrained in the oil and prevents the gas from disengaging to form a free phase when the pressure drops below the bubble point. This is accounted for by incorporating a "pseudo-bubble" point pressure into the model. The entrained gas serves to increase the compressibilty of the foamy oil "phase". A foamy oil simulation of a primary production incorporating the altered PVT properties was performed and compared to a simulation using normal black oil PVT properties. The comparison showed that the foamy oil simulation yielded a higher recovery and a low producing GOR. As well, the foamy oil simulation displayed a natural pressure maintenance. These characteristics are consistent with field observations.

Geilikman *et al* (1994a) presented a physics based model to represent sand production during the primary production of heavy oil. In their model, the formation yields and sand production begins at a critical pressure drawdown. As sand is produced, the yielded zone grows radially out from the wellbore. The flow of sand grains with the oil reduces the resistance to flow for the oil and enhances the fluid production rate. They later expanded their model to include a second mechanism for production rate enhancement (Geilikman *et al*, 1994b). They stated that the production of sand would result in an increase in the permeability in the yielded zone. The reduced resistance to flow due to the movement of sand grains would offer short term enhancement of flow rates while the increased permeability in the yielded zone would offer long term enhancement of production rates. The rate at which the drawdown of the well is increased will determine which mechanism dominates in the enhancement of flow rates. In a subsequent paper, Geilikman *et al* (1994c) analyzed the competition between cylindrical growth of the yielded zone and the

growth of channel type propagation of the yielded zone (i.e. wormholes). They concluded that cylindrical growth of the yielded zone would be stable when disturbances to the yield front velocity were small and smooth. However, in the later stages of sand production, the velocity of channel type propagation could exceed cylindrical front velocity. This would result in a wormhole type yielded zone being more prevelant in older more mature wells.

Tremblay *et al* (1995) performed an experimental study of sand production using X-ray computed tomography to visualize a cylindrical sand pack. The sand was densely packed and saturated with dead heavy oil. CT images of the sandpack were taken before and after sand and oil had been produced from a ¼" (.635 cm) orifice representing a single well perforation. They observed that a distinct wormhole with a porosity greater than 50 % had formed. The wormhole formed in the region of the sandpack that had a higher initial porosity. They concluded that the most likely explanation of high heavy oil production rates was that high permeability wormholes propagate from the well once a critical pressure gradient is established. A subsequent study (Tremblay *et al*, 1996) in which CT images were taken while the wormhole developed showed that high sand cuts occurred during the formation of the wormhole. Once the wormhole had been formed lower sand cuts were experienced as a result of loose sand being "scoured" from the walls of the wormhole. The high initial sand cuts followed by lower constant sand cuts are consistent with field observations.

Claridge and Prats (1995) proposed a mechanism to explain the increased productivity observed with foamy oils. In their mechanism, asphaltenes, which are initially present in the oil in as a colloidal dispersion, migrate with the resins to the surface of gas microbubbles that form when the pressure drops below the bubble point pressure. The asphaltenes and resins form a semi-rigid coating that prevents the bubbles from further growth and coalescence. As well, the removal of the asphaltenes and resins from suspension in the oil phase results in a reduction in the viscosity of the oil and therefore improves its mobility.

Geilikman *et al* (1995) believed that due to the low molecular diffusivity of gas in a viscous oil, a rate based model could describe foamy oil behaviour. They presented such a model. In the model, they proposed a kinetic bubble point that exists at a pressure below the thermodynamic bubble point when the rate of pressure decline is large. Small microbubbles form in the supersaturated oil. These small bubbles are compressed by capillary pressure and act rigidly. This makes the coalescence of these bubbles difficult and results in a stable foamy oil "phase". The authours did not test their model against experimental or field data. The authours also stated that failure of the formation, resulting in sand production, likely occurs at the foaming front.

Based on field observations and a simulation study Metwally and Solanki (1995) proposed a mechanism based on sand production and foamy oil that they found to match the enhanced primary production of heavy oil. They accredited foamy oil to improved pressure maintenance of the formation by preventing the formation of a continuous gas phase. Their simulation study showed that both improved pressure maintenance and increased permeability near the well bore caused by sand production had to be taken into account in order to predict heavy oil primary production.

Sheng *et al* (1995a) and Sheng *et al* (1995b) presented a rate based model to predict foamy oil volumes and compressibilities. In their model, foamy oil consists of three components: dead oil, solution gas and evolved gas. Kinetic equations for gas evolution and gas disengagement were developed. The volume of foamy oil was assumed to be the combined volumes of the three components. The compressibility of the foamy oil was calculated as the volume average of the compressibilities of the three components. Experiments performed with bulk oil in a PVT cell to test their model. Using two adjustable parameters, their model was able to represent the behaviour of the PVT cell test. However, no flow experiments in a porous media were performed to test the model.

Sheng *et al* (1995c) performed an experimental study to determine the factors affecting foamy oil stability. They measured the height of a given amount of foamy oil in a PVT cell as a function of time during a pressure depletion. They concluded that foamy oil

stability increased with increasing viscosity, asphaltene content, initial GOR, and larger initial foamy oil volumes resulted in a more stable foamy oil.

In Venezuela, de Mirabal *et al* (1996) observed high production rates for heavy oil reservoirs in the Hamaca area. The behaviour was similar to observations made in Canada. Well tests revealed a critical gas saturation of about 10 %. They were able to match the field behaviour using the kinetic models developed by Kraus *et al* (1993) and Sheng *et al* (1995a, 1995b).

Bora *et al* (1997) used glass micromodels to investigate foamy oil flow at the pore level. The model consisted of two glass plates pressed together with a pore network etched into one of the plates. A video camera with a magnifying lens was used to observe the foamy oil. Heavy oils with and without asphaltenes were used and different depletion rates were performed. The authours found that asphaltenes did not seem to affect bubble nucleation. Asphaltenes did appear to increase the degree of supersaturation needed to initiate bubble nucleation and seemed to hinder bubble coalescence. As well, higher flowrates made bubble coalesence difficult and resulted in bubble breakup. The presence of microbubbles could not be determined.

Pooladi-Darvish and Firoozabadi (1997) performed a series of depletion experiments on an unconsolidated sand pack using light oil and heavy oil to investigate the foamy oil phenomenon. Their conclusions contradicted the findings of previous authours. They found the critical gas saturation to be low (less than 5 %) and found there to be no enhancement of the oil mobility. As well, they found that the oil and gas flowed intermittently and not simultaneously with gas microbubbles. They proposed that the gas is present in the porous media as a discontinuous phase and that this results in a low gas phase mobility.

Treinen *et al* (1997) performed solution gas experiments on an unconsolidated sand pack with a Venezualan heavy oil. They measured produced and pore volume fluid compressibilities. A CT scanner was used to measure the gas saturation in the sandpack

at various stages of the depletion. Their results indicated a high critical gas saturation of about 9 % was responsible for the high oil recovery. The CT scans indicated free gas accumulating in regions as large as 2 cm with saturations as high as 70 % that were surrounded by areas with little free gas. They found that the producing GOR decreased before free gas was produced and noted that the pore fluid compressibility increased well before the produced fluid compressibility. From the experimental results the authours concluded that a trapped free gas phase was forming and that a high critical gas saturation existed in the sand pack.

In spite of all the research done on the mechanisms of heavy oil primary production, a sound understanding of the enhanced production that has been observed has not been obtained. From all the work there have been many contradictory findings. However, the conclusion that improved pressure maintenance exits during heavy oil primary production has been common. It is very likely that this is the case as a result of either low gas mobility or a high critical gas saturation. Sand production definitely plays a role in enhancing the recovery of heavy oil during primary production. However, the effects of sand production on secondary and enhanced recovery strategies performed after primary production are not known. There has been no published research to date that deals with this issue.

Horizontal well technology has also improved the viability of heavy oil primary production. Luhowy and Sametz (1993) reported a successful 14 horizontal well primary production project in the Cactus Lake area in western Saskatchewan. The horizontal wells allowed a longer section of well in the producing zone of the thin (16 m) formation. High production rates of the 10,000 cP oil resulted in favourable economics of the project. The rates were higher than expected, leading the authours to believe that the "foamy oil" phenomenon was occurring in the reservoir. However, they did not observe any significant sand production from the horizontal wells. A recovery of 12 % of OOIP from primary production was predicted.

Huang *et al* (1997) reported on a 10 horizontal well project in the Frog Lake area of Alberta. Oil with a viscosity between 20,000 cP and 50,000 cP was produced with the horizontal wells at rates three to four times the rates capable using vertical wells. As with most other "Cold Production" projects, high initial sand cuts of about 25 % were observed over the first six months. The sand cuts leveled off at about 5 %. Well servicing, including clean outs, and sand handling proved to be the two largest expenses.

2.2 Water Flooding

After primary production, water flooding can be performed as a secondary recovery technique for heavy oil. However, water flooding is limited to areas were the heavy oil is initially mobile in the reservoir. Jameson (1973) reported on water flooding in the Lloydminster region where the oil viscosity ranges from 500 to over 4,000 cP. Very low incremental recoveries were obtained through water flooding. The water floods were economic since connate water had to be disposed of anyway, leading to low incremental costs. Jameson stated that water flooding was not economic in primary depleted reservoirs. This was a result of increased viscosity of the oil due to loss of solution gases, causing an increasingly adverse mobility ratio between the oil and the injected water. This, along with the presence of zones of high gas saturation caused by evolving gas, led to severe channeling of the water.

Adams (1982) also reported on water flooding heavy oil in the Lloydminster area. He performed an in depth analysis of the production history of the field through primary production and water flooding. Well logs were used to evaluate water saturations in the reservoir. The water floods performed as well, and in some cases better than the theoretical predictions with high conformance efficiencies. This was surprising with the high mobility ratios involved. As well, it was believed that non-radial flow of injection water was occurring. Although areal conformance was believed to be good, well logs indicated that vertical conformance was quite poor. The contribution of solution gas drive and rock compressibility was believed to be a significant factor in the oil recovery. The effect of ceasing water injection was investigated by shutting in five injection wells in one of the fields and monitoring oil production. The shutting in of the injection well

was not found to be detrimental to the performance of the flood. The amount of water requiring handling in the field decreased by 40 % and the oil decline rate did not increase. Although there had not been enough production data to draw any definite conclusions, the oil production rate may have increased slightly. The authour concluded that the incremental recovery after primary production due to water flooding was only about 1 – 2 % of OOIP.

Smith (1990) provided an analysis of the mechanisms and unique features involved in heavy oil water floods. He stated that because of the high mobility ratios involved, viscous fingering of the water will occur. As a result, unlike conventional oil water floods where the residual oil is in the form of discontinuous ganglia, the residual oil in a heavy oil water flood is in the form of a continuous bypassed zone. This allows for economic oil production rates long after water break through. Smith also stated that water floods should be performed in order to maintain pressure support and control the produced GOR. In high permeability heavy oil reservoirs, when the pressure declines the oil and gas flow as an expanding mixture with the gas in the form of small entrained bubbles. However, if the gas phase becomes too large it will disengage from the oil phase and flow rapidly to the production well. This would lead to a rapid loss of energy from the reservoir. Therefore, water flooding should be used to control the rate of pressure decline in the reservoir so that the gas phase does not disengage from the oil. Smith states that this can be difficult if the water channels through to a production well causing a "short circuit" between the injector and the producer. This causes large amount of water to be recycled in order to maintain pressure support. It is suggested that altering the flood configuration may be a suitable method to combat "short circuiting".

More research needs to be performed on heavy oil water flooding. The topic has not been addressed thoroughly in the published literature. As well, there has been very little investigation on tertiary strategies for heavy oil recovery after water flooding. The unique continuous nature of the residual oil resulting from a heavy oil water flood would seem to make it a prime target as source of incremental recovery.

2.3 Enhanced Oil Recovery

The majority of enhanced recovery techniques currently being employed for heavy oil recovery are thermal in nature. The aim of these thermal techniques is to reduce the viscosity and therefore improve the mobility of the oil. Steam is the most common source of heat used.

Cyclic Steam Stimulation (CSS) is a single well "huff 'n puff" operation. It is one of the most widely used and successful thermal recovery techniques (Briggs *et al*, 1988). The process involves the injection of steam into the reservoir. This is followed by a soak period during which the well is shut in. The well is then opened for production until rates decline below economic values, after which the cycle is repeated. Production is encouraged due to a thermal reduction in the viscosity of the oil and stimulation of internal drive mechanisms such as solution gas drive (Briggs *et al*, 1988; Towson, 1997).

Steam flooding is a multi well process in which steam is injected into the formation and oil is produced along with water at nearby production well. Mobility of the oil between the injection and production wells is required. Poor sweep is experienced due to gravity override of the steam (Towson, 1997).

Steam Assisted Gravity Drainage (SAGD) is another thermal recovery technique (Butler and Stephens, 1981; Butler, 1985). The process involves the use of two parallel horizontal wells, one placed above the other. Steam is injected into the upper horizontal well. This causes a steam chamber to form in the reservoir. The steam chamber takes on the shape of an inverted triangle. The oil at the steam chamber interface is heated and its viscosity is reduced. The oil drains by gravity to the lower horizontal well where it is produced. Field scale projects have shown the process to be successful (O'Rourke *et al*, 1997; Towson, 1997). Variations of the process using vertical injectors and single horizontal well configurations have also been used (Towson, 1997).

In-situ combustion involves the downhole generation of heat by igniting a fraction of the oil in place. The combustion front is then fueled by the continuous injection of air or air

and water in the case of wet combustion. The heat generated by the combustion front mobilizes the remaining oil towards the production well. This process has been prone to control problems in the field (Farouq Ali, 1986; Briggs *et al*, 1988).

The thermal techniques mentioned above have been successful in certain areas. However, there are a number of heavy oil reservoirs where thermal techniques are not suitable. This is the case in thin formations or in formations where bottom water is present. In these cases, the heat losses are too large for thermal operations to be economical. In fact, over half the heavy oil in Canada, Venezuela and the United States occurs in reservoirs that are not suitable for thermal recovery techniques (Selby *et al*, 1989).

A number of non-thermal recovery techniques have been proposed specifically for the recovery of heavy oil. As well, a number of researchers have investigated applying techniques that have traditionally been used for conventional oil for heavy oil recovery.

There have been various gas injection techniques proposed for recovery of heavy oil. Kantzas *et al* (1991) investigated the recovery of heavy oil using horizontal wells and gravity drainage with inert gas injection for pressure maintenance. Experiments were performed using glass micromodels, vertical columns packed with sand and rectangular physical models. The micromodel and vertical column experiments indicated that water flooding followed by gravity drainage was more effective than water flooding or gravity drainage alone. However, very high sweep efficiency was obtained in those experiments. Gravity drainage with gas pressure maintenance was performed on the rectangular models without prior water flooding. Oil recoveries ranging from 23 % - 46 % of OOIP were obtained using heavy oils with viscosities from 600 cP to 12700 cP. Shutting in the models periodically after gas breakthrough resulted in increased recovery.

Islam *et al* (1994) performed an experimental study to investigate heavy oil recovery using horizontal wells and inert gas injection. A series of scaled experiments at low pressures were conducted. The gravitational forces were scaled in the experiments but

the pressure drops were not. Gas was injected from a horizontal well at the top of the model and fluids were produced from another horizontal well at the bottom. Two oils were used in the experiments, one with a viscosity of 1000 cP and the other with a 4000 cP viscosity. Nitrogen and carbon dioxide were the gases used for injection. Glass beads and coarse sand were used as a porous media with a permeability of about 66 darcies. The highest recovery obtained was about 70 % of OOIP. This was for the case of gravity drainage with the 1000 cP oil and Nitrogen as the gas. Applying an injection pressure caused an increase in the production rate but a decline in the ultimate recovery. Increasing the injection pressure to 15 psi resulted in unstable displacement and a recovery of only 7 % prior to gas break through. Trends were the same for the 4000 cP oil but ultimate recoveries and rates were lower. The use of carbon dioxide was found to decrease the recovery of the 1000 cP oil and increase the recovery of the 4000 cP oil. This was attributed to swelling of the 4000 cP oil. The presence of connate water was found to have a negligible effect on oil recovery.

The VAPEX (vapour extraction) process is a non-thermal variation of SAGD. Experimental studies have been performed with Hele-Shaw cells and physical models to investigate the process (Butler and Mokrys, 1991; Mokrys and Butler, 1993; Butler and Mokrys, 1993). The same two parallel horizontal well configuration used in SAGD is proposed. The process involves the injection of a light hydrocarbon solvent and hot water instead of steam. A rising solvent vapour chamber is formed. The heavy oil at the chamber interface is diluted by the solvent and its viscosity is reduced. The oil then drains by drainage to the lower horizontal well were it produced. The solvent is selected so that it is near its dew point at reservoir conditions to maximize its solubility in the oil. The hot water boils off the solvent from the heavy oil as it reaches the bottom of the vapour chamber. This serves to improve the growth of the vapour chamber. It is believed that most of the solvent can be recovered and re-injected into the formation. The production rates in the VAPEX process are expected to be much slower than the SAGD process since the thermal diffusivity that governs SAGD is much higher than the molecular diffusivity of the solvent into the oil that governs the VAPEX process. An added advantage of the process is that the ashpaltenes in the heavy oil are precipitated out

of the oil by the solvent, effectively "upgrading" the oil in-situ. The reduced viscosity of the oil is believed to more than compensate for any reduction in permeability caused by the asphaltene precipitation (Butler and Mokrys, 1993).

Lim *et al* (1996) performed an experimental study to investigate the recovery of heavy oil or bitumen using a light hydrocarbon solvent. Their proposed process is a variation of the VAPEX process. Instead of the traditional two horizontal well setup, the authours propose a single horizontal well cyclic stimulation configuration. The solvent is injected into the horizontal well until the pressure exceeds the saturation pressure of the solvent. The solvent rises into the formation forming a solvent chamber. The viscosity of the bitumen is reduced due to the presence of the dissolved gas. Production is performed through the same well following the injection portion of the cycle. The production is continued until the bottom hole pressure has decreased below the saturation pressure. The cycle is then repeated. The scaled results from the experiments indicate that for a 500 m horizontal well in a 25 m thick reservoir using ethane as a solvent the production rates would peak at about 40 m^3/d after 4 years and would decline to about 10 m^3/d 10 years later.

Srivastava *et al* (1997) investigated the injection of flue gas for the recovery of heavy oil in Saskatchewan reservoirs. Flue gas, which contains about 15 mol % CO_2 and 85 mol % N_2, is more readily available and cheaper than pure carbon dioxide in Saskatchewan. A series of linear core floods were performed to investigate different recovery strategies. Comparison of a secondary slug injection technique and a tertiary slug injection technique where a previous water flood had been performed showed the tertiary strategy to be less effective. A tertiary water alternating gas injection strategy was found to be more effective than the tertiary slug injection technique but still less effective than the secondary slug injection technique. Floods with pure CO_2 performed better than the floods with flue gas. However, the improvement was only marginal, with the pure CO_2 recovering only 2 to 4 additional percentage points of OOIP. Therefore, it is believed that flue gas may still be an effective recovery agent for heavy oil. The Srivastava *et al* (1997) believe two competing mechanisms exit in the flue gas floods, a free gas

mechanism provided by the nitrogen and a solubilization mechanism provided by the carbon dioxide.

Chemical flooding is another classification of EOR techniques that has been predominantly used for conventional oil recovery. There have been some applications of chemical flooding for heavy oil recovery (Selby *et al*, 1989). There is clearly potential for non-thermal chemical techniques to become an effective heavy oil recovery tool. The most prevalent chemical flooding techniques are surfactant flooding, emulsion flooding, alkali or caustic flooding and polymer flooding. Combinations of the three have also been used (Taber *et al*, 1996).

Surfactant flooding is performed with the aim of reducing the oil water interfacial tension. This causes a reduction in the residual oil saturaton. However, the process suffers from a number of drawbacks including adsorption of the surfactant to the reservoir rock as well as undesirable chemical interactions with the formation (Farouq Ali and Thomas, 1996).

Emulsion or micellar flooding involves the injection of a water/hydrocarbon microemulsion. The emulsion is achieved through the use of surfactants. A reduction of the aqueous phase mobility is caused by presence of small oil droplets. The emulsion displaces the oil in an apparent "miscible" fashion. The technique has been shown to be successful in watered out light oil reservoirs (Farouq Ali and Thomas, 1996).

Caustic flooding involves the injection of an alkali solution into the reservoir. The alkali solution reacts with the organic acids in the crude oil and results in the generation of surfactants in situ (Jennings *et al*, 1974). This results in the reduction of the interfacial tension between the aqueous and oil phases. This aids in mobilizing the residual oil. As well, the generated surfactants cause the creation of an emulsion. This reduces the aqueous phase mobility and improves the sweep efficiency of the flood. Caustic flooding can also cause a reversal in wettability from water-wet to oil-wet by changing the pH of

the injected water (Selby *et al*, 1989). This can change the residual oil from an immobile discontinuous phase to a mobile continuous phase.

Polymer flooding is performed by adding a water soluble polymer to the injection water. The most common polymers used are partially hydrolyzed polyacrylamides and biopolymers such as xanthan (Littmann, 1988). The resulting polymer solution has an elevated viscosity. This reduces the mobility of the aqueous phase. Further mobility reduction of the aqueous phase is caused by polymer retention in the reservoir rock (Littmann, 1988). This serves to reduce the mobility ratio and improve the conditions of the displacement for oil recovery. There are a number of reasons that a reduction in mobility ratio can improve oil recovery, including improved fractional flow, improved areal sweep efficiency and a reduction in viscous fingering.

Part of the Buckley-Leverett model includes the description of fractional flow in porous media (Craig, 1971). The fractional flow of water in a water flood is defined as the flow rate of water divided by the total flow rate of water and oil. The fractional flow of water is described by the simplified fractional flow equation as follows:

$$f_w = \frac{1}{1 + \frac{k_o \mu_w}{k_w \mu_o}} \qquad (2.1) \quad \text{(Craig, 1971)}$$

Which is equivalent to:

$$f_w = \frac{1}{1 + \frac{1}{M}} \qquad (2.2)$$

Where M is the mobility ratio of the displacement. Increasing the aqueous phase viscosity, and therefore reducing the mobility ratio, results in a decrease in the fractional flow of water corresponding to an increase in the fractional flow of oil. Therefore, at any given water saturation in an element of porous media, an increase in the displacing aqueous phase viscosity will result in an increase in the flow of oil from the element of porous media.

Reducing the mobility ratio of the displacement also results in an improvement of the areal sweep efficiency. Willhite (1986) summarizes a number of experimental and modeling studies on two dimensional immicsible displacements. In all cases the areal sweep efficiency increases as the mobility ratio decreases.

Viscous fingering results from instabilities of the displacement front. Sarma and Bentsen (1987) developed an instability theory for immiscible displacements in porous media. As well, they verified their theory experimentally. According to their theory, an increase in the mobility ratio results in an increase in the likelihood of an unstable displacement and the onset of viscous fingering. Poor sweep efficiency and a decreased ultimate recovery will result from viscous fingering.

Jameson (1973) reported on polymer flooding of heavy oil in the Lloydminster region. Although there was improvement in the sweep efficiency over water fooding, the economics at the time were marginal. Selby *et al* (1989) presented results from many field scale polymer flood operations on light heavy oils. The degree of success of the various projects varied over a large range indicating that the mechanisms involved are not fully understood. The potential of polymer floods to improve the sweep efficiency over water flooding makes it an attractive option for heavy oil recovery where water flood sweep efficiencies are quite poor. Since polymer flooding plays a significant role in this study it will be reviewed in further detail.

Pye (1964) noticed that aqueous solutions of certain high weight molecular polymers experienced a significant reduction in mobility in porous media. The observed reduction in mobility was 5 to 20 times greater than that expected based on the measured viscosity of the solutions. This indicated that only small amounts of polymer were required in order to improve the mobility ratio in water-oil displacements. Pye presented laboratory results that showed improved fractional flow characteristics when compared to brine displacements in experiments where oil was displaced by polymer solutions. As well field pilot tests of polymer flooding presented by Pye (1964) demonstrated substantial improvement over water flooding.

Sandiford (1964) investigated the use of solutions of partially hydrolyzed polyacrylamides to recover oil in a series of linear and radial displacement experiments. He noticed that the mobility of the polymer solution was substanially less than expected based on standard viscosity measurements of the solution. It was observed that at residual oil saturation, the presence of the polymer solution resulted in a substantial reduction in the mobility of the aqueous phase while the mobility of the oil essentially unaltered. Observations from the experiments indicated that microscopic displacement efficiency as well as the sweep efficiency was improved using a polyacrylamide solution instead of brine. Sandiford (1964) described field pilot tests of polymer flooding, including one in a Californian heavy oil reservoir. The results of the tests were very promising with increases in oil production rates being observed.

Mungan *et al* (1966) conducted an experimental study to investigate the rheology and adsorption of polymer solutions in porous media as well as the efficiency of polymer solutions for oil recovery. The shear thinning quality of a variety of polymer solutions was quantified. As well, the reduction of the viscosity of ionic polymer solutions caused by the presence of electrolytes such as sodium chloride was noticed. The reduction of the polymer solution mobility in porous media was attributed to an increase in the viscosity of the solution as well as adsorption and mechanical entrapment of polymer in the porous media. The effect of polymer adsorption in the porous media was observed when the mobility of brine was reduced in a core that had been previously flushed with polymer. Oil displacement experiments with polymer solutions were performed. Mungan *et al* (1966) concluded that little reduction in the residual oil caused by polymer flooding was achieved over water flooding. However, the volumetric sweep of polymer flooding was believed to be much better. When a tracer was co-injected with the polymer solution during a displacement, the tracer was detected at the production end of the core 1 pore volume ahead of the polymer. As well, a 48 % pore volume of tracer free water was produced before any tracer was detected. Therefore, the authours concluded that the connate water was being banked ahead of the polymer and that even if a polymer flood

was performed without any prior water flood it produced the same amount of oil because the banked connate water would act like a preceeding water flood.

In a laboratory study, Gogarty (1967) investigated the mobility of polymer solutions in porous media. He determined the size of the polymer molecules in solution using filtering techniques. The measured values were believed to be larger than some of the smaller pore throats in Berea cores in which the polymer had exhibited a considerable mobility reduction. It was hypothesized that polymer retention was taking place by adsorption and mechanical entrapment at these small pore throats essentially blocking them off. This was concluded to be the major cause of permeability reduction in the cores. Gogarty believed that the blocking of pore throats would cause an increase in the frontal velocity of the polymer. This increase in velocity would result in an increase in the shear rate of the polymer solution and a subsequent reduction in its viscosity. Therefore, the high effective viscosity of the polymer solutions observed at low shear rates was not being used efficiently due to the retention of polymer in the porous media.

Mungan (1969) performed a rheological study on partially hydrolyzed polyacrylamide solutions. He found that the viscosity of the polymer solutions decreased dramatically with increasing shear or salinity. It was also determined that the viscosity of the solutions dropped significantly when the pH was decreased below 7. Adsorption of polymer onto different silica sands was also quantified in the study with the maximum value of adsorption in porous media observed to be 160 micrograms polymer/gram rock.

In an experimental study, Smith (1970) investigated the behaviour of partially hydrolyzed polyacrylamides in porous media. In static adsorption tests with silica and carbonate, it was observed that adsorption increased with increasing salinity. The stated practical implications of polymer adsorption was that it would be detrimental to the polymer flood because the polymer losses to the reservoir rock would prevent deep penetration of polymer into the reservoir. Salinity was observed to reduce the apparent molecular size of the polymer in solution therefore reducing the viscosity of the solution. However, increased salinity did not appear to have a large effect on the reduction of the mobility of

the solution in porous media. This was attributed to the opposite effects of increased adsorption and reduction of apparent molecular size and therefore reduced mechanical entrapment caused by the increases in salinity. It was also observed that permeability loss was caused by flowing a polymer solution through a core sample. Even after flowing hundreds of pore volumes of brine through the core the original permeability could not be recovered.

In an investigation of the viscosity of ionic polyacrylamide solutions, Mungen (1972) fit a power law equations to a number of polymer solutions. Electrolytes were found to reduce the viscosity and the shear thinning characteristics of the polymer solutions. Divalent cations such as Ca^{2+} were found to have greater effect in the reduction of the solution visocosities.

Szabo (1975a) used a hydrolyzed polyacrylamide tagged with C^{14} to investigate retention of polymer in porous media. The tagged polymer allowed for an effective means of determining polymer concentration in produced fluids from core floods. When polymer in brine was injected in to a core it was observed that the polymer broke through at the production end ahead of the brine. From this result, it was estimated that at least 22 % of the pore volume was inaccessible to polymer flow. This led to the conclusion that since the polymer flows through only a portion of the pore volume and the brine flows through the entire pore volume, the concentration in the areas where the polymer does flow must be greater than the feed concentration. This could contribute to the fact the mobility of the solution is less than indicated by measured solution viscosities. Szabo (1975a) also concluded that in low permeability cores, rentention was dominated by mechanical entrapment while in medium and high permeability core adsorption was the dominant retention mechanism.

In another study (Szabo 1975b) performed a series of oil recovery tests in sand packs using polymer solutions. He found that polymer solutions did recover more oil than brine floods. In low permeability sand packs only small polymer concentrations and slug sizes were required to recover additional oil. In higher permeability sands larger amounts of

polymer were required to achieve improved oil recovery. As well, it was observed that if the polymer flood was initiated at connate water saturation in the core the residual oil saturation was reduced. However, if a previous water flood was performed, oil recovery was accelerated but no reduction in residual water saturation was observed. Displacements performed in layered sand packs with different permeabilities were very successful using polymer solutions. The reduction in aqueous phase mobility resulted in efficient recovery of oil from the low permeability layers.

Castagno *et al* (1987) performed a laboratory evaluation of synthetic polyacrylamides and polysaccharide biopolymers for a field project. The polysaccharide solutions had higher apparent viscosities than the polyacrylamide solutions. During oil displacement tests both polymer solutions gave similar production results. The retention of the polyacrylamide in core floods was found to be much greater than the polysaccharide. This led to the selection of the polysaccharide for the field test. Biological degradation of the polymer was controlled in the laboratory by the use of biocides. However, degradation was found to be a major problem in a field pilot test. As a result, a full field project using the polymer was not performed.

The propagation of polymer solutions through porous media was investigated by Zaitoun and Kohler (1987). They performed core floods with xanthan and polyacrylamide polymers. They investigated the effects on polymer propagation caused by adsorption, mechanical entrapment, inaccessible pore volume and the depletion layer effect. The depletion layer effect is caused by repulsive forces between the polymer macromolecule and the pore wall resulting in lower polymer concentration near the pore wall. Zaitoun and Kohler believed that the depletion layer effect was responsible for a lower mobility reduction than indicated by the polymer solution viscosity and the breakthrough of the polymer before a full pore volume was injected into the sand pack. Polymer adsorption was responsible for delaying polymer breakthrough, increasing the polymer mobility and reducing the permeability. Increasing the clay content in the porous media resulted in greatly increased polymer adsorption and led to poor propogation of the polymer solution. Breakthrough was greatly reduced in this case.

In high salinity reservoirs, it is often necessary to perform a fresh water pre-flush prior to injecting salt sensitive polymers. Sohn *et al* (1990) pointed out the short comings of performing a pre-flush. The low-viscosity fresh water flows through the high permeability paths in the reservoir, leaving portions of the reservoir uncontacted. Pre-flushing requires long injection times, which can be costly. As well, pre-flushing results in high water saturation areas in the reservoir. This effects the efficiency of the polymer flood since the polymer is used to displace large amounts of water. Sohn *et al* (1990) proposed using a small slug of polymer solution with a low degree of hydrolysis for a pre-flush. Polymers with a low degree of hydrolysis are less sensitive to salinity. However, a higher concentration of the polymer is required to attain a viscosity equal to solutions of polymer with a higher degree of hydrolysis. Therefore the authours recommend a small amount (10 – 15 % of total polymer slug) of the low-hydrolysis polymer be used. Laboratory and field results have shown the technique to be successful.

Huh *et al* (1990) developed a theoretical model for polymer retention in porous media. They considered a capillary bundle representation of a porous media. Their model accounted for both adsorption and mechanical entrapment. According to the model, the rate of polymer retention is proportional to the flux of polymer in the porous media. The rate of retention decreases linearly as retention increases until a maximum retention is attained. A series of core floods with xanthan were performed by Huh *et al* (1990) to compare with their model. Their model was shown to accurately predict the characteristics of the effluent polymer profiles. Both polymer frontal delay and a slow approach to the feed concentration were predicted by the model.

The ability of polymer solutions to selectively reduce the relative permeability of the aqueous phase over the oil phase has been investigated by a number of authours. Zaitoun and Kohler (1988) performed an experimental investigation on the effect of polymer adsorption on two phase flow in porous media. Both polysaccharides and polyacrylamides were used in the investigation. The adsorption of polymer to water-wet sand and sandstone was observed to have very little dependence on the presence of

residual oil. However, the reduction of the aqueous phase permeability was substantially larger with residual oil present. This was attributed to the reduction in flow cross section available to the aqueous phase. The relative permeability of the non-wetting oil phase was essentially unaltered by the adsorption of polymer to the porous media. Even though the polymer is expected to reduce the flowing cross section of the pore and reduce the permeability of all fluids it is believed permeability enhancement of the non-wetting phase is caused by a lubrication effect and an enhancement of the water wet nature of the rock. As well, polymer adsorption was observed to increase the irreducible water saturation.

Barrufet and Ali (1994) performed experiments using a starch based biopolymer. They also observed an increase in irreducible water saturation due to polymer adsorption. Polymer adsorption resulted in a significant reduction in the relative permeability to water. The effect of polymer adsorption on the oil relative permeability was varied depending on the rock formation. In some cases their was a slight reduction in the relative permeability while in others their was a significant increase in the oil relative permeability. The latter phenomenon was attributed to a lubrication effect caused by the adsorbed polymer.

Menella *et al* (1998) used a network model of a porous media to investigate the selective permeability reduction caused by polymer adsorption. They used a Sphere Pack Model to model the porous media and modeled the adsorbed polymer as a rigid layer impermeable to flow of any fluid. Core flood tests were performed to compare with the model. They found that the reduction in the absolute permeability and the reduction in the water relative permeability could be modeled adequately with the model. However, the thickness of the adsorbed polymer layer had to be reduced by an order of magnitude in order to match the reduction of the relative permeability of the non-wetting phase (oil or gas). From these observations it was proposed that the adsorbed polymer layer was not rigid but was prone to shrinking or swelling depending on the nature of the phase flowing through the pore. When oil is flowing through the pore, the hydrophilic polymer shrinks, expelling hydration water. Conversely, the polymer swells when water is

flowing through the pore. This would account for the disproportionate reduction in relative permeabilities.

Zaiton *et al* (1998) performed a series of experiments on both water wet and oil wet cores to investigate the disproportionate permeability reduction (DPR) caused by polymer adsorption to pore walls. They attributed DPR to three types of wall effects: steric effects, lubrication effects and wettability changes. Steric effects account for the polymer layer adsorbed to the pore wall that is impenetrable to fluid flow. Lubrication effects enhance the flow of the oil by supplying a film of water for the oil to flow over and for smoothing out the roughness of the pore wall. The adsorption of a hydrophilic polymer to the pore wall causes an enhancement of water wettability. Polymer adsorption was observed to cause an increase in the capillary pressure. This was attributed to an effective reduction in the size of pore throats due to the adsorbed polymer layer. In oil wet cores the increase in capillary pressure was attributed to a change in wettability to water wet as the capillary pressure was increased from negative values to positive values. As well, a significant reduction in the residual oil saturation was observed in the oil wet cores. This was also attributed to wettability reversal.

Zheng *et al* (1998) investigated the effect of partially hydrolyzed polyacrylamide adsorption on two phase flow in porous media. They performed core floods on water wet and mildly oil wet cores. An increase in the irreduceable water saturation was observed which was in agreement with previous studies. Very little change in residual oil saturation was observed. A selective reduction of the water relative permeability was observed. Changes in the relative permeability endpoints was found to vary with polymer concentration. A reduced polymer viscosity was observed in porous media when compared to the bulk measurements. This was attributed to the depletion layer effect. This effect as well as the changes in relative permeability endpoints where modeled and incorporated into a numerical simulator. Field scale simulations where performed that showed polymer floods to be an effective enhanced oil recovery tool.

The preceding review has summarized the development of polymer flooding since the technology was introduced. The low mobility of polymer solutions in porous media improves the conditions for displacement of the heavy oil. The fact that the mobility is reduced more than would be predicted based on viscosity alone allows for solutions with desired low mobilities with reduced chemical costs. The selective permeability reduction characteristics of polymer solutions that many researchers have observed are very beneficial for oil recovery. In the case of heavy oil, which already has a low mobility, the benefits of reducing the aqueous phase mobility with out reducing the oil mobility are even greater. Due to the high viscosity of heavy oil, polymer flooding is an attractive option for enhanced recovery of heavy oil.

CHAPTER THREE: DESCRIPTION OF APPARATUS AND PROCEDURES

3.1 Ambient Conditions Physical Models

3.1.1 Description

Two of the physical models used were constructed for running experiments at ambient conditions with dead oil. The models had two Plexiglas walls originally intended for visualization of the displacements. The Plexiglas walls were attached to a phenolic frame. An o-ring between the Plexiglas walls and the phenolic frame provided a seal. Due to the opaque nature of the heavy oils used in the experiments, direct visualization was not possible. The internal dimensions of the larger ambient model (Ambient Model #1) were 50 cm x 30 cm x 10.5 cm. The second ambient model (Ambient Model #2) had internal dimensions of 50 cm x 30 cm x 5 cm. A picture of Ambient Model #1 is shown in Figure 3.1. The well configurations of both models were the same. Figure 3.2 displays the configuration of these wells. There were six wells that penetrate into the thickness of the models that were arranged in two rows of three that were approximately 23 cm apart. These were the wells that are used for injection and production of fluids during the displacement experiments. The models could be laid down flat so that these wells were vertical or the models could be stood up to simulate displacements with horizontal wells. Each model also had two long wells that ran along the 50 cm length of the models. These long wells were used for saturating the sand pack with heavy oil. All wells were made from ¼" (0.635 cm) stainless steel tubing that had been drilled with perforations and then wrapped with wire mesh to prevent sand from entering the well.

Figure 3.1: Picture of Ambient Model #1

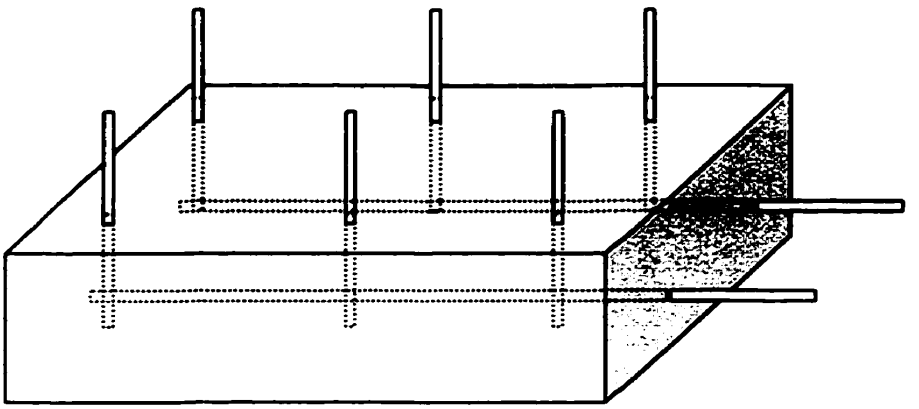

Figure 3.2: Well Configuration of Ambient Models

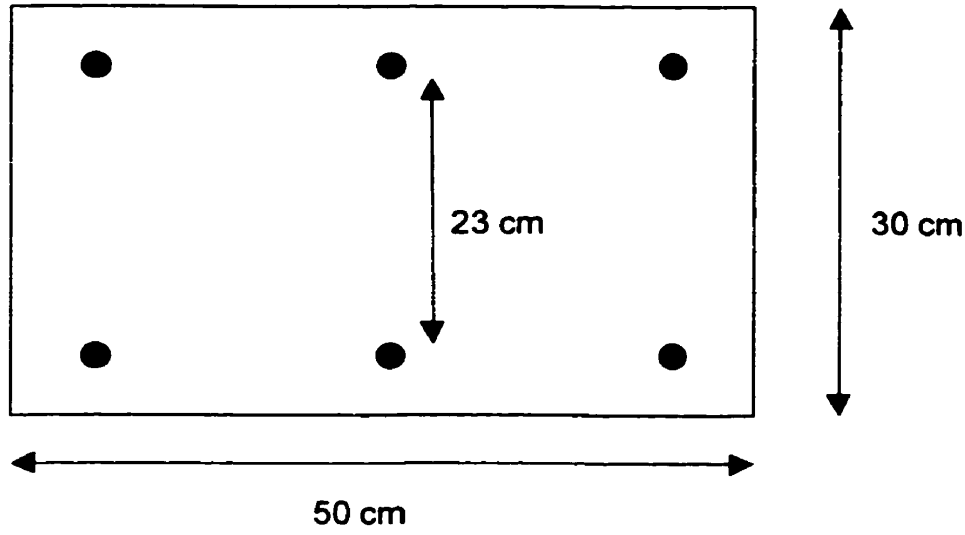

3.1.2 Saturation Procedure

Prior to packing, the models were assembled and slightly pressurized to ensure there were no leaks. The models were then opened and wet packed. This was done by maintaining a water level of about 2 – 3 cm above the sand while packing. The model was vibrated while packing.

The construction of Ambient Model #2 was different from that of Ambient Model #1 in the fact that Ambient Model #1 had a removable lid that made packing easier. There were three access ports in the top of Ambient Model #2 about 2 cm in diameter through which to pack the model. This made it difficult to get a tight pack right up to the top of the model. As a result, the quality of the sand pack tended to be better in Ambient Model #1.

The permeability and porosity of the sand pack were estimated by measuring these qualities with a core holder that had been packed with the same sand using the same packing technique. The absence of a confining overburden pressure on the sand packs of the Ambient Models made the determination of porosity and permeability difficult.

These difficulties are discussed in Chapter Four. The details of the porosity and permeability measurements are described further in section 3.6.

Once the Ambient Models were packed they were saturated 100 % with 2 % NaCl brine. Brine was injected into three wells and produced from three wells opposite to the injectors. The flow rates and pressure drops were measured. From these measurements a rough estimate of the permeability was made and compared to the value obtained from the core holder tests. The same procedure and apparatus was used to saturate each of the models. A 3.8 litre vessel was filled with dead heavy oil. The top of the vessel was connected to a compressed nitrogen cylinder. The models were placed so that the long wells were vertical. These wells were connected to the bottom of the vessel with the dead oil. The oil was then purged from the vessel out the bottom of the vessel at a constant pressure and injected into the model. The oil was injected from the top of the well so there was a gravity stable displacement of the brine by the oil. The displaced fluids were drained from the model through the six short wells. The dead oil was injected until no more brine was produced from the six injection/production wells. The injection pressure was maintained below 10 psi (69 kPa) to ensure the model remains sealed. The volumes of the displaced fluids were carefully tracked in order to determine the oil saturation of the models. As well, the amount of oil injected into the models was determined by weighing the vessels containing the oil before and after the saturation. The saturation of the Ambient Models took from two weeks to a month to complete.

3.1.3 Production Set-up

During the production phase of an experiment it was possible to orient the model so that the six injector/producer wells were either vertical or horizontal. Typically, one row of three wells was designated as injectors well the other row was designated as producers so that floods were performed in a line drive configuration.

All floods were performed under constant pressure drive to ensure that model remained sealed. For brine or aqueous polymer floods, a 3.8 litre vessel was filled with the brine or

aqueous polymer. The top of the vessel was connected to a compressed nitrogen cylinder. The bottom of the vessel was connected to the injector wells. The fluids were then injected into the model under constant pressure. For nitrogen floods, the injectors were connected directly to the regulator on the nitrogen cylinder. The produced fluids were collected at the production wells in either graduated cylinders or centrifuge tubes. The volumes of the produced fluids were then measured. The production set up of the Ambient Models is presented in Figure 3.3.

Figure 3.3: Production Set Up of Ambient Models

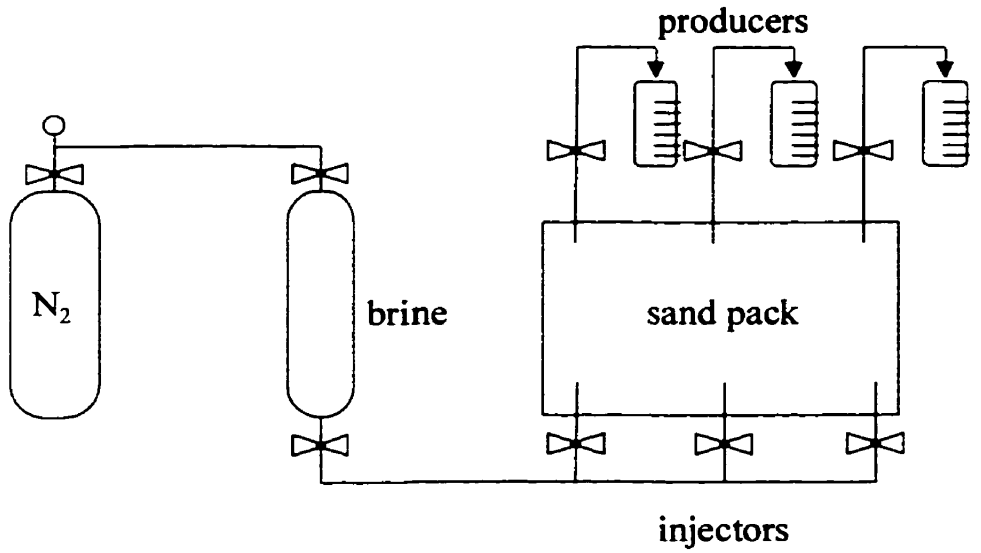

3.2 Reservoir Conditions Physical Models

3.2.1 Description

In addition to the two Ambient Models, two models had been constructed to operate at reservoir conditions. Both models were constructed of aluminum. They were pressure rated to 600 psi (4.1 MPa) and were used for live oil experiments. With these models primary production could be performed prior to any displacements. Both models had internal dimensions of 30 cm x 30 cm x 10 cm.

An overburden pressure could be applied to the sand pack. There was a small cavity engraved into the lid of each of the models. A viton diaphragm separated the lid from the

sand pack and provided a seal for the model. Compressed nitrogen was injected into the cavity in the lid of the model at the desired overburden pressure.

Both models had two horizontal wells that were used for saturating the model with oil. They were placed at opposite sides from each other and ran along the 30 cm length of the model. One of the horizontal wells was located in the upper corner while the other was in the lower corner.

Reservoir Model #1 had four vertical wells that ran into the 10 cm thickness of the model while Reservoir Model #2 had only three vertical wells. Top views of both models, presented in Figures 3.4 and 3.5, show the vertical well configurations. The well configurations allowed for testing of spot geometry. Performing a flood across the diagonal of the model from an injection well in one corner to a production well in the opposite corner represents a quarter of a five spot pattern. Wells for the reservoir condition model were constructed from 3/8" (0.9525 cm) stainless steel tubing that was drilled with perforations then wrapped with wire mesh.

Figure 3.4: Top View of Reservoir Model #1

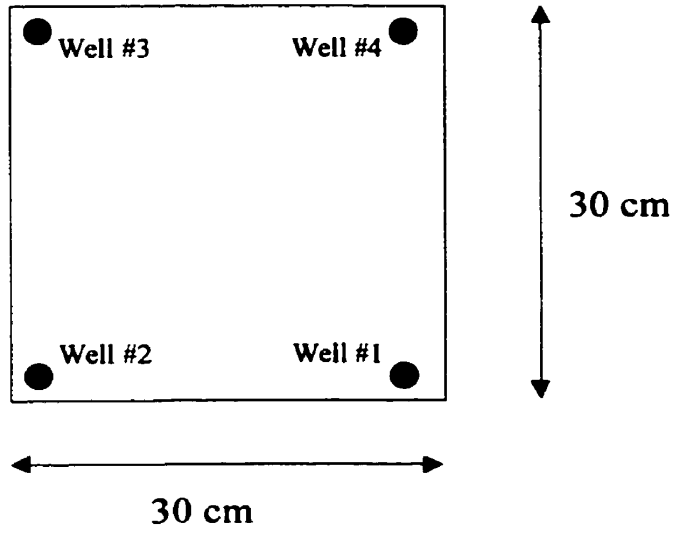

Figure 3.5: Top View of Reservoir Model #2

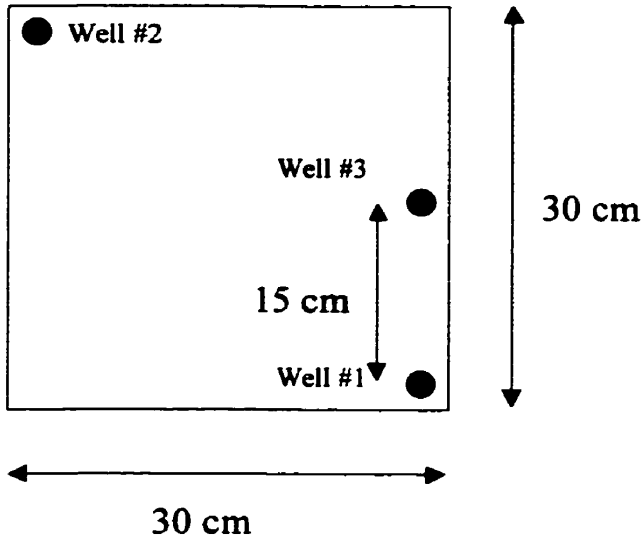

3.2.2 Saturation Procedure

Both models were wet packed in the same manner as the Ambient Models. The model was sealed and a 600 psi (4.1 MPa) overburden pressure was applied to the pack. A nitrogen dome back pressure regulator (BPR) was then connected to the lower horizontal well. The BPR was set to 500 psi (3.4 MPa) and the model was brought up to pressure by injecting brine in through the horizontal well that was in the opposite upper corner of the model. Multiple pore volumes of 2 % NaCl brine were injected into the model. The model was then pressure tested for any leaks.

Live oil was produced in the live oil generation apparatus as described below. Live oil was then pushed from the apparatus by methane into a 2 litre piston cylinder. The piston cylinder was connected to an ISCO piston pump which pumped water into the bottom of the piston cylinder. This moved the piston in the piston cylinder and pushed the live oil into the model via the upper horizontal well. The brine was thus displaced from the model out the bottom horizontal well and through the BPR in a gravity stable manner. The pump was set to inject oil into the models at a set rate of 15 cm^3/hour. The pump was also set to pump at a maximum pressure of 550 psi (3.8 MPa) so that the internal

pressure did not get too close to the overburden pressure. As a result, the pump did not always pump at the set rate.

As with the ambient models, the volumes of the displaced fluids were recorded along with the volume of oil injected. As well, the overburden and internal pressures were monitored to ensure that no leaks developed anywhere in the system. The oil was injected until no more brine was displaced. The lower horizontal well was then shut in and brine was displaced from each of the vertical wells. The entire saturation required about a month to complete.

3.2.3 Production Set-up

Primary production was performed by decreasing the set pressure on the BPR. The produced liquids were collected in 100 cm^3 centrifuge tubes. The produced gas was measured by a wet test meter.

During brine floods or aqueous polymer floods, an ISCO piston pump pumped distilled water into the bottom of a 1 litre vessel containing mineral oil. The top of this vessel was connected to a second 1 litre vessel containing brine. The brine was pushed by the mineral oil from the second vessel and into the injector well of the model at a constant rate. The produced liquids were collected in a graduated cylinder and the gas was measured with a wet test metre. Figure 3.6 presents the production set up. For immiscible gas floods, the injector well was connected to a compressed nitrogen and the nitrogen was injected into the model at a constant pressure.

Figure 3.6: Production Set Up for Reservoir Models

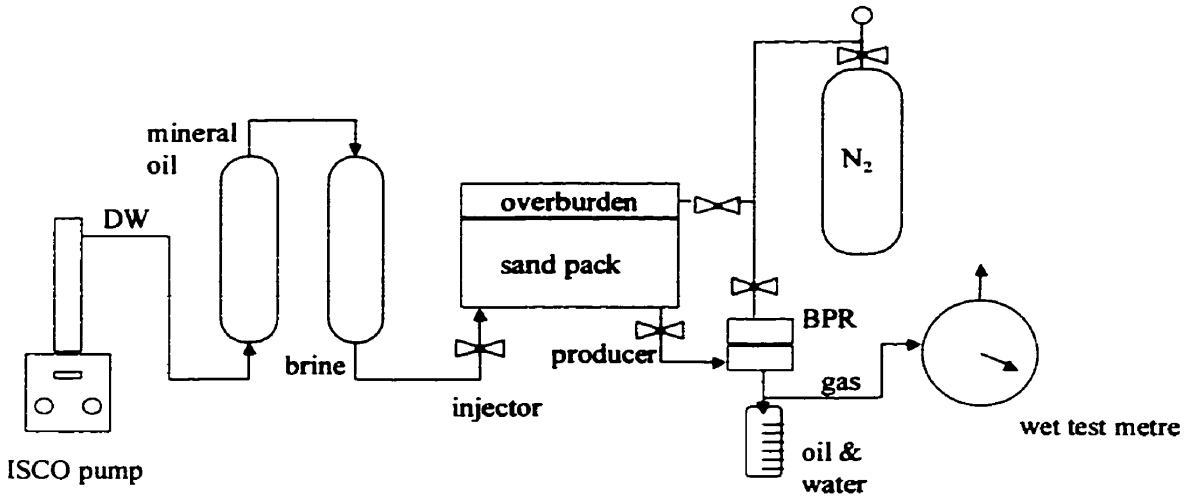

3.2.4 Modifications for Sand Production

Modifications were made to one of the wells of Reservoir Model #1 in order to perform experiments with sand production. The well consisted of two concentric tubes. The inner tube was a 3/8" (0.9525 cm) stainless steel tube with a single perforation approximately 3/4 cm in diameter located at mid-depth in the sand pack. This tube fit in the outer tube with enough tolerance to rotate within the outer tube. The outer had a perforation located at the same depth as the inner tube. Thus the perforation could be opened by turning the inner tube. The outer tube had been equipped with a tab that could be wedged into the corner of the model to ensure that the outer tube did not rotate with the inner tube.

Since it was not possible to produce sand through the back pressure regulator, the model was blown down to atmospheric pressure during primary production for sand production experiments. A stainless steel line was run from the production well to a stainless vessel were the fluids were collected. A tee was run from the line at the vessel and connected to a wet test metre to measure gas production. As the vessel filled up it was replaced with a new vessel.

Floods performed after sand production were performed under constant rate, as with non sand producing experiments. Since the models were at atmospheric pressure there was no need for a back pressure regulator at the exit of the production well. All produced fluids were collected directly from the production well into a graduated cylinder.

3.3 Live Oil Generation Apparatus

A live oil generation apparatus was set up to generate live oil for the reservoir condition models. The apparatus consisted of three 3.8 litre stainless steel vessels connected in series in a closed loop with ½" (1.27 cm) tubing. A recirculating pump was contained in the loop. One of the three vessels was packed with chain link to increase the mass transfer surface area. To generate live oil, the two other vessels were filled with dead heavy oil. The entire apparatus was pressurized by filling the vessel with the chain link packing with methane to the desired bubble point pressure which was 500 psi (3.4 MPa) for all the experiments. Heating pads were wrapped around the vessels and they were slightly heated in order for the pump to be able to initiate flow. The oil was then circulated through the three vessels until the desired GOR was obtained. Approximately one week was required for a GOR of about 10 cm^3/cm^3. The vessels were only heated for the first couple of days after which the oil was circulated at ambient temperature.

3.4 Aluminum Core Holder

A fifth physical model was used for visualization experiments that were performed with the CT scanner. The model was a core holder constructed of aluminum. Aluminum is X-ray transparent and allows for visualization of the sand pack contained in the core holder. The sand was packed in a rubber boot that was then placed in the aluminum core holder. An overburden could then be applied to the boot by injecting water or nitrogen into the annulus between the core holder and the boot. The sand pack in the core holder had a diameter of 8.89 cm and a length of 28 cm.

The core holder was wet packed and saturated with brine. A 600 psi overburden pressure was applied to the sandpack. The core holder was then scanned with the CT scanner acquiring an image every 5 mm along the sandpack. These scans were used to determine saturations during the experiment. The core holder was then placed vertically and the brine was displaced from the sandpack by the oil in a gravity stable manner. This was done at constant pressure similar to the manner in which the Ambient Models were saturated.

The production set up was also similar to the one used for the Ambient Models. Displacements were performed under constant pressure drive. The displacing fluid was contained in a 1 litre vessel that was connected at the top to a compressed nitrogen cylinder. The nitrogen displaced the liquid from the vessel into the injection end of the core holder. Produced fluids were collected in centrifuge tubes from the production end of the core.

3.5 Visualization Equipment

3.5.1 Gamma Ray Camera

The gamma ray camera was a Siemens Orbiter medical diagnostic camera interfaced to a Macintosh Power PC. The camera has 75 photo-multiplier tubes located behind a NaI(TI) detector crystal. In front of the crystal is a collimator. Gamma rays that pass through the collimator cause a scintillation event on the detector crystal. The photo-multiplier tubes and position logic circuits determine the position of the scintillation event. The coordinates of the event are passed on to the computer and displayed on the monitor. The total detection area of the camera has a diameter of 41 cm. The camera acquires an image consisting of a 128 x 128 pixel matrix. Each pixel represents a 3.2 mm x 3.2 mm area. The value stored in each element of the matrix represents the number of radioactive counts (scintillation events) detected by the camera during the length of time it is allowed to acquire an image.

The Ambient Models were used with the gamma ray camera. The radioisotope used was technetium 99m (^{99m}Tc). It is a radio-pharmaceutical with a half life of 6 hours and a peak energy of 140 eV. The short half life allowed for the radioactivity to decay in a matter of days, minimizing the down time of any equipment used for the experiments. The aqueous phase was tagged with ^{99m}Tc and therefore could be visualized with the camera. This allowed for determination of the area swept by the displacing phase. Images were taken with the gamma camera throughout the flood. For each image the camera was allowed to measure counts for one minute. Due to the smaller size of the detector of the camera it was necessary to take three images in order to acquire imaging for the entire area of the model. These three images were later combined into a single image.

3.5.2 X-ray CT Scanner

The CT scanner is a EMI 5005 second generation machine. The scanner contains an X-ray source and 30 detectors that move in a translation-rotation movement around the object to be visualized. The scanner operates at 140 kV and 28 mA with a resolution of 750 μm x 750 μm. The beam thickness is 3 mm.

The X-ray source and the detectors move around the object and measure the attenuation of X-rays from all angles. The scanner then uses that information to reconstruct an image of the cross section of the object. The image is a matrix of CT numbers. The CT number is the linear attenuation coefficient normalized to the linear attenuation coefficient of water. The CT number is proportional to the density and the effective atomic number of the object (Kantzas 1990).

3.6 Porosity and Permeability Measurements

As mentioned above, the permeability and porosity of the sands used in the experiments were determined using core holders packed with the same sands, packed with the same wet packing technique that was used to pack the models.

After being packed the core was flushed with methanol and evacuated over night with a vacuum pump. The pore volume and porosity were determined by measuring the amount of brine required to fill the core using a precision Ruska pump.

The sands used were silica sands with permeabilities in the order of multiple Darcies. Therefore, high flow rates and small pressure drops across the sand pack were expected. In order to perform the tests accurately the brine was injected at a constant head pressure. A Plexiglas "bucket" with an elevated drain at the top and a separate outlet at the bottom was used. The outlet at the bottom of the bucket was connected to the injection end of the core. Brine was constantly poured into the bucket by a second container above the bucket. Brine overflowed into the elevated drain maintaining a constant level of brine in the bucket. The bucket was elevated above the core causing brine to flow into the core. The flow rate of brine was measured at the outlet of the core and the height of the level of brine above the core is carefully measured. The flow rate was measured for multiple bucket elevations and Darcy's law was used to determine the permeability. The test could be performed with multiple overburdens applied to the sand pack to determine the effect of overburden on permeability.

Figure 3.7: Set Up for Permeability Measurements

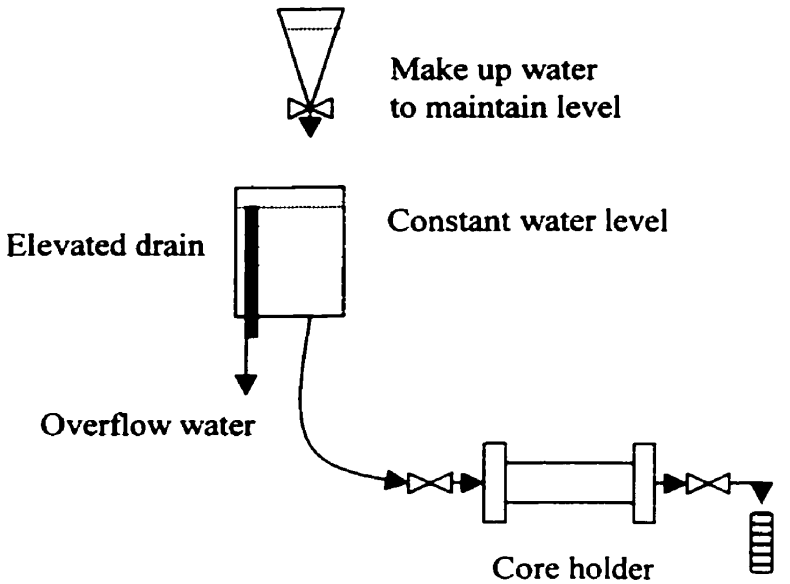

3.7 Measurement of Liquid Properties

Liquid viscosities were measured with a Wells-Brookfield cone/plate digital viscometer. The viscometer could measure viscosities at multiple shear rates and was accurate to within 1 % of full scale.

Densities were measured with an Anton Paar DMA 46 calculating density meter. The density meter was capable of measuring densities to within $5x10^{-4}$ g/cm^3.

CHAPTER FOUR: EXPERIMENTAL RESULTS AND DISCUSSION

The same sand was used for Experiments #1 to #5 and Experiment #7. The sand was nearly pure SiO_2, with traces of other compounds. Therefore the sand was water wet since that is the inherent nature of silica sands. The porosity and permeability were measured using the technique.described in Chapter Three. The measured porosity was 0.43. The permeability was measured for the sand starting with an overburden pressure of 30 psi. The overburden pressure was then increased in 30 psi increments and the permeability was measured at each overburden pressure. When the overburden pressure was increased from 210 psi to 240 psi, the overburden seal was compromised and the nitrogen used to apply the overburden pressure seeped into the sand pack. At this point the core was disassembled and repacked. Permeability measurements were redone starting at an overburden pressure of 100 psi and increasing the overburden in 100 psi increments to maximum of 600 psi. Figure 4.1 and Figure 4.2 show the measured permeability as a function of overburden pressure. All figures are presented at the end of the chapter. Figure 4.1 presents the results from the first test up to an overburden pressure of 210 psi while Figure 4.2 presents the subsequent test up to a 600 psi overburden pressure. In the overburden pressure range from 100 psi to 210 psi where there was overlap in the two tests, noticeable differences in the measured values can be observed. This illustrates the uncertainty of these tests. A possible source of this uncertainty is that the quality of the sand packs used in the different tests may not have been identical. Even though the same sand was used in the both tests and care was taken to pack the core holder in the same manner, it is very difficult to obtain sand packs that are identical. As well, due to high flow rates involved in the tests due to the high permeability of the sands, possible movement of fines may have altered the results. Because of these uncertainties in the permeability tests, the results obtained are used strictly as a rough estimate of the sand pack permeability.

The experiments using the Reservoir Models and the Aluminum Core holder were performed with a 600 psi overburden applied to the sand pack. The permeability for

these experiments can be taken directly from the measured values. The permeability measured with at an overburden pressure of 600 psi was 2.8 darcies.

No overburden was applied to the sand pack for the experiments performed using the Ambient Models. To estimate the permeability for these experiments it is necessary to extrapolate the permeability measurements to an overburden pressure of zero. The measurements from the first permeability test were used since the deviation of permeability with overburden pressure was observed to occur at overburden pressures under 150 psi. The measured data in Figure 4.1 was fitted with a trend line that is shown in the figure along with the equation for this trend line. The equation for the trend line has an asymptote at an overburden pressure of zero. Therefore, it was necessary to linearly extrapolate the line to an overburden pressure of zero. The slope of this trend line at the lowest measured permeability was determined by taking the derivative. The value of the permeability was estimated by linearly extrapolating back to an overburden pressure of zero using the slope determined by taking the derivative. The estimated value of the permeability with no applied overburden was 6.4 darcies. It is very possible that the relationship between permeability and overburden pressure is not linear at overburden pressures lower than 30 psi. If the relationship is higher order equation, permeability obtained from the linear extrapolation will be less than the true value of the permeability with no overburden pressure.

Flow tests were performed on the Ambient Models to get a rough estimate of the permeability to ensure it was in line with this estimated value. Once the models were packed and 100 % brine saturated, brine was injected in three of wells along one side of the at a constant pressure and produced from the opposite three wells. The produced flow rate was measured. The permeability was estimated using the linear form of Darcy's law along with the measured pressure drop and flow rate. The calculated permeabilities from these flow tests assumed the entire cross section of the model was used for flow. This would likely give permeability values that were smaller than the actual permeabilities. However, in some cases, permeabilities as high as 11 darcies were estimated from these tests. During history matching of the experiments with numerical simulators, which will

be described in detail in Chapter Five, permeabilities as high as 50 darcies were required in order to match the pressure drop in the experiments performed with the Ambient Models. This illustrates the difficulty in obtaining a good tight pack as well as the difficulty in determining a reliable estimate of permeability in the absence of an overburden pressure.

For Experiment #6 and Experiments #8 and #9 a second sand was used. It was also a silica sand. The measured porosity at an overburden pressure of 600 psi was about 0.43. The permeability measured with a 600 psi overburden pressure was 4.4 darcies.

In most cases the mass of sand used to pack the models was measured. This allowed for direct calculation of the porosity of the sand pack. In some cases with the Ambient Models the sand was wet before it was packed in the model. This occurred if the model had to be repacked due to leaks that were found in the model after packing. In these instances it was not possible to get an accurate measurement of the mass of sand used to pack the model due to the moisture in the sand. When this occurred the porosity that was measured using the core holder was used as an estimate. Deviations from the porosity values obtained with the core holder were only observed with the Reservoir Models, where porosities of about 0.40 were obtained.

It should be noted that great care was taken when packing the models to try to obtain as uniform a sand pack as possible. In spite of this it is quite likely that some variations in the quality of the sand pack did exist. This was especially the case in the Ambient Models where no overburden pressure was applied to the sand pack. In the Reservoir Models the overburden pressure was applied over the entire area of the sand pack. This helped maintain a good tight pack throughout the model.

Nine experiments were performed. Table 4.1 lists the experiments along with apparatus used and the operations that were performed. A detailed description of each experiment and the recoveries obtained follows.

Table 4.1: Summary of Experiments Performed

Experiment #	Model Used	Production Operations
1	Ambient Model #1	Water floods, gas floods, polymer floods
2	Ambient Model #2 (positioned vertically)	Water floods, gas floods, polymer floods
3	Reservoir Model #1	Primary, water floods, gas flood, polymer floods
4	Reservoir Model #2	Primary, water floods, polymer floods
5	Ambient Model #2 (with gamma camera visualization)	Water floods, polymer floods
6	Ambient Model #1 (with gamma camera visualization)	Water floods, polymer floods
7	Aluminum Core Holder (with CT scanner visualization)	Water flood, polymer flood
8	Reservoir Model #1	Primary (with sand production), water floods, polymer floods
9	Reservoir Model #2	Primary, water floods, polymer floods

4.1 Experiment #1

The first experiment was performed using Ambient Model #1. The experiment was performed with the model lying down flat so that the injection and production wells were vertical. Figure 3.2 represents a top view of the model. For the course of this experiment one row of three wells were designated as injection well while the other row of three were used as production wells. The floods were performed in a line drive configuration.

The initial conditions of the model after saturation are presented in Table 4.2. The oil used in the experiment was a heavy crude oil from the Lloydminster area.

Table 4.2: Conditions of Ambient Model #1 After Saturation, Experiment #1

Pore volume [cm^3]	6,765
Porosity [% p.v.]	0.43
Permeability [D]	6.4
OOIP [cm^3]	5,608
Initial Oil Saturation [%]	86
Oil Viscosity [cP]	5,800
Oil Density [g/cm^3]	0.968

The saturation of the model resulted in an initial water saturation of 14 %. This likely quite close to irreducible water saturation of the sand pack. However, due to the rectangular geometry of the model, some dead zones likely existed in the corners. The water saturation in these corners was probably higher than in the other regions of the sand pack. As a result, it is difficult to saturate the model with a uniform oil saturation right down to irreducible water saturation.

The first production cycle performed on Ambient Model #1 was a flood with 2% brine. All the injectors and producers were open. The flood was performed under constant pressure drive by applying a pressure of 2 psi to the brine filled vessel. Once the water cut reached 90 % for a particular producer, that producer was shut in. The cut off criteria of a 90 % water cut was selected to prevent the experiments from becoming excessively lengthy. Figure 4.3 shows the cumulative production for each producer well. The wells were numbered Producer 1, Producer 2 and Producer 3 from left to right. Figure 4.4 shows the water cut for each well. The production cycle lasted almost nine hours until the water cut for all the wells had reached 90 %. The oil produced amounted to 10.6 % of OOIP. The low recovery is to be expected due to the adverse ratio of the mobility of the water to that of the oil.

These experiments were not scaled. So the results do not imply that 10.6 % of OOIP can necessarily be recovered for a heavy oil of this nature by water flooding. However, the performance of the flood can be evaluated by comparing it to other recoveries obtained

using different recovery techniques on the models. Scaling of the results to field scale has been performed using numerical simulation and is described in detail in Chapter Five.

The stability of the flood was evaluated using the stability theory developed by Sarma and Bentsen (1987). They developed the following stability number:

$$I_{sr} = \frac{\mu_w v(M - 1 - N_g)}{k_{wro}\sigma_e} \frac{M^{5/3} + 1}{(M+1)(M^{1/3}+1)^2} \frac{4h^2b^2}{h^2 + b^2} \qquad (4.1)$$

Where v is the superficial velocity of the displacing water, h and b represent the height and width of the porous media respectively, M is the endpoint mobility ratio defined as:

$$M = \frac{\mu_o k_{wro}}{\mu_w k_{ocw}} \qquad (4.2)$$

N_g is the gravity number defined as:

$$N_g = \frac{\Delta\rho\, g\, k_{wro} \cos\alpha}{\mu_w v} \qquad (4.3)$$

Where $\Delta\rho$ is the density difference between the water and oil and α is the angle of deviation from vertical (horizontal, $\alpha = 90°$). The pseudo interfacial tension, σ_e, is defined as:

$$\sigma_e = A_c \phi (1 - S_{wc} - S_{or}) \qquad (4.4)$$

Where A_c is the area under the capillary pressure vs. saturation curve. According to the stability theory, a displacement is stable if I_{sr} is less than or equal to π^2. Sarma and Bensten (1987) confirmed this experimentally.

In order to use this criteria to evaluate the stability of the water flood performed in the experiment it is necessary to estimate some of the unknown variables. The approach taken in estimating the unknown variables was to make estimations that would favour a stable displacement, resulting in a lower value of I_{sr}. This was done because the displacement of such a high viscosity oil by water is expected to be unstable. Therefore, if the calculated stability number does indicate an unstable displacement, we can be confident that this is indeed the case.

The unknown quantities in the water flood are the endpoint relative permeabilities as well as the residual oil saturation and A_c required to calculate the pseudo interfacial tension. For the calculation of the mobility ratio M, the ratio of k_{wro} over k_{ocw} was assumed to be 0.1. This is a fairly low value and will reduce the value of the mobility ratio. The value of water relative permeability used to calculate I_{sr} was the value of the absolute permeability. The two assumption are not consistent, however, they will result in a reduced value of I_{sr}. Without any capillary pressure data, it is not possible to calculate the pseudo interfacial tension. Sarma and Bentsen (1987) performed stability analysis on water/oil displacements in high permeability sands. The largest value of pseudo interfacial tension that they measured was 3749 dyne/cm. This was the value assumed for calculating the instability number of the water flood performed in this experiment. Using these estimated variable values along with the directly measured variable values yielded a stability number value of 1203.7. This value is significantly lager than π^2, indicating an unstable displacement took place. This is not surprising considering the large mobility ratio involved in the water flood.

It also useful to calculate the capillary number, N_{ca}. The capillary number is the ratio of viscous forces to capillary forces and is defined as:

$$N_{ca} = \frac{\mu_w v}{\sigma_{ow}} \qquad (4.5)$$

Where v is the interstitial velocity. Most water floods operate with a capillary number in the order of 10^{-6}. If the capillary number is increased to 10^{-4} or greater, there will be a reduction in the residual oil and improved oil recovery will occur (Mungan, 1981). The average interstitial velocity of the water flood performed in the experiment prior to water breakthrough was estimated by dividing the distance between the wells by the time of water breakthrough. A value of 30 dyne/cm was used for the oil/water interfacial tension. This is a typical value for oil/water systems and will yield an approximate estimate of the capillary number. The calculated value of the capillary number for the water flood is 8.77×10^{-7}. Therefore the flood is controlled by capillary forces and the residual oil saturation is not "artificially" reduced by excessive viscous forces.

The second production cycle performed on the model was also a brine flood. However, the middle injection well was shut in for the duration of the flood. Again, as the water cut from each producer reached 90 % it was shut in. The model was shut in overnight between the first and second production cycles. In general, the shut in time between production cycles for all the experiments was minimized as much as possible and did not exceed more than two or three days. The cumulative production and water cuts are shown in Figure 4.5 and Figure 4.6 respectively. The production cycle lasted just over nine and a half hours. The outside wells, Producer 1 and Producer 3, reached a 90 % water cut in almost three hours. Once these wells were shut in the water cut of middle well, Producer 2, dropped moderately and required another seven hours to reach 90 % water cut. The incremental recovery was 8.7 % of OOIP. It is believed that this additional recovery of oil is a result of the flow pattern in the model being altered from the first flood. It is likely that the water flowed into previously unswept zones.

The next two production cycles were also 2 % brine floods. Production cycle 3 involved injecting through one of the outside injectors and producing through the production well in the opposite corner so that the flood was across the diagonal of the model. Production cycle 4 involved injecting through the other outside well and producing through the production well in the opposite corner, flooding across the other diagonal of the model. The water cut for both of these floods never dropped below 90 %. Insignificant amounts of oil were produced during both floods. The production to this point amounted to 19.6 % OOIP. This represents the maximum recovery from the model due to water flooding.

The four production cycles described above were then repeated using nitrogen instead of brine to investigate the performance of gas flooding as a tertiary recovery technique after water flooding. Gas flooding of heavy oil as a secondary recovery technique has been investigated previously (Kantzas *et al*, 1991; Islam *et al*, 1994). The nitrogen was injected into the model at a constant pressure of 2 psi. Very little oil was produced during these production cycles. The nitrogen broke through quickly and after breakthrough barely any liquids were produced. This result is quite different than the

results obtained by Islam *et al* (1994), who performed similar gas floods on sand packs to recover heavy oil. They obtained significant recoveries for all their floods, including those deemed to be unstable. However, their gas floods were performed on vertical systems, which may have improved stability of the floods to a certain degree. As well, they did not perform any water flood prior to the gas floods. This may also have affected the performance of the gas floods.

After the nitrogen floods another flood was performed with 2 % brine. All injectors and producers were used. Once again very little oil was produced.

For the tenth production cycle an aqueous polymer solution was injected into the model. The polymer used was Allied Colloids' ALCOFLOOD 935 which is a partially hydrolyzed polyacrylamide. The polymer has a molecular weight in the range of 6 – 9 million and a low degree of hydrolysis. A 5000 ppm solution of ALCOFLOOD 935 in fresh water was used. The resulting solution was a non-Newtonian shear thinning liquid. A plot of viscosity vs. shear for the solution is presented in Figure 4.7. The 5000 ppm concentration of polymer resulted in a solution with an elevated viscosity that was likely to be effective in displacing the high viscosity oil. As well, the concentration was low enough to keep the chemical cost from becoming excessive. All three injection wells and all three production wells were used for this flood. The flood lasted 103 hours and resulted in a large incremental recovery of 54.6 % of OOIP. After about 13 hours the water cut of all the producers decreased drastically. Figure 4.8 and Figure 4.9 show the cumulative production and the water cuts respectively. The large incremental recovery is likely due to the improved mobility ratio of the polymer flood as compared to the water flood. The reduction of the aqueous phase mobility was caused by its increased viscosity and possibly adsorption of polymer to the sand pack. As well, the presence of gas from the previously performed gas floods may have resulted in a reduction in the water relative permeability.

Performing the polymer flood involved constant monitoring and replacing graduated cylinders approximately every two hours. It was not possible to run the flood

continuously due to its length. The model was shut in overnight eight times. It was not shut in for the first time until the polymer had broken through to the production wells after about 20 hours into the flood once the water cut began to increase after reaching its minimum value. It was hoped that this would minimize any redistribution of fluids within the sand pack during shut in. The time the model was shut in was minimized as much as possible. This did not appear to have a significant effect on the performance of the flood. When the flood was restarted the flow rates and water cuts continued from where they were prior to shut in.

The polymer solution is a shear thinning power law fluid. The apparent viscosity as a function of shear rate can be defined by the power law equation.

$$\mu_a = H\gamma^{n-1} \qquad (4.6)$$

The viscosity vs. shear rate data for the polymer solution presented in Figure 4.7 can be fitted to this equation using H=770.1 cP/s and n=0.5118, with R^2=0.998886. The shear rate experienced by the polymer solution as it flows through a porous media can be determined using the following equation by Littmann (1988):

$$\gamma = \frac{3n+1}{4n}\sqrt{2}\frac{1}{\sqrt{k\phi}}v \qquad (4.7)$$

Using equations 4.6 and 4.7 along with the viscosity vs. shear data in Figure 4.7, an estimate of the apparent viscosity during the flood can be made. If we consider the middle injector and assume that the amount of polymer injected is equivalent to the total fluids produced from the middle producer, the flow rate can be approximated at 30 cm^3/hr. Assuming radial flow from the well we can estimate the superficial velocity as a function of radius, using a semi-circle to account for the well being at the edge of the model, and in turn the apparent viscosity. This analysis was performed and it was found that at a radius of merely 1.65 cm from the well the shear was equal to the lowest measured value presented in Figure 4.7, 1.92 s^{-1}. Therefore, beyond this radius the viscosity of the polymer solution was estimated to be equal to or greater than the maximum measured value of 557cP. This increase in the aqueous phase viscosity by two orders of magnitude would serve to increase the capillary number of the displacement.

However, it would not be enough to reduce the residual oil saturation of the flood. It would result in an increase in the fractional flow of oil. Therefore the polymer flood would reduce the amount of liquid injected that is required to achieve residual oil saturation in the sand pack.

The high incremental recovery and drastic reduction in water cut obtained from the polymer flooding is a very promising result. However, it should be noted that the combined liquid flow rate was approximately five times lower than that observed in the water floods after breakthrough. This is due to the lost injectivity as a result of an increase in the viscosity of the injected liquid. The potential consequence of this reduced production rate is that it may offset any economic gains obtained by the improved ultimate recovery, due to a lengthy delay in the production of the additional oil. An economic analysis on the field scale will have to be performed to evaluate whether this is the case.

The polymer solution was also used for the eleventh production cycle. For this cycle, the middle injection well was shut in. The rest of the injectors and all of the producers were open. The cumulative production and water cuts are presented in Figure 4.10 and Figure 4.11. The flood lasted for almost thirty hours. The incremental recovery was a modest 3.22 % of OOIP. The water cut of the middle production well did decline to about 78 % indicating that some additional oil was being swept by the polymer due to the altering of the flow patterns.

Another two polymer floods were performed. They were performed by injecting and producing in opposite corners to flood across the diagonals of the model. The water cuts never went below 90 % during either flood and very little oil was produced.

The final production cycle performed was a nitrogen flood with all injectors and producers. Nitrogen broke through in less than an hour and very little oil was produced. The total oil produced over all the production cycles performed during Experiment #1 was 79.29 % of OOIP. The remaining oil saturation in the model was 18 %. This low oil

saturation is likely to be close to the residual oil saturation. The numerous displacement performed during Experiment #1 resulted in an ultimate recovery that is probably close to the theoretical limit. Figure 4.12 shows the oil production and water cut over the course of the entire experiment.

4.2 Experiment #2

Ambient Model #2 was used for the second experiment. The model was erected up on its 50 cm length so that the injection and production wells were horizontal with one row of three along the bottom and the other row along the top. As a result Figure 3.2 represents a side view of the model for this experiment. After being packed, flow tests indicated that the permeability of the sand pack was higher than that measured in the core holder. The permeability was estimated to be approximately 11 darcies. As mentioned in Chapter Three, the construction of Ambient Model #2 made it difficult to obtain a good sand pack. This is the reason for the higher permeability. The initial conditions after saturation are presented in Table 4.3.

Table 4.3: Conditions of Ambient Model #2 After Saturation, Experiment #2

Pore volume [cm^3]	3,214
Porosity [% p.v.]	0.43
Permeability [D]	11
OOIP [cm^3]	2,877
Initial Oil Saturation [%]	89.5
Oil Viscosity [cP]	3,517
Oil Density [g/cm^3]	0.972

The first production cycle performed on Ambient Model #2 was a 2 % brine flood. The brine was injected through the lower three wells and the top three wells were used as production wells. A constant pressure of 2 psi was applied to the vessel containing brine. As with Ambient Model #1 the producers were shut in as they reached a water cut of 90 %. Figure 4.13 and Figure 4.14 display the cumulative production and water cuts of the individual wells. The flood lasted almost twelve hours. The oil recovered was 21.5 % of

OOIP. This amounted to more than double the recovery in the first water flood performed in Experiment #1. The stability number was calculated to be 20.6 using the same assumptions used in Experiment #1. Although this calculated value does indicate an unstable displacement, it is considerably lower than the valued obtained from the first water flood in Experiment #1. This may explain the improved oil recovery. The lower viscosity of the oil used in Experiment #2 reduced the mobility ratio, therefore improving the stability of the flood. The reduced thickness of the Ambient Model #2 also serves to reduce the instability number. As well, the vertical nature of the flood may have improved the conditions for oil recovery. The capillary number calculated for the flood was 2.05×10^{-6}. Again, this indicates that the residual oil is not influence by excessive viscous forces.

For the second production cycle, the middle injector on the bottom was shut in and another brine flood was performed with all the production wells open. However, the water cut never went below 90 % and an insignificant amount of oil was produced.

The higher recovery in the first flood as well as the poor performance of the second flood indicates that the flood performed in the first production cycle provided a better sweep efficiency then the water floods in Experiment #1. This is most likely due to the gravity stable nature of the flood.

For the third production cycle nitrogen was injected into the model. The nitrogen was injected through the top three wells and the bottom three wells were used as producers. The nitrogen broke through quickly and very little oil was produced. This was followed by another nitrogen flood with middle injector at the top shut in. Again, the oil production was insignificant.

The gas floods performed in Experiment #1 and Experiment #2 are very similar to the gas floods performed by Islam *et al* (1994), especially the vertical floods performed on Ambient Model #2. The dimensions of the models are even similar except for the thickness. However, the recoveries in Experiment #1 and Experiment #2 were

substantially lower than the 70 % OOIP reported by Islam *et al* (1994). Even their unstable displacement recoveries were much higher than the negligible amount of oil that the floods performed on the Ambient Models yielded. Islam *et al* (1994) only reported results that were scaled up to field scale, so no direct comparison of breakthrough times can be made. The major difference between their experiments and the ones performed here is that water floods had been performed prior to the gas floods performed on the Ambient Models. Therefore, there was a high mobility channel of water from the injector well to the producer well that the gas could pass through very quickly. As well, the model used by Islam *et al* was much thinner than that of the Ambient Models (0.65 cm vs. 5.5 cm). The thickness of the Ambient Models allowed for viscous fingering to occur in two dimensions not just one.

Even though oil recoveries due to gas flood were insignificant in Experiment #1 and Experiment #2, water was produced. In order to estimate the volume of oil that would have been recovered if water floods were not performed prior to the gas floods, the volumes of all liquids recovered were combined. The oil recovery was calculated considering this total volume to be oil. The volumes would account for a recovery of 6.2 % OOIP for the first gas flood in Experiment #1 and 7.8 % of OOIP for the first gas flood of Experiment #2. This is in agreement with the findings of Islam *et al* (1994) for unstable displacements. It should be noted that the viscosity of water is significantly lower than the oil, and that this may lead to a larger volume of produced liquids. However, it is also possible that the produced liquid volumes for the gas floods performed on the Ambient Models would be even greater if there was not a high mobility channel of mobile water for the gas to shoot through.

The fifth production cycle was a 2 % brine flood. The bottom three wells were used as injectors and the top three were used as producers. Once again, very little oil was produced.

The next production cycle a flood with an aqueous polymer solution. The solution consisted of 5000 ppm of ALCOFLOOD 935 in water. The polymer solution was

injected into the model from the bottom through the bottom three wells. The fluids were produced through top three wells. As each producer reached a water cut of 90 % it was shut in. A constant pressure of 2 psi was applied to the polymer vessel containing polymer.

The flood lasted just over 50 hours. The incremental recovery obtained during the flood was 45.7 % of OOIP. The cumulative production and water cuts are presented in Figure 4.15 and Figure 4.16 respectively. As shown by Figure 4.16 the water cut declines significantly after about 6 hours. Again, the reducing the aqueous phase mobility appears to very effective in recovering the heavy oil.

The polymer flood was not performed continuously for the same reasons mentioned above for the polymer flood performed in Experiment #1. As with Experiment #1, the flood was not shut in until the polymer had broken through to the production wells.

The next production cycle was an additional polymer flood. The polymer was injected at the bottom of the model with the middle well shut in shut in. All three upper wells were opened as producers. The flood was allowed to proceed for about 20 hours. However, the water cut of the three producers never did drop below 90 %. The recovery from the flood was 2.85 % OOIP.

The final production cycle performed on Ambient Model #2 was a nitrogen flood. The nitrogen was injected in the top three wells and the bottom three wells were all used as producers. However, after about 15 minutes the nitrogen broke through at the producers and very little oil was produced. The total recovery from Experiment #2 was 72 % OOIP. Figure 4.17 presents the oil recovery and water cut over the entire course of the experiment.

4.3 Experiment #3

Reservoir Model #1 was used for Experiment #3. The model was saturated with a live oil as described in Chapter Three. The initial conditions after saturation are presented in Table 4.4. In order to describe the production results the four wells that are in the corners of the model have been numbered 1 to 4 in a clockwise manner, as shown in Figure 3.4.

Table 4.4: Conditions of Reservoir Model #1 After Saturation, Experiment #3

Pore volume [cm^3]	3,587
Porosity [% p.v.]	0.403
Permeability [D]	2.8
Internal Pressure [psig]	500
Overburden Pressure [psig]	600
Live Oil GOR [vol. gas/vol. Oil]	7.2
OOIP [$STcm^3$]	2,957
Initial Oil Saturation [%]	82.5
Dead Oil Viscosity [cP]	1,100
Dead Oil Density [g/cm^3]	0.964

Prior to any flooding, primary production was performed. This was done by reducing the set pressure of the back pressure regulator (BPR) connected to Well #1 from 500 psi to 200 psi. In the early stage of the depletion the flow was restricted by throttling the valve at Well #1. This was done to prevent the breaking of the glassware used to collect the produced liquids. Figure 4.18 shows the cumulative production of all fluids. Figure 4.19 displays the produced and cumulative GOR. Primary production lasted just over six hours and resulted in a recovery of 18.2 % of OOIP. As can be seen in Figure 4.19 the initial gas production was about three times the original solution gas ratio. This indicates that there may have been some initial free gas in the model. A gas bubble could have been passed from the live oil generation apparatus to the model during saturation.

As with the experiments performed on the Ambient Models, the experiments performed on the Reservoir Models are not scaled. So, the above result does not imply 18.2 % of OOIP can be produced at the field scale with this type of oil.

The second production cycle was a brine flood. The brine consisted of 2 % NaCl in distilled water. Well #1 was the producer and Well #3 in the opposite corner of the model was the injector. The outlet pressure at the producer well was maintained at 200 psi by the BPR. The brine was injected into the model as described in Chapter Three at a constant rate of 10 cm^3/hr. As with the Ambient Models, the criteria for ending the production cycle was a 90 % water cut.

The flood lasted just over 150 hrs and resulted in an incremental recovery of 10.8 % OOIP. The brine broke though at the producer after about 20 hours. The cumulative production is presented in Figure 4.20. The water cut and GOR are presented in Figure 4.21. The presence of solution gases result in the reduction of the viscosity of the oil. This reduced viscosity must be estimated in order to calculate the stability number. A correlation from Butler (1991) for determining viscosity of heavy oils and bitumens as a function of pressure was used for an approximation of the oil viscosity. The effects of gas solubility are accounted for in the equation which is as follows:

$$\mu = \exp\left[\frac{\ln \mu_o \exp[0.00511938(P - .01)}{1 + 0.0093\, P \exp(343/T)}\right] \quad (4.8) \quad \text{(Butler, 1991)}$$

Where μ_o is the dead oil viscosity in cP at atmospheric pressure, P is the pressure in Mpa and T is the temperature in Kelvins. The estimated oil viscosity at the depleted model pressure of 250 psi (1.73 MPa) was 936 cP. Since the flood was performed across the diagonal of the model, the width of flowing cross sectional area varies along the path of the flood. In order to calculate the stability number a width must be chosen. If the width at the widest point (42.4 cm), mid-way along the flood path is used, a stability number of 20.3 is obtained. If a width of 5 cm is used, which would represent the situation closer to the injection or production well, a stability number of 4.3 is obtained. This latter value is less than π^2, and indicates that the flood may be stable close to the wells. However, it should be noted that most estimated parameters, such as the ratio of end point relative permeabilities, were made in favour of stability, so the calculated value of the stability

number is artificially low. Therefore, the flood may not be stable, near the wells. The capillary number of the flood was calculated to be 3.06×10^{-7}.

The next production cycle was another brine flood. The injector and producer positions were switched from the previous flood so that Well #1 was the injector and Well #3 was the producer. The flood lasted for almost 95 hours and resulted in an incremental recovery of 4.4 % OOIP. Figure 4.22 and Figure 4.23 display the cumulative production, water cut and GOR. It can be seen that the water cut did decrease during the first 25 hours resulting in increased recovery before the water cut began to increase.

The fourth production cycle was another brine flood. Well #4 was the injector and Well #2 was the producer. The flood lasted almost 55 hours and resulted in a recovery of 2.2 % OOIP.

A brine flood was again used for the fifth production cycle. The flow was reversed from the previous flood with Well #2 as the injector and Well #4 as the producer. The duration of the flood was almost 90 hours with a recovery of 3.4 % OOIP.

The brine floods performed on Reservoir Model #1 to this point were performed discontinuously. The 100 cm^3 glassware used for collecting the produced fluids were only large enough to collect liquids for about 5 to 6 hours due to the foaming of the oil. As a result it was necessary to shut in the model overnight. After the water floods larger glassware that could be attached to the BPR was obtained so that the remainder of the floods performed on the Reservoir Models could be performed continuously.

The sixth production cycle was a nitrogen flood with Well #2 as the injector and Well #4 as the producer. The nitrogen was fed to the injector directly from the compressed nitrogen cylinder at a constant pressure of 220 psi, so that there was a 20 psi pressure drop in across the sand pack. The nitrogen broke through at the producer after about half an hour. The production cycle was stopped after about 40 minutes when only gas was essentially being produced. No substantial amount of oil was produced. The failure of

the gas flood in this experiment as well as the experiments performed on the Ambient Models indicate that gas flooding may not be a suitable tertiary recovery technique to be performed after water flooding. The large difference in the mobility of the gas to that of the oil coupled with the presence of a high mobility channel caused by water flooding appear to adversely affect the stability of the displacement. Perhaps at lower flow rates (smaller pressure drops) the floods would be more stable and more successful. The pressure drops used in these experiments were the lowest possible that could be used with the equipment available.

This was followed by an aqueous polymer flood. The solution consisted of 5000 ppm of ALCOFLOOD 935 mixed in brine (2 % NaCl). Viscosity measurements performed on the polymer mixed in brine showed that the viscosity was approximately an order of magnitude less than polymer mixed in fresh water at any given shear rate. Accurate measurement of the polymer solution viscosity could not be made because the measured value was a very low percentage of full scale at each shear rate. The reduced viscosity is to be expected since polyacrylamide is a salt sensitive polymer (Littman, 1988; Mungan, 1972). Moreover, it is suspected that polymer adsorption increases with salt concentration (Smith, 1970). Therefore, it was hoped that the mobility of the aqueous phase would be reduced enough to recover significant incremental oil. Well #2 was the injector and well #4 was the producer. The flood lasted just over 250 hours and produced 7 % of OOIP. The cumulative production and water cut are shown in Figure 4.24 and Figure 4.25. This significant production is mainly a result of the long duration of the flood. The water cut was essentially above 90 % for the entire flood. So, unlike the floods performed on the Ambient Models using polymer mixed in fresh water, no oil bank was formed. The polymer seems to have been rendered ineffective by the brine.

To determine if the poor performance of the polymer flood was due to the salinity of the polymer solution, a flood with polymer mixed in fresh water was performed. Well #2 was the injector and well #4 was the producer. The polymer solution was injected at a constant rate of 10 cm^3/hr. The flood lasted almost 350 hours and resulted in an incremental recovery of 24.9 % OOIP. The cumulative production and the water cut and

GOR of the flood are presented in Figure 4.26 and Figure 4.27. As can be seen from Figure 4.27, after about 150 hours the water cut begins to drop significantly. The high oil recovery obtained this flood indicates that the brine used to make the polymer solution in the previous flood did indeed adversely affects the performance of the polymer.

The total recovery from recovery from Experiment #3 was 70.9 % OOIP. The cumulative recovery along with the water cut and the GOR over the duration of the experiment are presented in Figure 4.28 and Figure 4.29.

4.4 Experiment #4

Reservoir Model #2 was used for Experiment #4. The model was also saturated at an internal pressure of 500 psi. The GOR of the live oil was 11.5. During the saturation of the model, a pocket of methane that was used for mixing the live oil was inadvertently injected into the model. Even though, the live oil generation apparatus was checked to ensure it was not emptied out after the live oil was transferred to the piston cylinder for injection into the model, some gas bubbles must have been transferred with the live oil. This resulted in an initial gas cap being present prior to production. Although unintentional, useful information can still be gained from this experiment, since gas caps are often encountered in the field. A complete list of the initial conditions is presented in Table 4.5. There was some question about the initial amounts of gas and oil in the model due to presence of gas in the piston cylinder. After the experiment was completed, three core samples were taken from the sand pack. Dean Stark analysis was performed on the samples to determine the oil saturation in the sand pack after the experiment. The saturations obtained from the three samples were averaged to estimate the total amount of oil remaining in the model after the experiment. This was added to the total oil production to estimate the initial oil saturation and subsequently the initial gas saturation.

Table 4.5: Conditions of Reservoir Model #2 After Saturation, Experiment #4

Pore volume [cm^3]	3,559
Porosity [% p.v.]	0.398
Permeability [D]	2.8
Internal Pressure [psig]	500
Overburden Pressure [psig]	600
Live Oil GOR [vol. Oil/vol. Gas]	11.5
OOIP [$STcm^3$]	2,498
Initial Oil Saturation [%]	70
Initial Gas Saturation [%]	7.5
Initial Water Saturation [%]	22.5
Dead Oil Viscosity [cP]	1250
Dead Oil Density [g/cm^3]	0.96

Primary production was performed on Reservoir Model #2, depleting the internal pressure to 200 psi. The production was performed from Well #1 and resulted in the recovery of 12.6 % OOIP. There was water production during the depletion, indicating that a mobile water zone near the producer was present after saturation. Due to the geometry of the models it is not always possible to obtain perfect saturations. The cumulative production of all fluids is presented in Figure 4.30. The water cut and the GOR are shown in Figure 4.31. The smaller recovery obtained for the primary production performed on Reservoir Model #2 as compared to Reservoir Model #1 can likely be attributed to the presence of mobile water initially in the model. The combined volume of oil and water produced would amount to 20.7 % of OOIP if the entire volume were oil. However, the production would likely not be that high if it were entirely oil due to larger viscosity of the oil as compared to the water. The initial free gas saturation may also have contributed to the reduced recovery. The presence of a high gas saturation zone, likely at the top of the model was much more mobile than the oil. The larger amount of gas produced indicates that this mobile gas was produced. Since the wells were perforated over the entire thickness of the sand pack this gas would have been produced before it could have enhanced production by any gas cap drive effects. Even if the wells were only perforated at the bottom of the sand pack, the large pressure gradient (300 psi over a 10 cm thick sand pack) would likely have led to the gas fingering or

coning to the well before it could enhance production. Figure 4.32 shows that when the gas production leveled off after about 2 hours, so did the oil production. This indicates that the production of the mobile gas depleted much of the internal energy in the model. In the case of the primary production performed on Reservoir Model #1 the absence of an initial mobile gas phase along with the possible low mobility of gas due to foamy oil effects could have resulted in the higher oil recovery due to better pressure maintenance.

Primary production was followed by a water flood. Brine was injected into well #2 and well #1 as the producer. The flood was performed at a constant injection rate of 10 cm^3/hr. The recovery was 21.5 % OOIP. This recovery is considerably higher than any water flood performed on Reservoir Model #1. However, the combined recovery of the first water flood along with primary production was only recovered an additional 4 % of OOIP than the combined primary and first water flood of Reservoir Model #1. Figure 4.32 displays the cumulative production. The water cut and GOR are presented in Figure 4.33. Since the dimensions of the model are the same as Reservoir Model #1 and the same injection rate was used, the calculated values of the stability number were the same. The capillary number was calculated to be 5.02×10^{-6}.

This water flood was followed by an additional water flood in the reverse direction. The resulting recovery was 16.1 % OOIP. The cumulative production, water cut and GOR are shown in Figure 4.34 and Figure 4.35. An additional water flood was performed with Well #3 as the injector and Well #2 as the producer. Less than 2 % OOIP was recovered.

The significant recovery obtained by simply reversing the flood direction observed with Reservoir Model #2, and to a lesser extent Reservoir Model #1, is very interesting. Viscous fingering may offer a possible explanation for this observation. If fingering does occur during the initial water flood, water would channel through any finger that reaches the production well, leaving unswept areas around the production well. Once this well is converted to an injector, this region would be swept. Since viscous fingering is more severe in water flooding of heavy oil than conventional oil, this effect would be more prevalent in the case of heavy oil.

After water flooding was performed on Reservoir Model #2, a polymer slug was injected into the model that was chased with brine. A 27 % pore volume slug of 5000 ppm polymer in fresh water was injected into Well #1. This was chased by 2 % NaCl brine. Well #2 was the producer. The injection rate of the polymer and the brine was 10 cm^3/hr. After about 280 hours only 4.7 % of OOIP had been produced. The water cut did not decline at all. This is a poor recovery when compared to the 24.7 % OOIP obtained by polymer flooding in Experiment #3, and is believed to be a result of the instability of the slug of polymer. It is likely that the brine fingered through the polymer slug to the production well. To confirm this, a continuous polymer flood was performed with Well # 1 as the injector and Well #2 as the producer. The cumulative production is presented in Figure 4.36. The water cut, as shown in Figure 4.37, did decline during this flood. The flood lasted for approximately 370 hours and recovered 21.6 % OOIP.

Due to the unscaled nature of the experiment, the failure of the polymer slug chased with brined does not imply that this strategy would be unsuccessful. Using a polymer slug would be the only economically feasible manner to perform a polymer flood in the field. Tapering down the polymer concentration of the polymer slug prior to injecting brine may improve the stability of the brine/polymer displacement front. As well, optimization of the slug size may make the technique successful.

The ultimate recovery from Reservoir Model #2 during Experiment #4 was 77.5 %. The cumulative production, water cut and GOR over the duration of the experiment are presented in Figure 4.38 and Figure 4.39.

4.5 Experiment #5

Experiment #5 was performed using Ambient Model #2. The experiments were performed with the model lying flat so that the injector and producer wells were vertical, as was the case in Experiment #1. Visualization of the experiment was performed using

the gamma camera system described in Chapter Three. The initial conditions of the model after saturation are presented in Table 4.6.

Table 4.6: Conditions of Ambient Model #2 After Saturation, Experiment #5

Pore volume [cm^3]	3,214
Porosity [% p.v.]	0.43
Permeability [D]	6.4
OOIP [$STcm^3$]	2,996
Initial Oil Saturation [%]	93
Oil Viscosity [cP]	3,840
Density [g/cm^3]	0.9687

The first production cycle performed on Ambient Model #2 was a water flood with 2 % brine tagged with ^{99m}Tc. The amount of activity contained in the ^{99m}Tc was measured by acquiring an image of the sample prior to adding to the brine. The sample, which was no more than 2 cm^3, was then added to 3.5 litres of brine. For the first flood, one row of three wells were used as injectors and the other row of three was used as the producers so that the flood was performed in a line drive configuration as with the previous experiments. The flood was performed with a constant pressure of 2 psi applied to the vessel containing brine. Once again the criteria for shutting in the flood was a water cut of 90 %. The flood lasted just over 5 hours and resulted in a recovery of 16.3 % OOIP. Figure 4.40 and Figure 4.41 present the cumulative production and water cut for the flood respectively. A stability number of 128.3 was calculated for the flood indicating an unstable displacement. The capillary number was 2.86×10^{-6}.

Images were taken with the gamma camera throughout the flood. For each image taken the camera was allowed to measure counts for one minute.

The images show what areas of the model have been swept by the aqueous phase. This qualitative information is very useful. It was hoped that quantitative information, in the form of saturations, could be obtained as well. To do this a similar method to the one

used by Huang and Gryte (1988) was used. First the data from the image was corrected for decay back to the starting time of the flood. This was done with equation 4.9.

$$a_0 = a \cdot e^{\lambda t} \qquad (4.9)$$

Where t is the time in seconds from the start of the flood, λ is the time constant which is equal to 3.188 x 10^{-5} 1/s for ^{99m}Tc, a is the counts measured counts for a specific pixel and a_0 is the counts for the same pixel corrected back to the start of the flood.

A sand pack of the same thickness as that in the model was packed in a beaker saturated 100 % with brine tagged with ^{99m}Tc. An image was taken to obtain a baseline for the amount of activity for 100 % brine saturation. The saturation for each pixel was then determined with equation 4.10.

$$S_w = \left(\frac{a_0 / C}{a_b / C_b} \right) \qquad (4.10)$$

Where S_w is the calculated average water saturation over the thickness of the sand pack for the pixel, C is the concentration of activity used for the flood, a_b is the counts measured from the 100 % brine saturated baseline and C_b is the concentration of activity used for the baseline. Once the saturation for each pixel is determined, the amount of oil produced from the model can be calculated by determining the increase in water saturation from connate water saturation and multiplying it by the pore volume in each pixel. The total oil produced from all pixels can be compared to the actual oil produced to evaluate the accuracy of the saturations calculated. As well, the area of the sand pack that is swept can be calculated.

Figure 4.42 shows an image of Ambient Model #2 at the completion of the first water flood. The three injectors are along the bottom of the image while the producers are along the top. It can be seen from this image that channeling played a major role in this displacement. The coloured areas indicated areas where the brine has flowed in the sand pack and the black and white areas are where no counts where measured. There are three

"lobes" of water swept areas. The areas between these "lobes" are unswept and indicates that the three injector/producer pairs are not in communication with each other. The dark spot in the middle lobe is due to a bolt on the surface of the model that attenuates some of the radiation. The image shows the flow seemed to be more linear in nature than radial. This behaviour contributes to the poor sweep and low recovery of the water flood.

This image also displays the saturations as calculated by the method described above. There is an obvious problem with the saturations obtained. Some pixels have saturations higher than 100 %, the highest being 126 %. This is clearly impossible. It is possible that an error was made in measuring the amount of activity used for the flood as well as for measuring the baseline. The method of using the camera to measure the activity may not be accurate enough. As well, scattering of the radiation in the sand pack may have contributed to this erroneous result. It may also be possible that the ^{99m}Tc may have adsorbed to the sand pack and that in some areas of the pack radioactive counts could have accumulated. Small differences in the porosity of the baseline sand pack and the sand pack in the model may have also contributed to the error in the calculated saturations. An attempt was made to fit the image data to the mass balance. This was done by increasing the value of the number of counts at 100 % water saturation, a_b, until the saturation map obtained corresponded with the amount of oil produced during the flood. However, saturations above 100 % were still obtained. Clearly more work needs to be done to work out the "bugs" of obtaining saturations from the image. The calculated areal sweep efficiency for the first water flood was 43 %.

An image of Ambient Model #2 was taken from the side after the flood was complete. Activity was observed over the entire thickness of the sand pack indicating that gravity underride of the brine did not occur. As well, images were taken a day after the flood had been shut in and no redistribution of the fluids in the sand pack was observed.

The second production cycle was another water flood. For this flood the middle injector was shut in. The brine tagged with ^{99m}Tc and images were taken during the flood. Again

a 2 psi constant pressure was applied to the vessel containing brine. The flood lasted 4 hours and yielded an incremental recovery of 4.6 % OOIP. The cumulative production and water cut are presented in Figure 4.43 and Figure 4.44. Initially all producers produced at a high rate and a high water cut. Almost one hour into the flood the right and left producer were shut in. After this the water cut of the middle producer dropped. Figure 4.45 shows an image of the sand pack at the completion of the flood. The values associated with each pixel in this image are the counts acquired during imaging. In the image the radioactivity from the first flood has decayed and is not visible. As a result the area in the middle of the image appears to not have any brine. The brine from the first flood is likely still there, it is just not visible. It can be seen that some of the previously unswept regions are now swept. The left and right lobes are much larger and cover areas that were not covered in the previous flood (see Figure 4.42).

After the water floods a polymer flood (5000 ppm ALCOFLOOD 935) was performed on Ambient Model #2. As with the water floods the polymer solution was tagged with ^{99m}Tc. The flood lasted almost 50 hours with a constant pressure drive of 2 psi. The cumulative production and water cut are shown in Figure 4.46 and Figure 4.47. The incremental recovery from the flood was 38 % OOIP. As can be seen from Figure 4.47 the water cut drops substantially after about 4.5 hours. This behaviour is consistent with the earlier experiments performed on the Ambient Models.

Due to the length and radioactive nature of the flood it was not possible to run the flood continuously. Once the radioactive polymer was almost all injected the flood was shut down. It was then necessary to allow the radioactivity to decay for a couple of days before any of the equipment, such as glassware could be cleaned and reused. The flood was then restarted using polymer that was not radioactive. As a result, it was only possible to obtain images during the first day of the flood. The flood was first shut in after 16 hours. Figure 4.48 shows an image of the model at 4.5 hours into the flood. This is about the same time when the water cut began to decline drastically. It can be seen that the polymer solution has only proceeded a short distance from the injector wells. As well, it should be noted that the area swept by the polymer at this point has not exceeded

any area that has not been previously swept in the previous water floods as shown in Figure 4.42 and 4.45. Therefore the reduction in water cut that occurs at the time this image was taken is not a result of improved sweep efficiency over the water floods, but is a result of additional oil being mobilized from these previously swept zones. The improved mobility ratio of the polymer flood as compared to the water flood has resulted in an increase in the fractional flow of oil in the previously swept zones.

The additional oil mobilized by the polymer could have collected in front of the polymer front forming an oil bank. Once this oil bank reached the production wells, the water cut would decline as was observed during the polymer floods. Another possible explanation is that the high viscosity of the polymer reduced the volume of aqueous phase required to displace the oil. During the water floods, the water channeled through to the production wells creating highly water saturated pathways. Once these pathways were established, water flowed through the pathways at a very high rate. Large volumes of water were required to displace much smaller volumes of oil. This resulted in a high water cut. Once polymer was injected into the model it entered the highly water saturated pathways displacing water and oil from these pathways. Due to the reduced mobility of the polymer, the flow rate of the aqueous phase through the pathways was greatly reduced. The reduction in the volume of the aqueous phase passing through the model would result in a reduction of the water cut as was observed.

The ultimate recovery from Ambient Model #2 in this experiment was 58.9 % of the OOIP. Figure 4.49 present the cumulative recovery and the water cut over the entire course of the experiment.

4.6 Experiment #6

Ambient Model #1 was used for Experiment #6. Again, the model was laid down flat so that the injection wells and the production wells were vertical. As with Experiment #5, the gamma camera system was used to visualize the experiment. The initial conditions of the model are presented in Table 4.7.

Table 4.7: Conditions of Ambient Model #1 After Saturation, Experiment #6

Pore volume [cm^3]	6,653
Porosity [% p.v.]	0.42
Permeability [D]	6.4
OOIP [$STcm^3$]	6,379
Initial Oil Saturation [%]	95
Oil Viscosity [cP]	623
Oil Density [g/cm^3]	0.9579

The oil used in this experiment had considerably lower viscosity than the oils used in the other experiments. The oil came from the same field as the oil used with Reservoir Models in Experiments #3, #4, #8 , and #9. It may have been taken from a different location in the field and as a result had different properties.

The first production cycle performed on Ambient Model #1 was a water flood using 2 % brine tagged with ^{99m}Tc. Due to the lower viscosity of the oil the flood was operated with a reduced constant pressure of 0.8 psi applied to the vessel containing brine. The flood lasted 2 hours and yielded a recovery of 17 % OOIP. The cumulative production and water cut are presented in Figure 4.50 and Figure 4.51. The water cut at the end of the flood was about 80 %. The flood was shut off at this point because almost all of the brine in the vessel had been injected into the model and all the glassware had been used collecting the produced fluids. Due to the radioactive nature of the effluent the glassware with the effluent had to be set aside to decay and could not be cleaned and reused right away. The calculated stability number of the flood was 275.8. The capillary number was calculated to be 1.49×10^{-5} which is higher than a typical water flood but not high enough to cause a reduction in the residual oil saturation.

Images were taken throughout the flood. As with Ambient Model #2, an attempt was made to determine saturations from the images. The procedure that was described previously was used. Figure 4.52 shows the saturations for the model calculated from an image taken at the end of the flood. All calculated saturations were well below 100 %.

However, when the amount of oil produced from the model was calculated from the change in saturations, a substantially lower value than the actual produced oil is obtained. So again it appears more work is needed before quantitative information can be determined from the images. Comparing Figure 4.52 with the image of the first water flood performed in Experiment #5 (Figure 4.42) we can see that the areal sweep is better than that observed in Experiment #5. The calculated value of the areal sweep efficiency from the image of the model is 50 %. The better sweep is likely due to the lower viscosity of the oil used in this experiment. The mobility ratio of the oil and the aqueous phase was more favourable. We would expect there to be higher oil saturations in the swept zones of Ambient Model #1 than we had for the initial water flood of Ambient Model #2. This is due to the fact that they both produced very similar percentages of OOIP even though there was a greater areal sweep of Ambient Model #1. However, if the flood of Ambient Model #1 was allowed to proceed to 90 % water cut as it was with Ambient Model #2 it would be likely that the saturations in the swept zones would be similar.

The water flood was followed by a polymer flood. The polymer used was Allied Colloids' ALCOFLOOD 1275A. This polymer is a higher molecular weight polymer (18 - 22 million) than ALCOFLOOD 935 (6 - 9 million) that had been used in the previous polymer floods. For this flood 5000 ppm of the polymer was mixed in 2 % NaCl brine. The viscosity vs. shear relation for ALCOFLOOD 1275A in brine is shown in Figure 4.53 along with similar data for ALCOFLOOD 935 in fresh water. It can be seen that for a given rate of shear the viscosity of ALCOFLOOD 1275A in brine is approximately two thirds that of ALCOFLOOD 935 in fresh water. This indicated that ALCOFLOOD 1275A would be a good candidate to be used with brine since the viscosity of ALCOFLOOD 935 mixed in brine was at least an order of magnitude less than ALCOFLOOD 935 mixed in fresh water.

Three injectors and three producers were used for the polymer flood. The polymer was tagged with ^{99m}Tc and was injected with a constant pressure of 0.8 psi applied to the polymer containing vessel. The flood lasted just over 20 hours and resulted in an

incremental recovery of 46.1 % of OOIP. The flood was not run continuously. The vessel containing the polymer could hold 3.8 litres of polymer. This volume was injected before the water cut reached 90 %. Due to the radioactive nature of the experiment it was necessary to allow the radioactivity to decay for a couple of days before glassware and other equipment could be cleaned and reused. The cumulative production and water cut vs. time are presented in Figure 4.54 and Figure 4.55 respectively. It can be seen from Figure 4.55 that the water cut declined sharply almost immediately and then slowly recovers to 90 %. The "spike" in the water cut seen at about 6 hours occurred when the flood was restarted after stopping it for the reasons stated above. Smaller spikes in the water cut are observed at times of the other stoppages. It is possible that this is due to the oil and water segregating during the shut in periods.

The sharp decline of the water cut is consistent with results from previous polymer floods performed on Ambient Models with ALCOFLOOD 935 in fresh water. This indicates that ALCOFLOOD 1275A was effective even when mixed in brine. However, it should be noted that the oil in this experiment had a lower viscosity than the oils used in the other experiments and further work needs to be done to determine the effectiveness of ALCOFLOOD 1275A with brine on higher viscosity oils.

Due to the reasons similar to those mentioned for Experiment #5, it was only possible to obtain images in the early stages of the flood. Figure 4.56 shows an image of the Ambient Model#1 at 5 hours into the flood when the water cut has reached its lowest value. When compared with an image of Ambient Model#1 after the first water flood (Figure 4.52) it can be seen that the polymer only occupies areas of the sand pack that had been previously swept in the first flood. As seen with the floods performed in Experiment #5 this indicates that the polymer mobilizes oil from previously swept zones and does not only improve sweep efficiency.

The total recovery from Ambient Model #1 during Experiment #6 was 63.1 % of OOIP. Figure 4.57 shows the cumulative production and water cut over the entire course of the experiment.

4.7 Experiment #7

The Aluminum Core Holder was used for Experiment #7. The X-ray CT scanner was used for visualization of the experiment. As mentioned in Chapter Three, the core was scanned every 5 mm along its length with the CT scanner prior to being saturated with oil. These scans at 100 % brine saturation were later used for calculating the local oil saturations during the floods. In order to increase the contrast in CT number between the oil and water phase it was necessary to dope one of the phases. Since doping of the aqueous phase may adversely affect the properties of the polymer solutions it was decided to dope the oil phase. The oil used in this experiment was a heavy oil with a viscosity of 40,000 cP. This oil was doped with approximately 15 % 1-iodododecane. The resulting mixture had a viscosity of 6275 cP and a CT number of 512, which is high enough to be distinguished from the aqueous phase. The 1-iodododecane also caused the density of the oil to be increased to 1.008 g/cm^3. The conditions of the core holder after saturation are presented below in Table 4.8.

Table 4.8: Conditions of Aluminum Core Holder After Saturation, Experiment #7

Pore volume [cm^3]	695
Porosity [% p.v.]	.40
Permeability [D]	2.3
OOIP [STcm^3]	500
Initial Oil Saturation [%]	72
Oil Viscosity [cP]	6,275
Oil Density [g/cm^3]	1.008
Overburden Pressure [psi]	600

After being saturated the core was once again scanned every 5 mm. Since the CT number is a linear function of saturation (Kantzas *et al*, 1990), we can determine the CT number for each slice at 100 % oil saturation. This information is used to estimate the saturations during the floods. The average saturation of a slice can be estimated using equation 4.11.

$$S_o = \frac{CT_{measured} - CT_{100\% brine}}{CT_{100\% oil} - CT_{100\% brine}} \qquad (4.11)$$

The CT number at 100 % oil saturation ($CT_{100\%\ oil}$) can be estimated for each slice, assuming that for each slice it is a greater than the CT number at 100 % brine saturation ($CT_{100\%brine}$) by a constant value.

$$CT^{i}_{100\%oil} = CT^{i}_{100\%brine} + b \qquad (4.12)$$

Where $CT^{i}_{100\%oil}$ is the CT number for slice i at 100 % oil saturation, $CT^{i}_{100\%brine}$ is the CT number for slice i at 100 % brine saturation, and b is a constant for all slices. Using the scans after saturation and the scans of the core saturated 100 % with brine, a value of b was determined so that the calculated average saturations correspond with the amount of oil in the core that was known from the mass balance performed after it was saturated.

The first production cycle performed on the Aluminum Core Holder was a water flood with 2 % NaCl brine. The brine was injected at a constant pressure of 15 psi. This higher injection pressure, when compared to the other constant pressure floods, was required in order to instigate flow in the core. The higher viscosity of the oil and the low permeability of the sand necessitated the higher pressure. The flood lasted 12.5 hours and resulted in a recovery of 11.4 % OOIP. The cumulative production and water cut are presented in Figure 4.58 and Figure 4.59 respectively. A stability number of 116.8, calculated for the flood indicated an unstable displacement. The capillary number was calculated to be 1.25×10^{-6}.

The second production cycle was a flood with 5000 ppm of ALCOFLOOD 935 mixed in fresh water. This flood lasted 20 hours and resulted in an incremental recovery of 41.2 % of OOIP. The cumulative production and water cut are presented in Figure 4.60 and Figure 4.61 respectively. As can be seen in Figure 4.61, the water cut declines almost immediately until about 7 hours into the flood, then it increases until the end of the flood. However, the water cut does not decline as steeply as it did with the two dimensional models. This is because no improvement in the areal sweep efficiency due to improved mobility ratio is realized in the one dimensional core flood. Improved fractional flow of oil and a reduction in viscous fingering would have contributed to the reduction in water cut in this case.

The polymer flood was performed with the core holder in the CT scanner gantry. Five positions along the length of the core were selected, 10 mm from the injection plate, 75 mm, 140 mm, 205 mm, 270 mm. During the course of the flood these positions were scanned repeatedly. From these scans it was possible to determine the average saturation of the core at these positions during the course of the flood. This was possible by determining the average CT number of the scans and calculating the average saturation of the slice by linearly interpolation, using the average CT numbers for that same slice at 100 % brine saturation and 100 % oil saturation. It was also necessary to use a mass balance to account for any energy drift that may have occurred. The scans gave saturations at each of the five positions as a function of time. Therefore, it was possible to monitor how the oil was being displaced by the polymer. Figure 4.62 presents the saturations of each of the five positions as a function of time. The saturations in Figure 4.62 are normalized to the initial value prior to the polymer flood. This allows for better comparison, since all the slices started with different saturations due to the water flood that was performed prior to the polymer flood. It should be noted that the actual initial saturation for the measured first position (10 mm) prior to the polymer flood was 0.57. This value was higher than the other four positions. This indicates that the water flood performed on the core may have been subject to end effects. The injected fluid enters the core through a port located at the centre of the endplate. As a result, the injected water only flowed through the centre of the sand pack near the injection end of the core holder before the flow could become fully distributed over the cross sectional area of the sand pack. Therefore, the sweep near the injection end endplate may have been poor. The initial oil saturations for the other four positions followed the expected pattern, with the lowest oil saturation (0.49) occurring at the second position of 75 mm and then increasing along the length of the core to the last position of 270 mm with an oil saturation of 0.55.

It can be seen from Figure 4.62 that the saturation declines right from the start of the flood at 10 mm, 75 mm and 140 mm from the injection plate. Aside from the position at 10 mm where the end effects occurred, these are the areas that would have experienced the most sweep from the initial water flood. So again the improved mobility ratio of the

displacement has resulted in additional oil being swept out of these previously swept regions with the polymer. Farther away from the injection plate the saturation maintains its value before it declines later in the flood. However, the water cut in the produced fluids declines right from the start of the flood. There is no significant increase in oil saturation at any position along the core. This indicates that an oil bank is not being formed. It is more likely that the polymer solution is displacing both the oil and water in the core, but due to the reduced mobility of the polymer solution the volume of the aqueous phase passing through the core has been greatly reduced. As well, it is likely that the oil being mobilized near the injection end of the core moves to the perimeter of the core where the oil saturation is higher and therefore the relative permeability is higher. Since the residual oil from water flooding for heavy oil is in the form of a continuous region of bypassed oil, the oil can be mobilized through this continuous region of high saturation and higher relative permeability to the production end of the core. This explanation can also be applied to the Ambient Model experiments were imaging showed that initial water flooding left large areas of bypassed oil. Subsequent polymer flooding resulted in a drastic decline in the water cut even though the polymer had only progressed a short distance from the injection wells.

Figure 4.63 shows an example of the scans taken during the polymer flood. The images are saturation maps taken at 75 mm from the injection end of the core. This is the position where the most change was seen. The image at the top left was taken at the beginning of the flood. The images are in chronological order (from left to right, top to bottom) with the end of the flood being represented by the image at the bottom right. The darker blue regions represent higher saturation of the aqueous phase. It can be seen that darker regions begin to appear as small dots that grow as the flood progress. This would indicate that viscous fingering is occurring. The images at the other four positions did not show as much of a change as time progressed. Scans of a conventional oil water flood where fingering did not occur would show a sudden change from low water saturation to high water saturation. The cross sectional image would appear like the first scan in Figure 4.63 and then very quickly appear like the last scan in Figure 4.63.

The total recovery from the Aluminum Core Holder in Experiment #7 was 52.6 % of OOIP. Figure 4.64 shows the cumulative oil production and the water cut over the duration of the experiment. The total recovery for Experiment #7 is significantly lower than the previously described experiments. End effects present in the core floods may have contributed to this. As well, the higher viscosity of the oil and the lower permeability of the sand would likely lead to a reduced recovery.

4.8 Experiment #8

Reservoir Model #1 was used for Experiment #8. The well designed for sand production was installed as Well #1 for this experiment. The model was wet packed and saturated in the same manner as previously described in the other experiments performed with the Reservoir Models. However, water was not drained from the well designed for sand production as the perforation was kept closed for saturating. As well, prior to injecting the live oil into the model, the piston cylinder was over pressured and a sample was drawn off the top to ensure there was no free gas in the cylinder. The initial conditions of the model after saturation are presented in Table 4.9.

Table 4.9: Conditions of Reservoir Model #1 After Saturation, Experiment #8

Pore volume [cm^3]	3,553
Porosity [% p.v.]	0.39
Permeability [D]	4.4
Internal Pressure [psig]	500
Overburden Pressure [psig]	600
Live Oil GOR [vol. Gas/vol. oil]	12.6
OOIP [$STcm^3$]	2,883
Initial Oil Saturation [%]	81.0
Dead Oil Viscosity [cP]	1,250
Dead Oil Density [g/cm^3]	0.96

Primary production with sand production was the first production cycle performed on Reservoir Model#1. As mentioned in Chapter Three, the model was blown down to atmospheric pressure. Fluids and sand were collected in stainless steel vessels. The pressure declined to atmospheric pressure from 500 psi in about 2 hours. The majority of

production occurred in the first 2 minutes of production. It is believed that the rate of gas production during the first moments of the depletion exceeded the capacity of the wet test metre. This is because the total amount of gas produced during the blow down (25.14 litres) was less than the amount of total amount of gas in solution believed to be initially in the model (36.3 litres). As a result, the measured gas production is lower than the amount actually produced.

Early in the depletion the overburden punctured through the viton bladder. However, the volume between the lid and the bladder is very small and it is believed that the very small amount of nitrogen that may have invaded the sand pack would not have had much of an effect on the production. Prior to subsequent flooding the lid was removed and the hole in the bladder was sealed with silicon. There was some subsidence of the sand pack. Above the bladder, any subsidence was filled in with wax to ensure the bladder would not rise apart from the sand during flooding.

Four vessels were used to collect the produced solids and fluids. The vessels were weighed prior to removing any of the contents. Dichloromethane was used to separate the sand from the liquids. The water was decanted off and the dichloromethane was allowed to evaporate from oil phase so that the volumes could be determined. Evaporation of the dichloromethane from the oil required at least three weeks. A mass balance performed after the evaporation showed that there was approximately 10 % loss of the total mass. A test where a known amount of oil was diluted with dichloromethane and then allowed to evaporate showed that some of the oil, likely the light ends, did indeed evaporate with the dichloromethane. The amount that evaporated was close to the 10 % that was lost from the produced samples. As a result, the lost mass was attributed to the oil phase.

The resulting oil recovery from primary production was 23.9 % OOIP. As well, 10.6 % of the original sand in place was produced. Figure 4.65 shows the cumulative production during the first 2 minutes. It should be noted that a significant amount of water was produced indicating the presence of mobile water in the model after saturation.

The second production cycle was a water flood with 2 % NaCl brine. The flood was performed with brine being injected at a constant rate of 10 cm^3/hr. The same well that was used for production during primary (Well #1) was used as the producer for the first water flood. Well #3, located in the opposite corner of the model from the producer, was used as the injector so that the flood was performed across the diagonal of the model. The flood lasted almost 165 hours and resulted in an incremental recovery of 12.4 % OOIP. Figure 4.66 and Figure 4.67 show the cumulative production and water cut respectively. There was some produced sand observed in the bottom of the graduated cylinders, however, it was too small an amount to measure. Over the entire flood it can be estimated that no more than 5 grams of sand were produced. For the calculation of the instability the same result were obtained as with Experiments #3 and #4. The flood was shown to be stable away from the wells and stable near the wells. The capillary number was calculated to be $1.76x10^{-7}$.

The third production cycle was an additional water flood with 2 % brine. The direction of the flood was reversed from the previous flood (i.e. the injector and producer switched positions). The flood lasted just over 100 hours and resulted in an incremental recovery of 3.7 % OOIP. One more water flood was performed on Reservoir Model#1. The flood was perform across the diagonal of the model perpendicular to the direction of the two previously described floods. Well #4 was the injector and Well #2 was the producer. The flood lasted 62 hours and an insignificant amount of oil was produced.

The water floods were followed with a polymer flood. The polymer solution used was a 5000 ppm solution of ALCOFLOOD 935 in fresh water. The well with sand producing capabilities used during primary production (Well #1) was used as the producer and Well #3 in the opposite corner of the model was used as the injector. The flood lasted just over 330 hours and resulted in an incremental recovery of 24.1 % OOIP. The cumulative production and the water cut are presented in Figure 4.68 and Figure 4.69 respectively. As can be seen from Figure 4.69, the water cut seems to decline right at the start and then increase to about 75 % where oscillates until the end of the flood. This is different from

the behavior of the previous polymer floods performed on the Reservoir Models. In the previous experiments the water cut remained high for about 150 hours then it declined before recovering. In those previous experiments there were two major differences in the conditions. First there was no sand production, second the models were only blown down to 200 psi and maintained at that pressure for all of the displacements. To determine the effect of sand production on the various stages of production it was necessary to produce a Reservoir Model in the same manner as Reservoir Model#1 eliminating sand production. This has been done with Reservoir Model#2.

After all the floods were completed the model was x-rayed to determine the location of any wormhole that was formed during primary production. The x-ray image was taken at the at the completion of the entire experiment because it was necessary to remove the valves from the outlets of the wells in order to remove the model from its stand. Doing this right after primary production would have resulted in the loss of fluids from the model and would have been detrimental to the floods performed during the remainder of the experiment. Alteration of the oil saturation in the sand pack should not effect the x-ray image since the density of the undoped oil and water are quite similar. Figure 4.70 shows the X-ray image. The production well is located just outside the circular area of the image at the bottom left. As indicated by the lighter area, a definite wormhole appears to have formed. The wormhole extends out from the production well to the centre of the sand pack. There seems to be a transition zone separating the wormhole from the undisturbed matrix where the porosity gradually decreases moving away from the wormhole. Samples were cored from different areas of the sand pack. The amount of sand, oil and water were determined from Dean Stark analysis. The porosity calculated from the Dean Stark analysis of the core samples ranged from 37 % in the undisturbed portion of the sand pack to 63 % in the wormhole close to the production well. The porosities from all the cored samples along with positions in the sand pack where the samples were taken are shown in Figure 4.71. The well that was used for primary production is positioned in the bottom right corner in Figure 4.71. The area where the sand pack had subsided is also shown in the figure.

The total cumulative production for Ambient Model #1 during Experiment #8 was 64.1 % of OOIP. Figure 4.72 presents the cumulative production and water cut over the entire course of the experiment.

4.9 Experiment #9

Reservoir Model #2 was used for Experiment #9. The same oil with same GOR as was used in Experiment #8 was used to saturate the model. The wells installed in the model were the standard wells that were not equipped for sand production. The initial conditions of the model after saturation are presented in Table 4.10.

Table 3: Conditions of Reservoir Model #2 After Saturation, Experiment #9

Pore volume [cm^3]	3559
Porosity [% p.v.]	0.39
Permeability [D]	4.4
Internal Pressure [psig]	500
Overburden Pressure [psig]	600
Live Oil GOR [vol. Gas/vol. oil]	12.6
OOIP [$STcm^3$]	2560
Initial Oil Saturation [%]	72.0
Dead Oil Viscosity [cP]	1250
Dead Oil Density [g/cm^3]	0.96

As mentioned above, Reservoir Model #2 in Experiment #9 was produced in the same manner, except for sand production, as Reservoir Model#1 in Experiment #8.

First primary production was performed by blowing the model down to atmospheric pressure. Well #1 was used as the production well. The valve at the outlet of the production well was throttled slightly to prevent the gas being produced in excess of the capacity of the wet test metre. The depletion lasted about two hours and resulted in an oil recovery of 19.3 % OOIP. The cumulative production is presented in Figure 4.73.

The second production cycle was a water flood with 2 % brine. The same well used during primary production (Well #1) was used as the producer well. Well #2 in the

opposite corner was used as the injector. The flood lasted 105 hours and resulted in an incremental recovery of 4.1 % OOIP. Figure 4.74 and Figure 4.75 show the cumulative production and water cut respectively. Again, the stability analysis showed a stable displacement near the wells and an unstable displacement near the wells. The capillary number was calculated to be 8.7×10^{-7}.

This was followed by an additional water flood with 2 % brine. The direction of the flood was reversed. The flood lasted 134 hours and resulted in an incremental recovery of 12.0 % OOIP. The cumulative production and water cut are shown in Figure 4.76 and Figure 4.77 respectively. It is interesting to note that reversing the direction of the flood resulted in a higher oil recovery than the initial flood.

A third water flood was performed on Reservoir Model#2. The same injector, Well #1, that was used in the previous water flood was used. The producer was Well #3, the offset well located halfway along the wall adjacent to the well located in the opposite corner. This flood lasted 51 hours and resulted in an incremental recovery of less than 1 % of OOIP.

After the water floods, a polymer flood was performed with 5000 ppm of ALCOFLOOD 935 in fresh water. Well #1 was used as the producer. Well #2 located in the opposite corner was used as the injector. The flood lasted just over 360 hours and resulted in an incremental recovery of 31.4 % of OOIP. The cumulative production and water cut are presented in Figure 4.78 and 4.79 respectively. The water cut, as shown in Figure 4.79, behaves similarly to the polymer floods of the other Reservoir Models without sand production. The water cut remains high for a prolonged period before it declines.

The total production during the experiment was 67.5 % of OOIP. Figure 4.80 presents the cumulative production and water cut over the entire course of the experiment.

When comparing the performance of the experiment with sand production against the experiment without sand production a few observations can be made. First the recovery

during primary production was higher with sand production. This was to be expected. The production of sand resulted in a high permeability wormhole being formed that allowed for easier flow of the viscous oil.

As far as the effect of sand production on subsequent recovery schemes, it does not appear that the production of sand during primary production had a detrimental effect on further recovery. It could have been possible for the wormhole to provide a high permeability channel through which any injected fluid may flow through and bypass large portions of the sand pack. This does not appear to have happened. The ultimate recoveries of both experiments were quite close. However, it is not possible to make any general conclusion from just these two experiments. It should be noted that the initial oil saturation was higher in Experiment #8 than it was in Experiment #9. This could have had an effect on the recoveries obtained during the experiments. The remaining average oil saturations at the end of the experiments were calculated based on the initial porosities. For Experiment #8 with sand production the estimated average oil saturation was 0.29 compared with 0.23 for Experiment #9 without sand production. So it is possible that sand production may have had a small negative impact on oil recovery. More experiments need to be performed with sand production to ensure that the observed trends are consistent.

Figure 4.1: Permeability vs. Overburden
Silica Sand Used For Experiments #1 - #5,#7

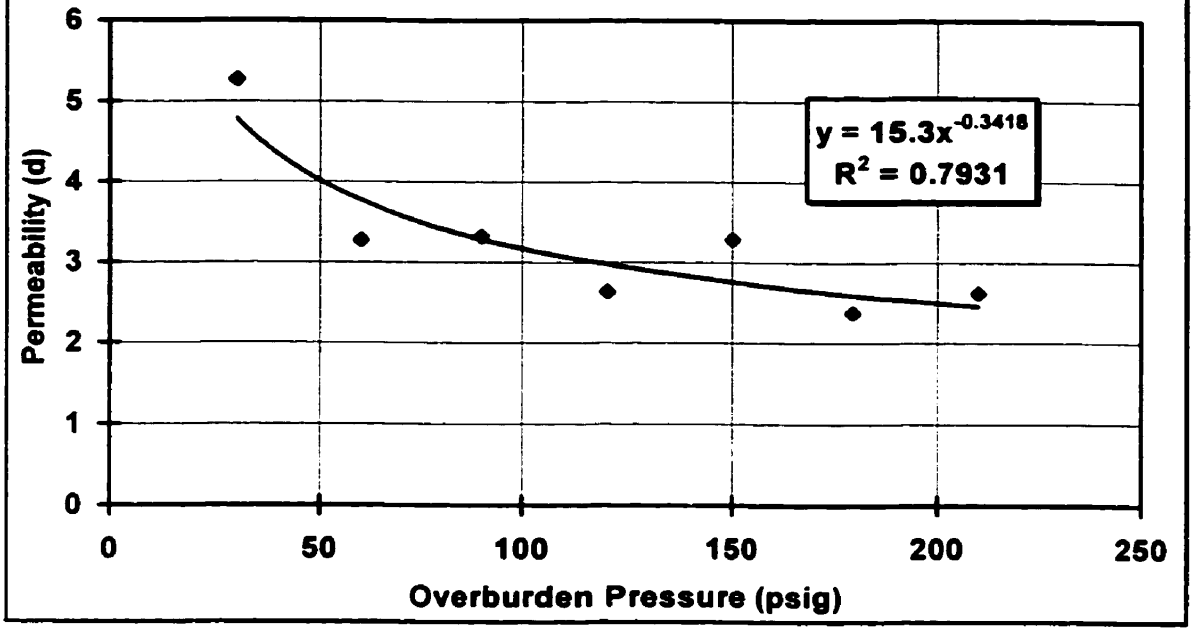

Figure 4.2: Permeability vs. Overburden
Silica Sand Used for Experiments #1 - #5, #7

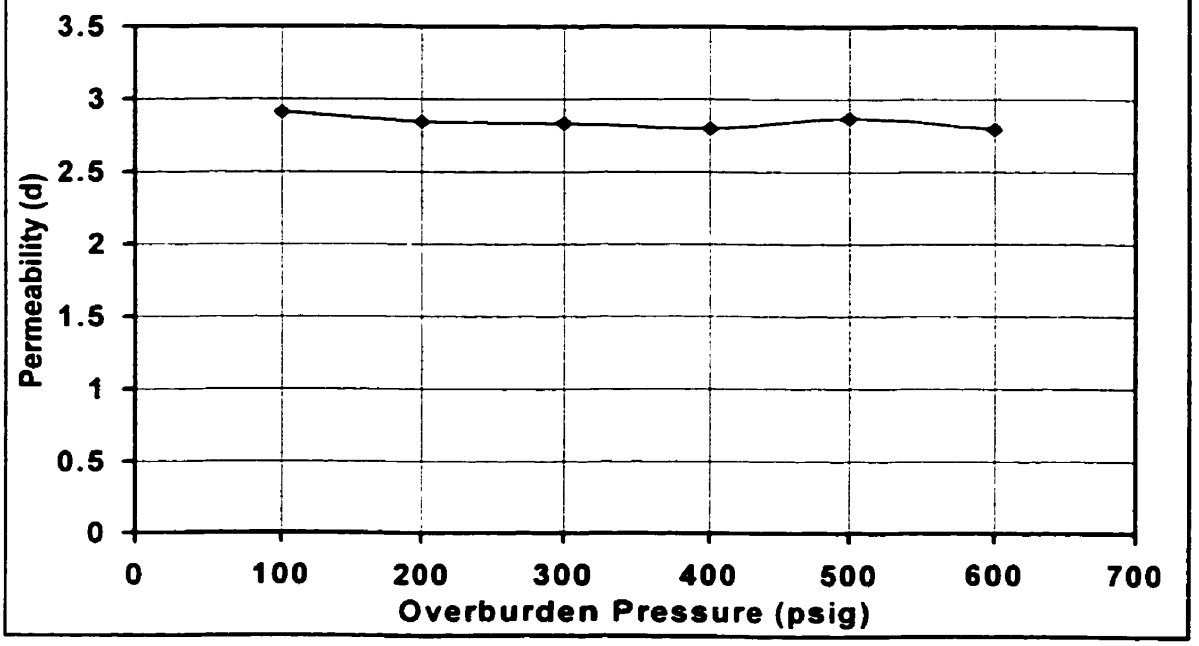

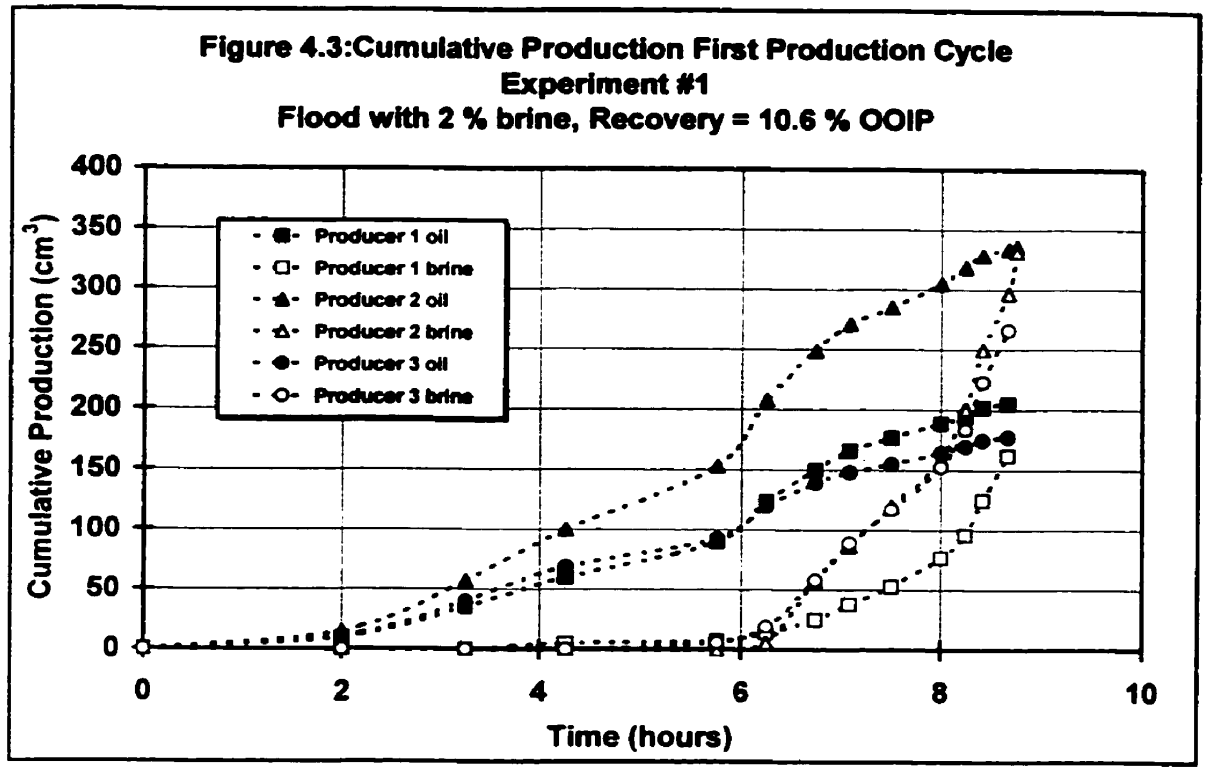
Figure 4.3:Cumulative Production First Production Cycle
Experiment #1
Flood with 2 % brine, Recovery = 10.6 % OOIP
Cumulative Production (cm3)
400
350
300
250
200
150
100
50
0
0
2
4
6
8
10
Time (hours)
Producer 1 oil
Producer 1 brine
Producer 2 oil
Producer 2 brine
Producer 3 oil
Producer 3 brine

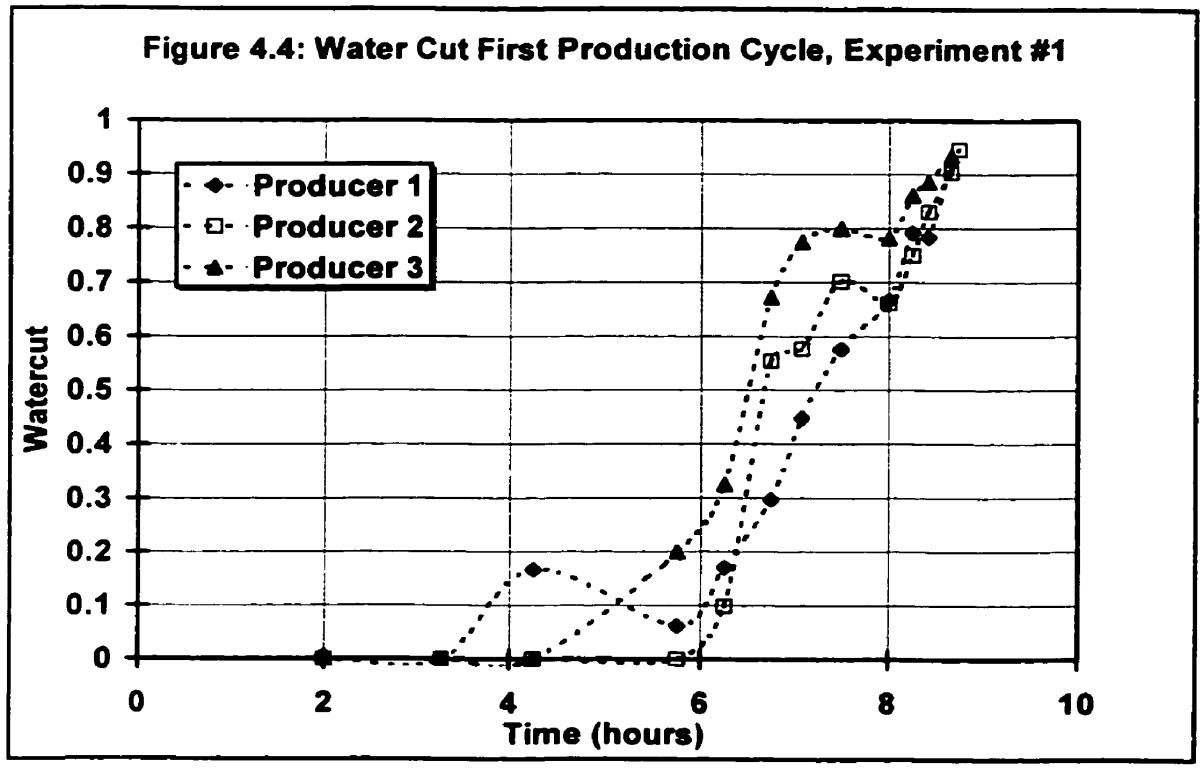
Figure 4.4: Water Cut First Production Cycle, Experiment #1
Watercut
1
0.9
0.8
0.7
0.6
0.5
0.4
0.3
0.2
0.1
0
0
2
4
6
8
10
Time (hours)
Producer 1
Producer 2
Producer 3

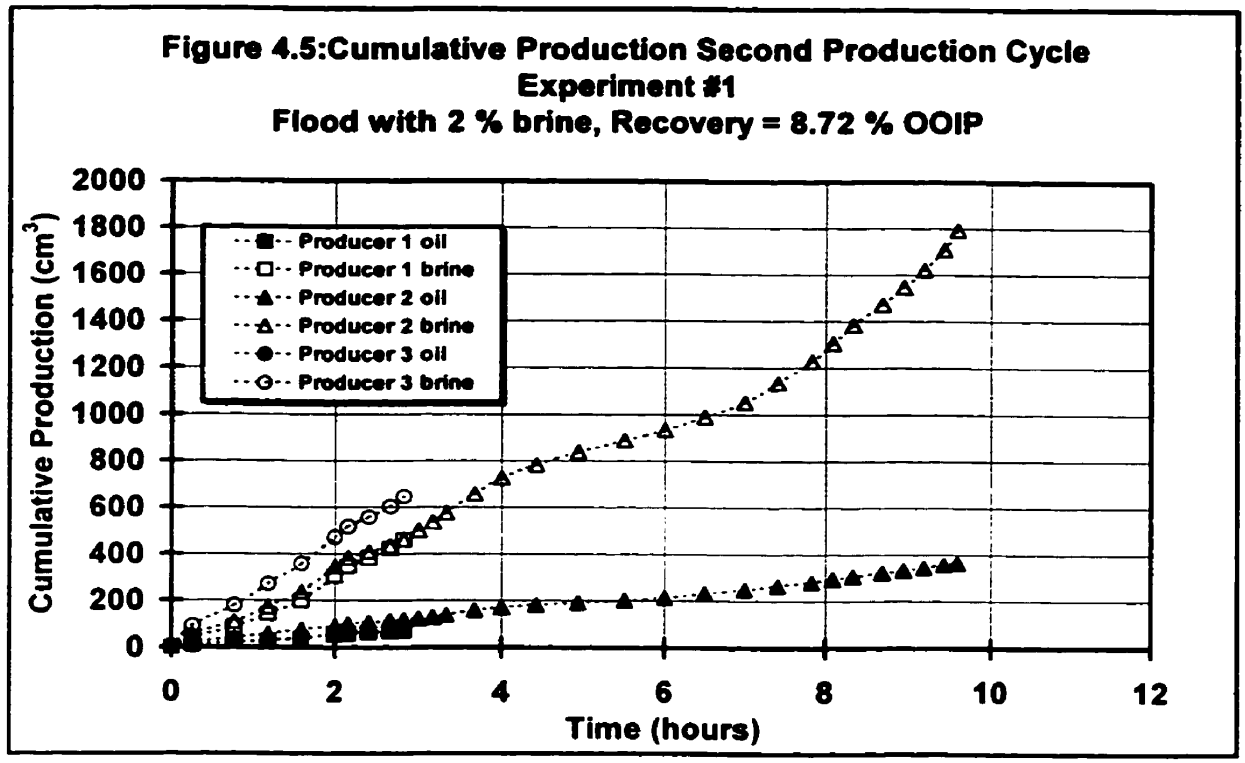
Figure 4.5:Cumulative Production Second Production Cycle
Experiment #1
Flood with 2 % brine, Recovery = 8.72 % OOIP
Cumulative Production (cm3)
2000
1800
1600
1400
1200
1000
800
600
400
200
0
Producer 1 oil
Producer 1 brine
Producer 2 oil
Producer 2 brine
Producer 3 oil
Producer 3 brine
0
2
4
6
8
10
12
Time (hours)

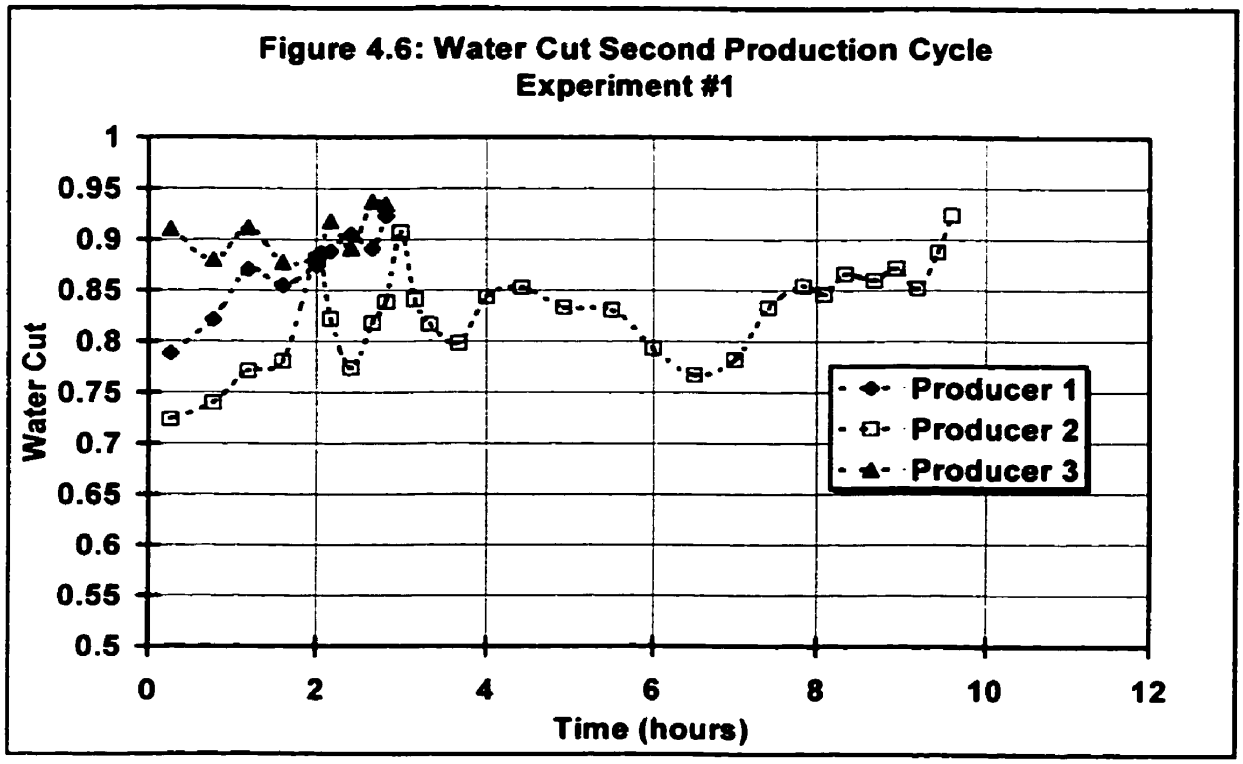
Figure 4.6: Water Cut Second Production Cycle
Experiment #1
Water Cut
1
0.95
0.9
0.85
0.8
0.75
0.7
0.65
0.6
0.55
0.5
Producer 1
Producer 2
Producer 3
0
2
4
6
8
10
12
Time (hours)

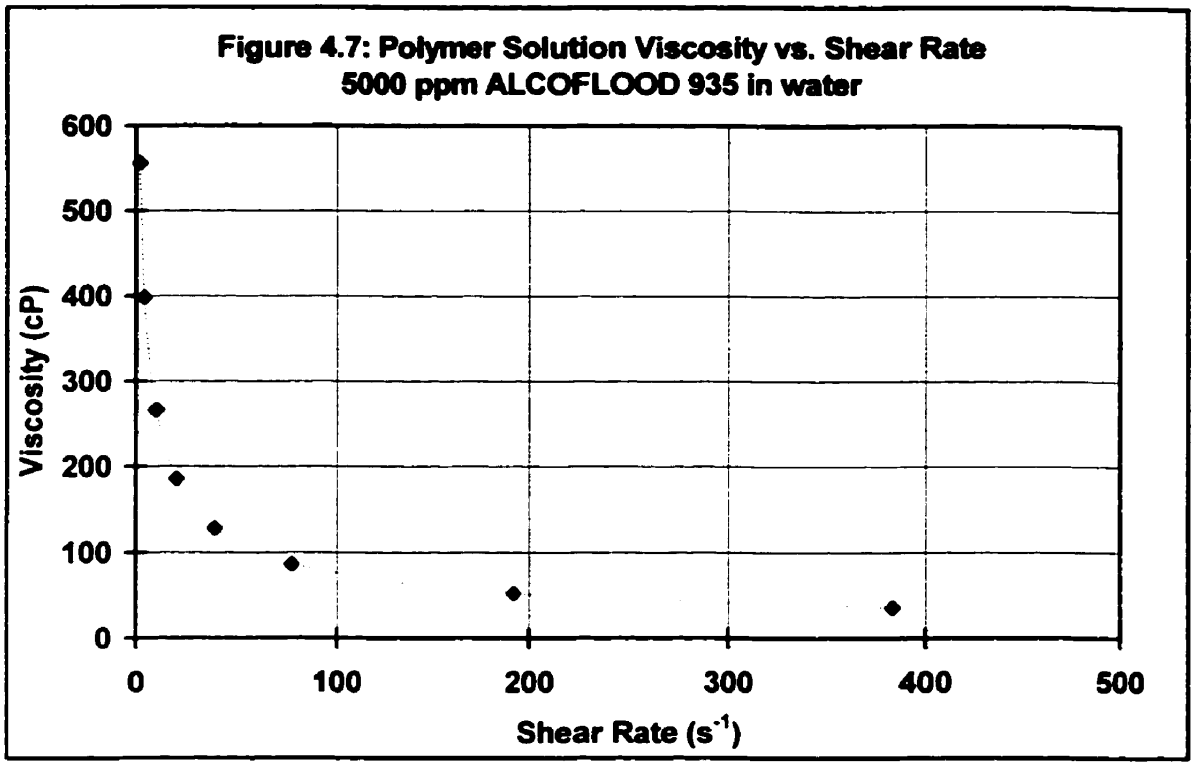
Figure 4.7: Polymer Solution Viscosity vs. Shear Rate
5000 ppm ALCOFLOOD 935 in water
Viscosity (cP)
600
500
400
300
200
100
0
0
100
200
300
400
500
Shear Rate (s-1)

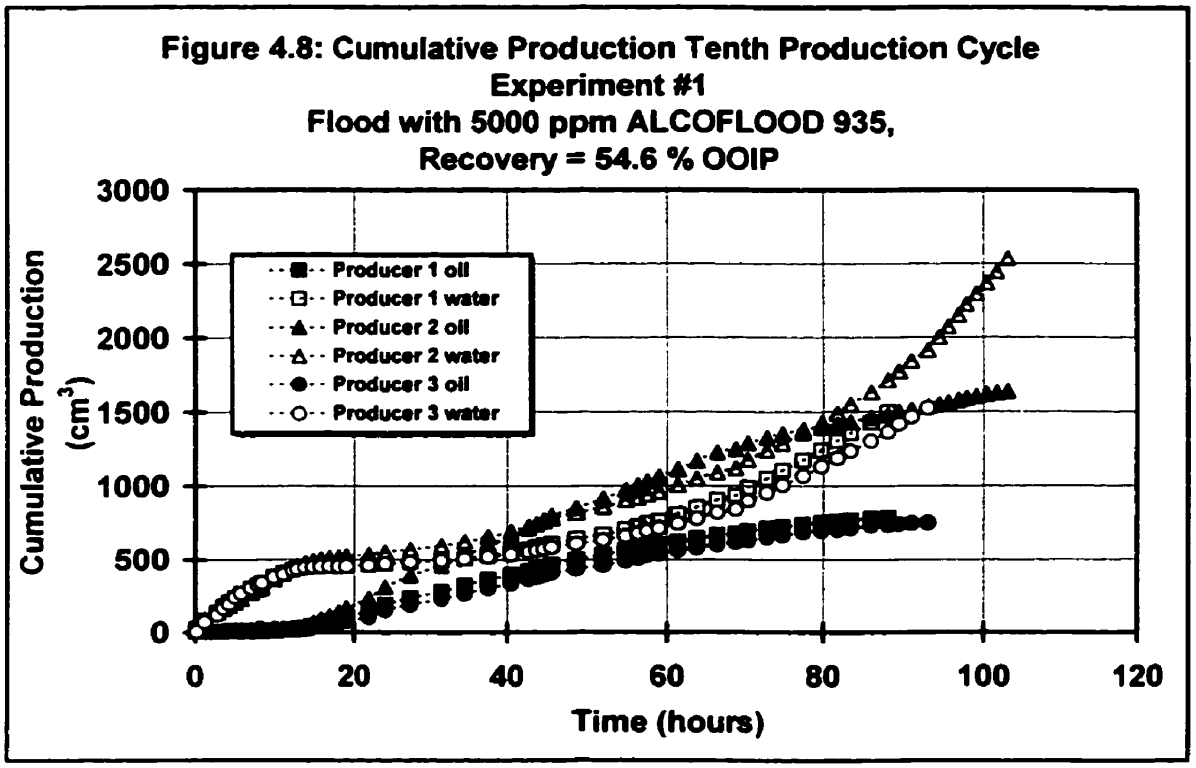
Figure 4.8: Cumulative Production Tenth Production Cycle
Experiment #1
Flood with 5000 ppm ALCOFLOOD 935,
Recovery = 54.6 % OOIP
Cumulative Production (cm3)
3000
2500
2000
1500
1000
500
0
Producer 1 oil
Producer 1 water
Producer 2 oil
Producer 2 water
Producer 3 oil
Producer 3 water
0
20
40
60
80
100
120
Time (hours)

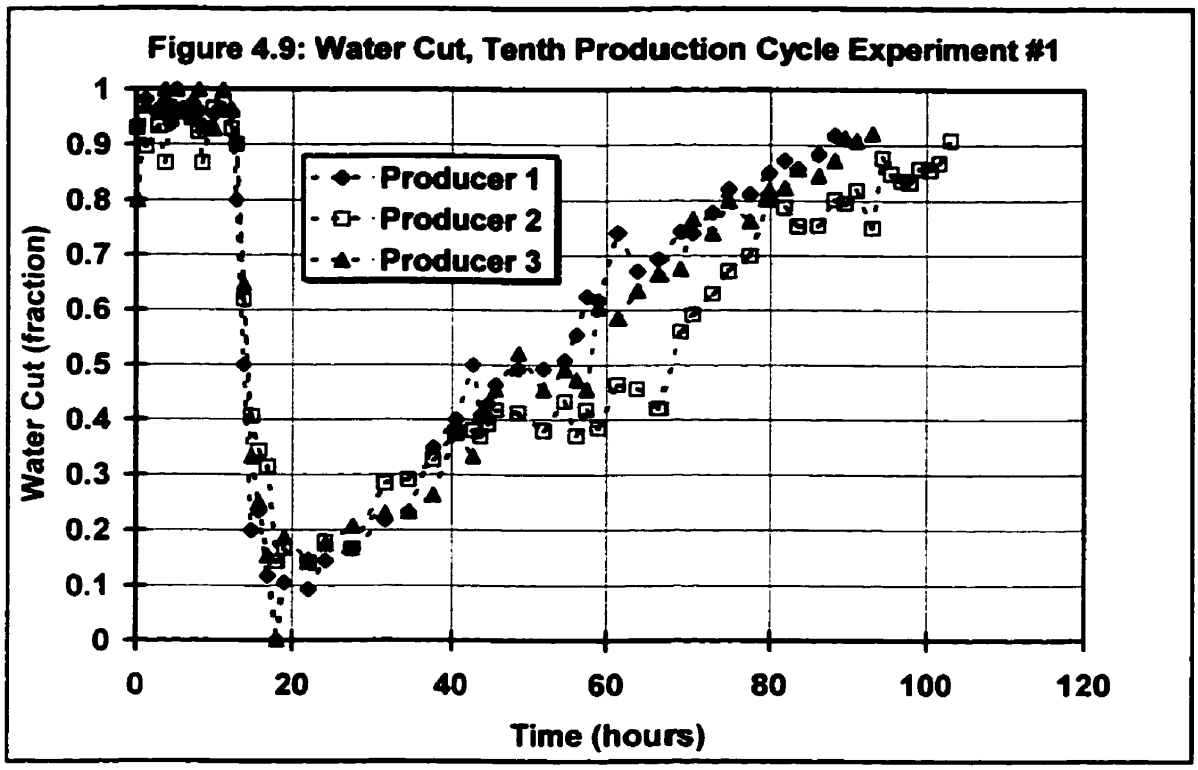

Figure 4.9: Water Cut, Tenth Production Cycle Experiment #1

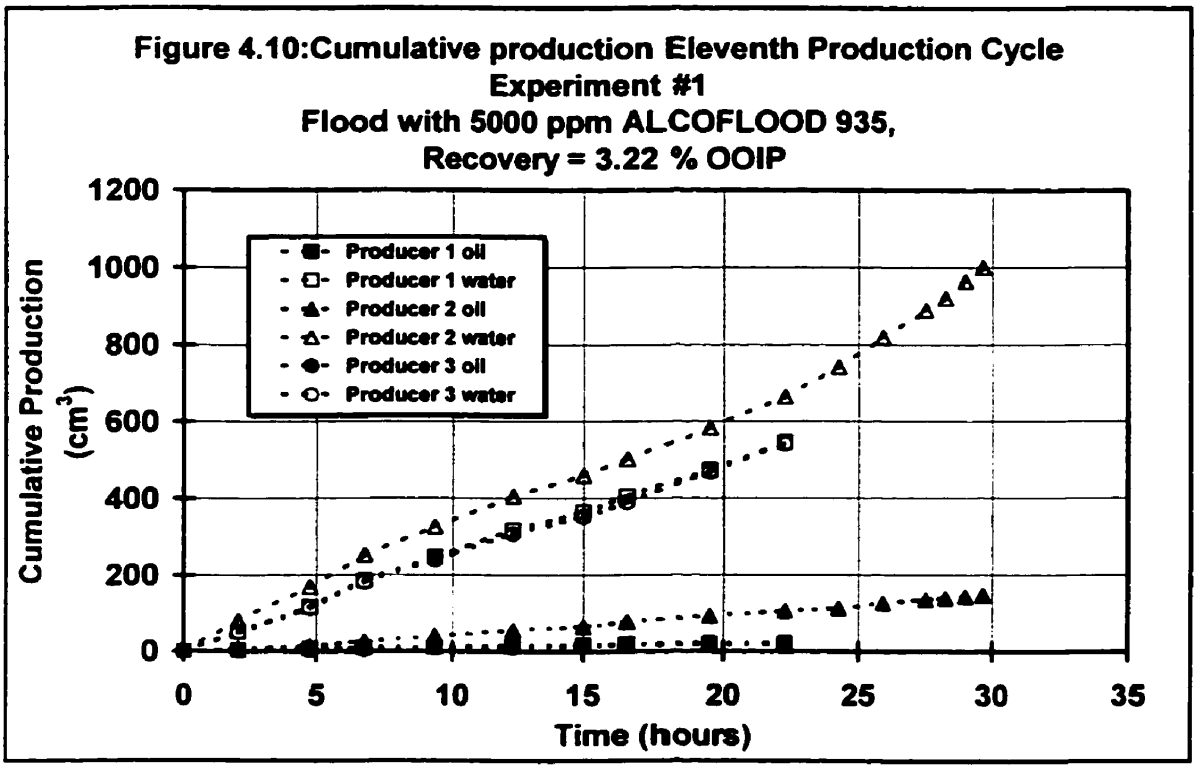

Figure 4.10:Cumulative production Eleventh Production Cycle Experiment #1
Flood with 5000 ppm ALCOFLOOD 935,
Recovery = 3.22 % OOIP

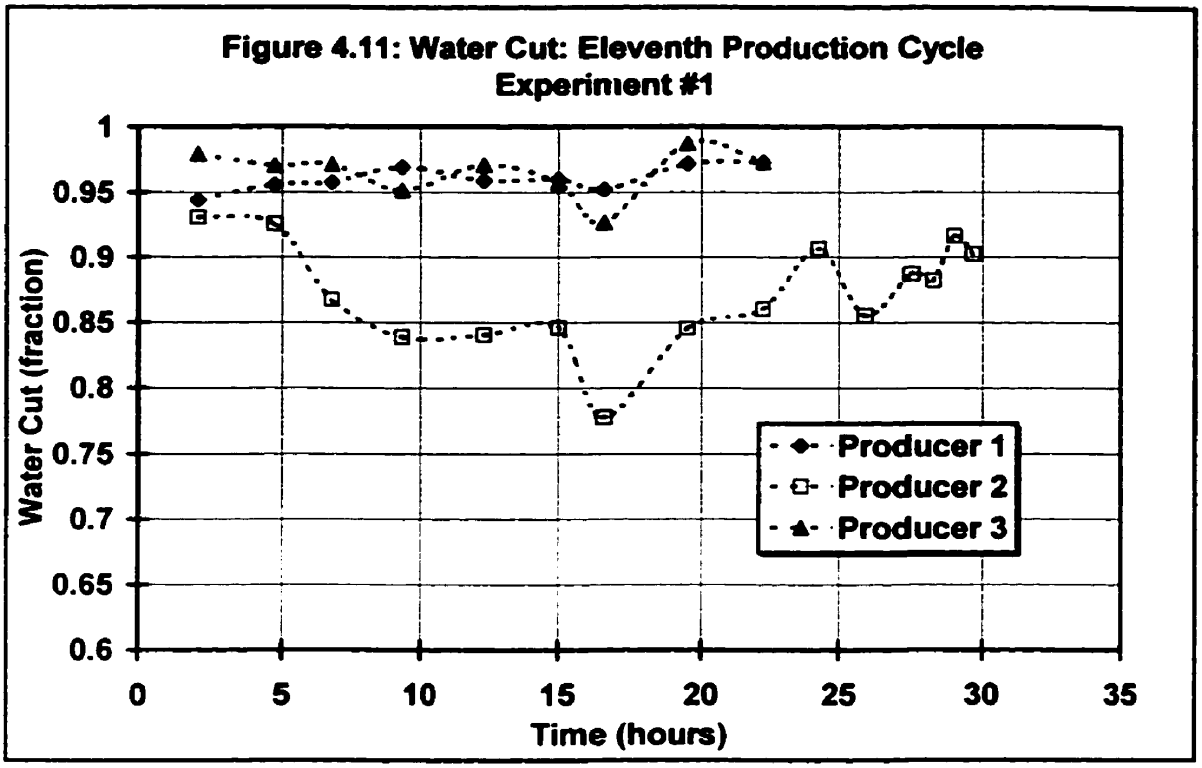
Figure 4.11: Water Cut: Eleventh Production Cycle
Experiment #1
Water Cut (fraction)
1
0.95
0.9
0.85
0.8
0.75
0.7
0.65
0.6
0
5
10
15
20
25
30
35
Time (hours)
Producer 1
Producer 2
Producer 3

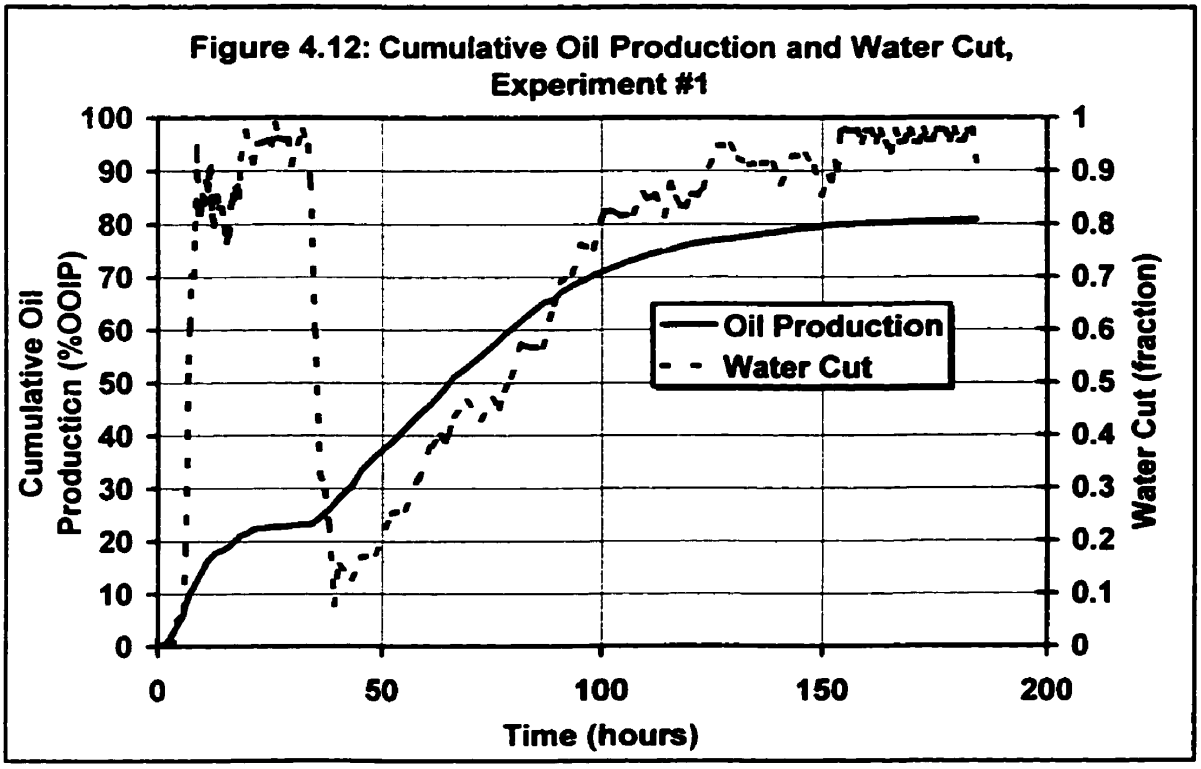
Figure 4.12: Cumulative Oil Production and Water Cut,
Experiment #1
Cumulative Oil Production (%OOIP)
100
90
80
70
60
50
40
30
20
10
0
Water Cut (fraction)
1
0.9
0.8
0.7
0.6
0.5
0.4
0.3
0.2
0.1
0
0
50
100
150
200
Time (hours)
Oil Production
Water Cut

Figure 4.13: Cumulative Production First Production Cycle
Experiment #2
Flood with 2% brine, Recovery = 21.5 % OOIP

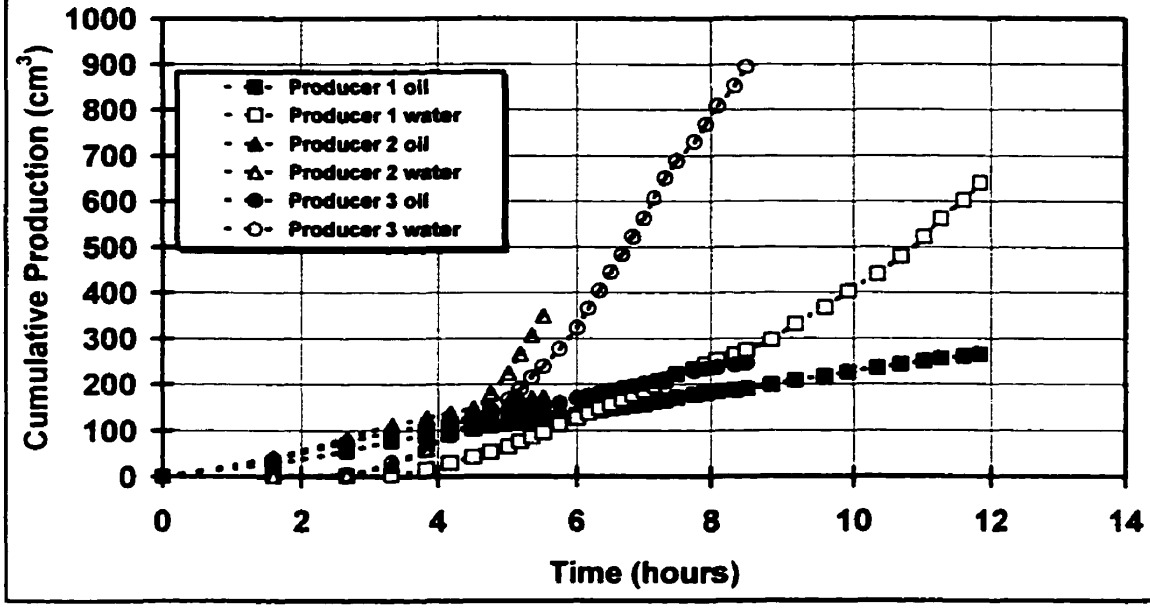

Figure 4.14: Water Cut First Production Cycle
Experiment #2

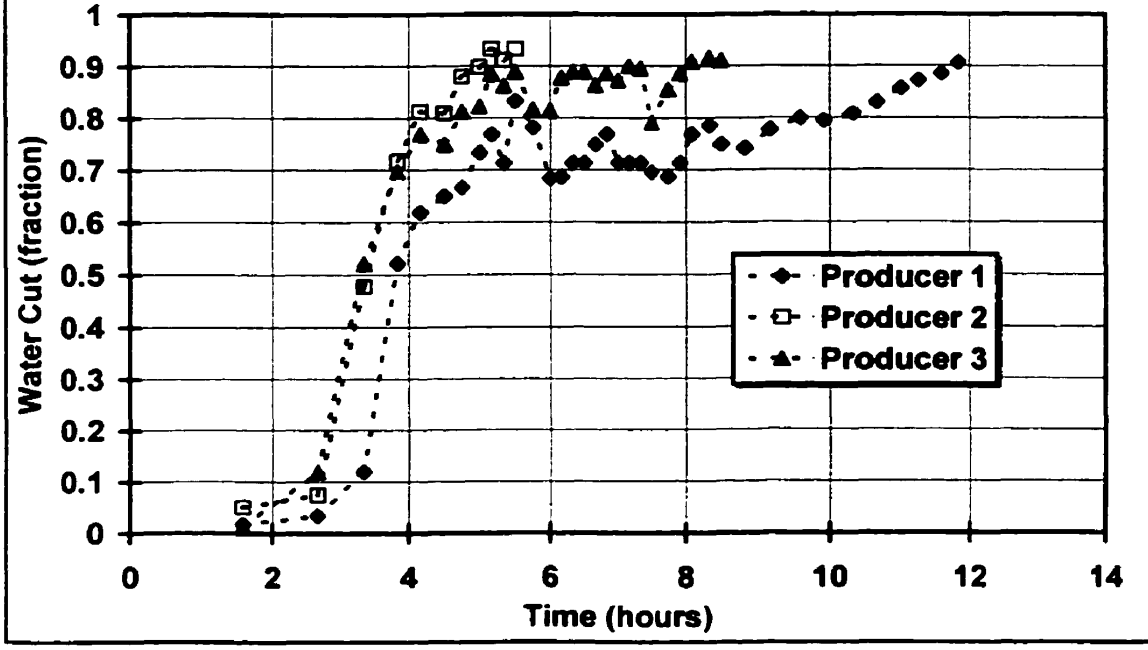

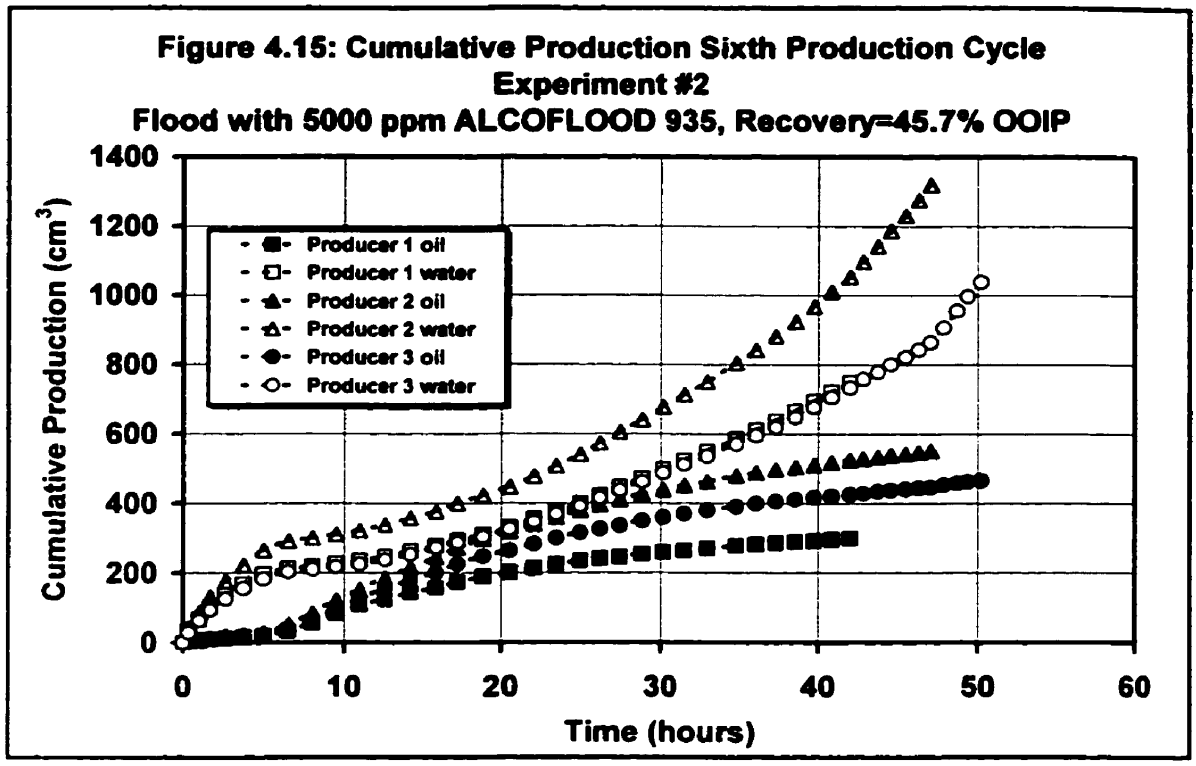
Figure 4.15: Cumulative Production Sixth Production Cycle
Experiment #2
Flood with 5000 ppm ALCOFLOOD 935, Recovery=45.7% OOIP
Cumulative Production (cm3)
Time (hours)
Producer 1 oil
Producer 1 water
Producer 2 oil
Producer 2 water
Producer 3 oil
Producer 3 water
0
200
400
600
800
1000
1200
1400
0
10
20
30
40
50
60

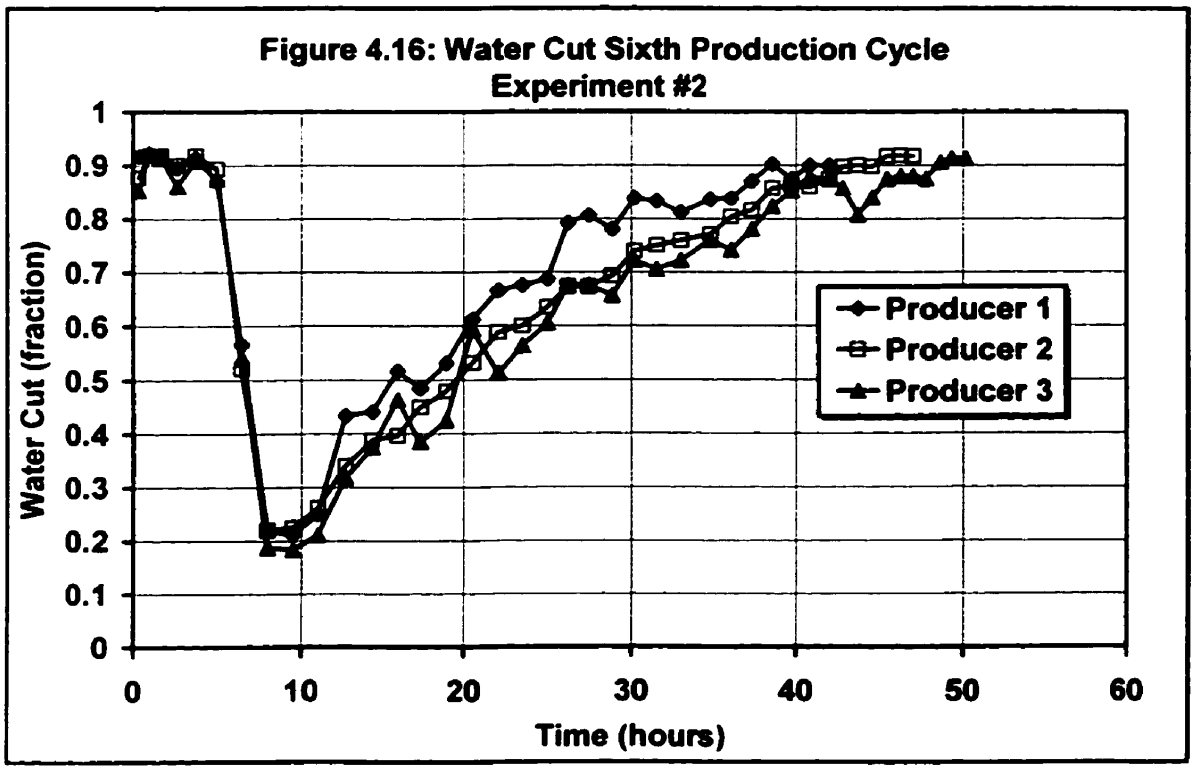
Figure 4.16: Water Cut Sixth Production Cycle
Experiment #2
Water Cut (fraction)
Time (hours)
Producer 1
Producer 2
Producer 3
0
0.1
0.2
0.3
0.4
0.5
0.6
0.7
0.8
0.9
1
0
10
20
30
40
50
60

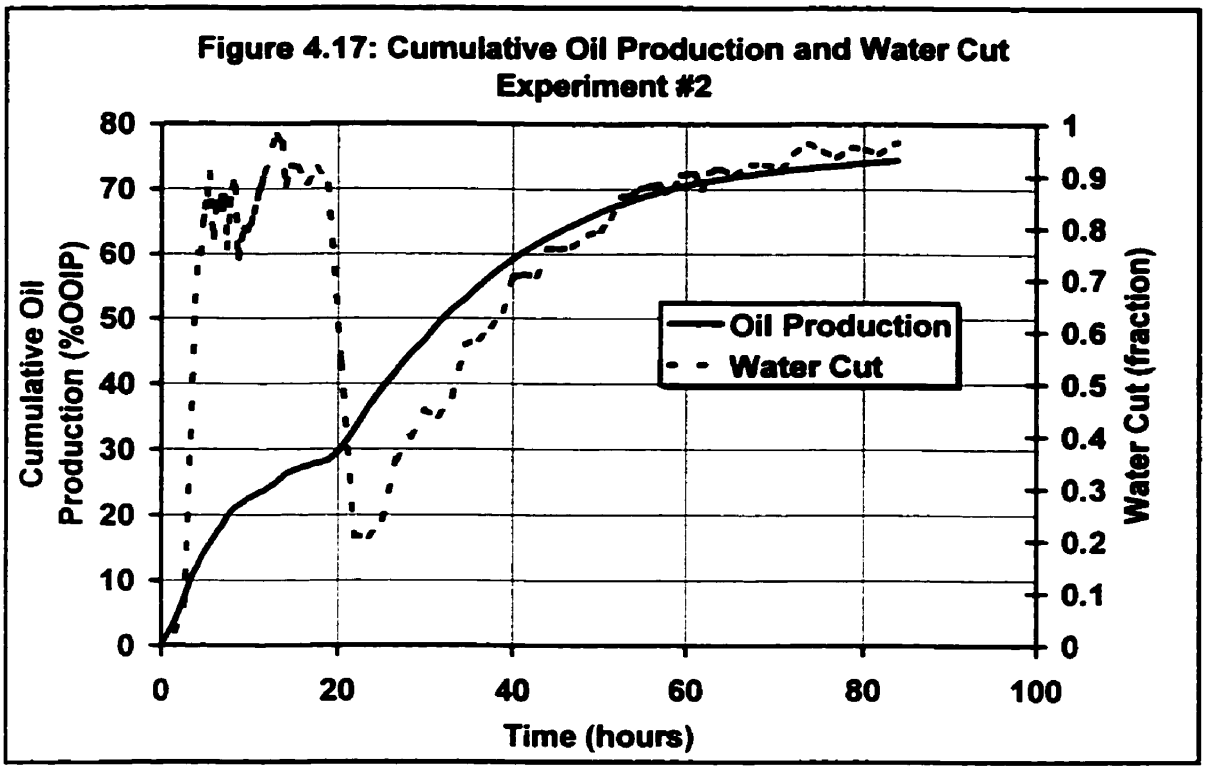
Figure 4.17: Cumulative Oil Production and Water Cut
Experiment #2
Cumulative Oil Production (%OOIP)
Water Cut (fraction)
Time (hours)
Oil Production
Water Cut
0
10
20
30
40
50
60
70
80
0
0.1
0.2
0.3
0.4
0.5
0.6
0.7
0.8
0.9
1
0
20
40
60
80
100

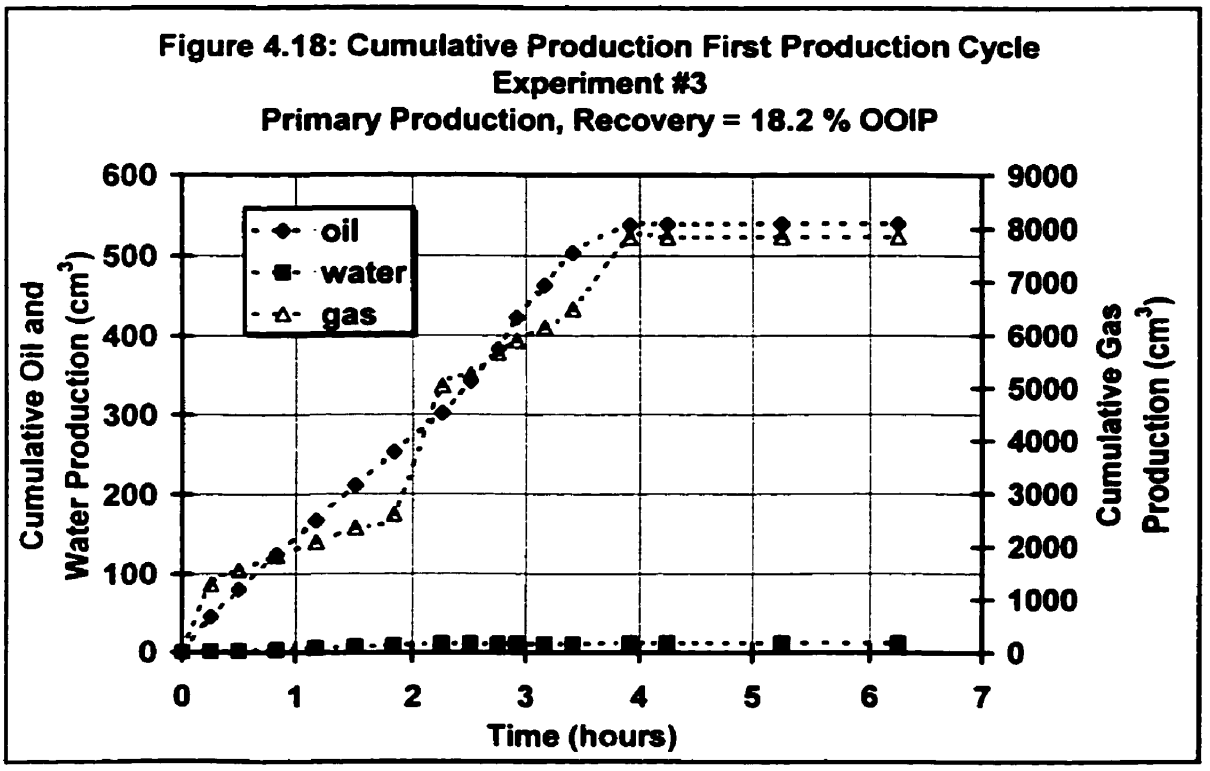
Figure 4.18: Cumulative Production First Production Cycle
Experiment #3
Primary Production, Recovery = 18.2 % OOIP
Cumulative Oil and Water Production (cm3)
Cumulative Gas Production (cm3)
Time (hours)
oil
water
gas
0
100
200
300
400
500
600
0
1000
2000
3000
4000
5000
6000
7000
8000
9000
0
1
2
3
4
5
6
7

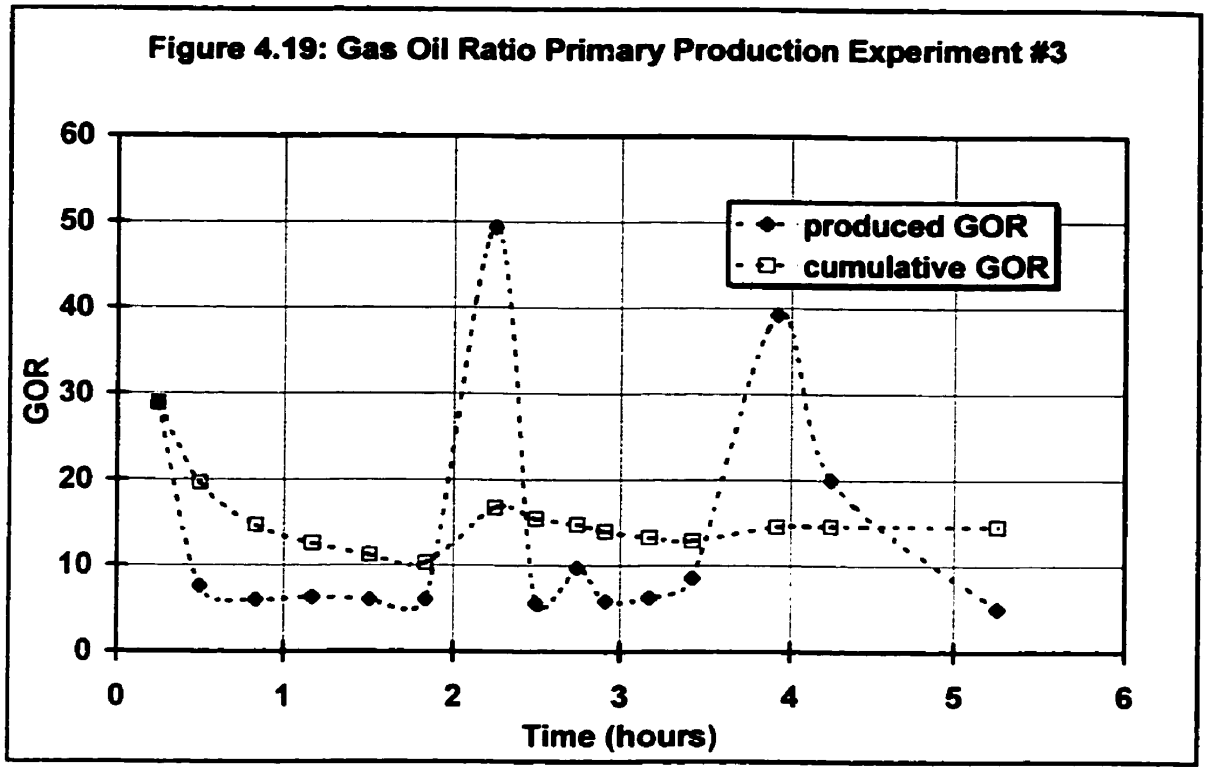
Figure 4.19: Gas Oil Ratio Primary Production Experiment #3
GOR
Time (hours)
produced GOR
cumulative GOR
0
10
20
30
40
50
60
0
1
2
3
4
5
6

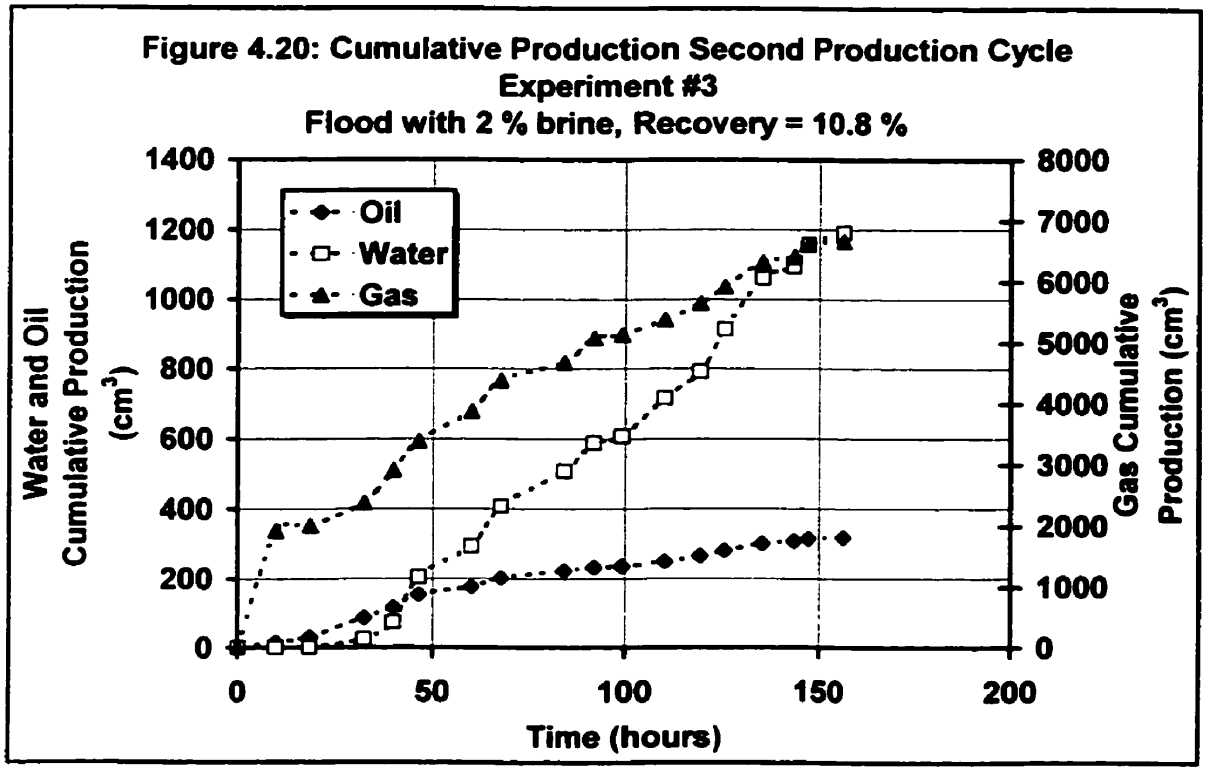
Figure 4.20: Cumulative Production Second Production Cycle
Experiment #3
Flood with 2 % brine, Recovery = 10.8 %
Water and Oil Cumulative Production (cm3)
Gas Cumulative Production (cm3)
Time (hours)
Oil
Water
Gas
0
200
400
600
800
1000
1200
1400
0
1000
2000
3000
4000
5000
6000
7000
8000
0
50
100
150
200

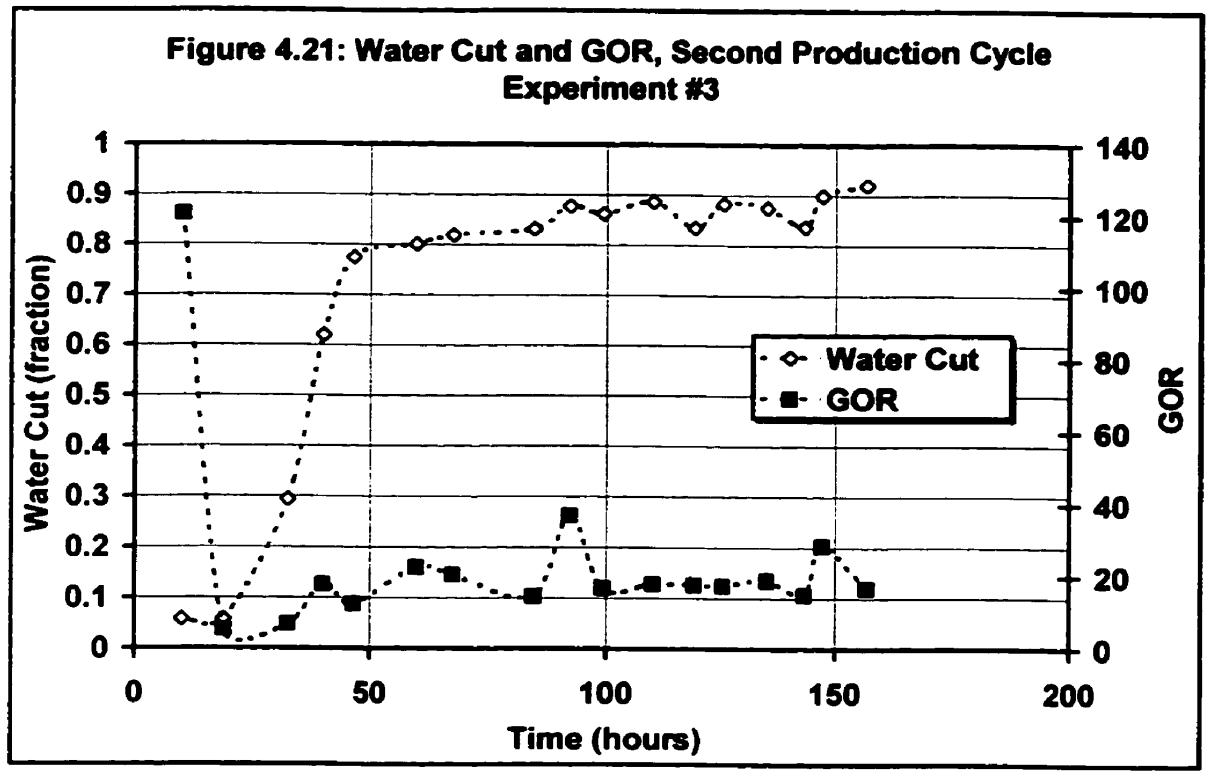
Figure 4.21: Water Cut and GOR, Second Production Cycle
Experiment #3
Water Cut (fraction)
GOR
Time (hours)
Water Cut
GOR
0
0.1
0.2
0.3
0.4
0.5
0.6
0.7
0.8
0.9
1
0
20
40
60
80
100
120
140
0
50
100
150
200

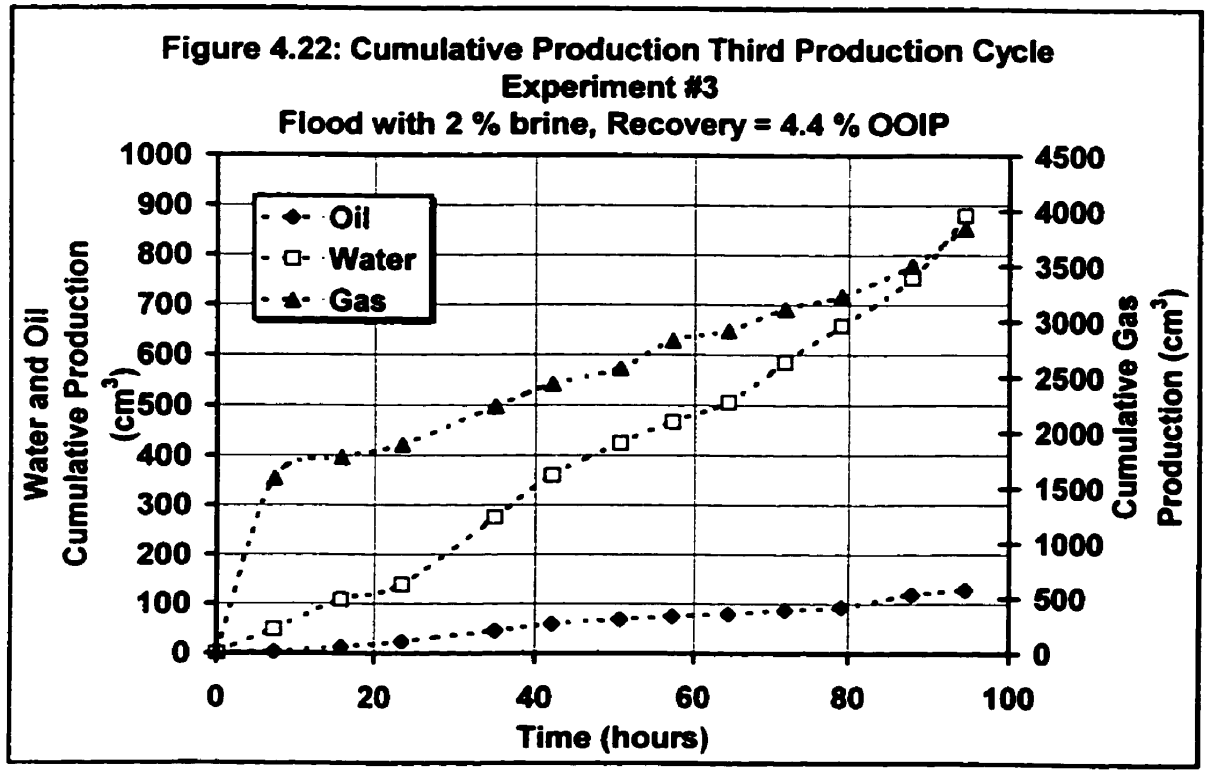
Figure 4.22: Cumulative Production Third Production Cycle
Experiment #3
Flood with 2 % brine, Recovery = 4.4 % OOIP
Water and Oil Cumulative Production (cm3)
Cumulative Gas Production (cm3)
Time (hours)
Oil
Water
Gas
0
100
200
300
400
500
600
700
800
900
1000
0
500
1000
1500
2000
2500
3000
3500
4000
4500
0
20
40
60
80
100

Figure 4.23: Water Cut and GOR, Third Production Cycle
Experiment #3

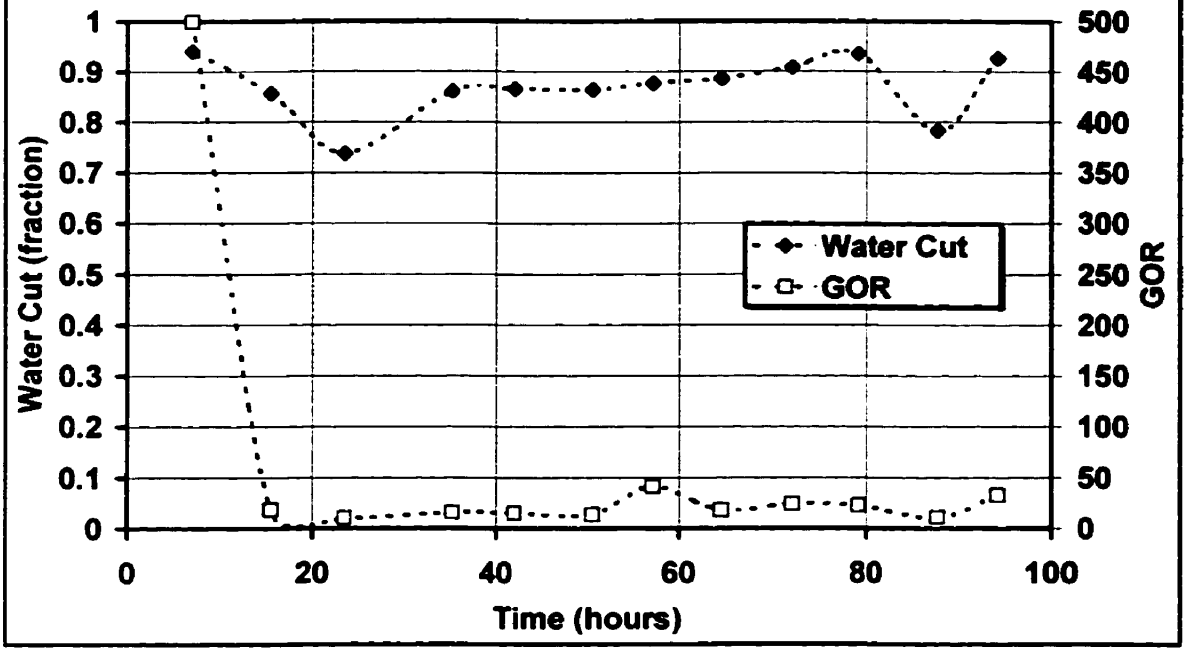

Figure 4.24: Cumulative Production Seventh Production Cycle
Experiment #3
Flood with 5000 ppm ALCOFLOOD in 2 % brine,
Recovery = 7 % OOIP

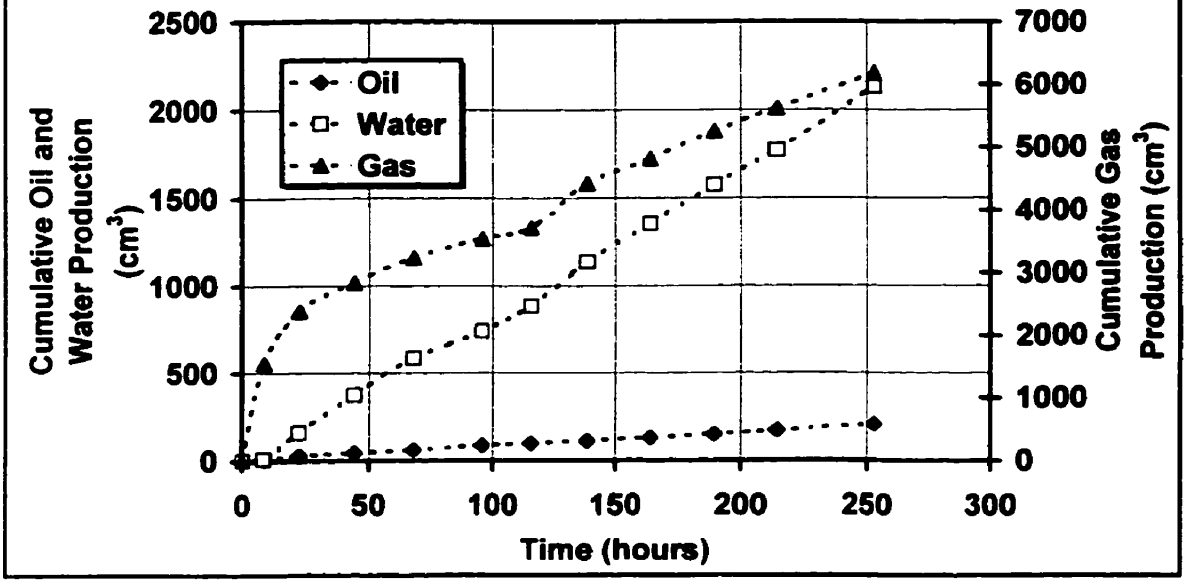

Figure 4.25: Water Cut and GOR, Seventh Production Cycle
Experiment #3

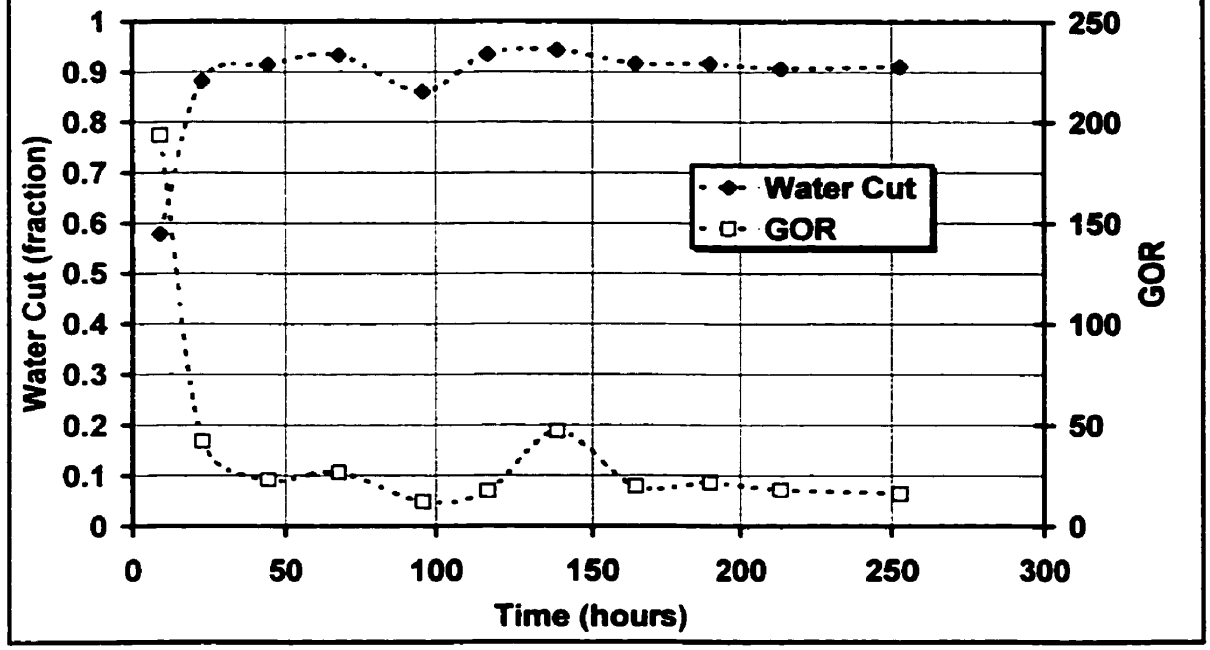

Figure 4.26: Cumulative Production, Eighth Production Cycle
Experiment #3
Flood with 5000 ppm ALCOFLOOD 935 in water,
Recovery = 29.5 % OOIP

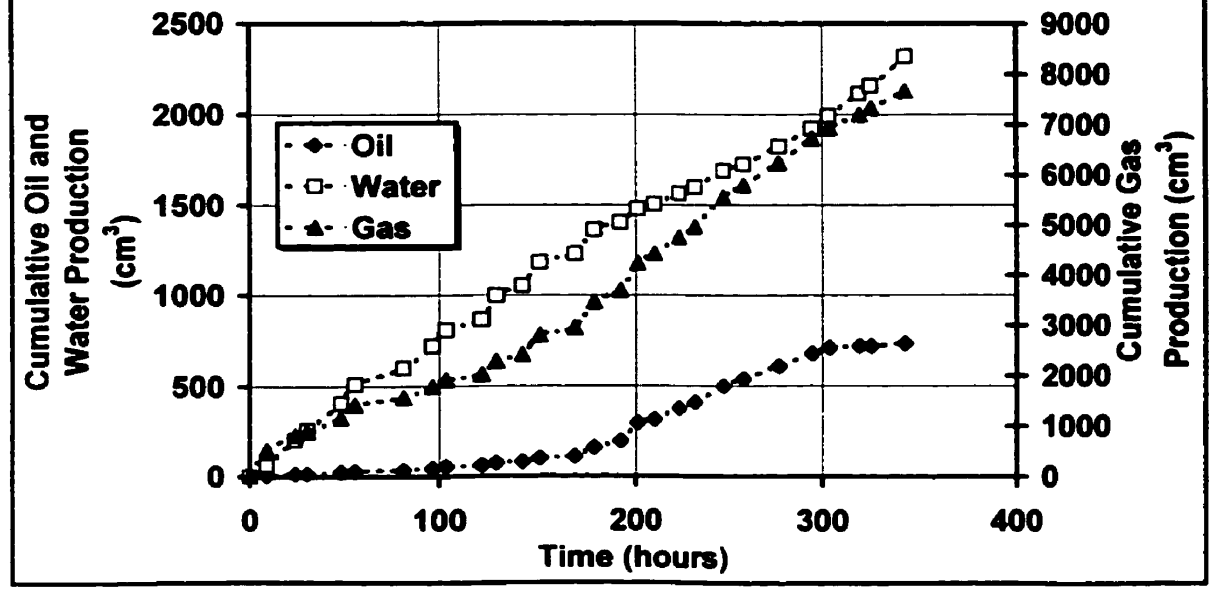

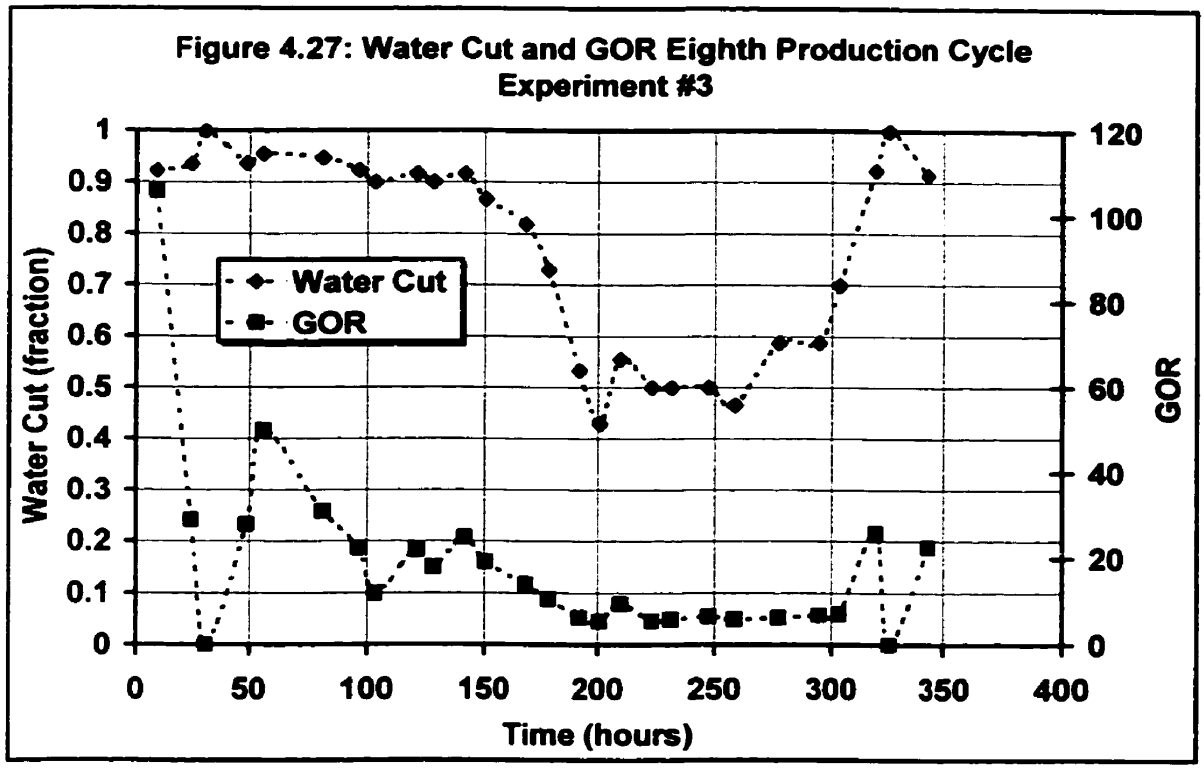
Figure 4.27: Water Cut and GOR Eighth Production Cycle
Experiment #3
Water Cut (fraction)
GOR
Time (hours)
Water Cut
GOR
0
0.1
0.2
0.3
0.4
0.5
0.6
0.7
0.8
0.9
1
0
20
40
60
80
100
120
0
50
100
150
200
250
300
350
400

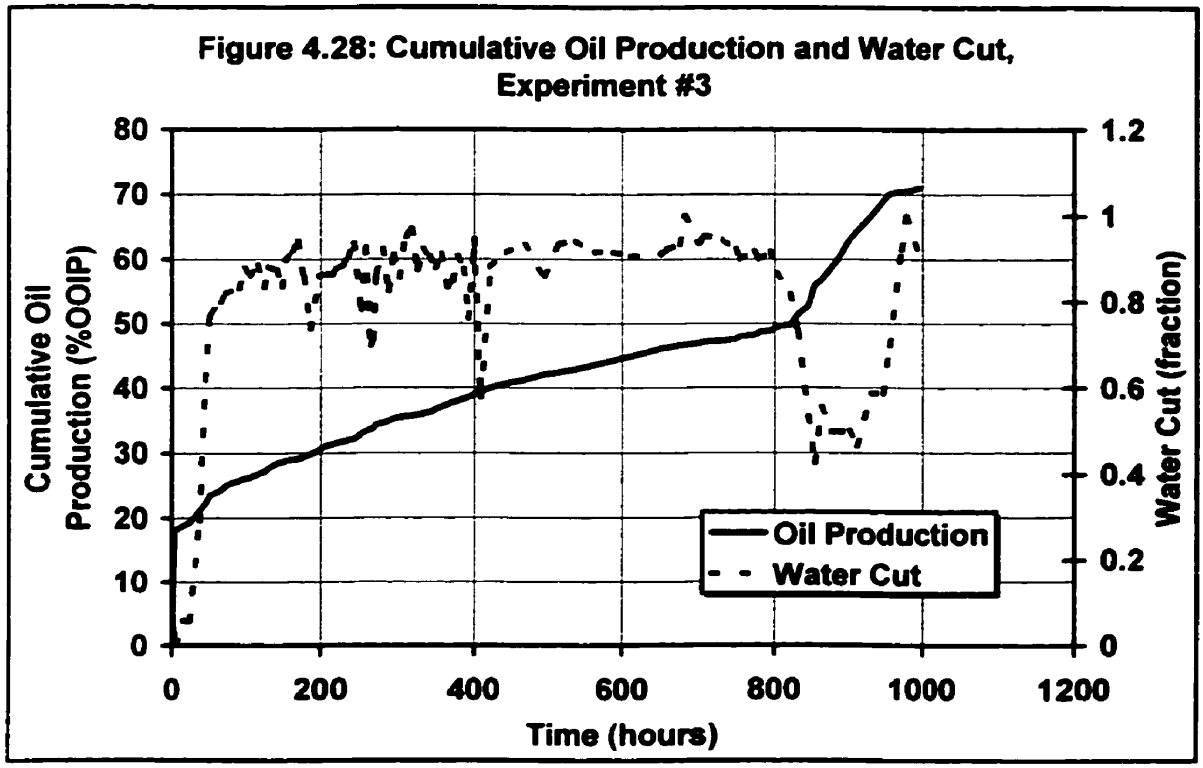
Figure 4.28: Cumulative Oil Production and Water Cut,
Experiment #3
Cumulative Oil Production (%OOIP)
Water Cut (fraction)
Time (hours)
Oil Production
Water Cut
0
10
20
30
40
50
60
70
80
0
0.2
0.4
0.6
0.8
1
1.2
0
200
400
600
800
1000
1200

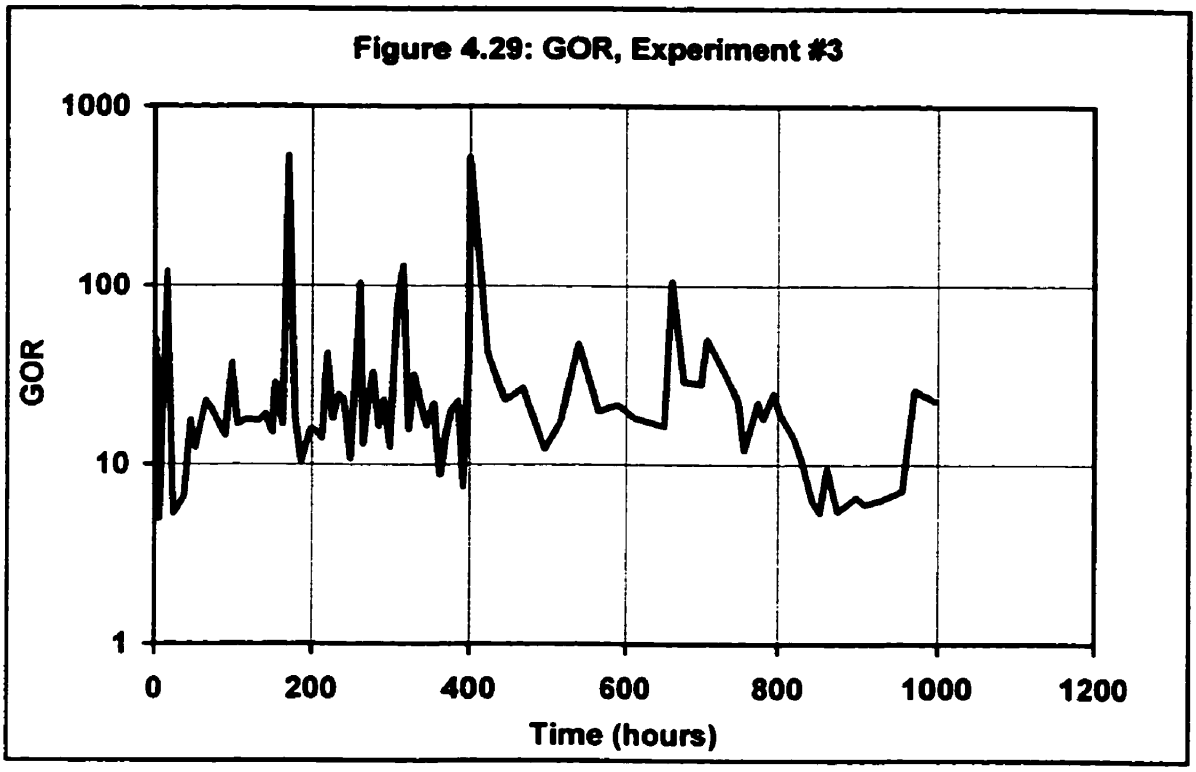
Figure 4.29: GOR, Experiment #3
1000
100
10
1
GOR
0
200
400
600
800
1000
1200
Time (hours)

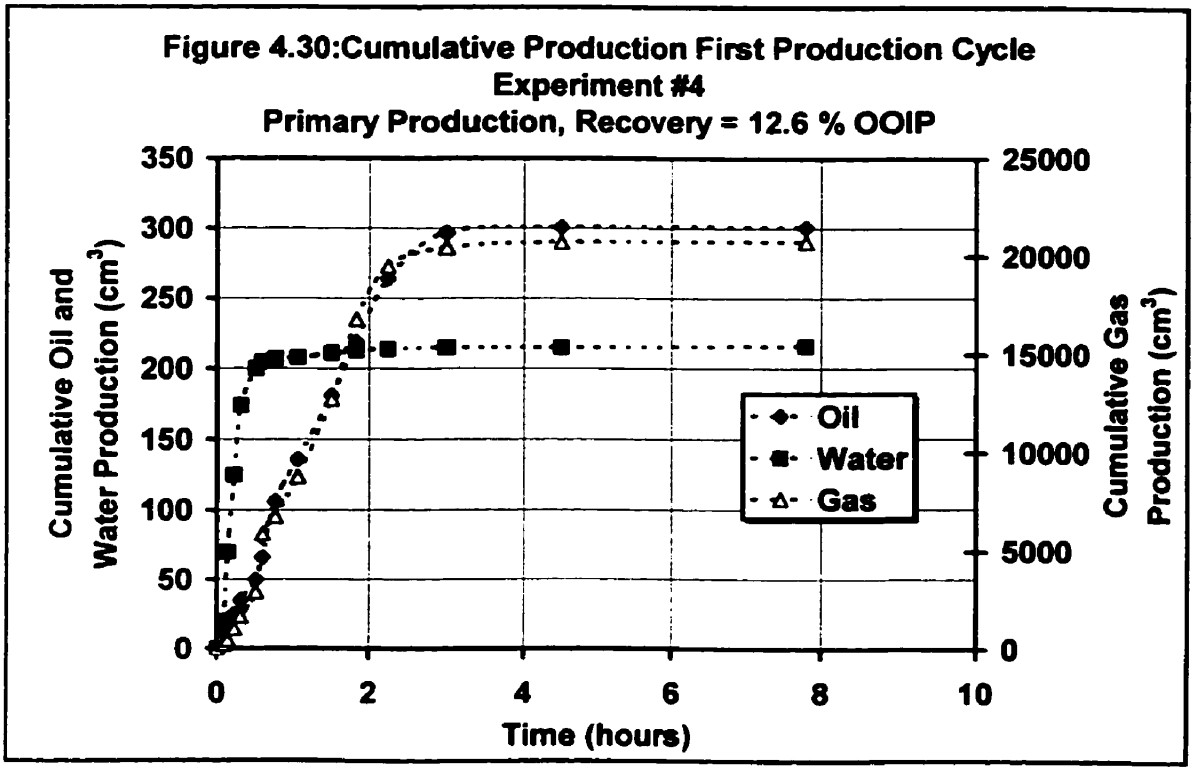
Figure 4.30:Cumulative Production First Production Cycle
Experiment #4
Primary Production, Recovery = 12.6 % OOIP
350
300
250
200
150
100
50
0
Cumulative Oil and Water Production (cm3)
25000
20000
15000
10000
5000
0
Cumulative Gas Production (cm3)
0
2
4
6
8
10
Time (hours)
Oil
Water
Gas

Figure 4.31: GOR and Water Cut, First Production Cycle
Experiment #4

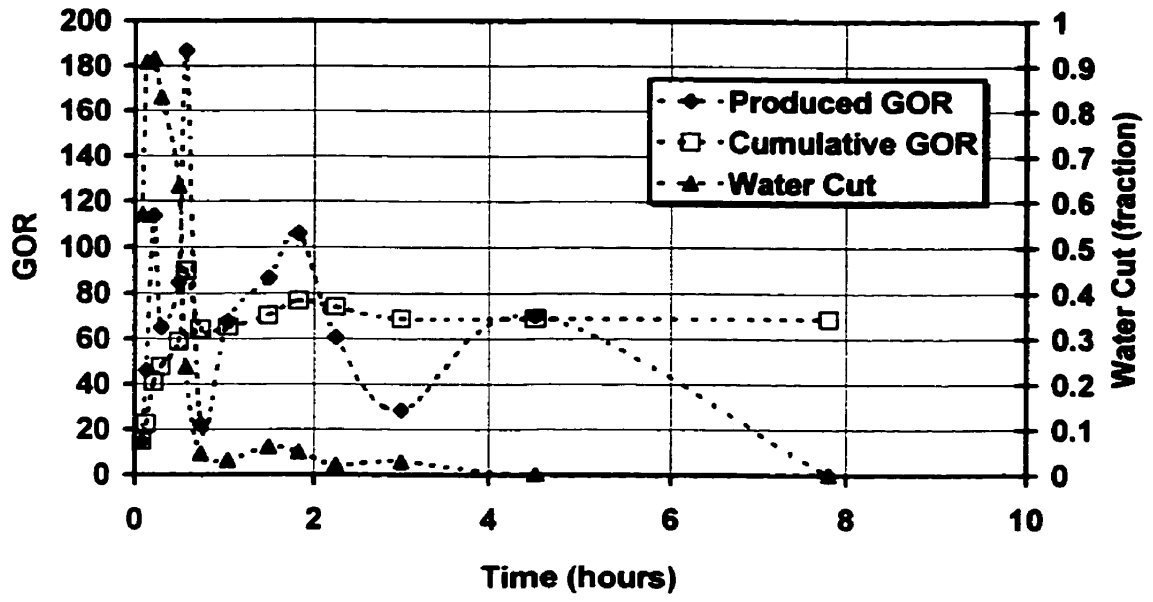

Figure 4.32: Cumulative Production, Second Production
Experiment #4
Flood with 2 % brine, Recovery = 21.5 % OOIP

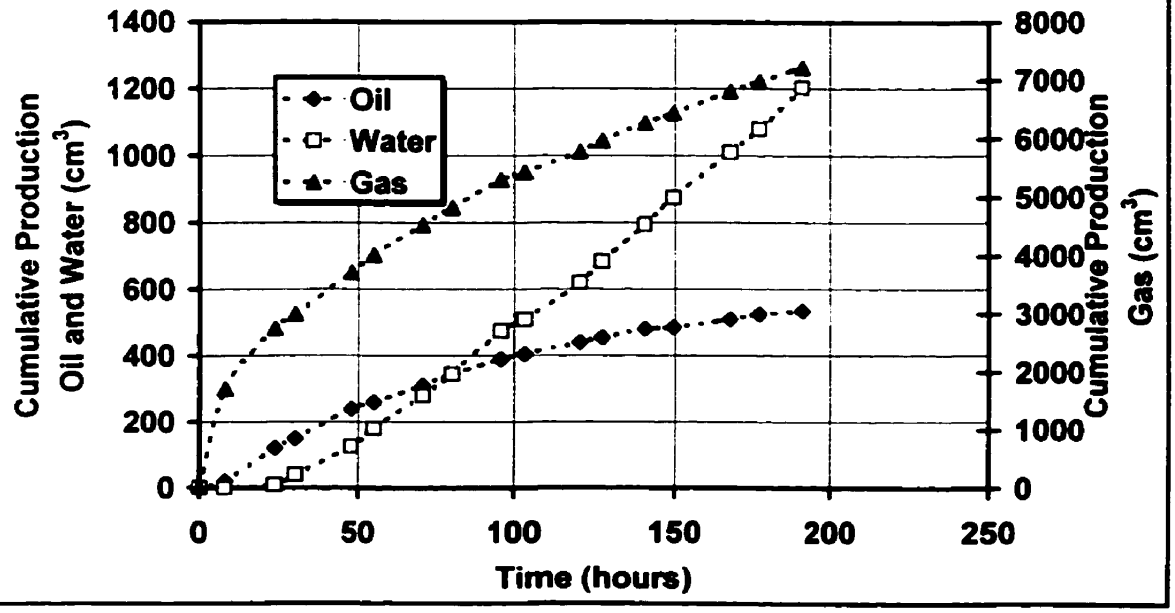

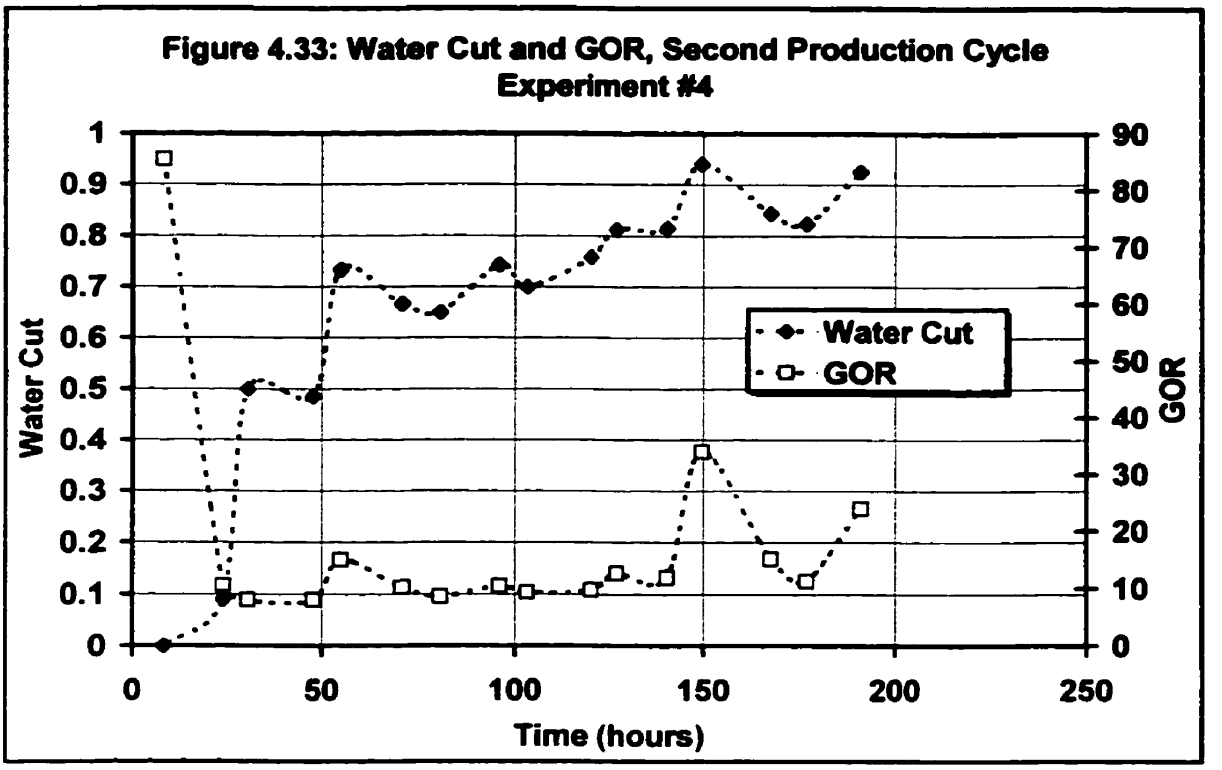

Figure 4.33: Water Cut and GOR, Second Production Cycle Experiment #4

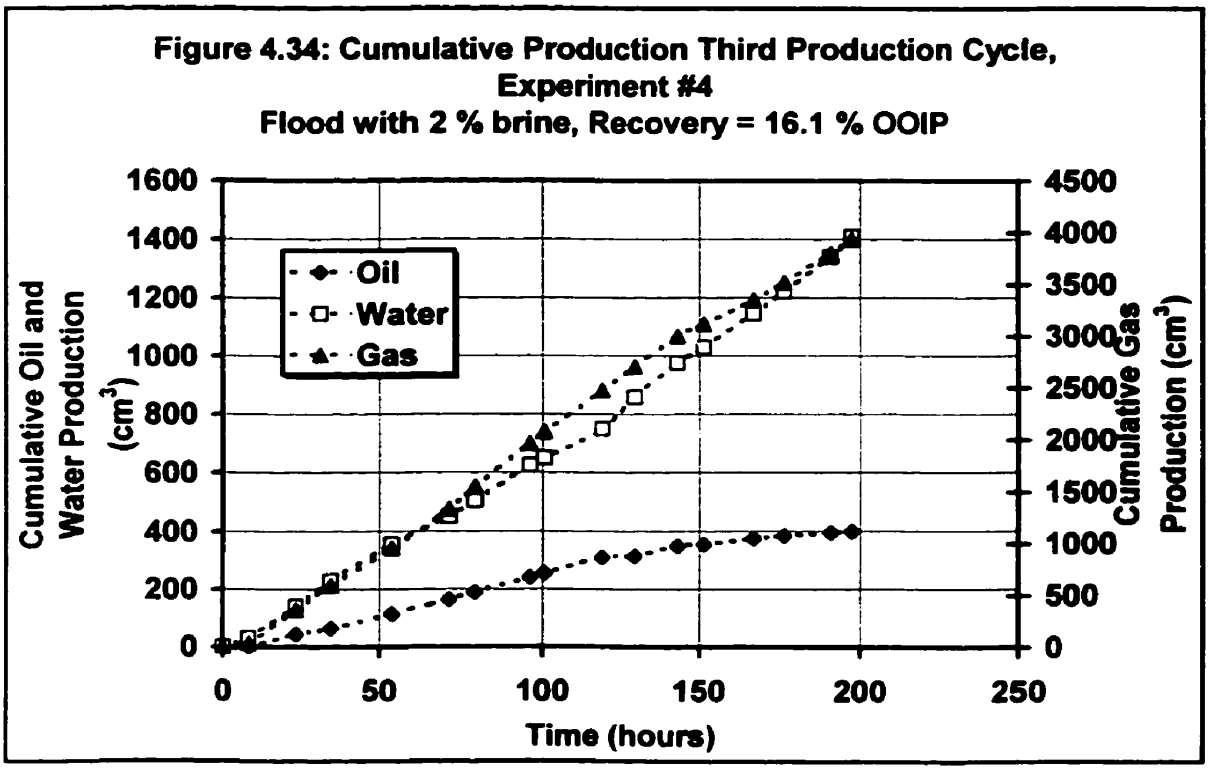

Figure 4.34: Cumulative Production Third Production Cycle, Experiment #4
Flood with 2 % brine, Recovery = 16.1 % OOIP

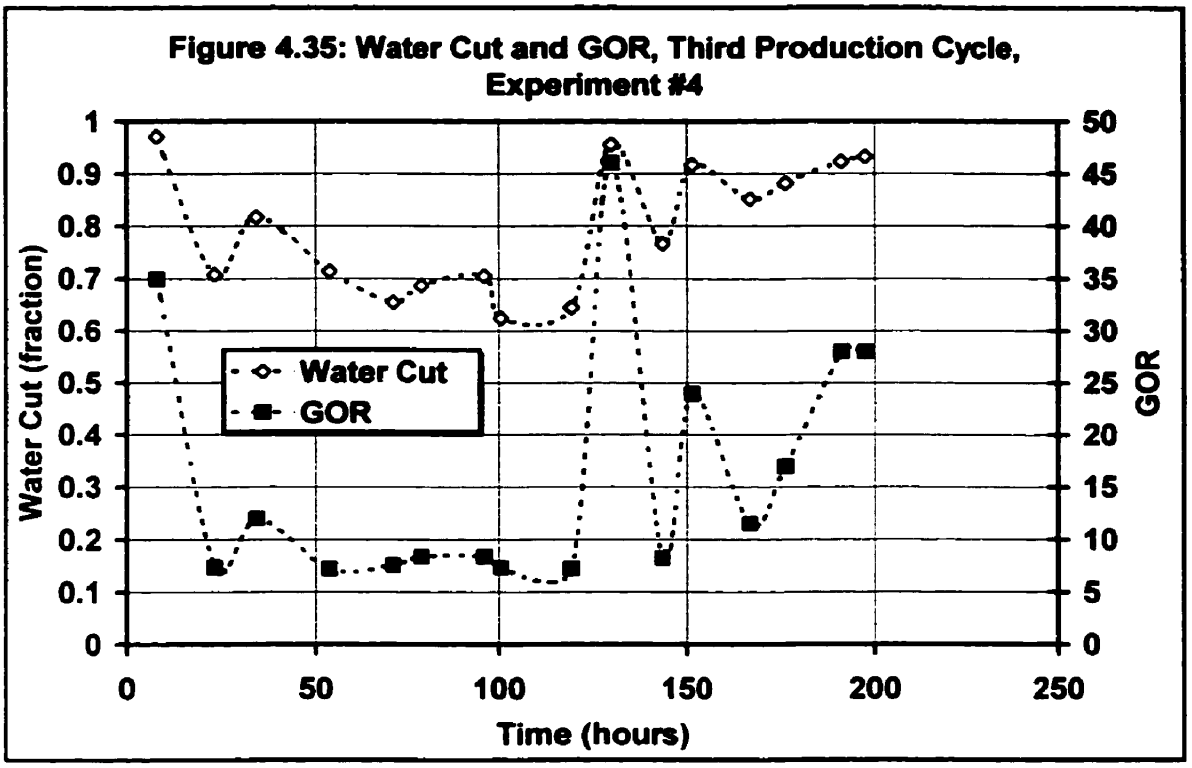

Figure 4.35: Water Cut and GOR, Third Production Cycle, Experiment #4

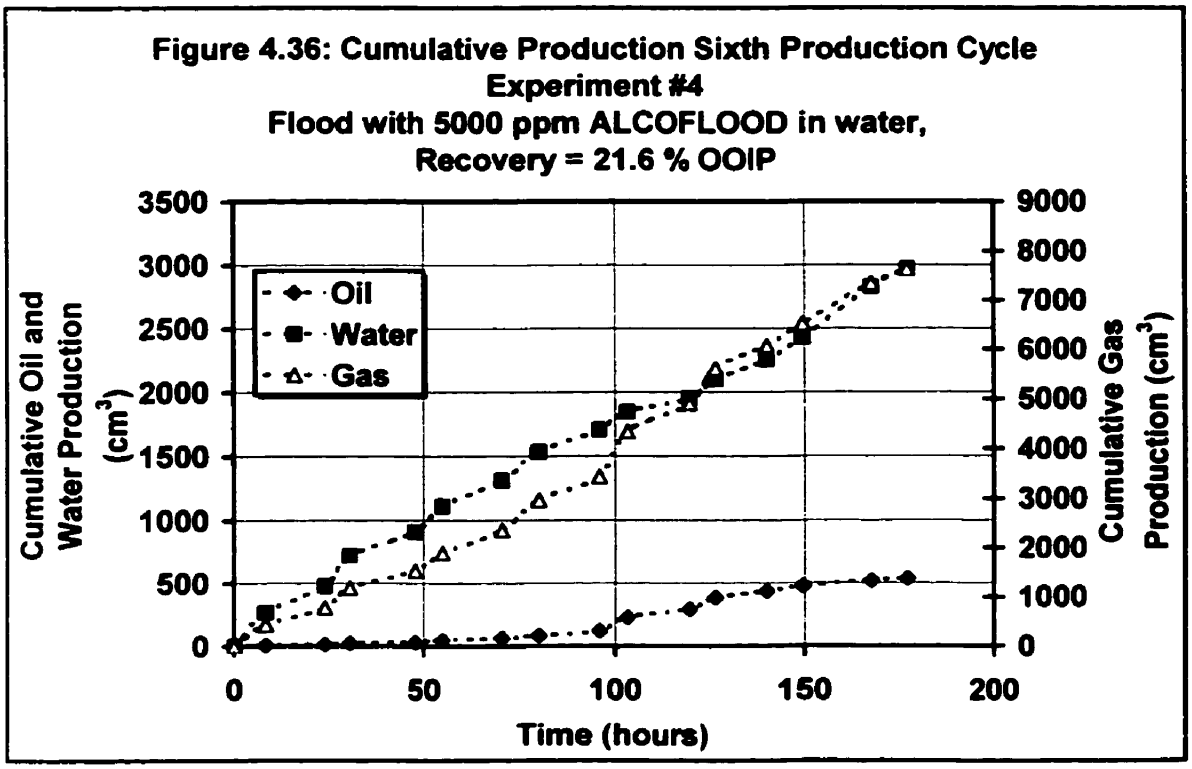

Figure 4.36: Cumulative Production Sixth Production Cycle Experiment #4 Flood with 5000 ppm ALCOFLOOD in water, Recovery = 21.6 % OOIP

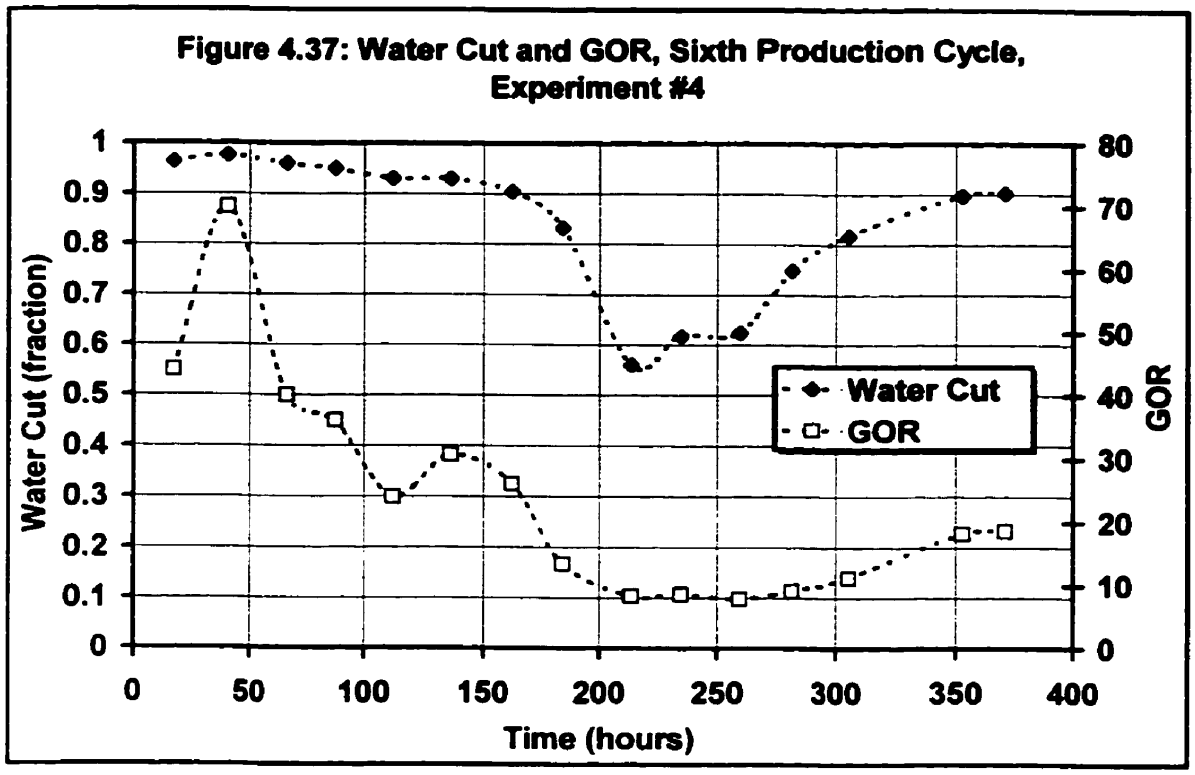
Figure 4.37: Water Cut and GOR, Sixth Production Cycle, Experiment #4
Water Cut (fraction)
GOR
Time (hours)
Water Cut
GOR
0
0.1
0.2
0.3
0.4
0.5
0.6
0.7
0.8
0.9
1
0
10
20
30
40
50
60
70
80
0
50
100
150
200
250
300
350
400

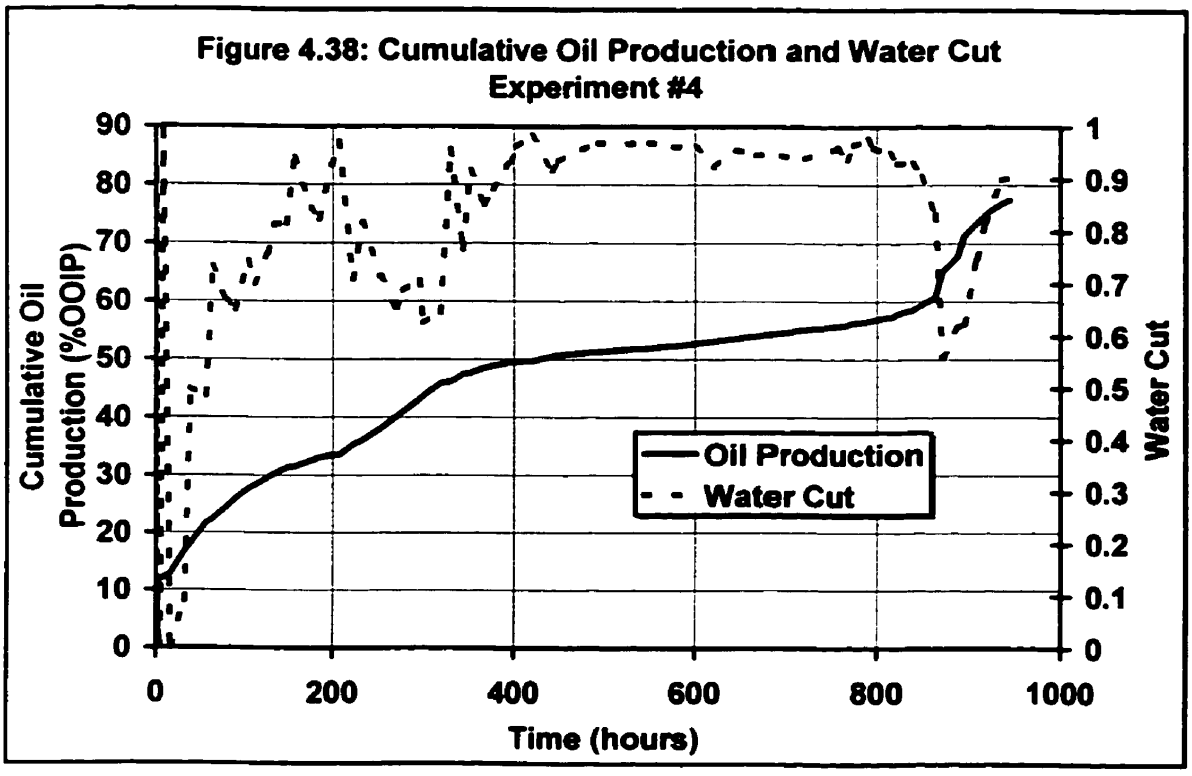
Figure 4.38: Cumulative Oil Production and Water Cut Experiment #4
Cumulative Oil Production (%OOIP)
Water Cut
Time (hours)
Oil Production
Water Cut
0
10
20
30
40
50
60
70
80
90
0
0.1
0.2
0.3
0.4
0.5
0.6
0.7
0.8
0.9
1
0
200
400
600
800
1000

Figure 4.39: GOR, Experiment #4

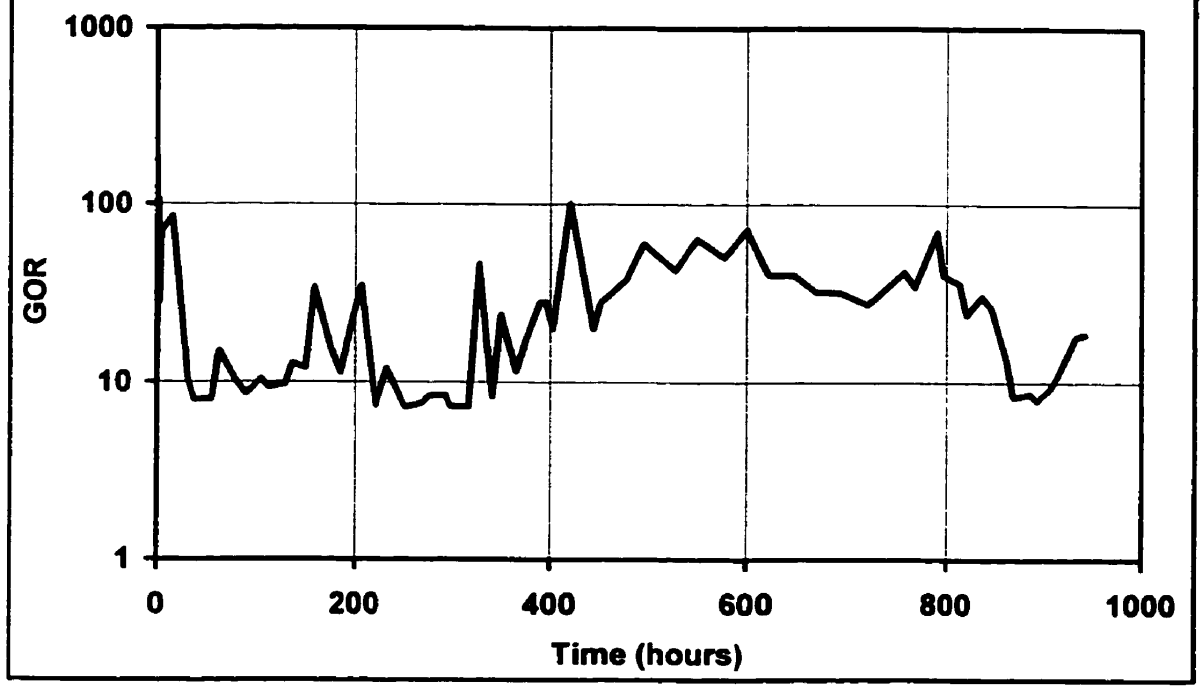

Figure 4.40: Cumulative Production, First Production Cycle, Experiment #5
Flood with 2 % brine, Recovery = 16.3 % OOIP

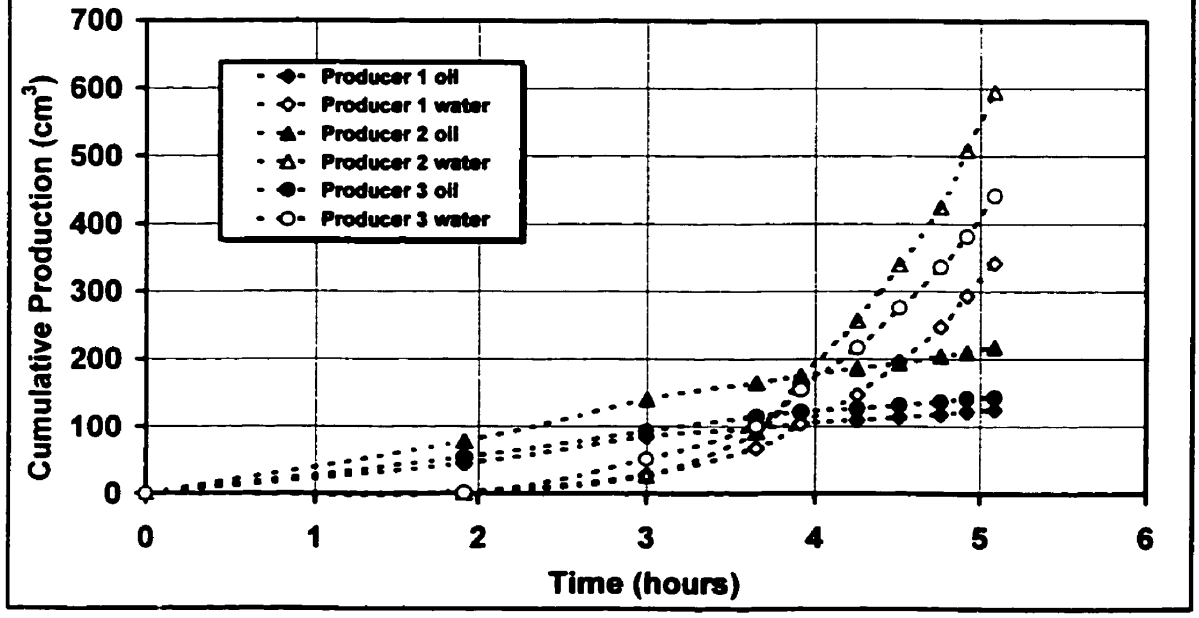

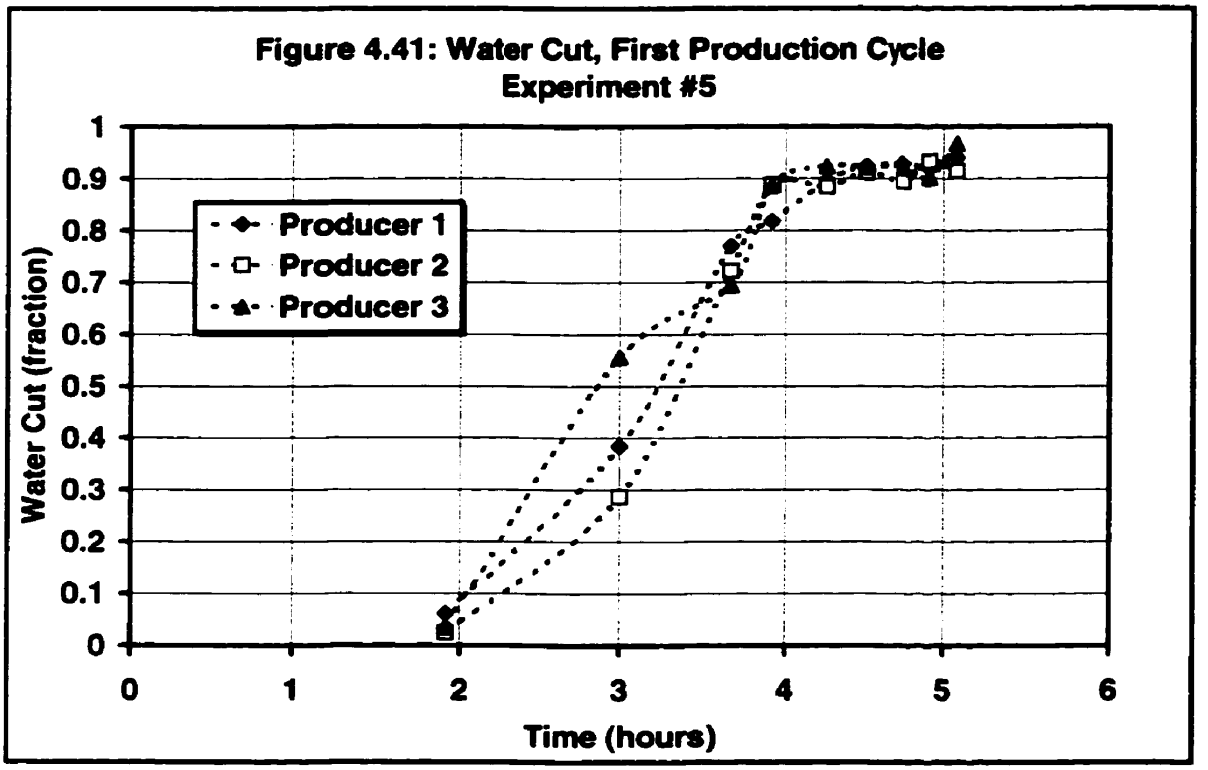

Figure 4.42: Image of Ambient Model #2 After First Water Flood

Figure 4.43: Cumulative Production Second Production Cycle, Experiment #5
Flood with 2 % brine, Recovery = 4.6 % OOIP

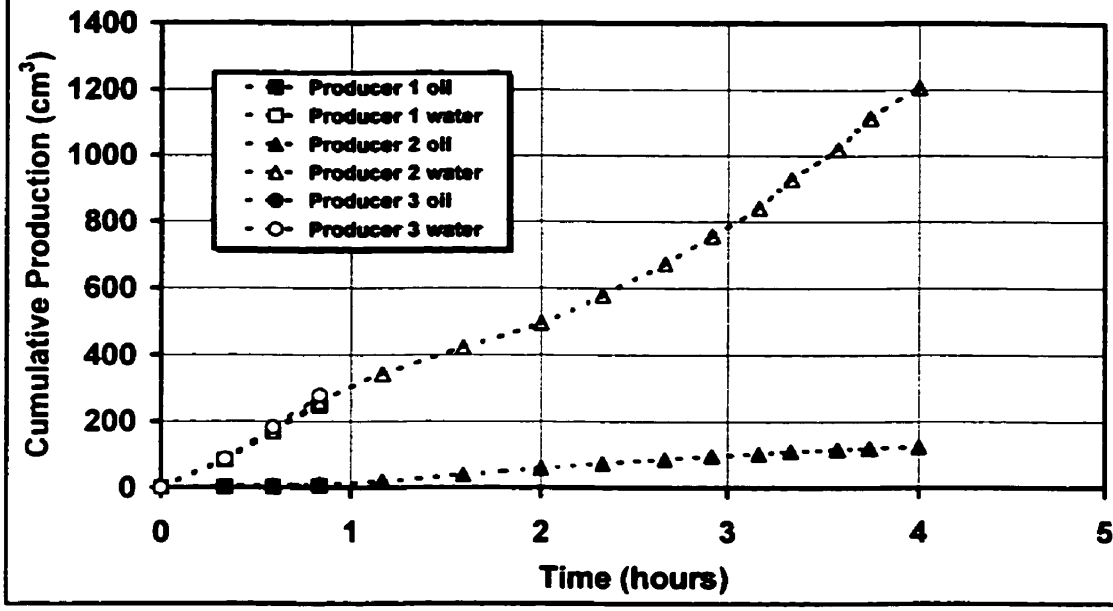

Figure 4.44: Water Cut, Second Production Cycle, Experiment #5

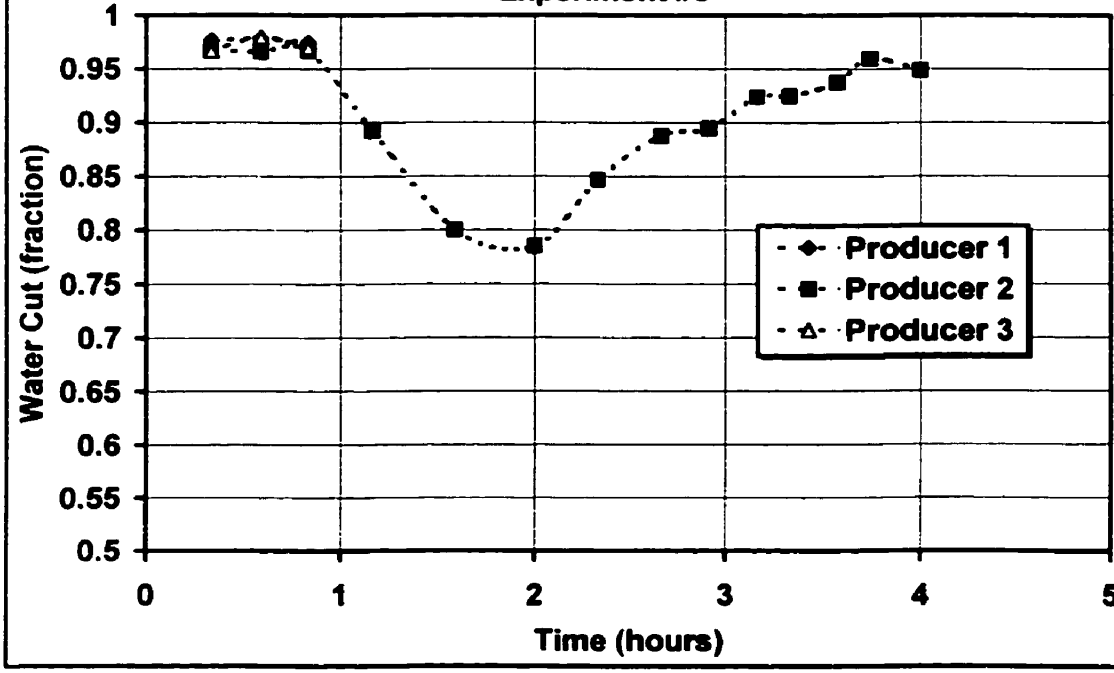

Figure 4.45: Image of Ambient Model #2 After Second Water Flood

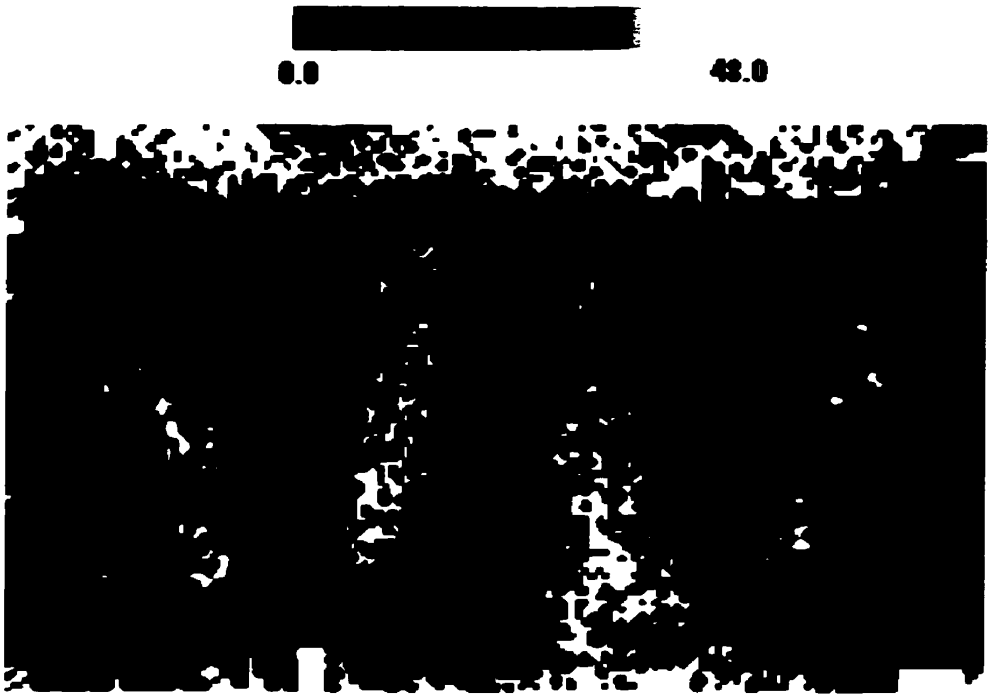

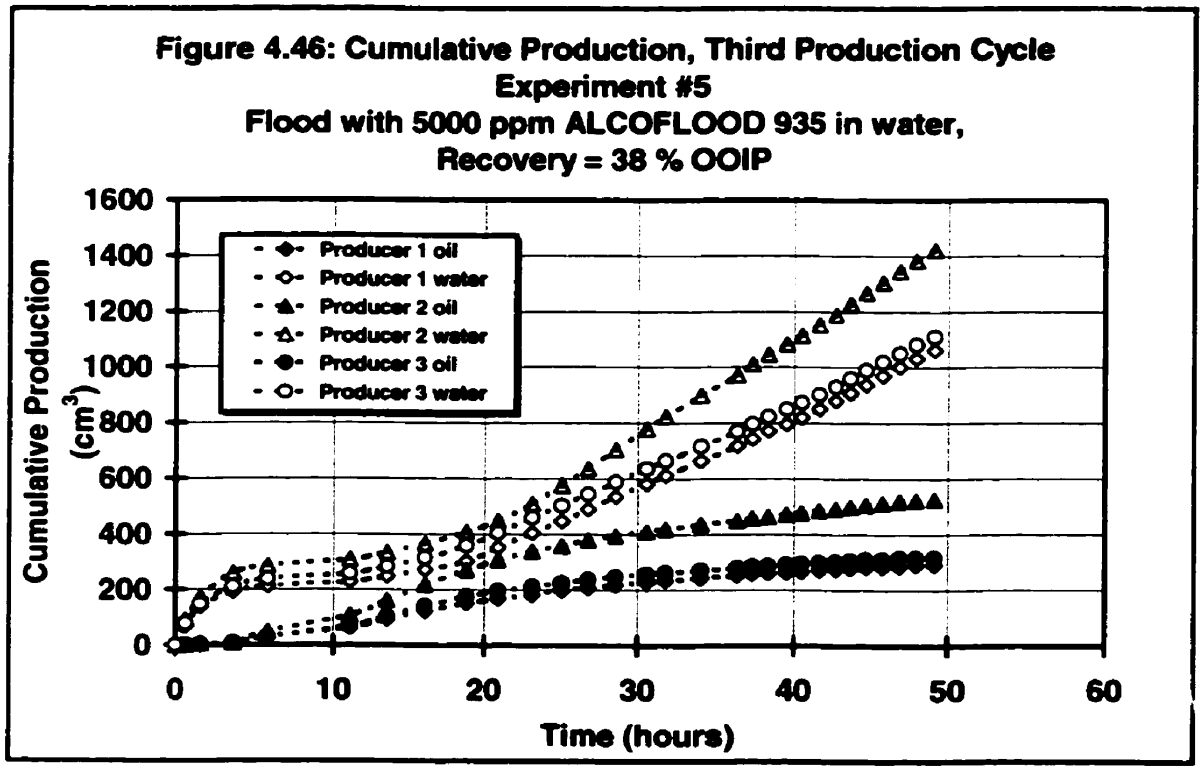

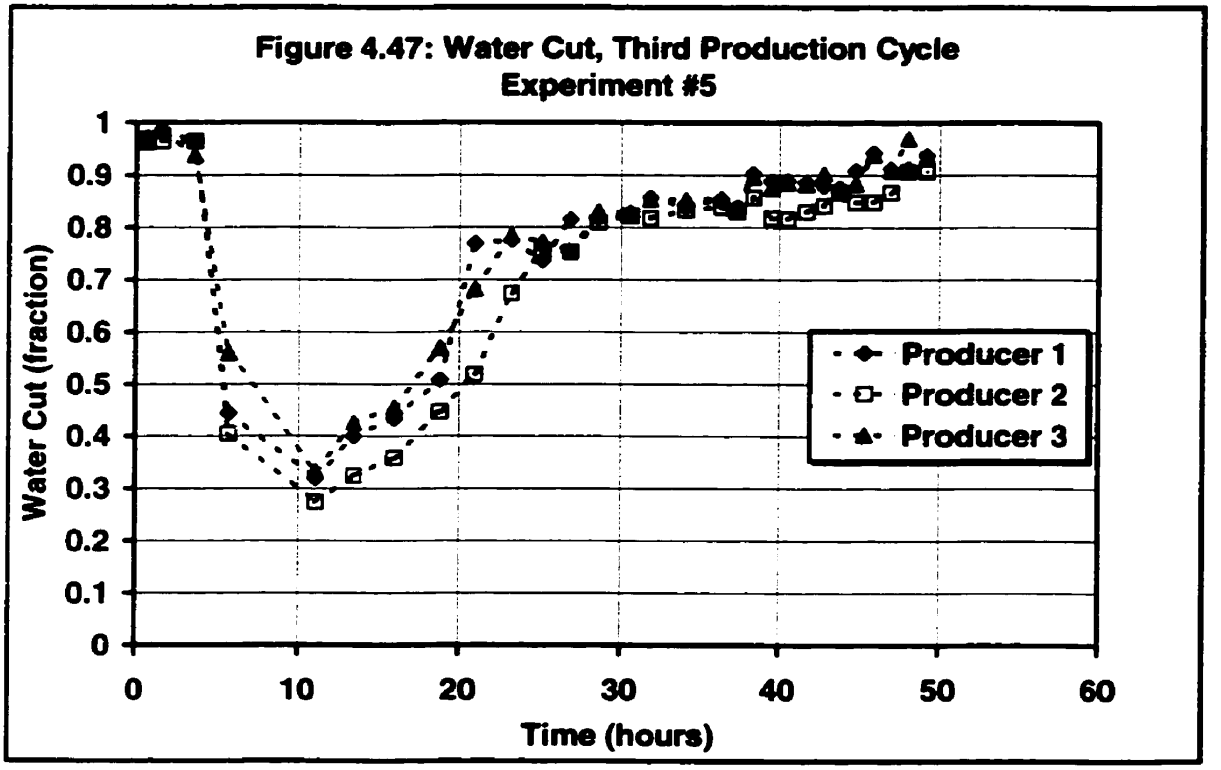

Figure 4.48: Image of Ambient Model #2 at 4.5 hours into Polymer Flood

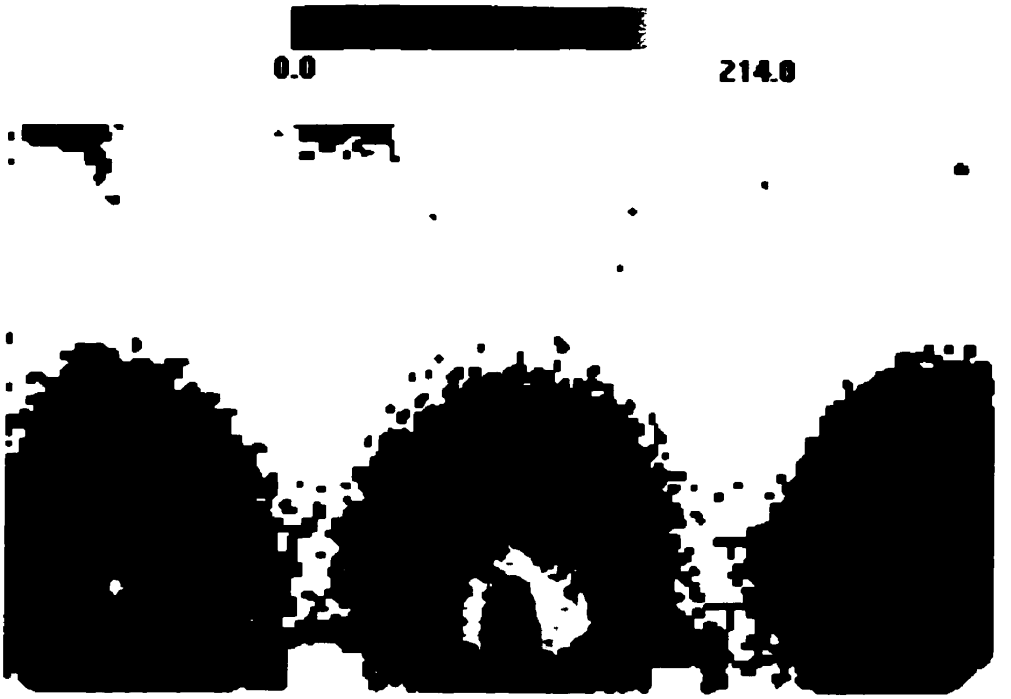

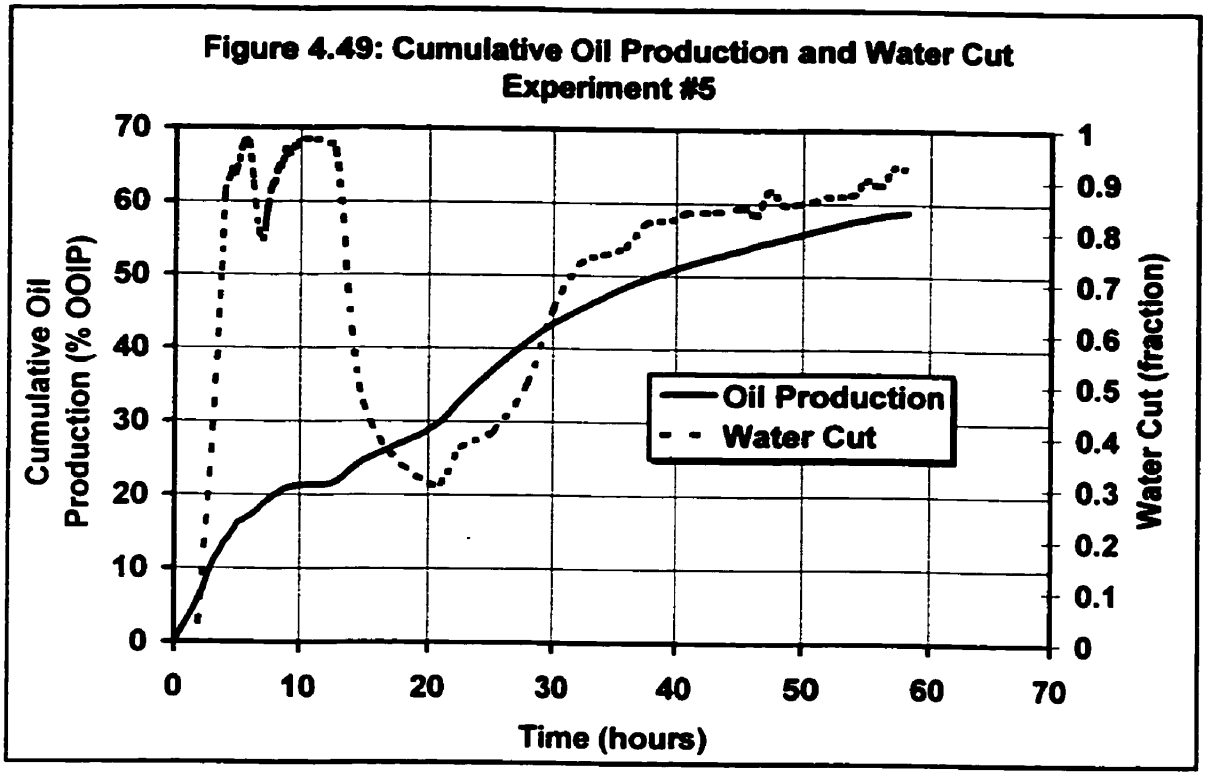
Figure 4.49: Cumulative Oil Production and Water Cut
Experiment #5
Cumulative Oil Production (% OOIP)
Water Cut (fraction)
Time (hours)
Oil Production
Water Cut
0
10
20
30
40
50
60
70
0
0.1
0.2
0.3
0.4
0.5
0.6
0.7
0.8
0.9
1

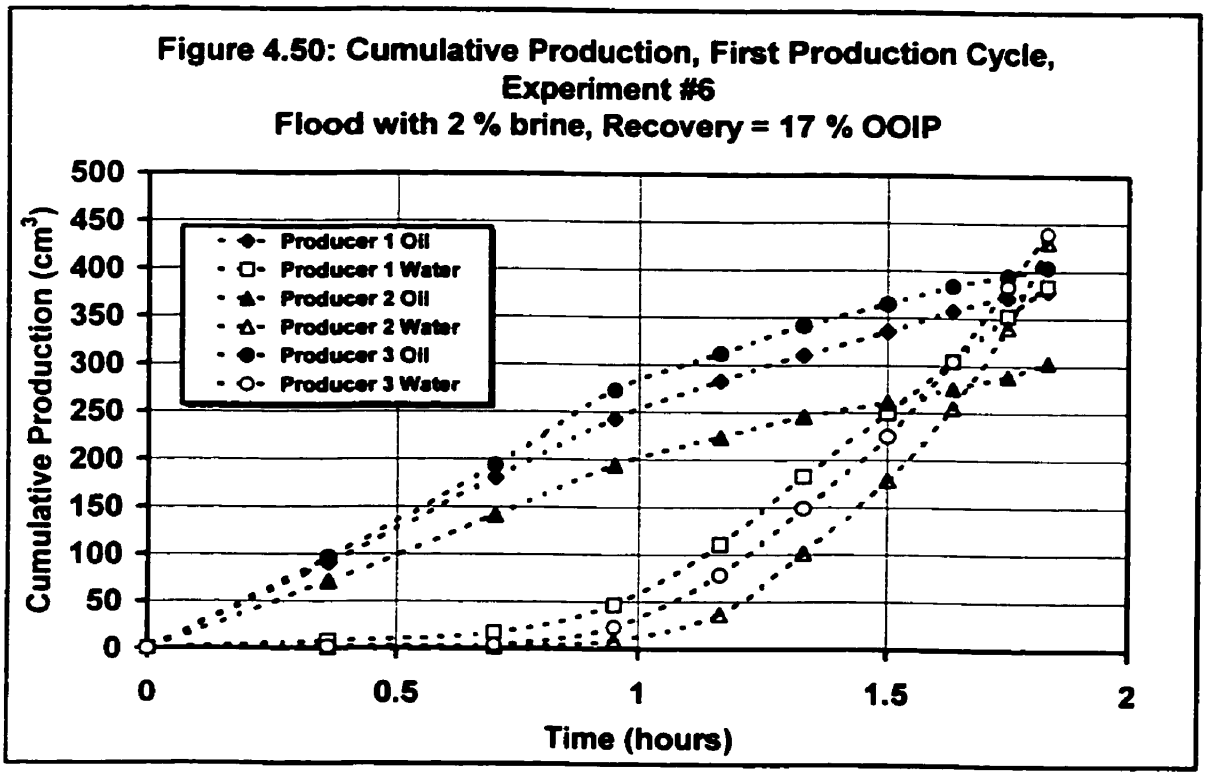
Figure 4.50: Cumulative Production, First Production Cycle,
Experiment #6
Flood with 2 % brine, Recovery = 17 % OOIP
Cumulative Production (cm3)
Time (hours)
Producer 1 Oil
Producer 1 Water
Producer 2 Oil
Producer 2 Water
Producer 3 Oil
Producer 3 Water
0
50
100
150
200
250
300
350
400
450
500
0
0.5
1
1.5
2

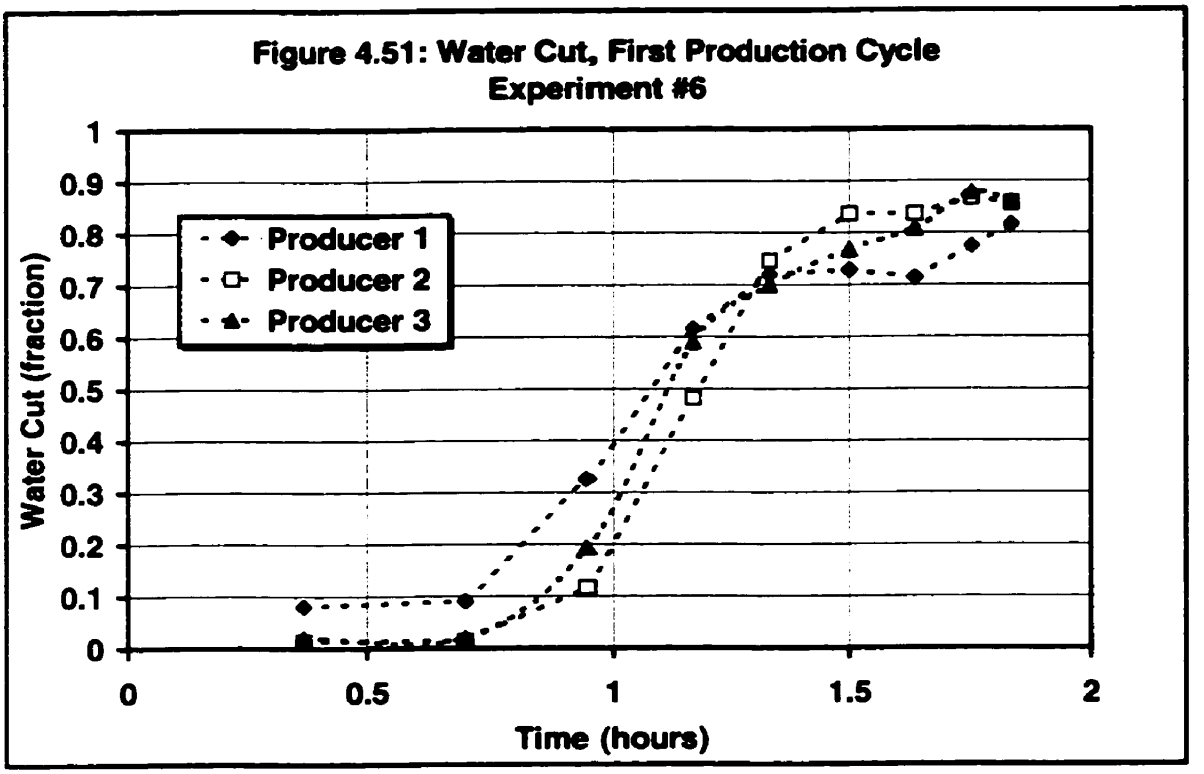

Figure 4.52: Image of Ambient Model #1 After First Water Flood

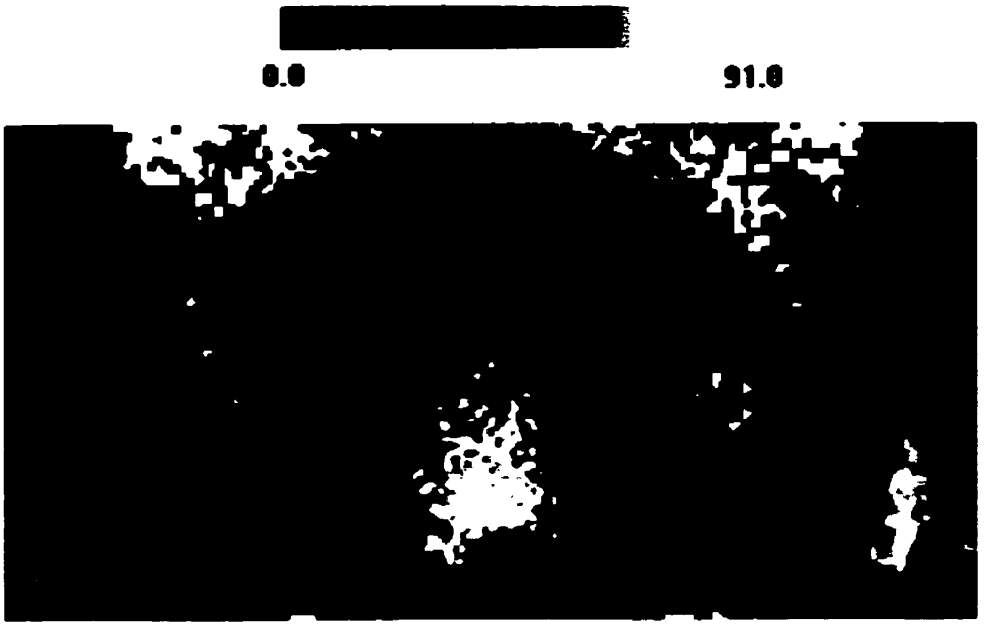

Figure 4.53: Polymer Solution Viscosity vs. Shear Rate
ALCOFLOOD 1275A in brine and ALCOFLOOD 935 in water

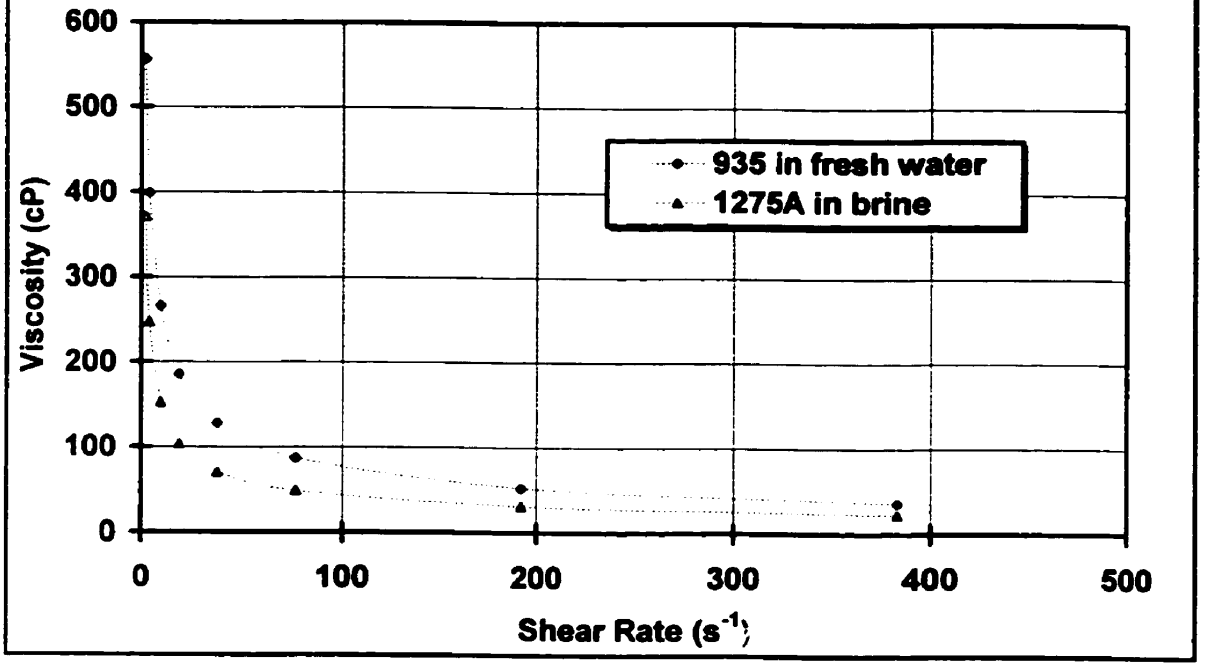

Figure 4.54: Cumulative Production, Second Production Cycle Experiment #6
Flood with 5000 ppm ALCOFLOOD 1275A in 2 % brine
Recovery = 46.1 % OOIP

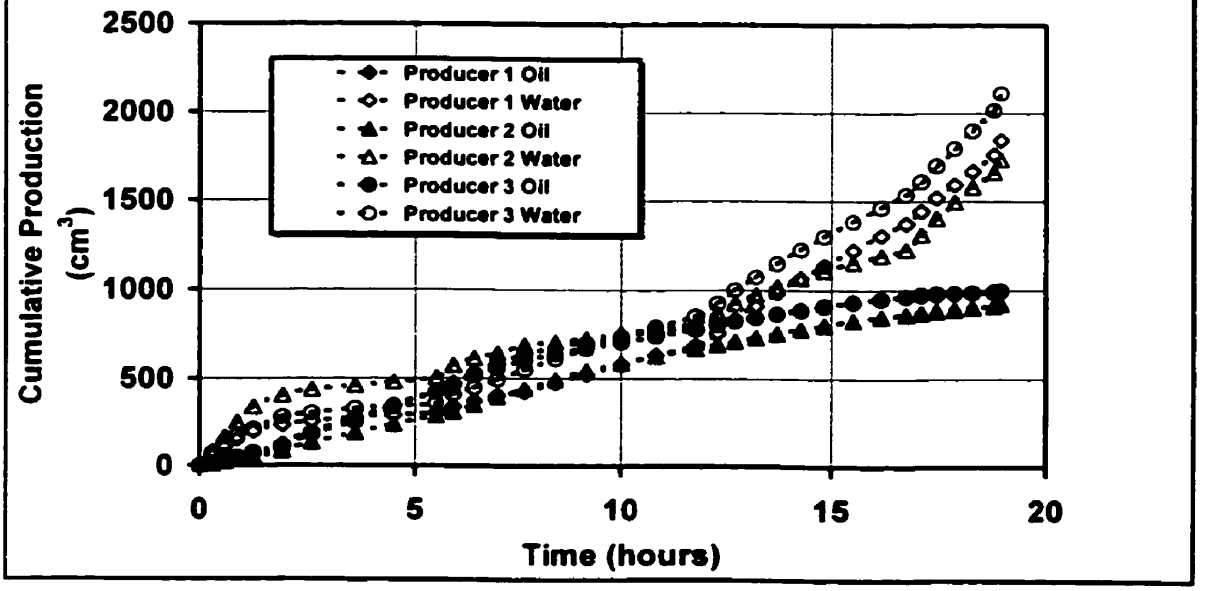

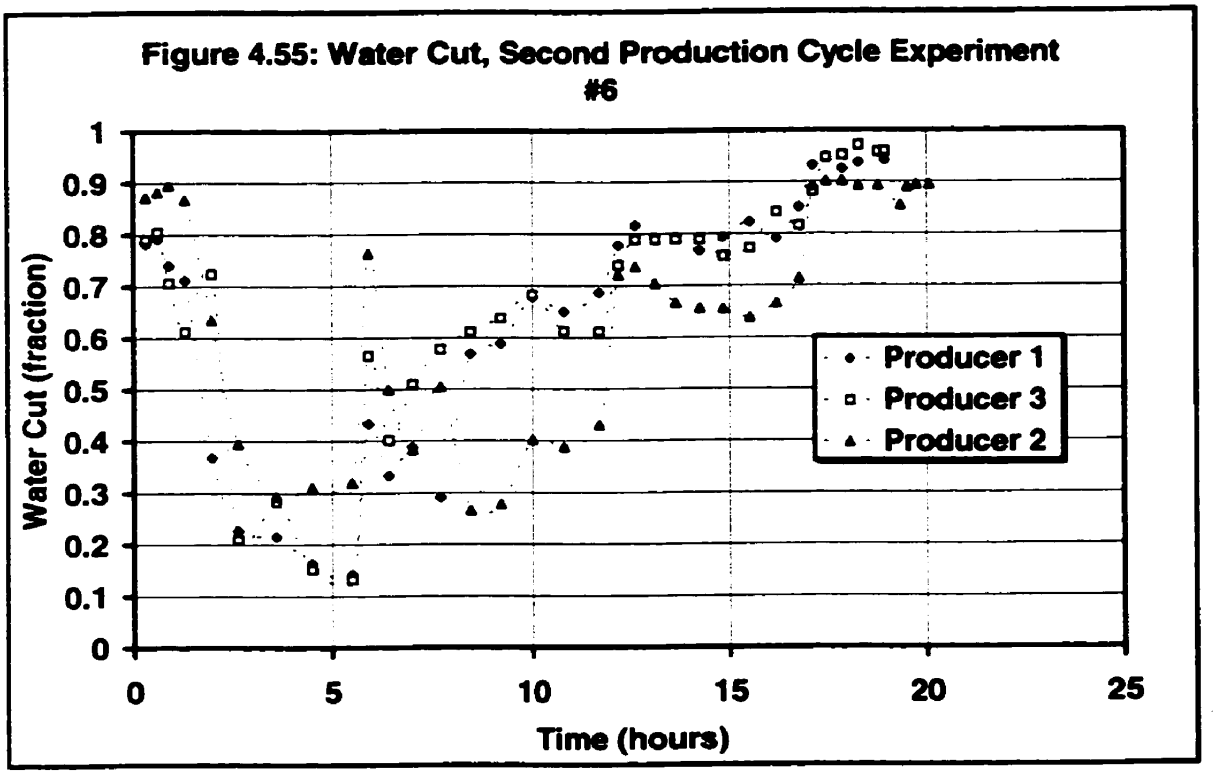

Figure 4.56: Image of Ambient Model #1 5 hours into Polymer Flood

Figure 4.57: Cumulative Oil Production and Water Cut, Experiment #6

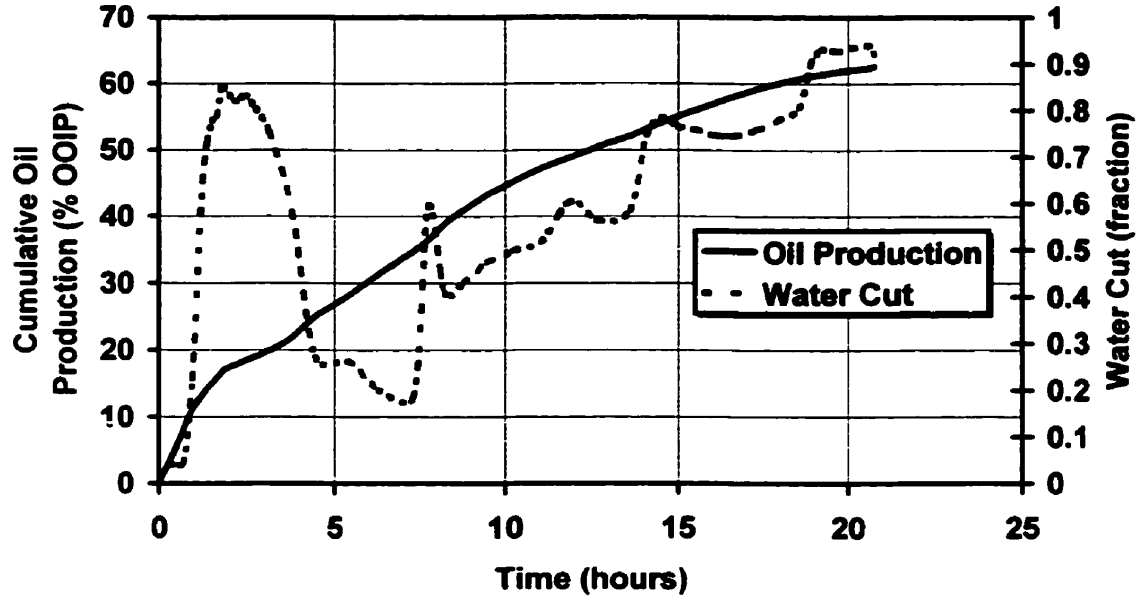

Figure 4.58:Cumulative Production, First Production Cycle
Experiment #7
Flood with 2 % Brine, Recovery 11.4 % OOIP

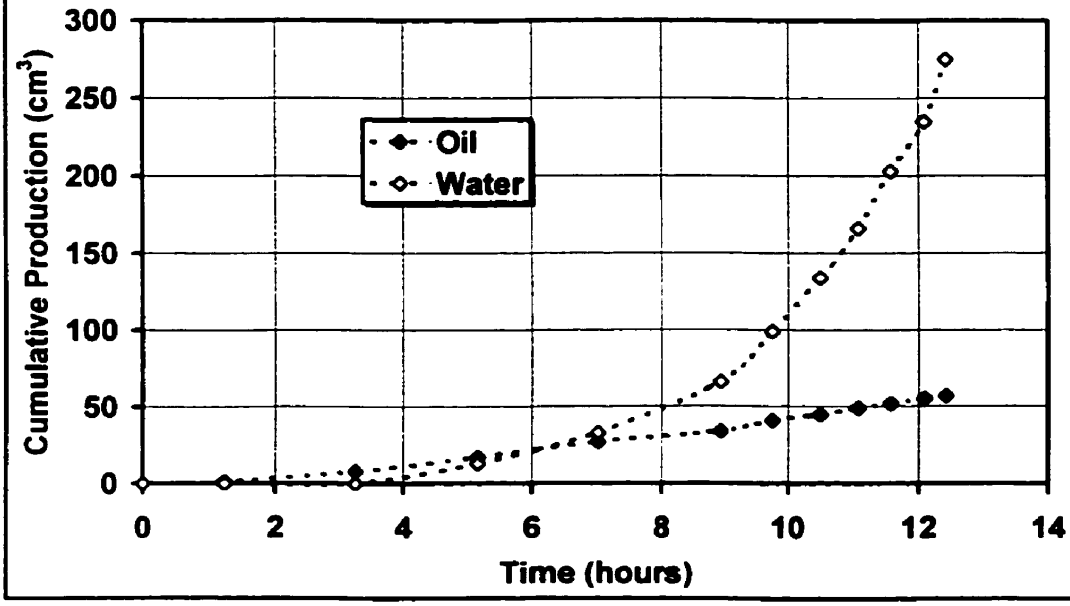

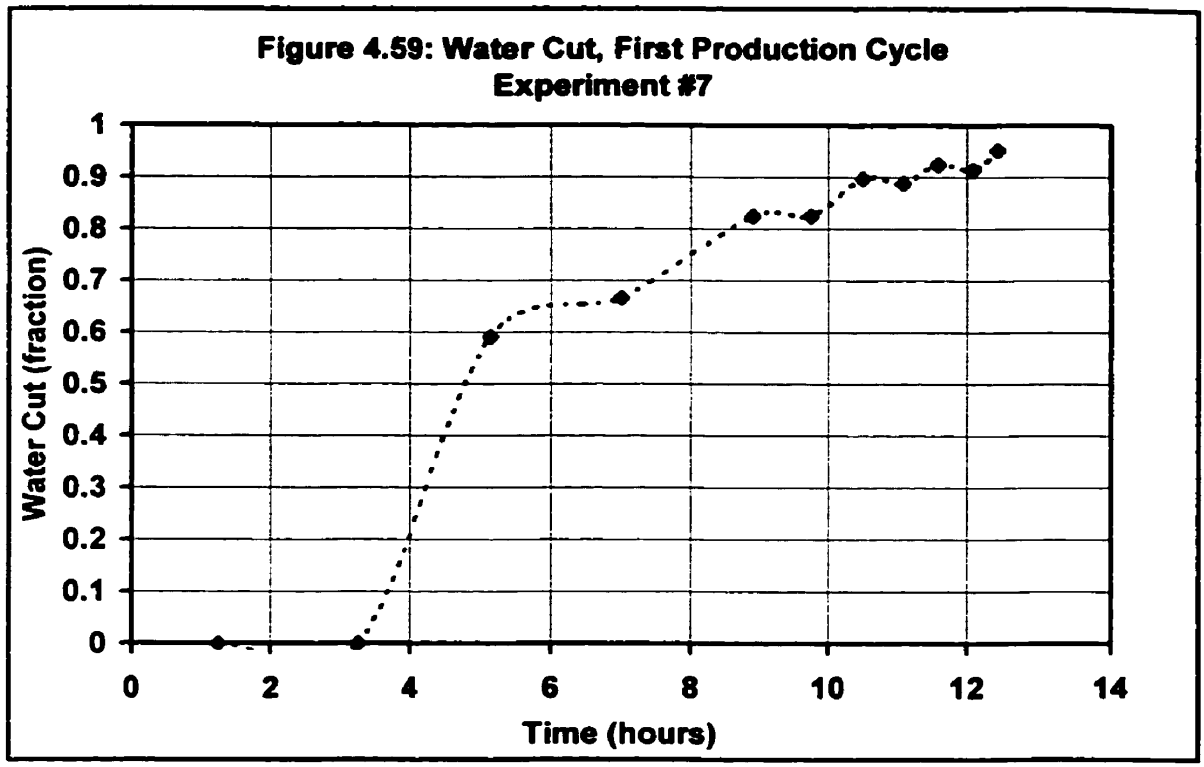
Figure 4.59: Water Cut, First Production Cycle
Experiment #7
Water Cut (fraction)
1
0.9
0.8
0.7
0.6
0.5
0.4
0.3
0.2
0.1
0
0
2
4
6
8
10
12
14
Time (hours)

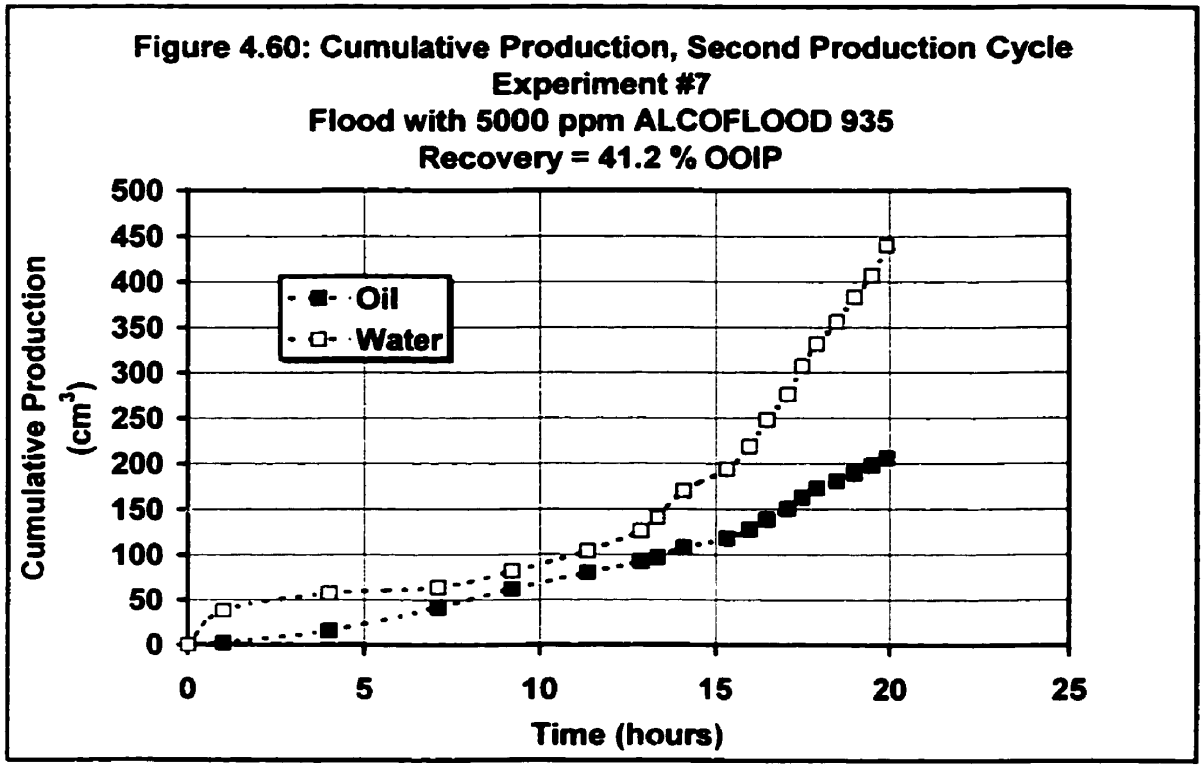
Figure 4.60: Cumulative Production, Second Production Cycle
Experiment #7
Flood with 5000 ppm ALCOFLOOD 935
Recovery = 41.2 % OOIP
Cumulative Production (cm3)
500
450
400
350
300
250
200
150
100
50
0
Oil
Water
0
5
10
15
20
25
Time (hours)

Figure 4.61: Water Cut, Second Production Cycle Experiment #7

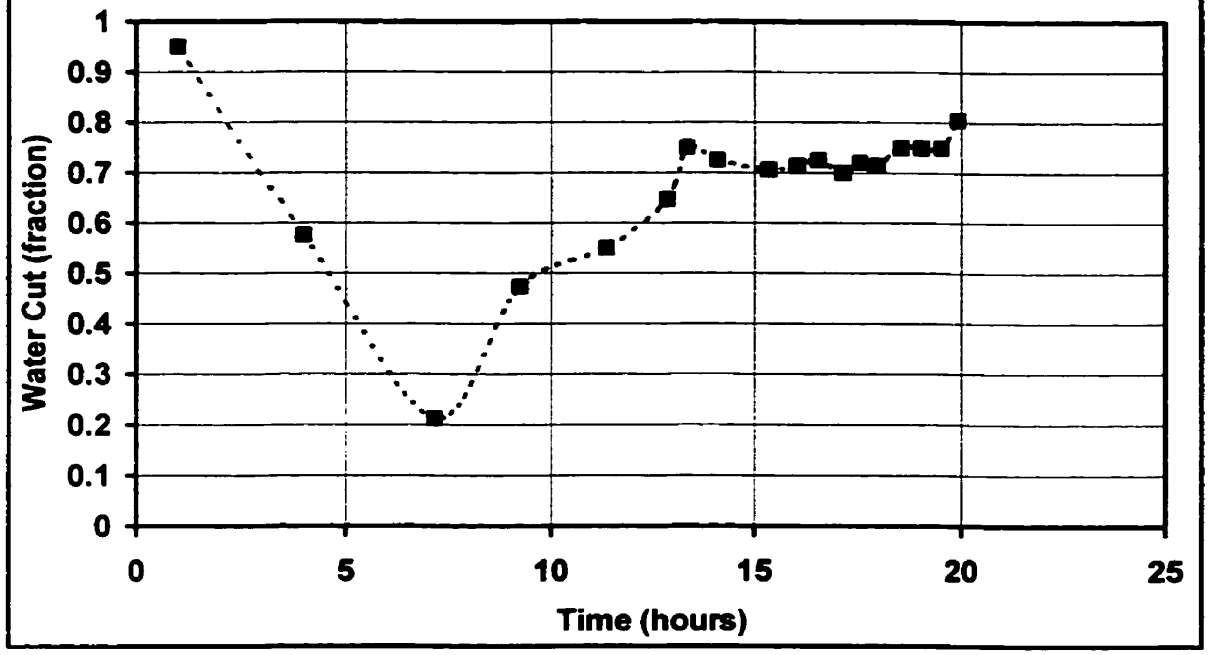

Figure 4.62: Saturation vs. Time, Second Production Cycle Experiment #7

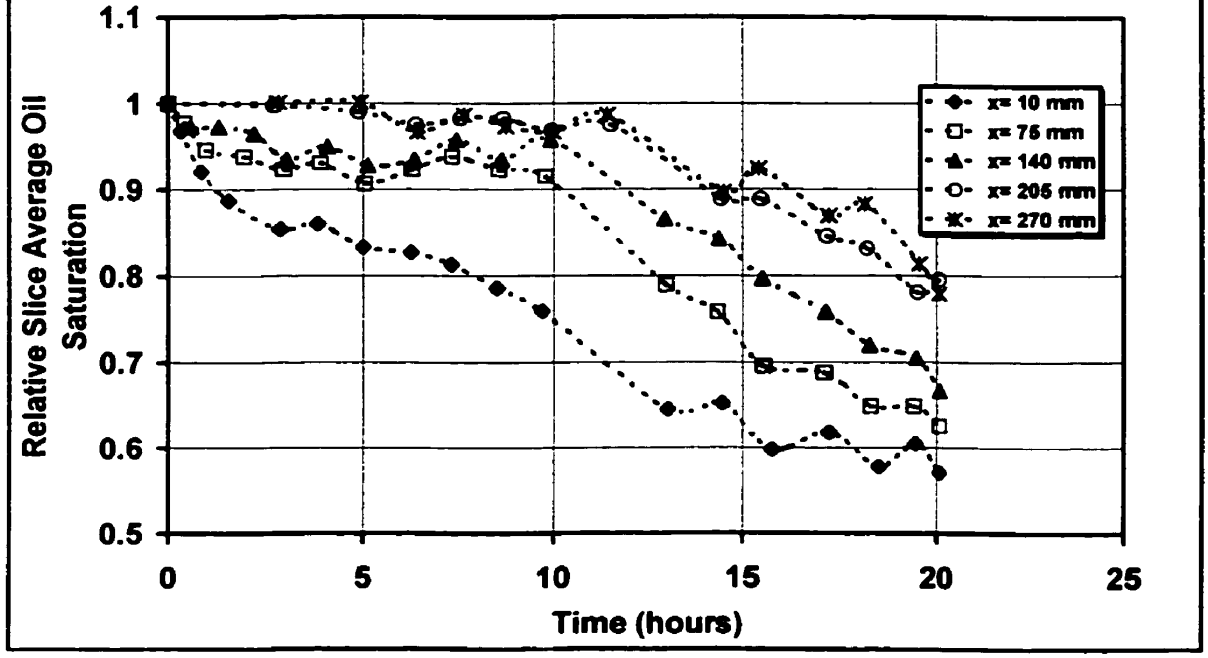

Figure 4.63: Images of Aluminum Core Holder During Polymer Flood at 75 mm from Injection Plate

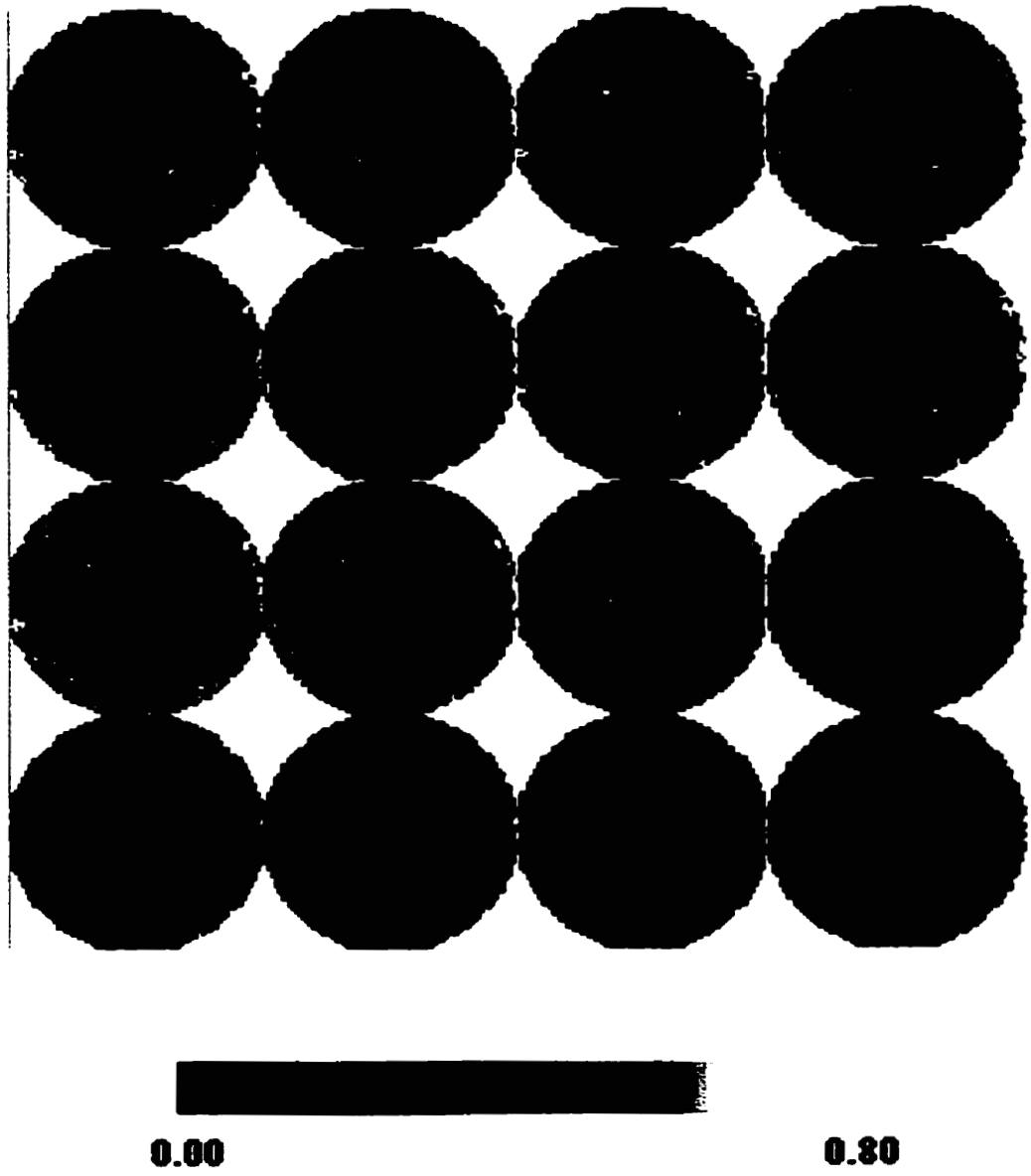

Figure 4.64: Cumulative Oil Production and Water Cut
Experiment #7

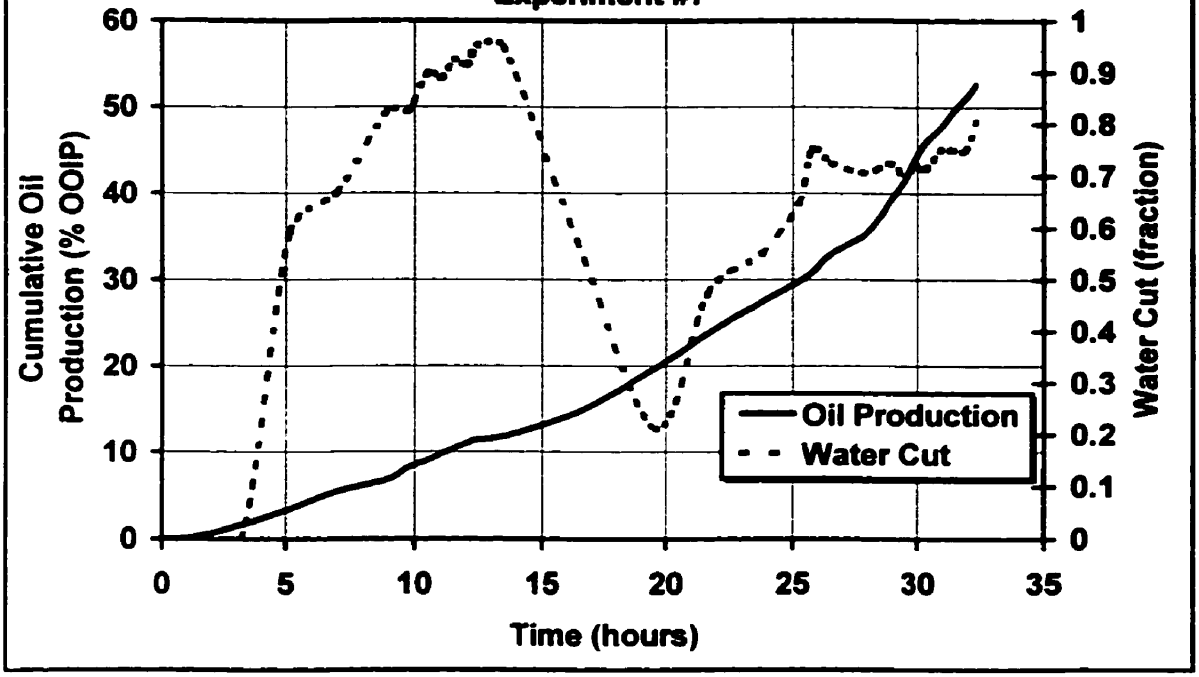

Figure 4.65: Cumulative Production, First Production Cycle
Experiment #8 (initial 2 minutes)
Primary Production, Recovery = 23.9 % OOIP

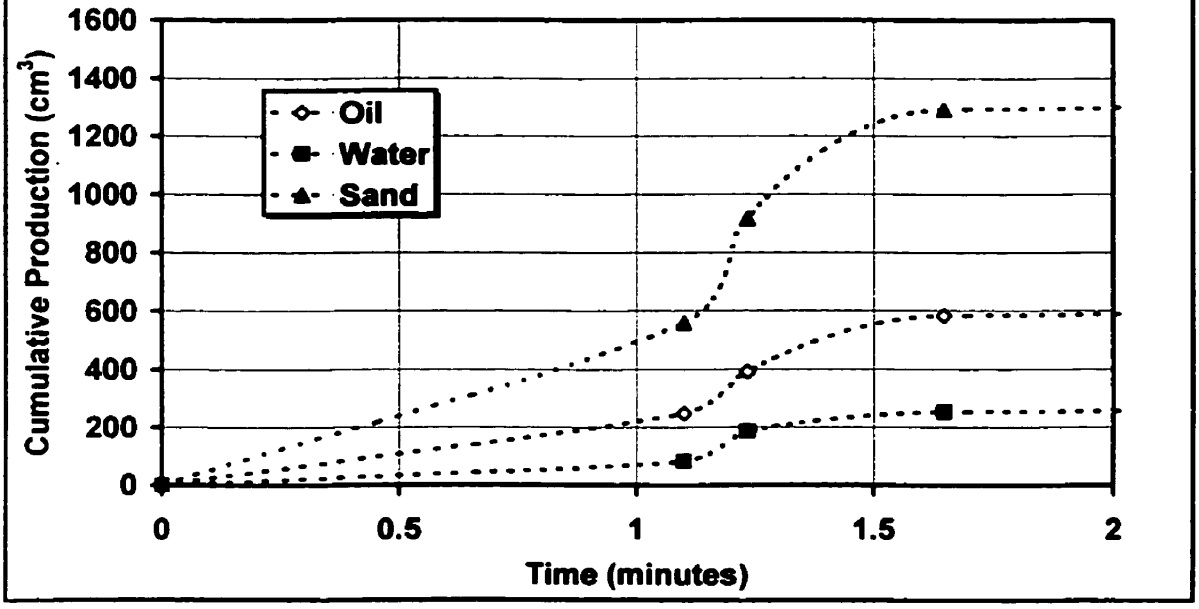

Figure 4.66: Cumulative Production, Second Production Cycle
Experiment #8
Flood with 2 % Brine, Recovery = 12.4 % OOIP

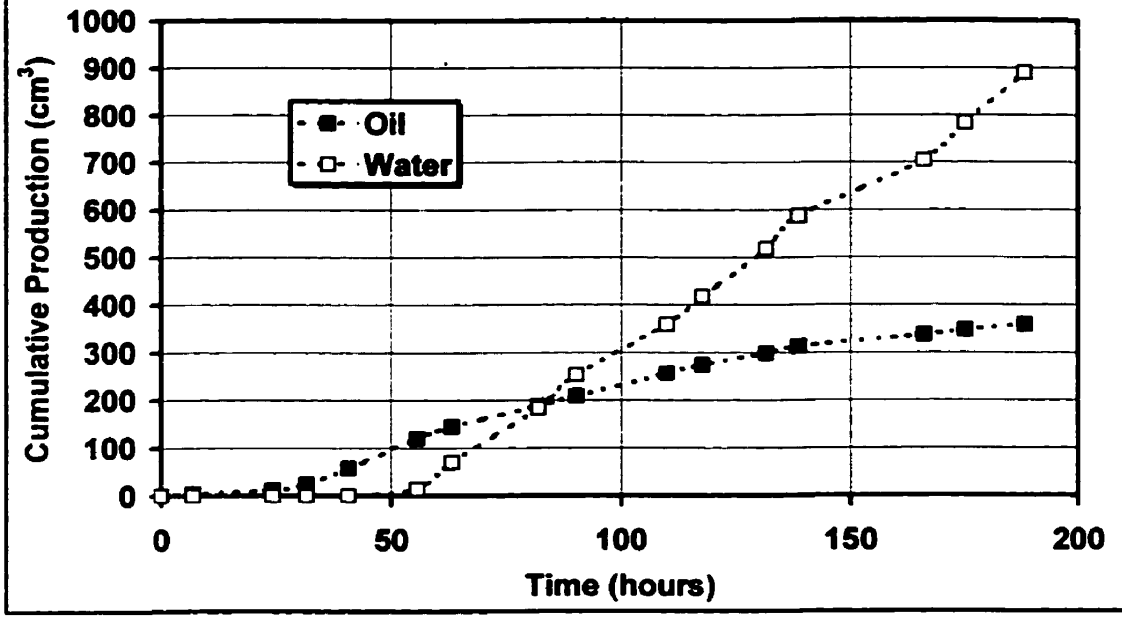

Figure 4.67: Water Cut, Second Production Cycle
Experiment #8

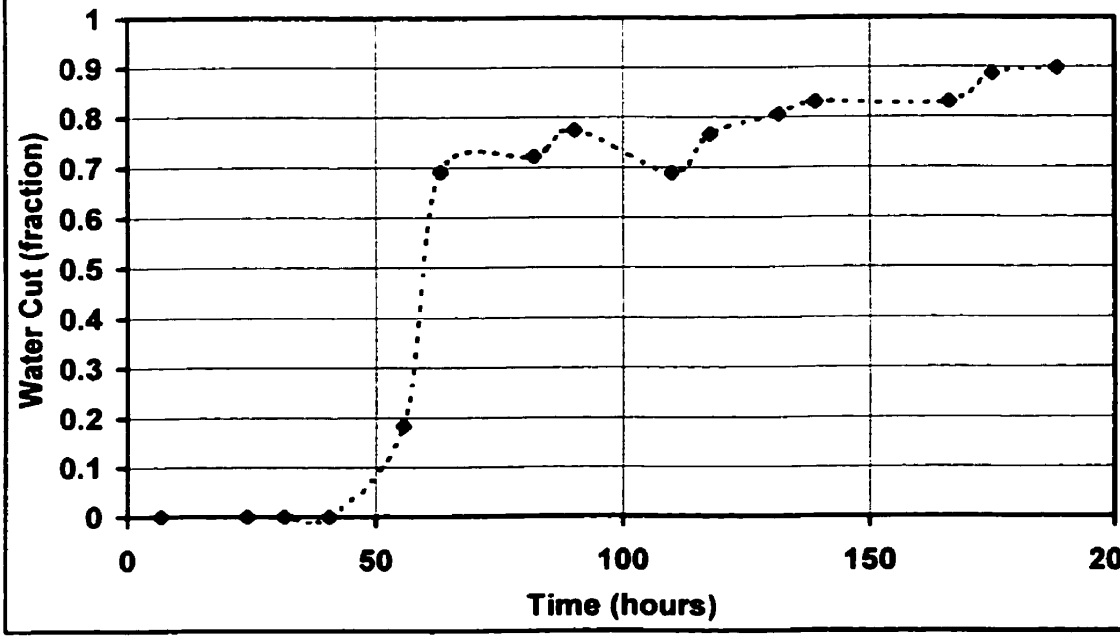

Figure 4.68: Cumulative Production, Fourth Production Cycle
Experiment #8
Flood with 5000 ppm ALCOFLOOD 935
Recovery = 24.1 % OOIP

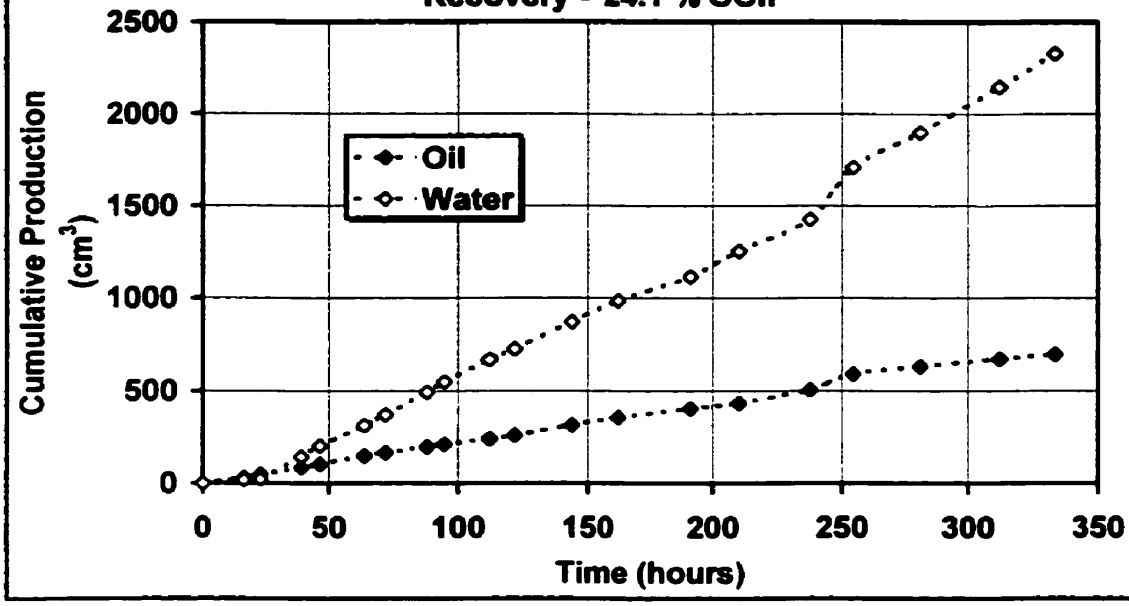

Figure 4.69: Water Cut, Fourth Production Cycle
Experiment #8

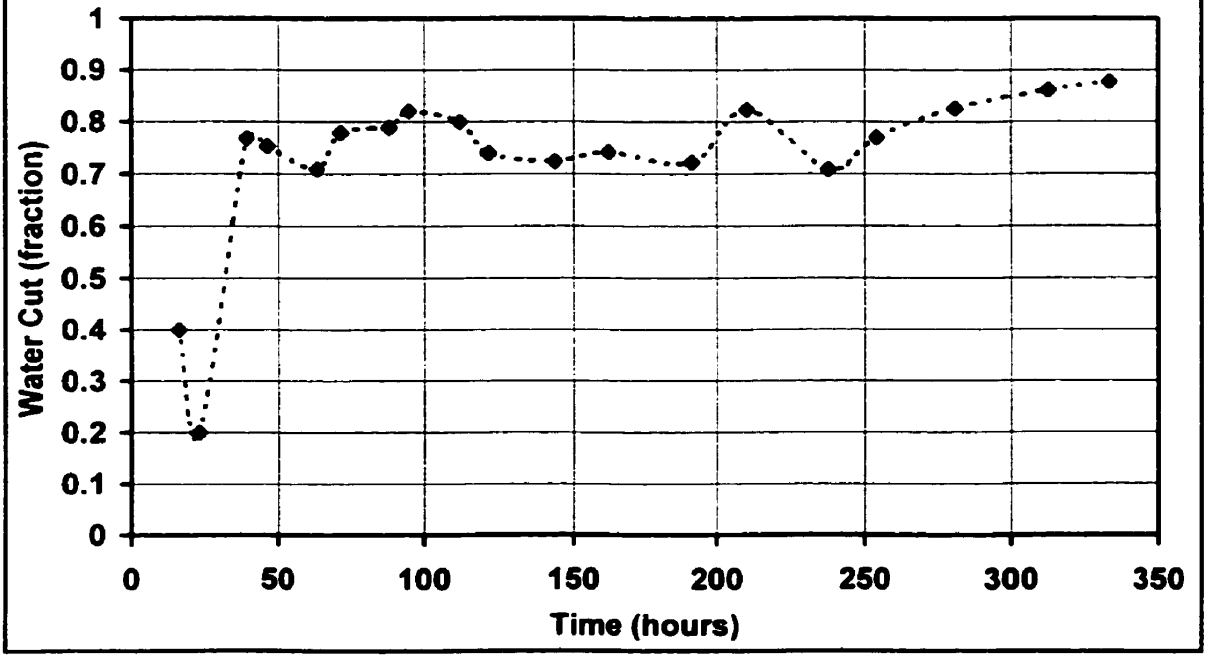

Figure 4.70: X-ray Image of Reservoir Model #1 After Experiment #8

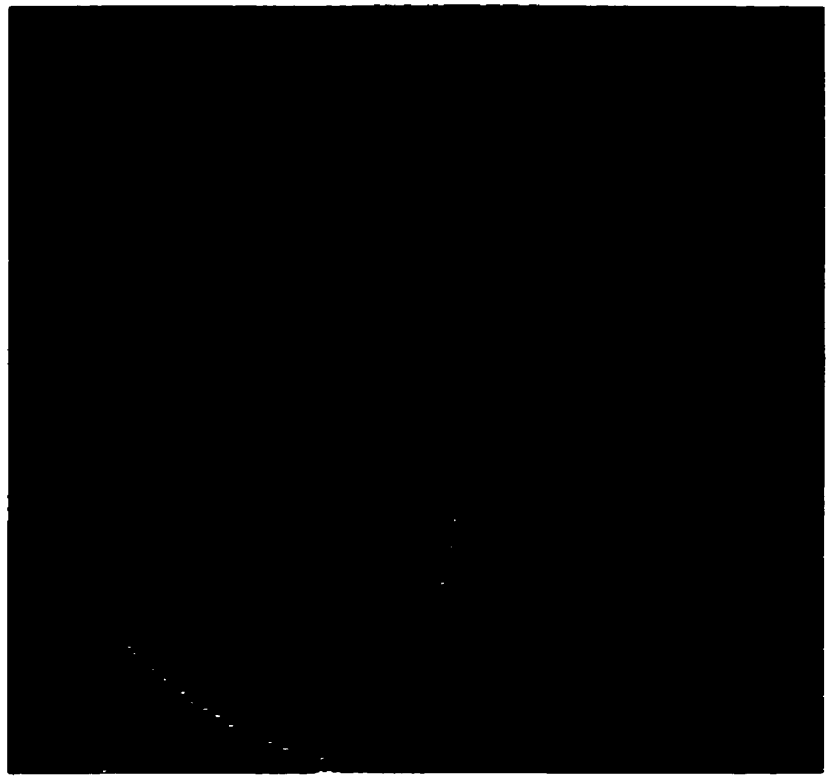

Figure 4.71: Porosities of Sand Pack After Experiment #8

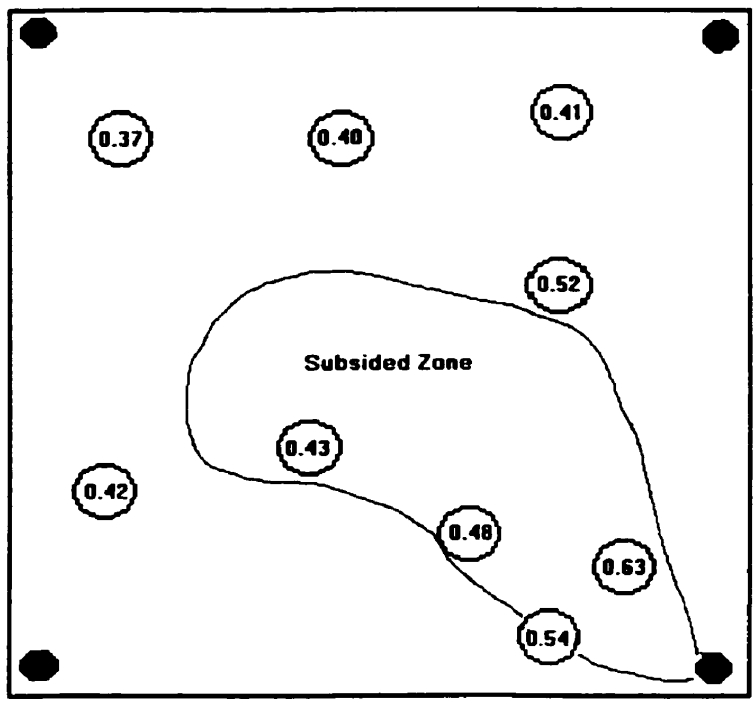

Figure 4.72: Cumulative Oil Production and Water Cut, Experiment #8

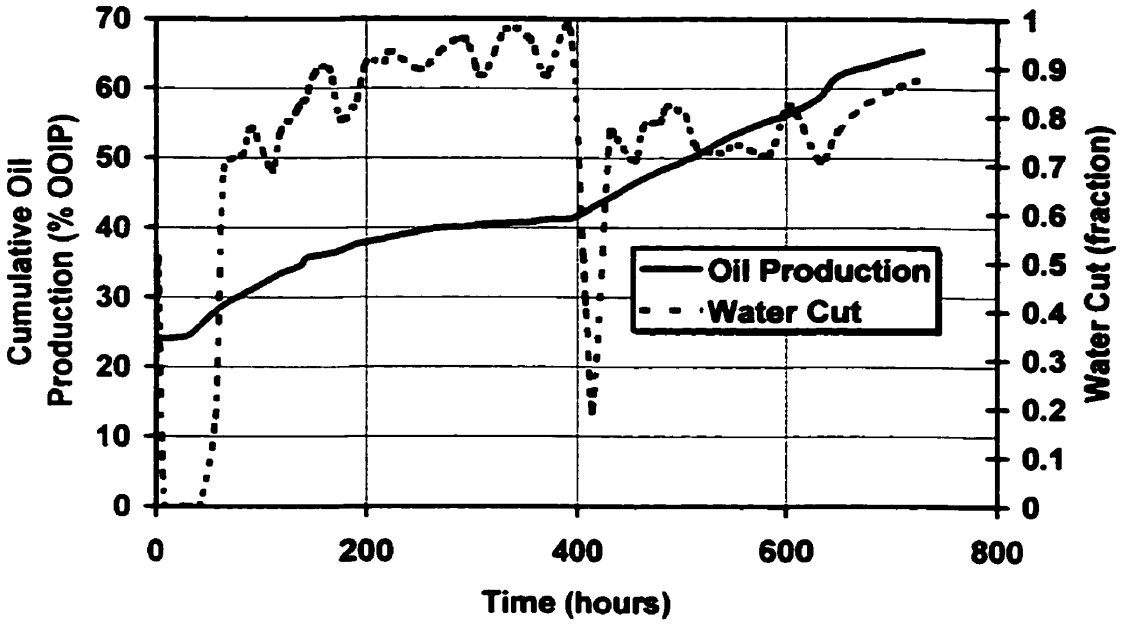

Figure 4.73: Cumulative Production, First Production Cycle Experiment #9
Primary Production, Recovery = 19.3 % OOIP

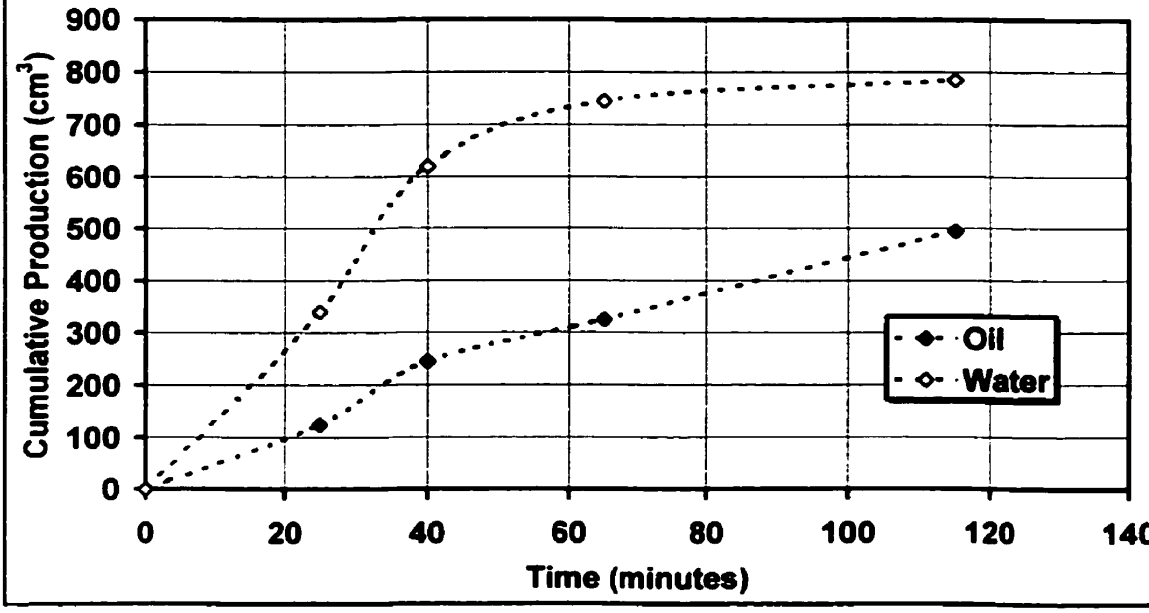

Figure 4.74: Cumulative Production, Second Production Cycle
Experiment #9
Flood with 2 % Brine, Recovery = 4.1 % OOIP

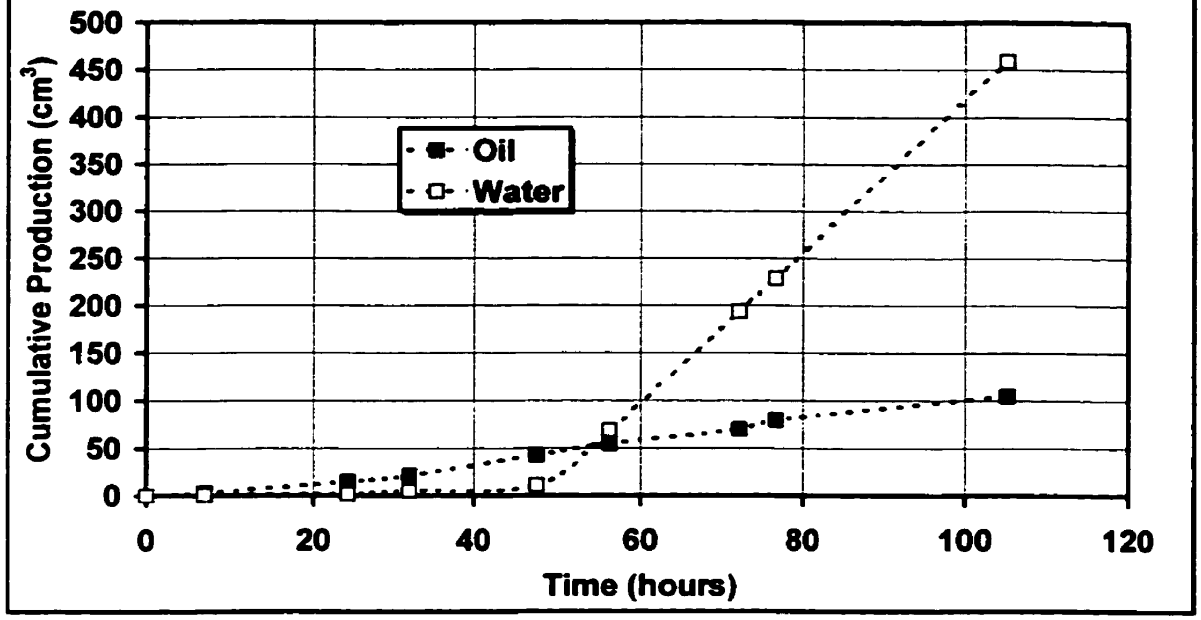

Figure 4.75: Water Cut, Second Production Cycle
Experiment #9

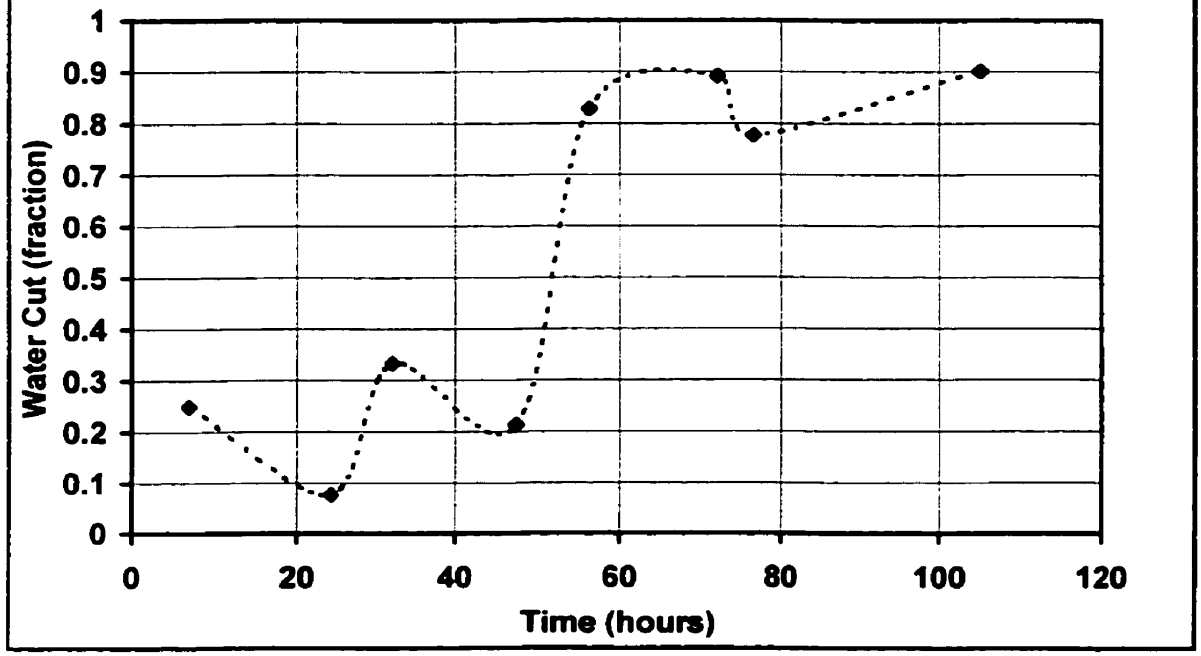

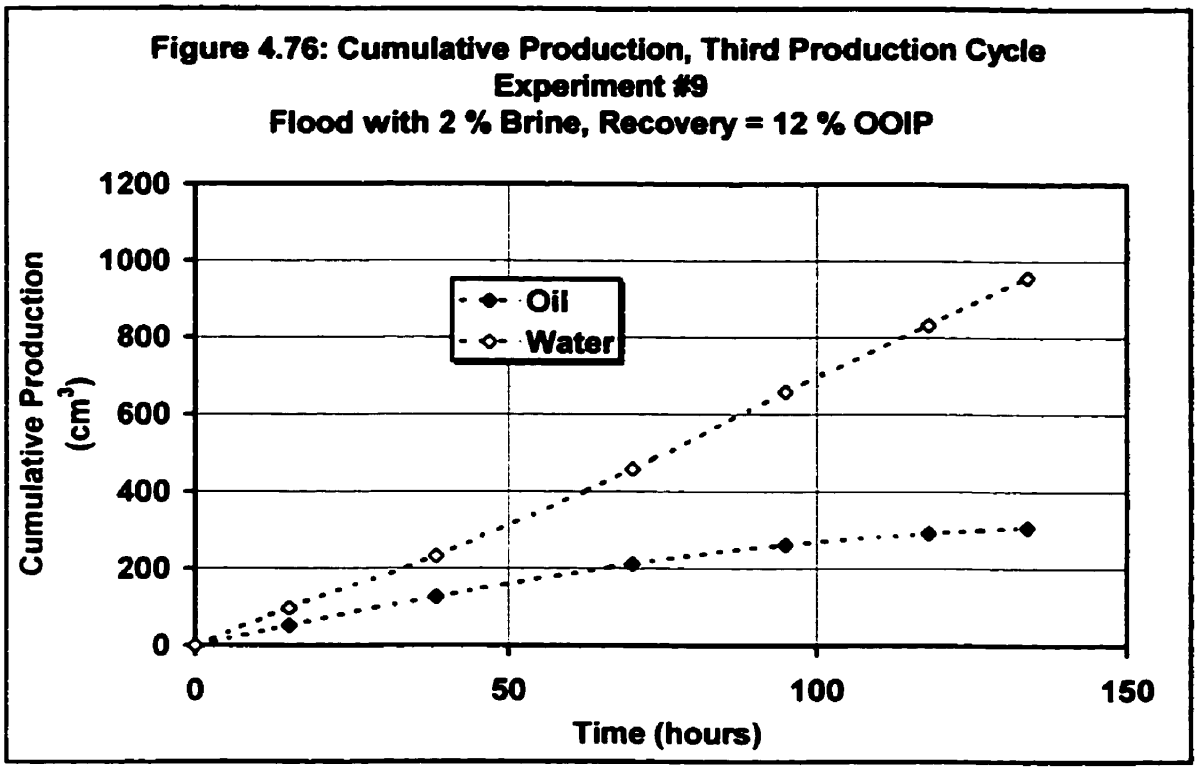
Figure 4.76: Cumulative Production, Third Production Cycle
Experiment #9
Flood with 2 % Brine, Recovery = 12 % OOIP
Cumulative Production (cm3)
1200
1000
800
600
400
200
0
Oil
Water
0
50
100
150
Time (hours)

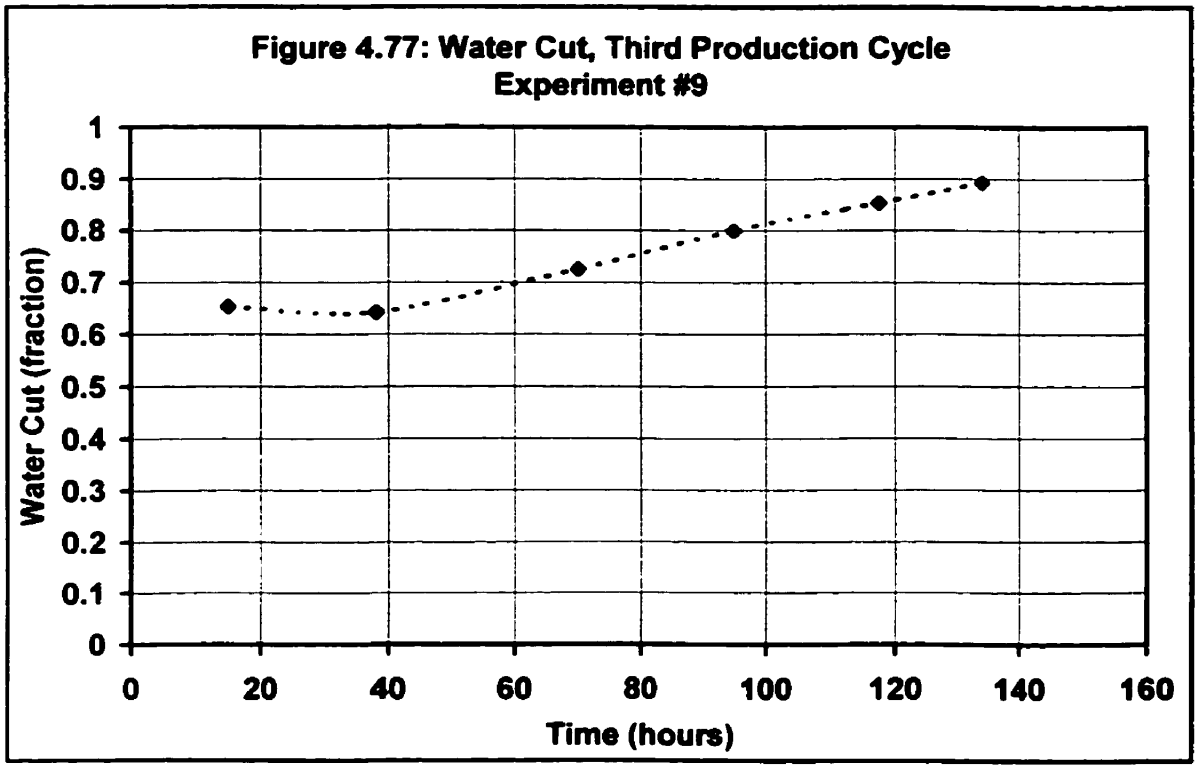
Figure 4.77: Water Cut, Third Production Cycle
Experiment #9
Water Cut (fraction)
1
0.9
0.8
0.7
0.6
0.5
0.4
0.3
0.2
0.1
0
0
20
40
60
80
100
120
140
160
Time (hours)

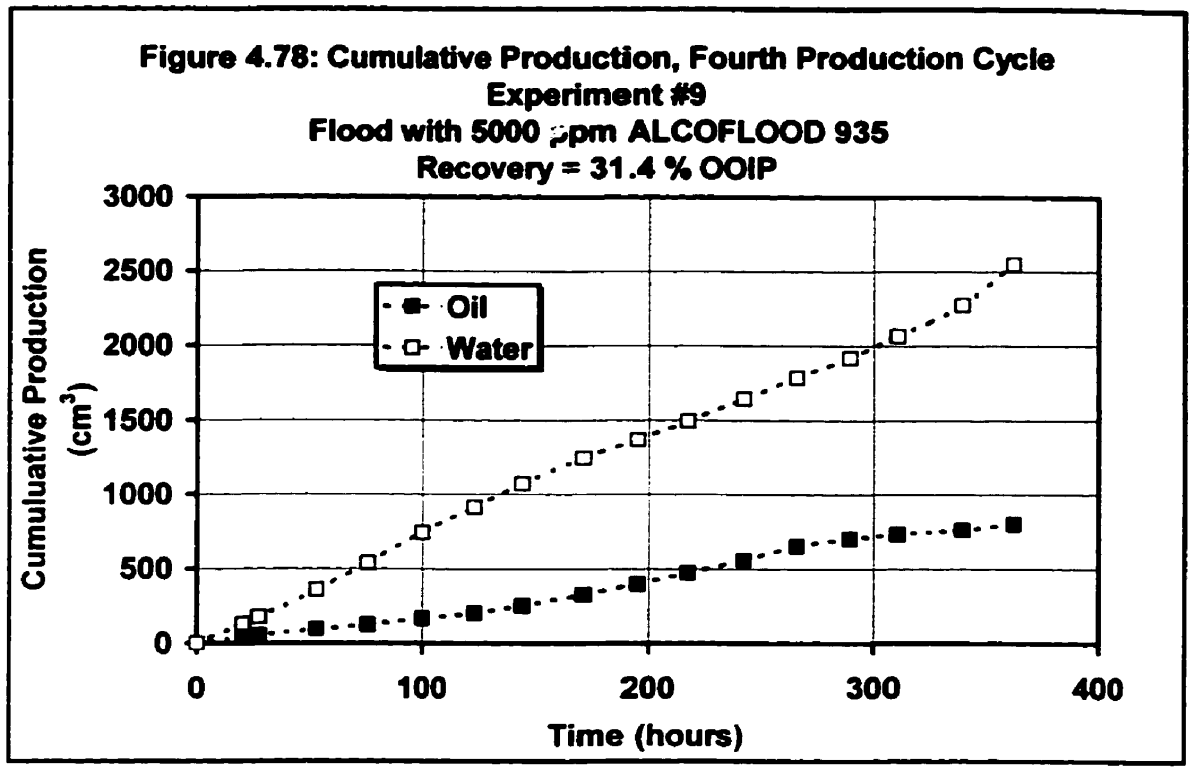
Figure 4.78: Cumulative Production, Fourth Production Cycle
Experiment #9
Flood with 5000 ppm ALCOFLOOD 935
Recovery = 31.4 % OOIP
Cumulative Production (cm3)
3000
2500
2000
1500
1000
500
0
Oil
Water
0
100
200
300
400
Time (hours)

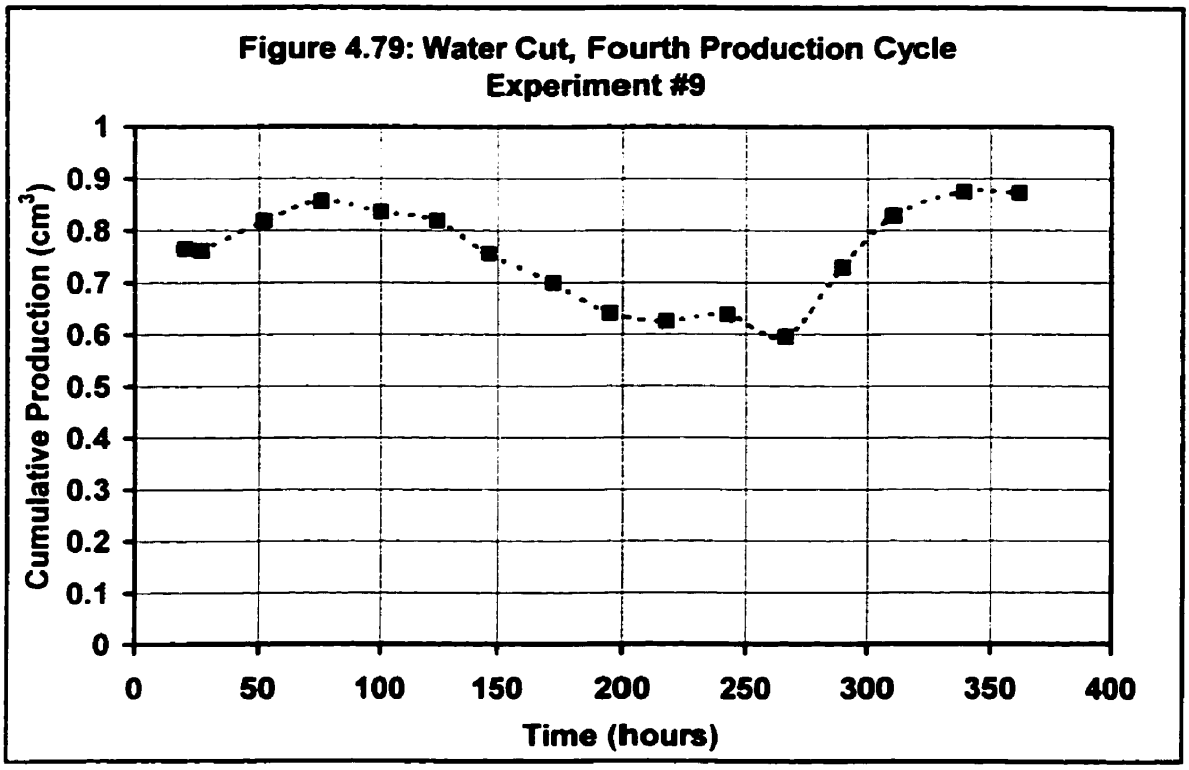
Figure 4.79: Water Cut, Fourth Production Cycle
Experiment #9
Cumulative Production (cm3)
1
0.9
0.8
0.7
0.6
0.5
0.4
0.3
0.2
0.1
0
0
50
100
150
200
250
300
350
400
Time (hours)

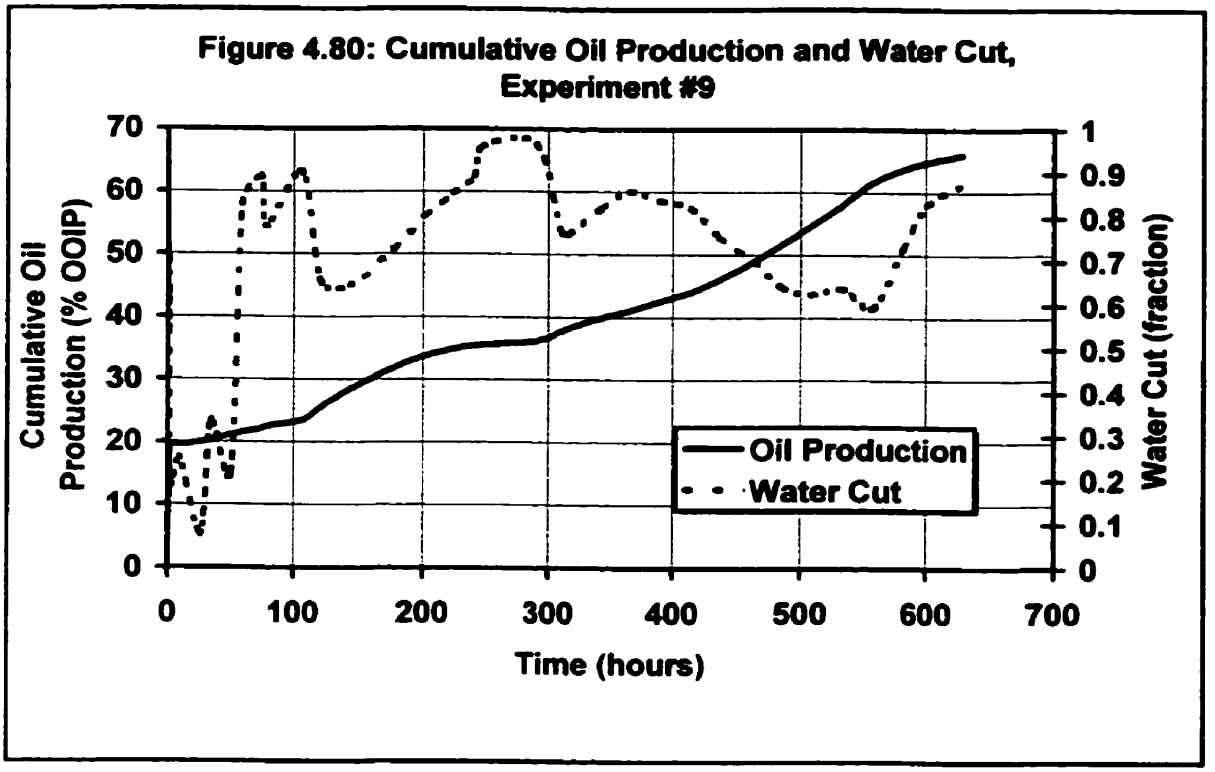
Figure 4.80: Cumulative Oil Production and Water Cut, Experiment #9
Cumulative Oil Production (% OOIP)
Water Cut (fraction)
Time (hours)
Oil Production
Water Cut
0
10
20
30
40
50
60
70
0
0.1
0.2
0.3
0.4
0.5
0.6
0.7
0.8
0.9
1
0
100
200
300
400
500
600
700

CHAPTER FIVE: SIMULATION RESULTS AND DISCUSION

Numerical simulation can be a useful tool for evaluating flow through porous media. The objective for using numerical simulation in this study was to be able to evaluate the experimental results discussed in Chapter Four on a field scale and determine the feasibility of the recovery techniques. The experimental results were to be history matched with the simulator in order to obtain unknown parameters such the relative permeability curves and the characteristics of the polymer during the flood, such as adsorption. The simulation package used was Eclipse-100 black oil reservoir simulator by Geoquest with the Eclipse-200 polymer option used for simulating the polymer floods.

The objective of the study was to explore possible recovery techniques for heavy oil that are inexpensive. As a result, the experimental results of Experiment #2 were not simulated due to the high costs of horizontal wells when compared to vertical wells. The history matching was first performed on Experiment #5 because it was a simple two-phase system and the match could be validated with both the production history and the areal sweep obtained from the gamma camera imaging.

5.1 Experiment #5

The methodology used in history matching the experimental data from Experiment #5 was to first match the water floods to obtain the oil/water relative permeability curves. Once the water floods were matched the polymer floods could be matched to obtain the polymer characteristics of the flood, such as adsorption, residual resistance factor and inaccessible pore volume, using the permeability curves obtained from the water flood match.

The first step in setting up the model for simulation was to construct a grid to represent the 50 cm x 30 cm x 5 cm sand pack in Ambient Model #2. This was done with a 25 x 30 x 5 grid consisting of 3750 grid cells each with dimensions of 2 cm x 1cm x 1cm. Figure 5.1 shows the top layer of the grid with the well locations indicated by the black dots. Each grid cell was then assigned the values of porosity and permeability that were

estimated for Experiment #5, 0.43 and 6 darcies respectively. The permeability was assumed to be isotropic. The properties of the oil were assigned the viscosity and density as listed in Table 4.6. The formation volume factor of 1 was used for both the oil and the water.

The top of the sand pack was chosen as the datum depth and the datum pressure was specified to be atmospheric pressure. The simulator then initializes the conditions in all the grid cells at equilibrium with respect to the datum conditions. Connate water saturation is set at the first saturation entered in the oil/water relative permeability table.

The well locations were specified along with their dimensions. A value of zero was assigned as the skin factor for all the wells. At first, an attempt was made to run the simulation with both the injection and production wells on bottom hole pressure control. In this manner the constant pressure drive nature of the flood could be simulated precisely. However, the simulator could not converge on a solution and error messages were received at run time. Therefore, the injection wells were converted to rate control with the production wells remaining on bottom hole pressure control, with the injection well bottom hole pressures being an additional parameter to be matched. The bottom hole pressure of the production wells was set to atmospheric pressure. The rates of the three injectors were specified as a function of time. The actual injection rates of the experiment were not constant due to the constant pressure drive nature of the experiment. Since the imaging of the first water flood in Experiment #5 showed three separate flow patterns, the injection rates for the three wells were set to the total liquid production of the production well opposite it for any given time step. For the second water flood where the middle injector was shut in, the injection rate of the two open injection wells was set to half of the total liquid production for the given time step.

The oil/water relative permeability curves were the main adjustable parameter used in the history matching. Exponential curves were created from estimated endpoints and an exponent to describe the curvature of the curves. The capillary pressure was set to zero for all oil/water saturations. A search of the literature for capillary pressure data to use in

the simulation was not successful. The uniqueness of capillary pressure curves to specific porous media made it difficult to find suitable data. For a high permeability sand, such as the one used in Experiment #5, the capillary pressure is expected to be low. Therefore, having no capillary pressure curves should not have a major impact on the validity of the simulation. Capillary pressure accounts for the difference in pressure between the oil and water phase at a given water saturation. At the flood front, capillary pressure results in a smooth transition form high water saturation to low water saturation. The effect of neglecting the capillary pressure is likely to be more significant in the field scale simulations where the displacement velocities away from the well bore are much smaller than in the laboratory experiments. This is because capillary pressure is an equilibrium phenomenon and in the laboratory the flood front travels across the fairly short distance of the model quicker. If strict conditions are to be met, the capillary pressures for drainage and imbibition must be obtained from separate tests. This was not done. Instead, it was hoped that the effect of capillary pressures could be accounted for in the relative permeability curves obtained through the history match. Thus the obtained relative permeability curves will be different from their true value due to the effect of capillary pressures. This will not be a true representation of the effects of capillary pressure, but it should be acceptable for the purposes of the simulations performed in this study.

Initial simulations revealed that at the specified injection rates taken from the experimental data, the injection well bottom hole pressures were about an order of magnitude larger than the constant 2 psi used in the experiment. It was necessary to increase the absolute permeability to 50 darcies in order to reduce the injection well bottom hole pressure to the desired values. The estimated value of 6.4 darcies, obtained from flow tests assumed the entire cross-sectional area of the model was being used for flow. This would likely have led to estimates of permeability that were lower than actual value since the flow path of the brine in the flow tests would have a smaller cross-sectional area. Therefore an actual permeability of 50 darcies for the sand pack is quite possible. The lack of an overburden pressure and possible bulging out of the Plexiglas plates are likely factors that led to the high permeability of the sand pack. The presence

of wall effects is another possible explanation. It is possible that the sand pack may not have been tight against the walls of the model. However, in simulations performed where the permeability in the grid blocks at the edge of the sand pack were increased, the production and the bottom hole pressures could not be matched. As well, the sweep of the floods did not match the gamma camera images taken of the floods. Therefore it is not likely that significant gaps between the sand pack and the walls existed.

The water floods performed in the first two production cycles of Experiment #5 were history matched by altering the water/oil relative permeability curves. Figure 5.2 shows the total cumulative oil production for the best match along with the actual production from the experiment. The relative permeability curves used to obtain this match are presented in Figure 5.3. These curves look very similar to steady state relative permeability curves measured for heavy oil that were presented by Maini (1998). As can be seen by, Figure 5.2 the match is quite good. The total oil production of the water floods was determined to be 655 cm^3. This is within 5 % of the 626 cm^3 actually produced. Figure 5.4 shows the simulated water cut as function of time along with the actual water cut. The simulated water cut follows the same trends as the actual water cut. The decline in the actual water cut at about 6 hours corresponds to the flood pattern alteration. The simulated water cut declines at the same time, however the decline is not as drastic as the actual water cut. The cumulative oil productions from the individual wells are presented in Figure 5.5. As can be seen in the figure, Producer #3 was matched very well. The production of middle well, Producer #2, was slightly under predicted by the simulation, while Producer #1 seemed to be over predicted by the same amount. This indicates that there may have been some communication between Injector #1 and Producer #2.

The areal sweep of the simulated water flood can be compared with the gamma camera images taken during the actual water flood. Figure 5.6 shows the water saturation of the third layer after the first water flood. When compared to the gamma camera image in Figure 4.42 it can be seen that the simulation closely matches the sweep of the actual

flood. This along with the close match of the oil and water production indicates that the simulator is capable of describing a heavy oil water flood.

Figure 5.7 shows a cross sectional view of the water saturations of the sand pack after the first water flood. As seen in the figure, all of the layers have been swept evenly by the injected water and there is little difference in the water saturations of each layer. This confirms that gravity under ride was not an issue in the experiment.

Once the water floods were matched, and the relative permeability curves were obtained, the polymer floods were matched. The simulations were run as restarts from the end of the water floods. The simulator requires the polymer solution viscosity to be expressed as a function of concentration. A straight line relationship was used with the maximum measured viscosity of 556.8 cP for ALCOFLOOD 935 at a concentration of 5000 ppm and the viscosity of water, 1 cP at a concentration of 0 ppm. The shear thinning property of the polymer solution was also considered by the simulator. The viscosity as a function of velocity was entered into the input. This data was taken from the viscosity measurements of the polymer solution at different shear rates that was presented in Figure 4.7. The shear rates were converted to velocities using the equation by Littmann (1988) that was presented in Chapter Four as equation 4.7.

As with the water floods, the simulations were performed with the production wells on bottom hole pressure control and the injection wells on rate control. The injection rates were estimated in the same manner as with the water floods using the total liquid production rates from the opposite production well.

The adjustable parameters in the history match were the dead pore space of the porous media, the residual resistance factor, the amount of polymer adsorption to the sand and the Todd-Longstaff mixing parameter. The dead pore space represents the pore volume that is inaccessible to polymer flow. The effect of the dead pore space is to increase the velocity of the polymer solution relative to that of polymer free water, which flows through all of the pores. The residual resistance factor is a number greater than one that

accounts for the reduction of the water phase relative permeability at maximum polymer adsorption. The reduction in water phase relative permeability results in a reduction in the mobility ratio and better oil recovery. The polymer adsorption is represented by a table of adsorption of polymer, expressed by mass of polymer adsorption per mass of sand, as a function of polymer solution concentration. A straight line relationship was used with no adsorption occurring at zero polymer concentration and the maximum adsorption occurring at a polymer concentration of 5000 ppm. This is a rough approximation of the adsorption behaviour of the polymer. Further study needs to be done to determine the exact relationship between polymer adsorption and concentration.

The Todd-Longstaff mixing parameter is a number that is used to help describe miscible displacements for reservoir simulation. Since the phases in each grid block are described by one set of PVT parameters, the properties of a mixture of two miscible fluids in the same phase can only be represented by one set of parameters. The Todd-Longstaff mixing parameter is a value between 1 and 0 and it describes the degree of mixing of two miscible fluids within a grid block. A value of 1 for the mixing parameter means that the two miscible fluids are completely mixed within the grid block. A value of 0 represents immiscible fluids with no mixing. In the simulation of the polymer floods the mixing parameter represents the degree of mixing of the polymer with the brine that is in the sand packs from the previous water floods. The viscosity of the mixed aqueous phase is dependent on the mixing parameter. The mixing parameter was found to have a significant effect on the simulation results. Initially a mixing parameter of 1 was used. This resulted in the simulated water cut declining too soon and too much oil being produced. It is believed that this was due to the simulator having the polymer propagate through the sand pack too quickly. As soon as the polymer entered the grid block it was mixed completely with the water in the grid block and then the aqueous phase with the increased viscosity proceeded to the next grid block where it was mixed completely again. It was necessary to reduce the mixing parameter in order to slow down the propagation of the polymer.

The Eclipse-200 polymer option also had a brine sensitivity capability. This option would take into account a reduction in the polymer solution viscosity caused by the presence of salt. An attempt was made to incorporate this into the simulation of the polymer flood. However, the addition of the brine option resulted in the simulator having difficulties converging. As a result, this option was not incorporated into the simulation.

For the best match of the polymer flood a dead pore volume of 0.005 was used, a residual resistance factor of 1.5, a maximum polymer adsorption of 0.0004 g polymer/g rock, and a Todd-Longstaff mixing parameter of 0.7. Figure 5.8 shows the cumulative oil and water production from both the simulation and the actual experiment for the entire course of the experiment. Figure 5.9 presents the water cut over the course of the experiment for the simulation and the actual experiment. The total oil production as determined by the simulation was 2043 cm^3. This was just over 15 % of the actual 1764 cm^3 produced. The reason for the over prediction can be seen in Figure 5.9. The simulated water cut follows the actual water cut quite well for the early portion of the experiment during the water floods. During the early portion of the polymer flood the match is still quite good. The simulated water cut declines at about the same time as the actual water cut and declines to nearly the same level. However, the simulated water cut remains lower for about 5 hours longer than the actual water cut. It then rises quickly and attains the same level as the actual water cut. The prolonged lower level of the simulated water cut accounts for most of the over predicted oil production. Once the simulated water cut rises, the simulated and actual cumulative oil curves continue to rise with increasing time, almost parallel to each other.

It was possible to perform a simulation using different parameter for the polymer flood and get a match that was closer than 15 % to the actual production. However, it was believed that these simulations did not represent the behaviour of the actual experiment as well as the accepted simulation case described above. Figure 5.10 shows an example of one such simulation along with the accepted case and the actual experimental data. The rejected simulation over predicts the oil production for the experiment by only 9.5 %. However, as can be seen in Figure 5.10, this simulation first under predicts the oil

production during the early part of the polymer flood, then the production increases above the actual oil production. This is because the water cut in this simulation declines later than the actual water cut and it doesn't decline as low as in the accepted case. Like the accepted case, the water cut in the rejected case remains low longer than the actual water cut. This is why the oil production "catches up" with the actual oil production and then exceeds it, resulting in the over prediction. So the same deviation exists in the accepted case also exists in the rejected case. However, an additional deviation, where the water cut declines later than in the actual experiment, also exist. Therefore, even though the simulated results of the rejected case show less deviation from the actual results than the accepted case, it was believed the accepted case represented the behaviour of the floods better.

Figure 5.11 shows the water saturations from the simulation for the fifth layer at 4.5 hours into the polymer flood. As with the water floods, there was very little difference in the water saturations between layers. The water saturations in Figure 5.11 are very similar to the gamma camera image taken of Ambient Model #2 at 4.5 hours into the polymer flood, shown in Figure 4.48. A map of the polymer concentrations from the simulation at 4.5 hours into the polymer flood is almost identical to the water saturation map in Figure 5.11. This indicates that the high water saturation areas in Figure 5.11 are the areas occupied by the polymer solution. Ahead of the high water saturation areas in Figure 5.11 is a uniform high oil saturation zone. It appears that in the simulation the oil has collected in front of the polymer solution forming an oil bank. This behaviour is contrary to the observations made with the CT scanner during the polymer flood of the Aluminum Core Holder, where there was no increase in the oil saturation at any location during the flood. It is possible that banking did occur during polymer flooding of the Ambient Models and that differences in the radial flooding vs. the linear flooding in the Aluminum Core Holder resulted in different flood behaviour. The good history match of the production data, indicates that the simulator has replicated the behaviour of the polymer flood. Therfore, it is quite possible that banking did occur. More experiments should be performed where oil saturations are monitored during polymer flooding to determined if banking does indeed occur.

5.2 Experiment #6

Experiment #6 was also history matched with the simulator. The same approach that was used to history match Experiment #5 was used for matching Experiment #6. The water flood was matched first to obtain the oil/water relative permeability curves. Then the polymer flood was matched.

The same 25 x 30 x 5 grid was used to describe the sand pack of Ambient Model #1 in the simulation of Experiment #6 as was used to describe the sand pack of Ambient Model #2 in the simulation of Experiment #5. However, the thickness of the grid cells was increased from 1 cm to 2.1 cm to account for the additional thickness of the sand pack. Each grid cell was assigned a porosity of 0.43. As with the simulation of Experiment #5, an increased value of the absolute permeability was required in order to obtain injection well bottom hole pressures that approximated actual injection pressure of approximately 0.8 psi. A value of 50 darcies was used for the absolute permeability.

The liquid production rates during Experiment #6 differed from all other experiments performed on the Ambient Models in that the production rates of the middle well, Producer #2, were lower than both of the outer wells. The exact cause of this is uncertain. At first, the injection rates were estimated for the simulation in the same manner they were estimated for the simulation of Experiment #5, by using the production rates of the opposite production well. By estimating the injection rates this way, the middle injector had a lower injection rate than the two outer wells. It was possible to match the total oil production this way, however, the middle production well had higher production rates than the outer two wells. This led to the conclusion that the cause of the reduced production rates of the middle well had more to do with the middle production well than the middle injection well.

The production data of the other experiments performed on the Ambient Models was analyzed. The data for these experiments showed that the middle production well

accounted for about 45 % of the total production while the remaining 55 % was split between the two outer wells. Therefore, the injection rates for the water floods performed during Experiment #6 were estimated by assigning 45 % of the total production rate to the middle injector and assigning 27.5 % of the of the total production rate to each of the two outer wells. To reduce the production rate of the middle producer, a skin factor of 3 was assigned to the production well. This resulted in a good match of both the total oil production and the oil production of the individual wells. Figure 5.12 and Figure 5.13 show the cumulative productions and the water cut respectively. The individual well productions are shown in Figure 5.14. This match was obtained using the oil/water relative permeability curves shown in Figure 5.15. The simulated oil production from the water flood of 1099 cm^3 is approximately 1.1 % greater than the actual 1087 cm^3 produced. However, just under an hour into the water flood, the simulation under predicts the oil production by 7.7 %. This is because the simulated water cut increase before the actual water cut, as can be seen in Figure 5.13.

Figure 5.16 shows the simulated water saturations for the fifth layer. When compared to the actual saturation profiles in Figure 4.52, the areal sweep of the simulation appears to be almost the same as the sweep in the experiment. As with the Experiment #5, there was very little difference in the sweep between the different layers.

Again, to match the polymer flood the dead pore space, the residual resistance factor, the maximum polymer adsorption and the Todd-Longstaff mixing parameter were adjusted. The viscosity of the solution of ALCOFLOOD 1275A in brine as a function of velocity was determined from the data in Figure 4.53 and the equation by Littmann (1988).

The cumulative productions for the experiment with the best match of the polymer flood are presented in Figure 5.17. This match was attained with a dead pore space of 0.005, a residual resistance factor of 1.1, a Todd-Longstaff mixing parameter of 0.7, and a maximum polymer adsorption of 0.0001 g polymer/g rock. The differences in the adsorption and residual resistance factor between Experiment #5 and Experiment #6 can be attributed to the use of the different polymer products. The simulation over predicted

the oil production by 16 %. The reason for this can be seen in Figure 5.18, which shows the water cut for the simulation along with the actual measured values. The simulated water cut matches the actual water cut well during the water flood and the early portion of the polymer flood. Shortly into the polymer flood, the simulated and the actual water cut decline at the same time and to about the same level. However, the simulated water cut does not follow the sudden increase that the actual water cut does at the point in time where the flood was restarted. This accounts for the majority of the deviation in the oil production.

5.3 Experiment #1

The same grid was used to describe Experiment #1 as was used to describe Experiment #6 since both experiments were run using Ambient Model #1. Again, the water floods were matched first. The gas floods were then simulated followed by the polymer flood. Each grid block was assigned a porosity of 0.43. As with the previously described simulations, the absolute permeability needed to be increased to match the injector bottom hole pressures. A permeability of 30 darcies was assigned to each grid block. The injection rates were determined as they were with the simulation of Experiment #5, using the liquid production rates from the opposite production wells.

The cumulative oil and water productions for best match for the water floods and the gas floods, leading up to the polymer flood, are shown in Figure 5.19. The oil/water relative permeability curves used to obtain this match are shown in Figure 5.20. Gas relative permeability curves were also used to obtain the match. However, due to the short duration of the gas floods and the small amount of oil recovered, the impact of the gas permeability curves on the simulation results was minor. As can be seen from Figure 5.19, the simulation matches the cumulative productions very well up to this point. In fact the simulated cumulative oil production of 1288 cm^3 was only 5 cm^3 less than the actual production of 1293 cm^3.

The first polymer flood was history matched with the simulator. The subsequent gas and polymer foods were not matched since little oil was recovered during these floods. The best match for the polymer flood used a dead pore volume of 0.005, a residual resistance factor of 1.4, a maximum polymer adsorption of 0.0001 g polymer/g rock, and a Todd-Longstaff mixing parameter of 0.7. The polymer adsorption obtained from the match of the polymer flood is different than the value obtained by matching Experiment #5, even though the same polymer product was used in both experiments. The presence of gas in the model during polymer flood of Experiment #1 may have had an effect on the amount of polymer adsorbed. As well, it is quite possible that the true adsorption value was the same as that obtained by matching Experiment #5, but the effects of a gas saturation being present were accounted for by the simulator through an artificial adjustment of the polymer adsorption value. Figure 5.21 shows the cumulative oil and water production obtained from both the simulation and the experiment. The simulator under estimated the oil recovery by about 10 %. The water cut from the simulation and the experiment are presented in Figure 5.22. The simulated water cut matches the actual water cut quite well up to the early portion of the polymer flood. A water cut of zero is given by the simulator briefly during the gas flood. During the polymer flood, the simulated water cut declines about four hours earlier than the actual water cut. However, it does not decline quite as low as the actual water cut and rises more quickly than the actual water cut. This accounts for the under prediction of the total oil production. The simulated water cut declines over the last few hours of the polymer flood after rising steadily for about 50 hours. This was the point in time during the experiment when the two outside wells were shut in because their water cut had exceeded 90 %. The water cut did not decline during the experiment during this period of the polymer flood. At this late stage in the polymer flood, only small amounts of oil were being produced. As a result, the error in the simulation during this portion of the polymer flood did not significantly affect the cumulative production.

5.4 Reservoir Models

Experiment #8 and Experiment #9 were not considered for simulation due to the rapid blow down that was involved in each experiment. Such a rapid blow down involves many non-equilibrium conditions that would have been very difficult to simulate. The black oil simulator calculates thermodynamic properties from a table and assumes equilibrium. Even though the primary production performed during Experiment #3 and Experiment #4 may have been too quick to be simulated, it was hoped that a reasonable match of the primary production could be made so that the subsequent floods could be history matched. However, it proved difficult to obtain a match. The oil production could be matched quite well, but the gas production could not be matched. This was attributed to the uncertainty of the initial amount of gas in the model and its distribution within the sand pack. As well, it is likely that the oil was supersaturated with gas during the rapid blow down. This would have delayed the formation of a mobile free gas phase. The black oil simulator assumes thermodynamic equilibrium between all the phases and does not account for any non-equilibrium kinetic effects. Efforts were made to match the gas production by altering the initial amount of the free gas in the model and altering its placement in the sand pack, but a good match could not be obtained. As well, it was believed that with the manipulation of so many variables, that any obtained match may not be a unique solution. Therefore, the effort to match the experiments performed on the Reservoir Models was given up.

5.5 Field Scale Simulations

The good matches of the Ambient Model experiments illustrate that simulator is capable of reproducing the behaviour observed in the water flooding and polymer flooding of heavy oil. The history matches have provided information about the floods, such as the relative permeability characteristics. This allowed for simulations to be performed on the field scale to give a rough evaluation of the performance of water flooding and polymer flooding of heavy oil. The simulations will not provide an exact scaling of the experimental results to the field scale, but will provide valuable insight into the issues that may exist when operating at the field level.

The field scale simulations were performed on a line drive pattern similar to that of the Ambient Models. The wells were spaced 200 m apart, which corresponds to approximately a 10 acre spacing. A grid of 21 x 11 x 5 was used for the simulation. The grid cells had the dimensions of 20 m x 20 m x 5 m so that the grid represented a portion of a reservoir that was 420 m x 220 m x 5 m. A porosity of 0.43 and a permeability of 5 darcies were assigned to each grid block. Figure 5.23 shows a top view of the grid with the well locations indicated by the black dots. The grid was set up as an element of symmetry type model. This was done by multiplying the pore volumes of the corner gird blocks by 0.25 and the remaining edge grid blocks by 0.5. The transmissibility in the x direction was multiplied by half for the grid blocks located on the edges of the grid that runs in the x direction. While the grid blocks located on the edges of the grid that run in the y direction had their transmissibility in the y direction multiplied by a factor of 0.5. The transmissibility in the z direction was multiplied by 0.5 for all blocks along the edge of the grid, except for the grid blocks on the corners where the transmissibilities in the z direction were multiplied by 0.25. This effectively eliminated the gray area of the grid in Figure 5.23. As well, the connection factor of the wells in the corner grid blocks were multiplied by 0.25 and the connection factor of the two middle wells that were located on the edge of the grid were multiplied by 0.5. The result of this is that the simulations with the four quarter wells and two half wells would represent the production from two wells, an injector and a producer, in a line drive configuration.

It was desired to evaluate the performance of the water flooding and polymer flooding on a depleted reservoir, since primary production would precede any flooding in an actual reservoir. In order to obtain the conditions of a depleted reservoir for running the simulations of the floods, a simulation was performed of a primary production of a reservoir that was at virgin conditions. The depleted reservoir provided the initial conditions for the simulations of the water floods and polymer floods. The oil used in the simulation was given the properties of the oil used in Experiment #5, with a dead oil viscosity of 3840 cP. The reservoir was initialized at a pressure of 3.5 MPa and an initial GOR of 10. The GOR was a linear function of pressure, which is consistent with data

presented by Butler (1991). The viscosity of the live oil as function of pressure was calculated using the equation by Butler (1991) presented in Chapter Four as equation (4.7). At the initial pressure of 3.5 MPa, the oil had a viscosity of 1847 cP. The gas was assigned the properties of methane. The oil/water relative permeability curve obtained in the match of Experiment #5 was used. However, the curve was shifted, as shown in Figure 5.24, so that the connate water saturation was a more reasonable 0.15. Gas/oil relative permeability curves were constructed in order to simulate primary production. The curves are shown in Figure 5.25. The gas had a critical gas saturation of 0.05. At low gas saturations, the gas permeability was very low. This was done to obtain an enhanced oil recovery that is often associated with primary production of heavy oil.

The simulation of primary production was performed with oil being produced from all the wells, with a bottom hole pressure of 0.68 MPa. The simulation was run until the reservoir was completely depleted down to the bottom hole pressure. The simulated recovery obtained from the blow down was 8.3 % of OOIP. This is consistent with recoveries obtained from heavy oil fields by cold production (Dusseault, 1993). After the primary production the reservoir was at 0.68 MPa with an immobile gas saturation of 0.05. At a pressure of 0.68 MPa the oil had a GOR of 1.7 and a viscosity of approximately 3080 cP. These were the conditions that served as the initial conditions for the water flood.

A simulation was performed of a water flood, with one row of wells as the injectors and the other row as the producers. This simulation would serve as the base case to evaluate the performance of the water floods with an altered flood pattern and polymer floods. The simulated water flood was performed with the water injected at a constant bottom hole pressure of 80 MPa. There were no flow limits placed on the injection or production rates. The water flood was simulated for 20 years. The cumulative production and water cut are shown in Figure 5.26. If a water cut of 98 % is considered the economic limit, the water flood would last 13 years and result in an incremental recovery of just under 10 % OOIP. The oil and water production rates as a function of time are shown in Figure 5.27. The rates shown in the figure are the total from the two quarter and one half production

well and therefore represent the production from a single well. The oil rate declines slowly over the course of the water flood. However, the water rate increases significantly, with a rate of 143 m^3/day after 13 years. The handling of this large amount of produced water can be a significant operating cost. Figure 5.28 shows the water saturations for a profile view of the reservoir. A significant amount of gravity under ride occurs between the five layers, with very little oil being swept from the top layer. The sweep in the bottom layer is quite good, as shown in Figure 5.29.

In order to evaluate the effect of altering the flood pattern, a simulation was performed of a water flood where the middle injector well was shut in after 13 years. All the producers remained open and the flood was simulated for 5 years. In the 5 years, the flood with the shut in injector recovered 3.2 % of OOIP. However, the water cut continued to rise above 98 %. As well, the additional recovery of 3.2 % OOIP is less than would have been recovered if the water flood was continued for five more years with all the injectors open. Continuing the water flood with all the injectors open for five more years would have recovered an additional 3.5 % OOIP at a water cut similar to the altered flood. A simulation was performed with the middle injector shut along with the outside producers shut in an effort to sweep the water toward the middle of the reservoir. This only served to reduce the recovery further without reducing the water cut. These results indicate that the improved recovery with a decline in water cut observed in the experiments does not scale up to the field level. This may be due to the difference in the degree of gravity segregation between the lab scale and field scale water floods. In the experiments, there was essentially no gravity under ride. The majority of unswept oil was due to poor areal sweep. On the field scale, the majority of the unswept oil was due to poor vertical sweep. The altering of the flood pattern would help improve areal conformance but is not likely to improve vertical conformance.

Simulations were performed to evaluate the performance of polymer flooding of heavy oil at the field level. The properties of the polymer obtained from the history matches of the experiments were used for the field scale simulations. The exception was the Todd-Longstaff mixing parameter. With the grid cell in the field scale simulations represent a

much larger volume, it stands to reason that the mixing in this larger volume would be much less than in the smaller grid cell used to simulate the experiments. Therefore it was necessary to reduce the Todd-Longstaff mixing parameter. There is no accepted way to scale the mixing parameter. A general rule of thumb, is to use a value of 0.7 for lab scale simulations and 0.5 for field scale (Baker 1999). A Todd-Longstaff mixing parameter of 0.5 was used for all field scale simulations of polymer floods.

A simulation was performed of a polymer flood that was started after 13 years when the water cut of the water flood had reached 98 %. The polymer was assigned the properties of ALCOFLOOD 935 in fresh water. The dead pore volume, residual resistance factor and polymer adsorption properties obtained from the match of Experiment #5 were used. The polymer solution was injected for one year, after which water was injected. The injection well bottom hole pressures were maintained at 80 MPa. The simulation was run for 15 years. Figure 5.30 presents the cumulative oil production and water cut. Over the 15 years the flood recovers an additional 8 % of OOIP. The water cut does decline, however, it does not decline until 5 years after the polymer injection. The water cut declines to about 87 % and then slowly increases. Even at the end of the simulation, 14 years after polymer injection had stopped, the water cut was about 96 %, still below the economic limit of 98 %. This indicates that polymer flooding has the capability to extend the life of a heavy oil reservoir. However, polymer flooding may not be economic in the short term. This is illustrated in Figure 5.31, which shows the oil and water production rates. When the polymer is injected at 13 years into the water flood, both the oil and water production rates decline dramatically. This is caused by the reduced injectivity of the viscous polymer solution. The oil production rate does not recover to pre-polymer injection levels until 20 years into the flooding. This can have serious implications on the economics, since oil recovered earlier in the life of a project has more influence economically than oil produced later. If the water flood were continued after 13 years, more oil would be recovered with extended water flood at the 20 year mark than would be with the polymer flooding scenario described above. However, the amount of water produced is significantly less in the case of the polymer flood. After 13 years of water flooding the water production rate was 143 m^3/day. Once the polymer was injected it

declined drastically to 8.5 m^3/day. It then increased when the total liquid production rates increased due to the re-injection of water. After rising to about 60 m^3/day at 18 years, the water production rate declines again due to a reduction in the water cut. At 29 years, 15 years after polymer injection, the water production rate is 75 m^3/day, well below the pre-polymer injection level of 143 m^3/day. Therefore, if the produced water handling costs are significant, the economics of the polymer flooding may be favourable. If not, the sharp decline in oil production rates in the short term after polymer injection will make polymer flooding economically unattractive. If polymer flooding can be made economic it has the potential to significantly increase the life and recoverable reserves of heavy oil reservoirs.

The behaviour of field scale polymer flood simulation differed from the polymer floods performed in the laboratory experiments. The decline in water cut was not as dramatic in the field scale simulations as it was in the experiments. One of the main differences in the field scale polymer flood simulation when compared to the laboratory experiments is that the polymer was injected as a slug chased with water in the field scale simulation. As a result the polymer solution would be subject to dispersion and dilution, reducing its effectiveness. As well, in the field scale simulations the majority of the unswept oil prior to polymer flooding was due to gravity under ride of the water flood. In the experiments the unswept oil was due to poor areal conformance of the water floods. The effectiveness of the polymer flood in improving vertical conformance as opposed to areal conformance may be significant. If the polymer is sweeping additional oil from the previously swept regions, as it appeared to in the experiments, it is unclear if it would sweep this oil vertically upward into the high oil saturation zone and mobilize the oil in that zone. The mechanisms involved in the polymer floods performed in the laboratory may not apply to the field scale simulations.

Figure 5.32 shows the water saturation for the bottom layer at 13 years into the polymer flood. This is when the water cut begins to decline. As with the simulation of the laboratory polymer floods, the polymer appears to be banking the oil in the field scale simulations. A high oil saturation zone has formed ahead of the polymer. Figure 5.33

shows a profile view of the water saturations. As with the water flooding, gravity under ride is prevalent with differences in the water saturations of the five layers. However, the vertical conformance is better than it was for the water flood as shown in Figure 5.28. This would have contributed to the reduction in water cut observed at the production well. This mechanism for recovering additional oil was not a factor in the polymer floods performed in the experiments where vertical conformance was good.

Another simulation was performed of a polymer flood. The simulation used the properties of ALCOFLOOD 1275A in brine and the polymer flood characteristics obtained from the history match of Experiment #6, except for the Todd-Longstaff mixing parameter which was assigned a value of 0.5. The polymer flood was simulated the same as the previously described simulation. The polymer was injected after 13 years of water flooding. The polymer solution was injected for one year, followed by water injection for 14 more years. The cumulative oil production and water cut are shown in Figure 5.34. Both the cumulative production and the water cut curves have the same pattern as the previously described polymer simulation that used the more viscous ALCOFLOOD 935 in fresh water. The recovery from the polymer flood was an additional 9.7 % OOIP. This is higher than the 8 % OOIP recovered from the simulation of the ALCOFLOOD 935. Figure 5.35 shows the water and oil production rates for the simulation with the polymer flood using ALCOFLOOD 1275A in brine. When the polymer is injected at 13 years into the simulation the production rates of the decline drastically due to the reduced injectivity of polymer solution. In this case the oil production rates recover about 2 years earlier than in the case of the flood with ALCOFLOOD 935 in fresh water. As well, the rates for the remaining portion of the flood are slightly higher. The ALCOFLOOD 1275A in brine, is just as effective at reducing the water production rates, even though it has a lower viscosity than the ALCOFLOOD 935 in fresh water. Due to the reduced viscosity of the polymer solution, the loss of injectivity of the injection wells is not sustained as long as it is in the case of the more viscous ALCOFLOOD 935 in fresh water. This makes the use of ALCOFLOOD 1275A in brine the more economically attractive option, which is convenient since reservoir brine is likely the most plentiful and

least expensive solute available, adding to the economic advantage of using ALCOFLOOD 1275A.

The result of the simulation of ALCOFLOOD 1275A in brine indicates that a more viscous polymer solution is not necessarily better. In fact a less viscous, less concentrated (and therefore less expensive) solution may actually be a more effective oil recovery agent. There is likely an optimum solution viscosity that maximizes the oil recovery by balancing the negative effects of injectivity loss and positive effects of water cut reduction. Further study on this issue is recommended.

A simulation was performed to see whether more oil could be recovered by injecting the polymer earlier in the life of the water flood. Instead of waiting for the water cut to reach 98 % before injecting the polymer, the polymer was injected once the water cut reached 90 %. This occurred 6 years into the water flood. The polymer solution injected was ALCOFLOOD 1275A in brine. After 6 years the polymer was injected for one year followed by 14 years of water injection. Figure 5.36 shows the cumulative oil production and the water cut from the simulation. The water cut declines four years after polymer was first injected. The total recovery of the flooding at the end of the simulation at 22 years was 15 % OOIP. This is slightly higher than the 14.5 % OOIP recovered 22 years into the simulation where the polymer was injected later. The oil and water production rates are presented in Figure 5.37. As with the other simulations, the production rates of both the oil and the water decline drastically when the polymer is injected. The oil rate recovers to pre-polymer injection levels after five years, as it did in the case where the polymer was injected later. The results of the simulation indicate the ultimate recovery is improved only marginally by injecting the polymer earlier. However, the loss of recovery earlier in life of reservoir makes injecting polymer earlier a less economically attractive option since the oil recovery is delayed for a number of years.

The final scenario considered, was the case in which the slug size was reduced. A simulation was performed in which ALCOFLOOD 1275A was injected after 13 years of water flooding. The polymer was injected for half a year, followed water injection for

15.5 years. The cumulative oil production and the water cut are presented in Figure 5.38. The total production recovered from the flooding was 19.5 % OOIP. This is slightly less than the 19.6 % OOIP recovered for the case where the polymer was injected for a year. The water cut declines at the same time for both cases, four years after polymer injection began. The water and oil production rates are shown in Figure 5.39. The production rates of both oil and water decline sharply when the polymer is injected. This is consistent with the previously described simulations. After five years the oil production rate has increased back up to pre-polymer injection levels. Reducing the size of the polymer slug seems to have very little effect on both the ultimate oil recovery and the oil production rates. However, the water recovery rates increase more quickly after polymer injection for the case where the slug size is reduced. In fact, at the end of the simulation the water production rate had increased to 113 m^3/day. This is nearly twice the water production rate of 65.5 m^3/day at the end of the simulation where the polymer was injected for an entire year. If these higher water production rates can be tolerated, the reduced polymer slug size may be more attractive due to the lower chemical costs. However, a larger slug size may be required if the water handling costs figure significantly into the economics of the project.

The field scale simulations described in this chapter have revealed some of the important issues involved in water flooding and polymer flooding of heavy oil. It should be stressed that these simulations are only intended to provide a rough indication of the possible recoveries available at the field level. Further study, in which an actual heavy oil reservoir is modeled and simulations are performed on the model would be useful. This would allow for estimation of logistics and the actual costs incurred by performing water floods and polymer floods on heavy oil. A detailed economic analysis of the recovery techniques could then be performed.

Figure 5.1: Simulation Grid for Experiment #5

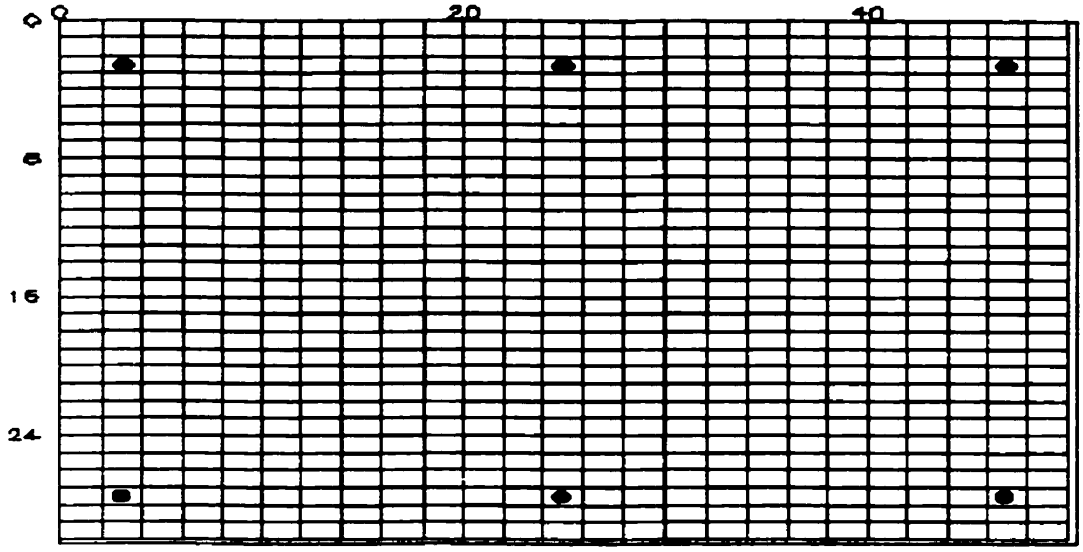

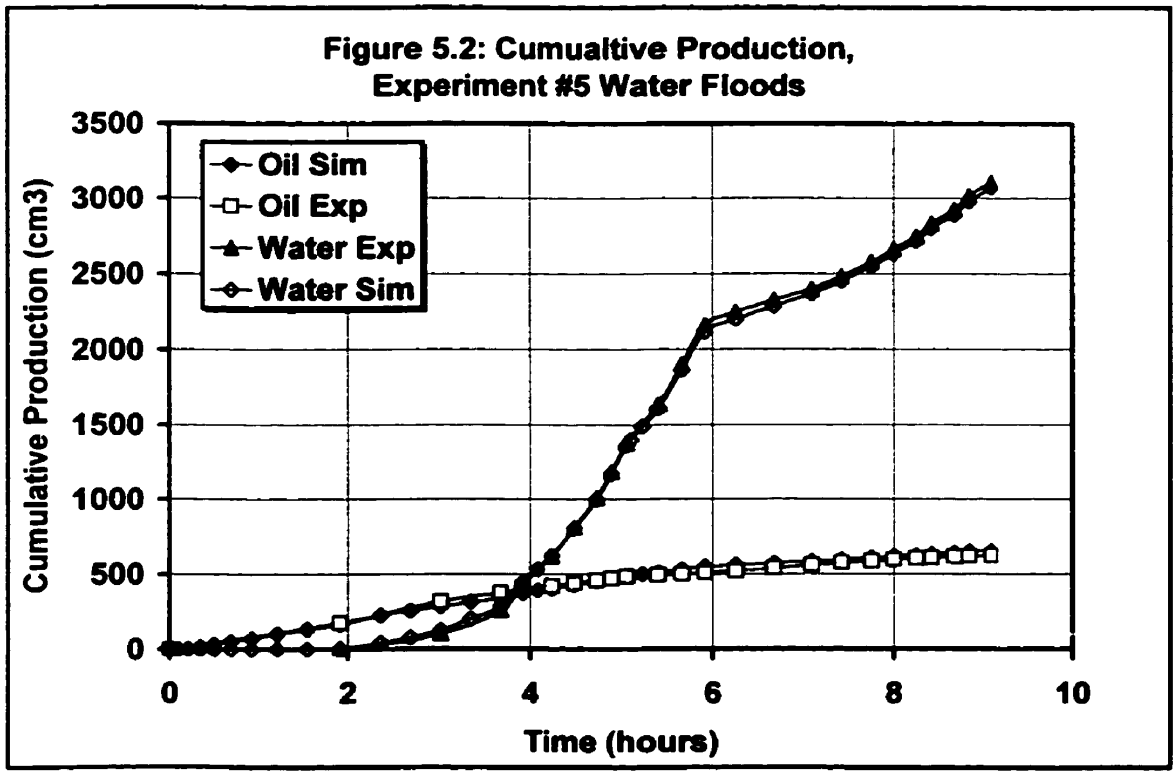

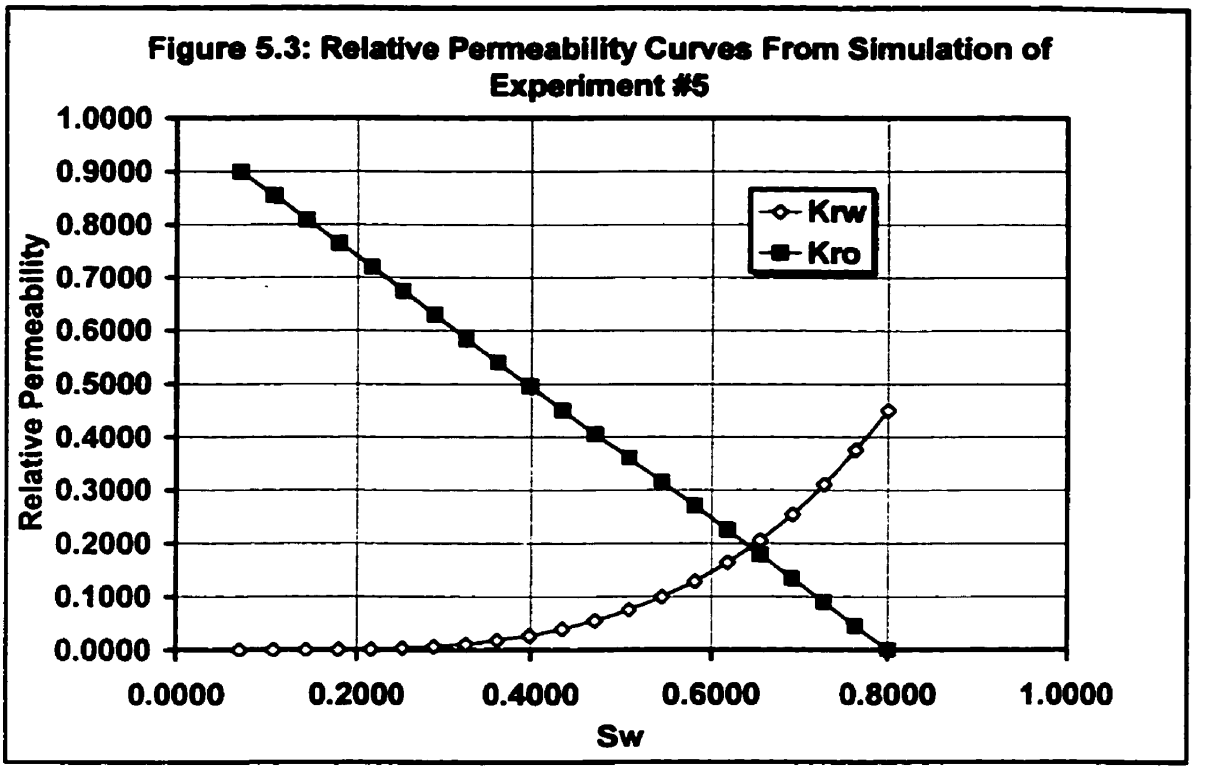
Figure 5.3: Relative Permeability Curves From Simulation of Experiment #5
Relative Permeability
1.0000
0.9000
0.8000
0.7000
0.6000
0.5000
0.4000
0.3000
0.2000
0.1000
0.0000
Krw
Kro
0.0000
0.2000
0.4000
0.6000
0.8000
1.0000
Sw

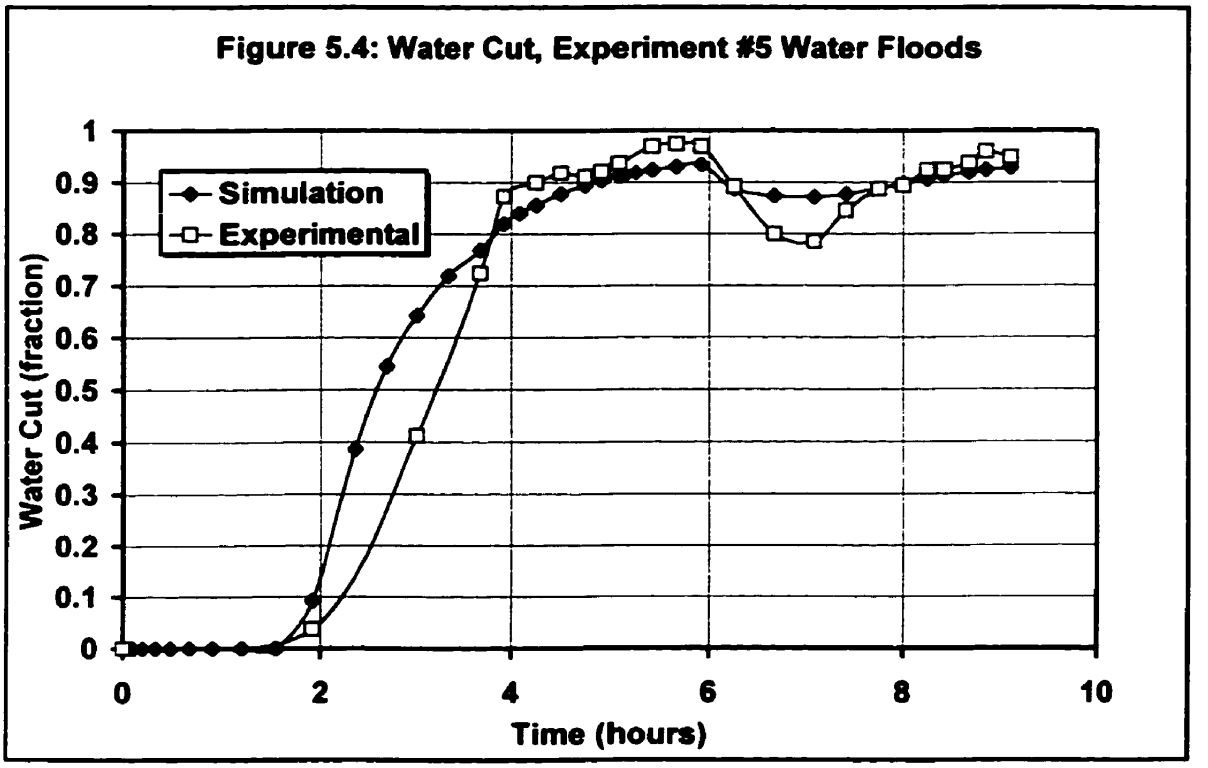
Figure 5.4: Water Cut, Experiment #5 Water Floods
Water Cut (fraction)
1
0.9
0.8
0.7
0.6
0.5
0.4
0.3
0.2
0.1
0
Simulation
Experimental
0
2
4
6
8
10
Time (hours)

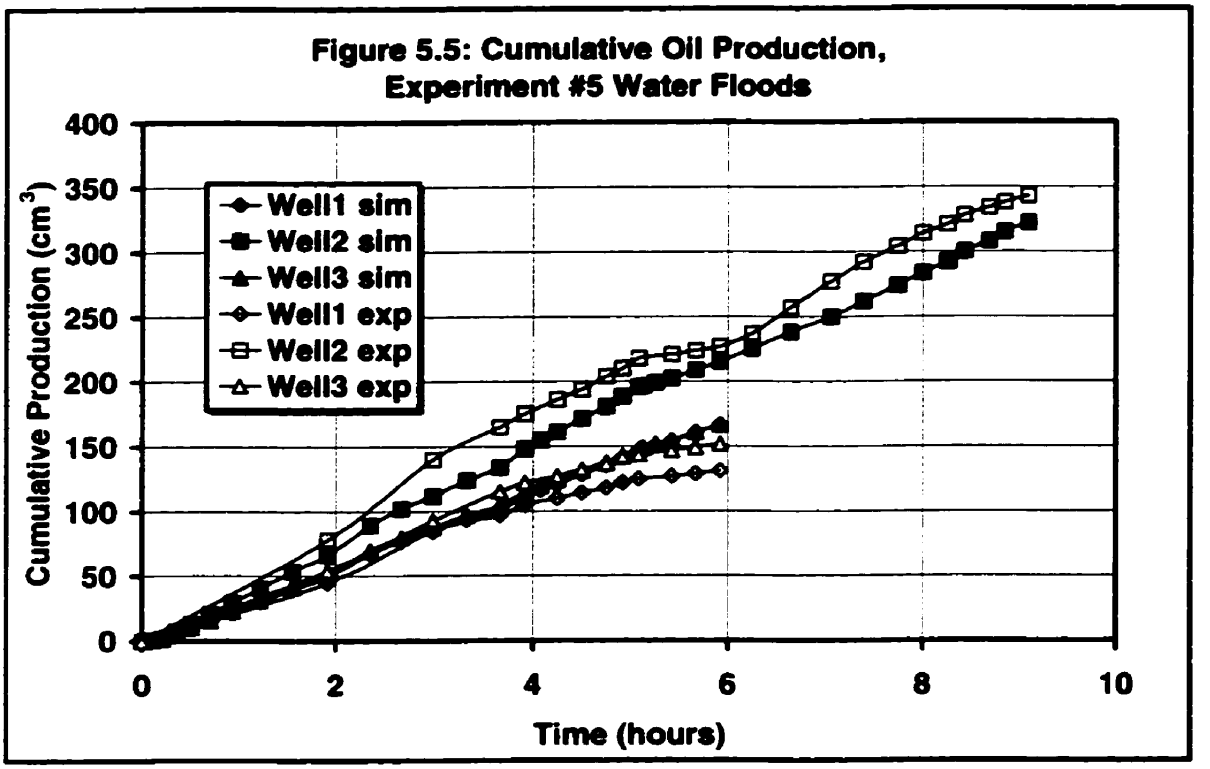

Figure 5.6: Water Saturations After Simulation of First Water Flood, Experiment #5, Areal View

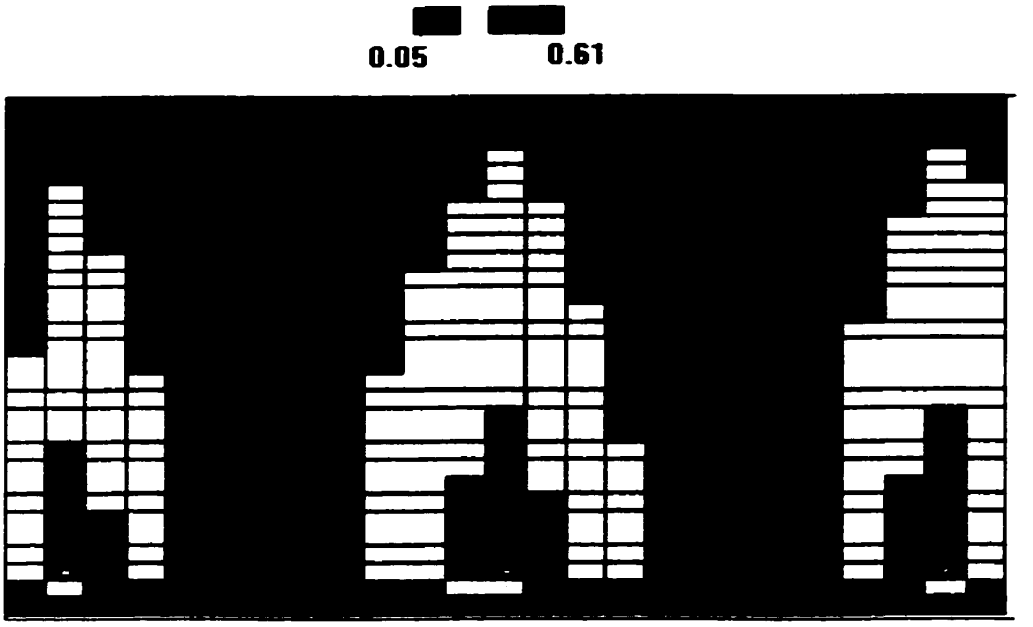

Figure 5.7: Water Saturations After Simulation of First Water Flood, Experiment #5, Profile View

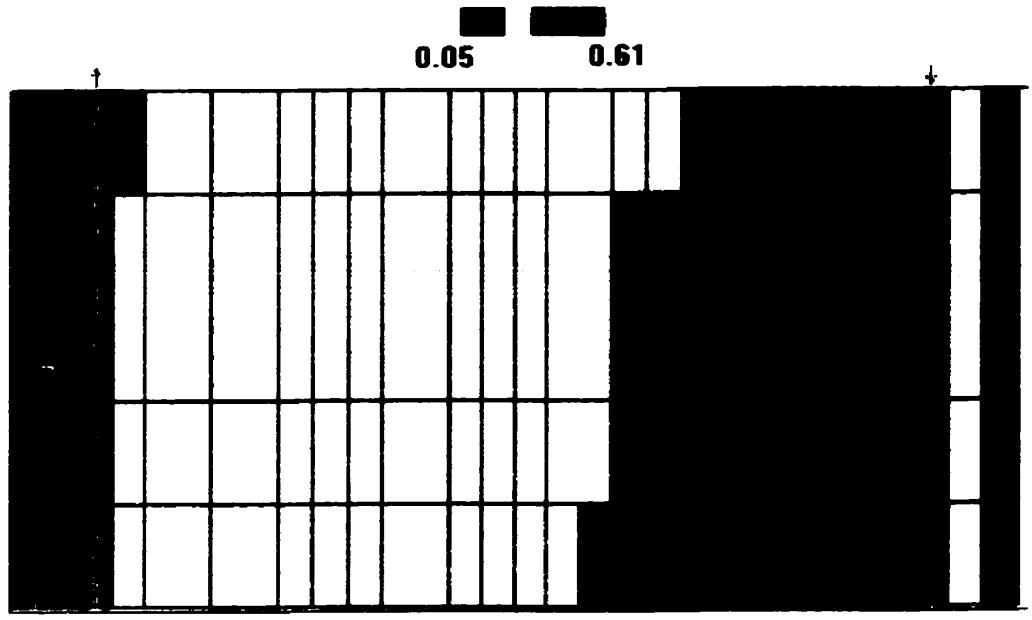

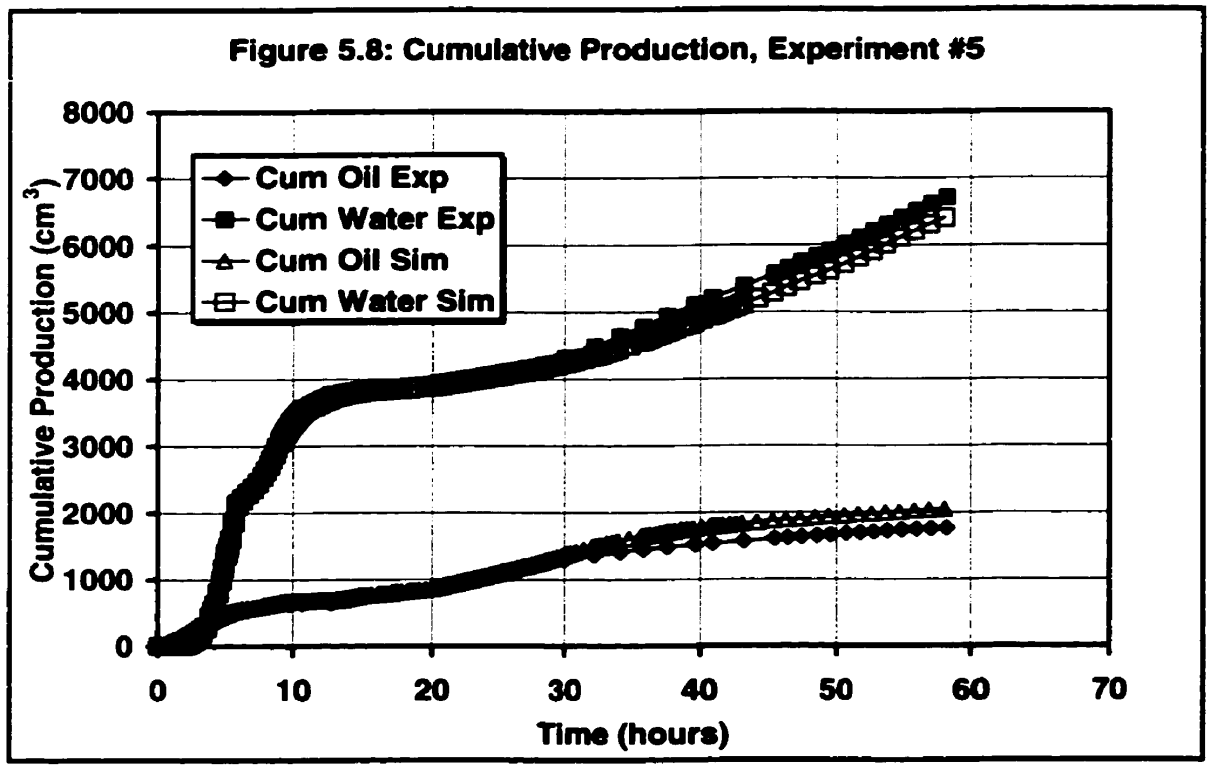

Figure 5.9: Water Cut, Experiment #5

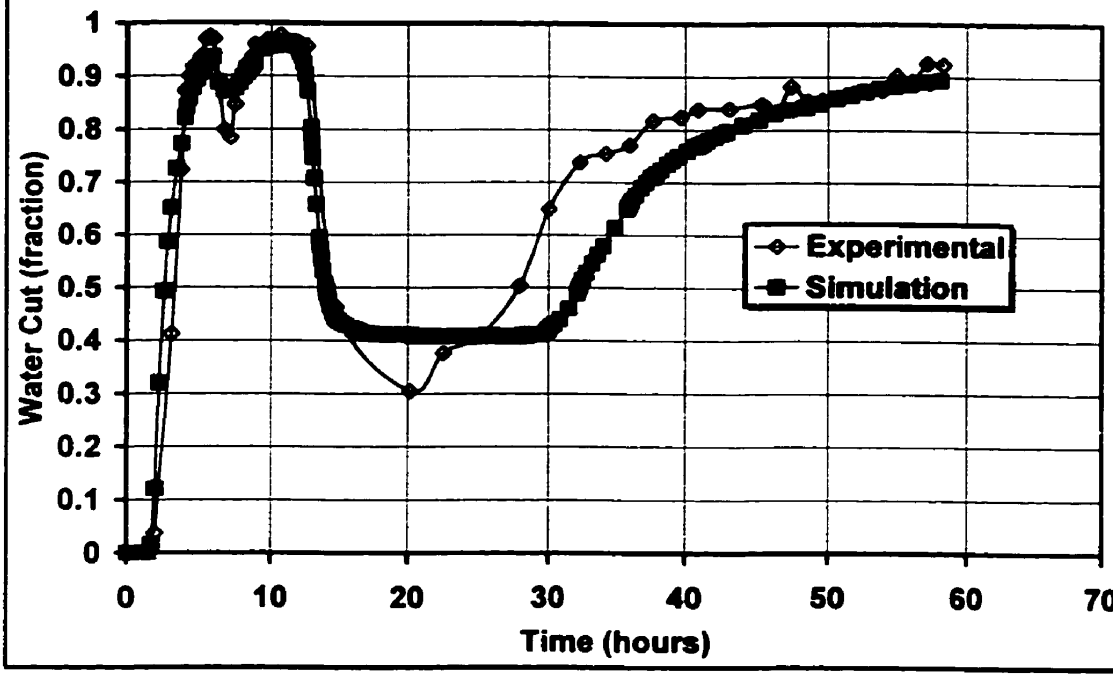

Figure 5.10: Cumulative Oil Production, Experiment #5

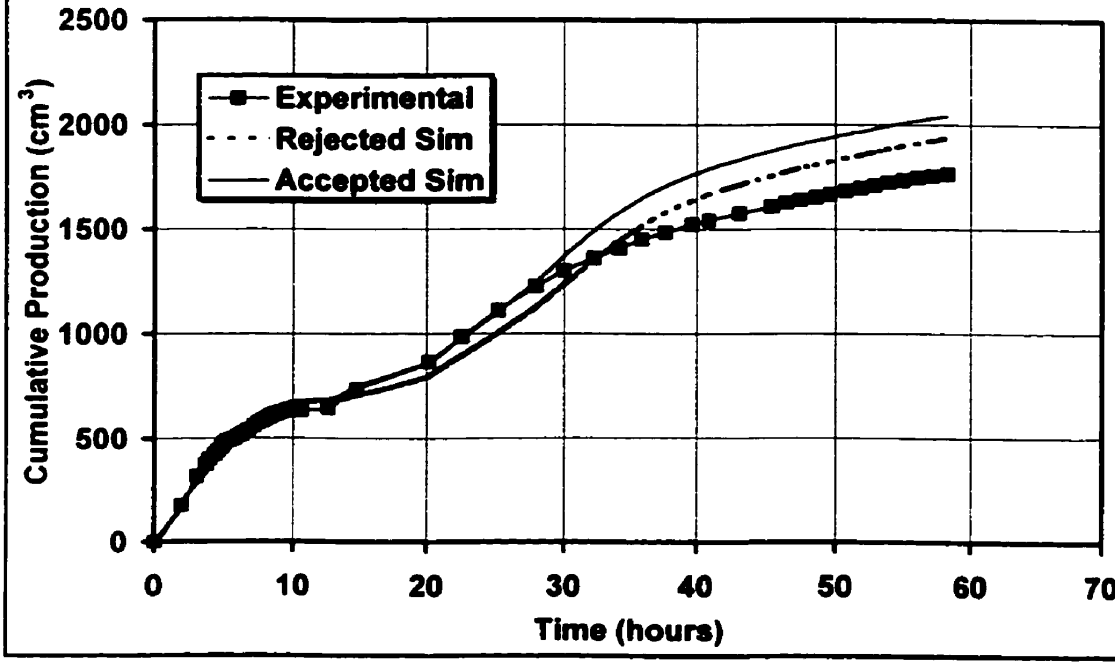

Figure 5.11: Water Saturations 4.5 hours into Simulation of Polymer Flood, Experiment #5, Areal View

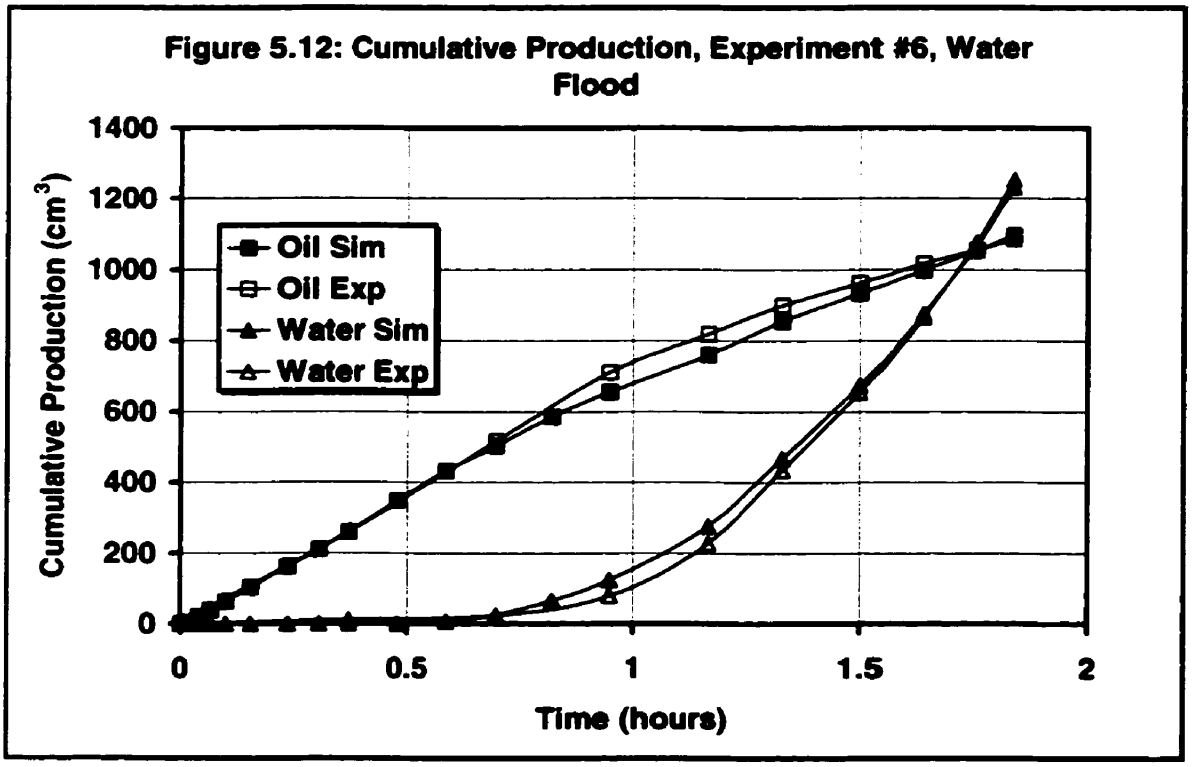

Figure 5.13: Water Cut, Experiment #6, Water Flood

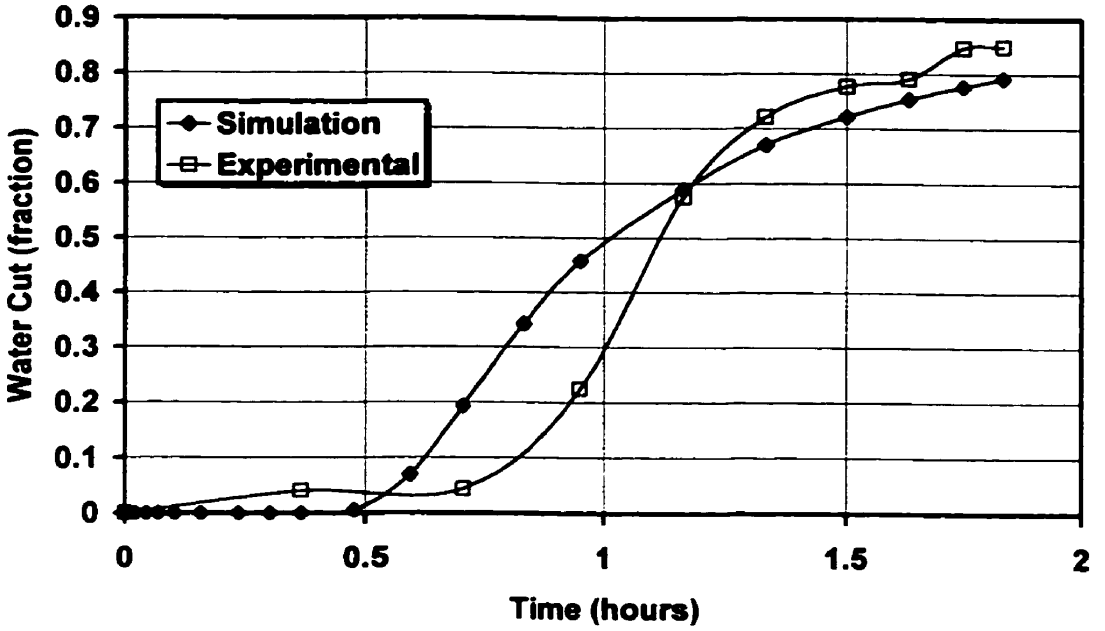

Figure 5.14: Cumulative Oil Production, Experiment #6, Water Flood

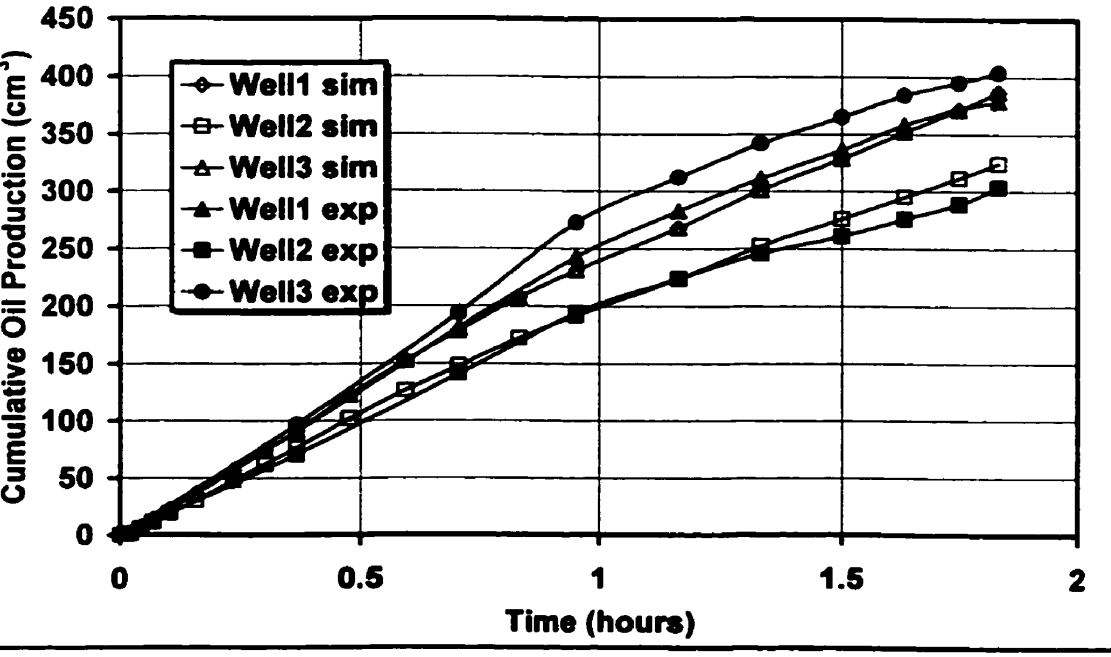

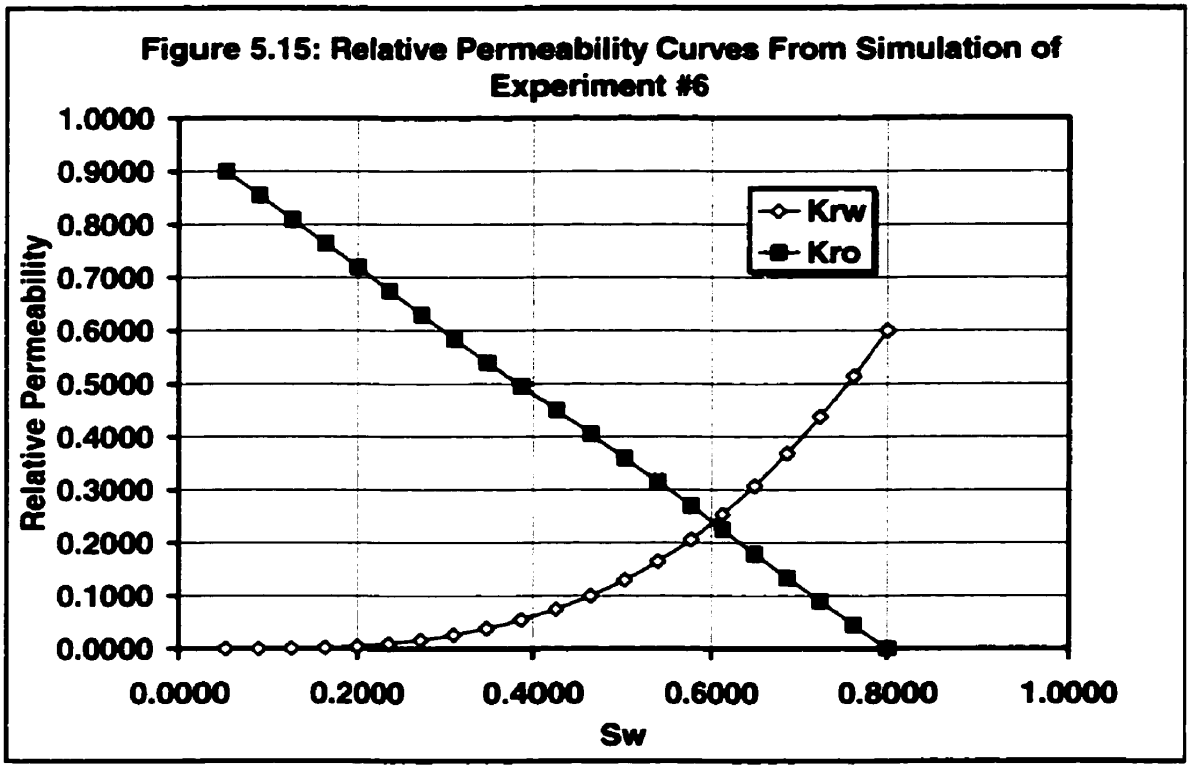

Figure 5.16: Water Saturations After Simulation of Water Flood, Experiment #6, Areal View

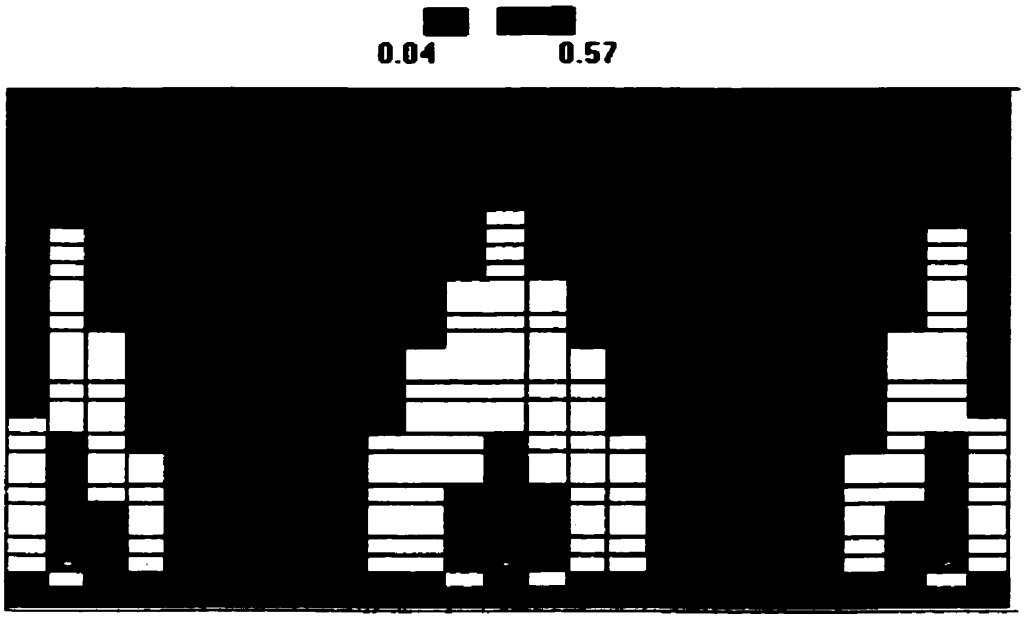

Figure 5.17: Cumulative Production, Experiment #6

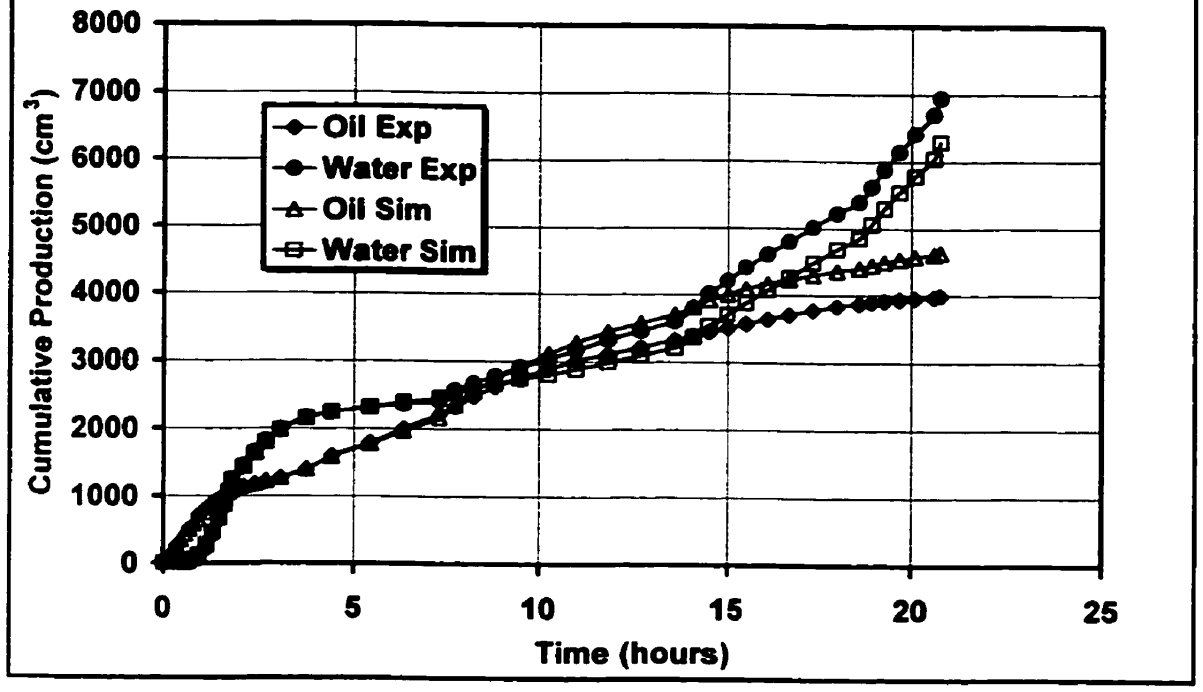

Figure 5.18: Water Cut, Experiment #6

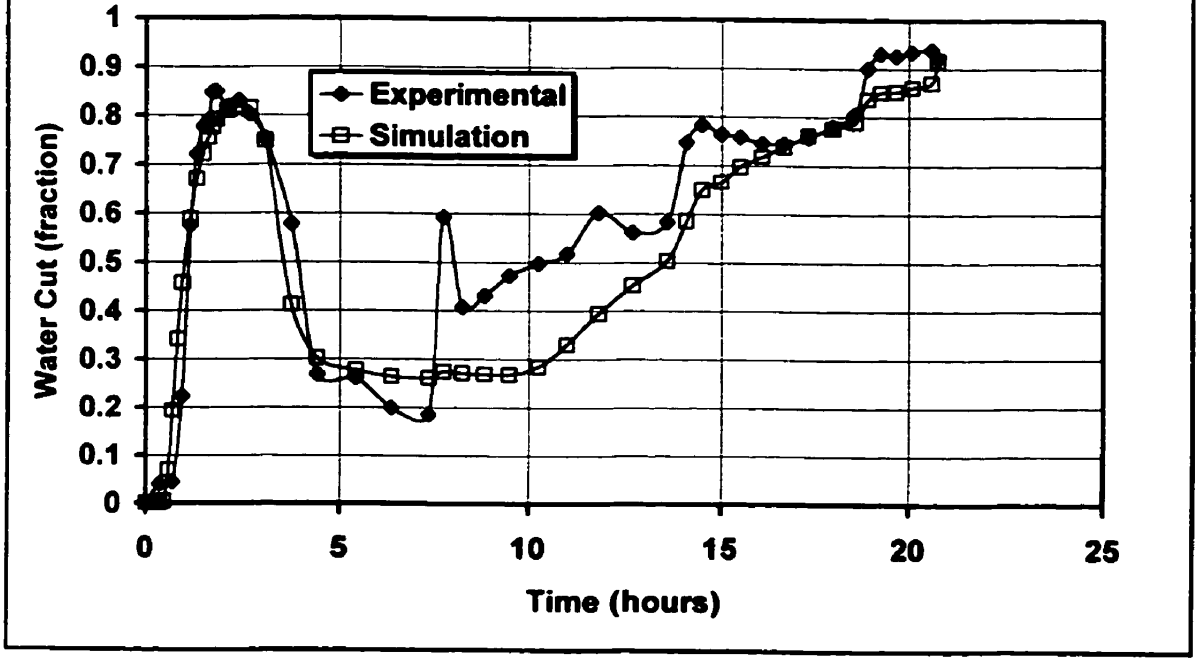

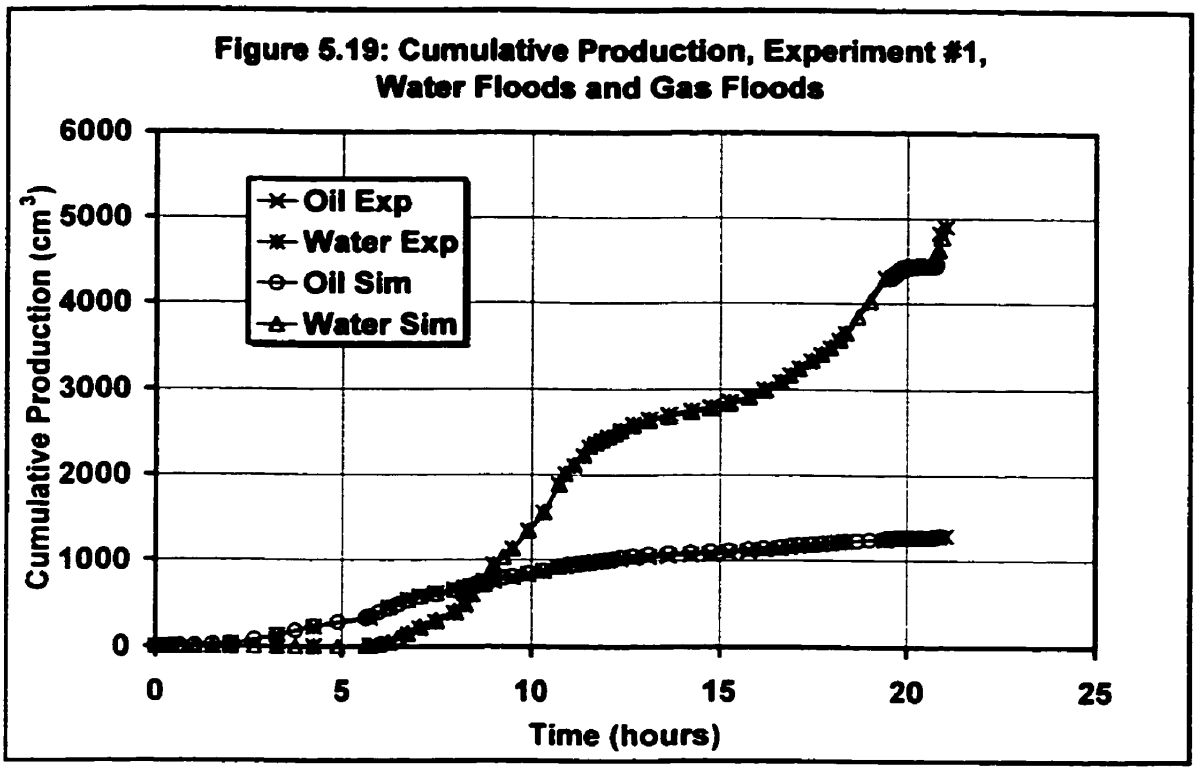
Figure 5.19: Cumulative Production, Experiment #1, Water Floods and Gas Floods
Oil Exp
Water Exp
Oil Sim
Water Sim
Cumulative Production (cm3)
6000
5000
4000
3000
2000
1000
0
0
5
10
15
20
25
Time (hours)

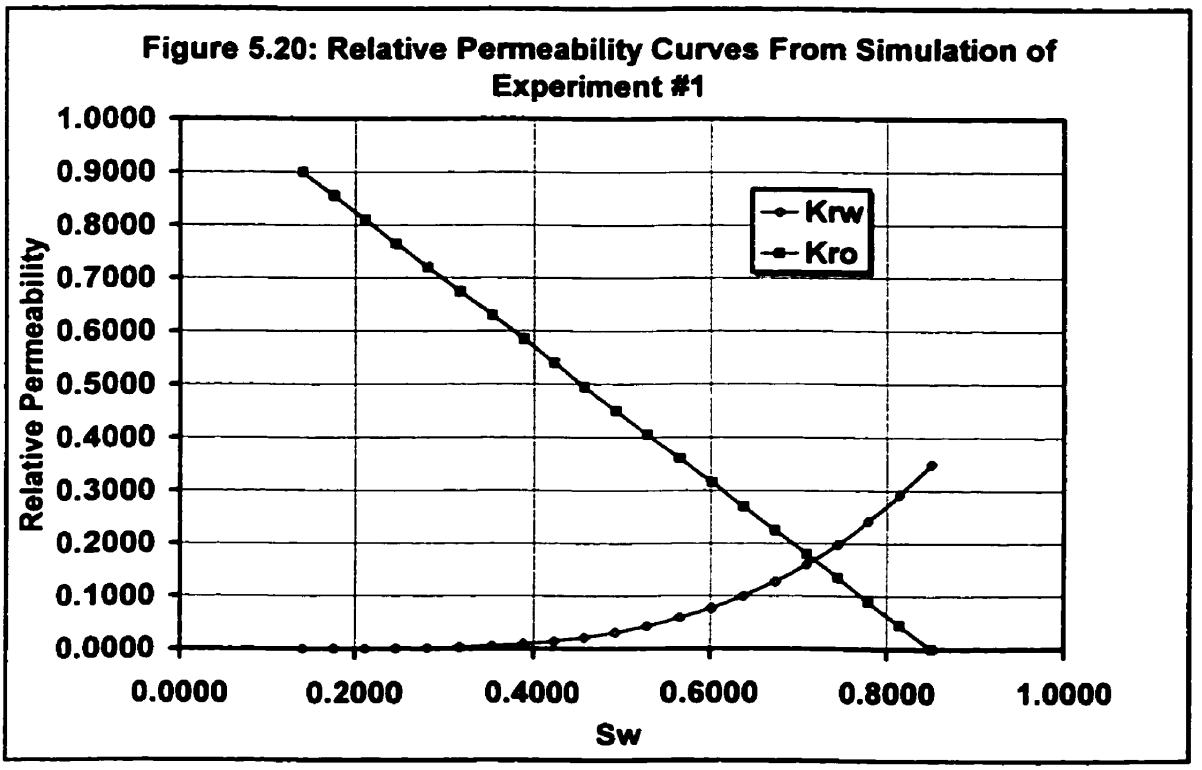
Figure 5.20: Relative Permeability Curves From Simulation of Experiment #1
Krw
Kro
Relative Permeability
1.0000
0.9000
0.8000
0.7000
0.6000
0.5000
0.4000
0.3000
0.2000
0.1000
0.0000
0.0000
0.2000
0.4000
0.6000
0.8000
1.0000
Sw

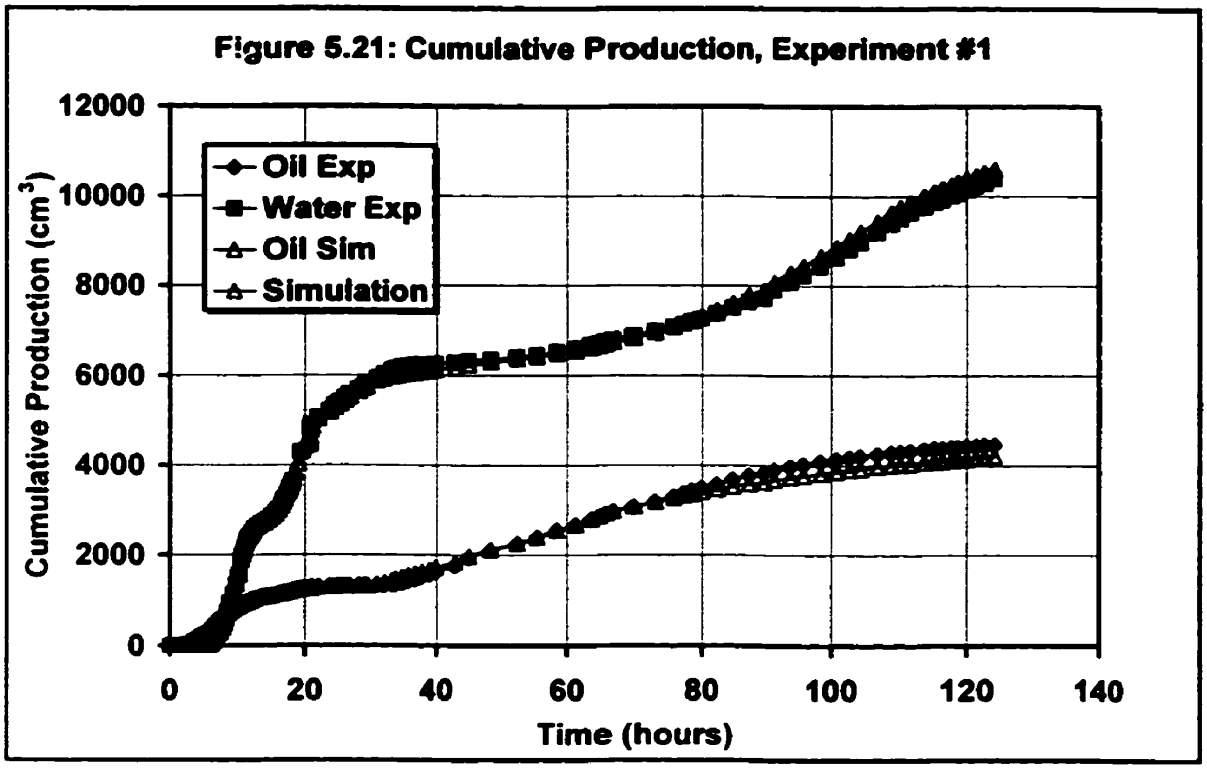
Figure 5.21: Cumulative Production, Experiment #1
Cumulative Production (cm3)
12000
10000
8000
6000
4000
2000
0
0
20
40
60
80
100
120
140
Time (hours)
Oil Exp
Water Exp
Oil Sim
Simulation

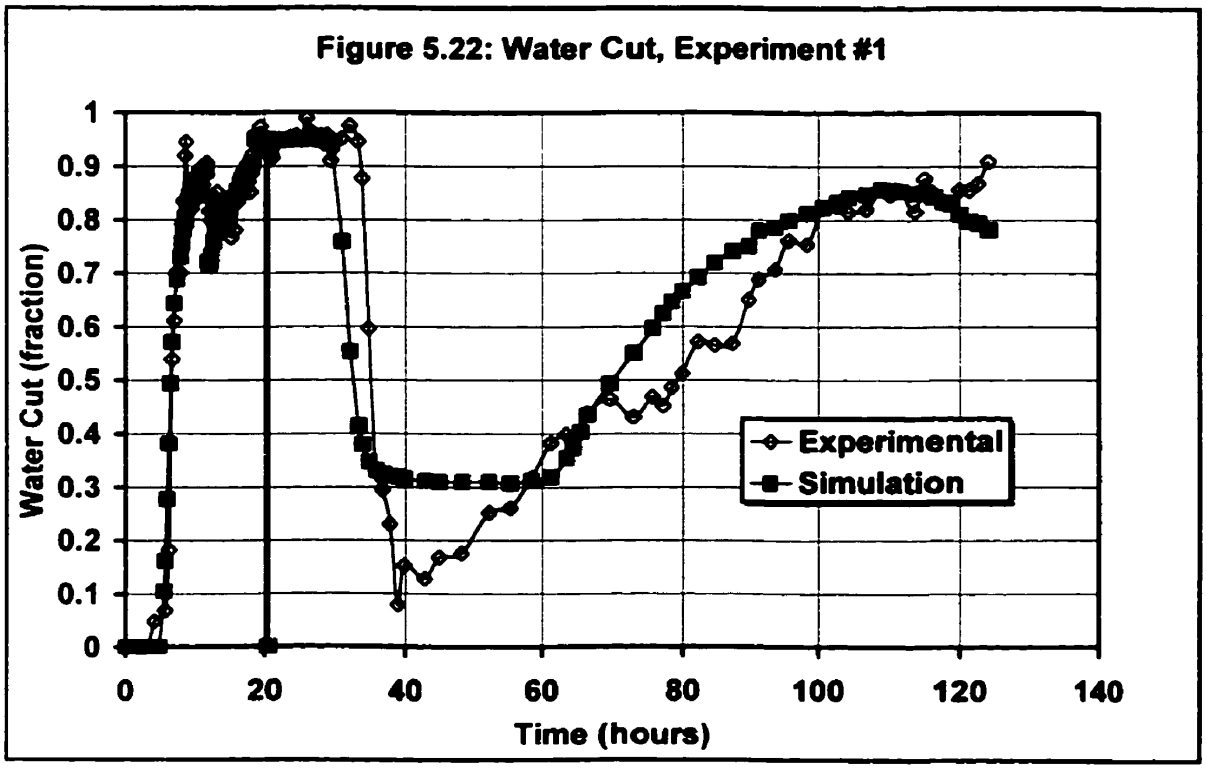
Figure 5.22: Water Cut, Experiment #1
Water Cut (fraction)
1
0.9
0.8
0.7
0.6
0.5
0.4
0.3
0.2
0.1
0
0
20
40
60
80
100
120
140
Time (hours)
Experimental
Simulation

Figure 5.23: Simulation Grid for Field Scale Simulations

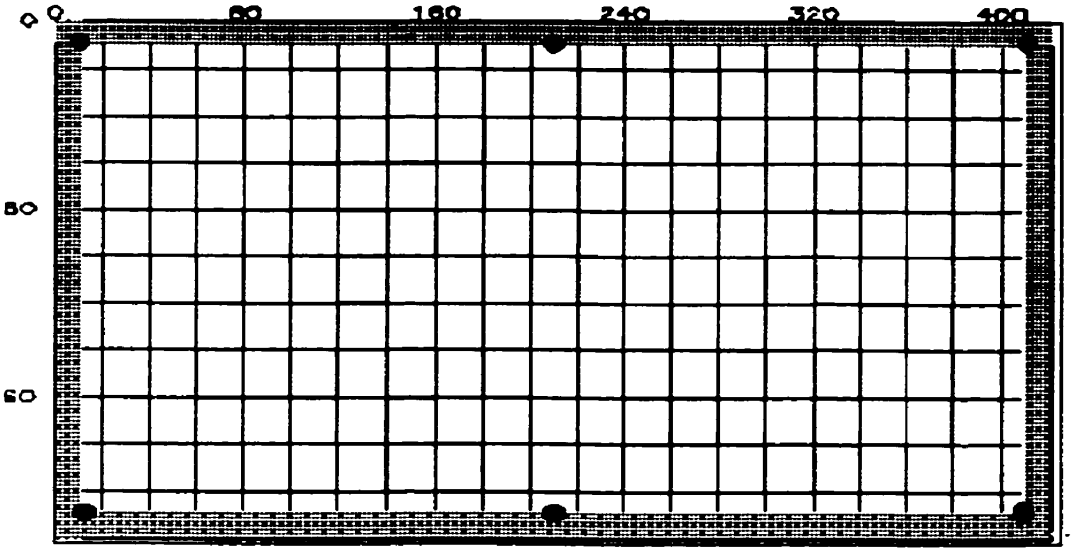

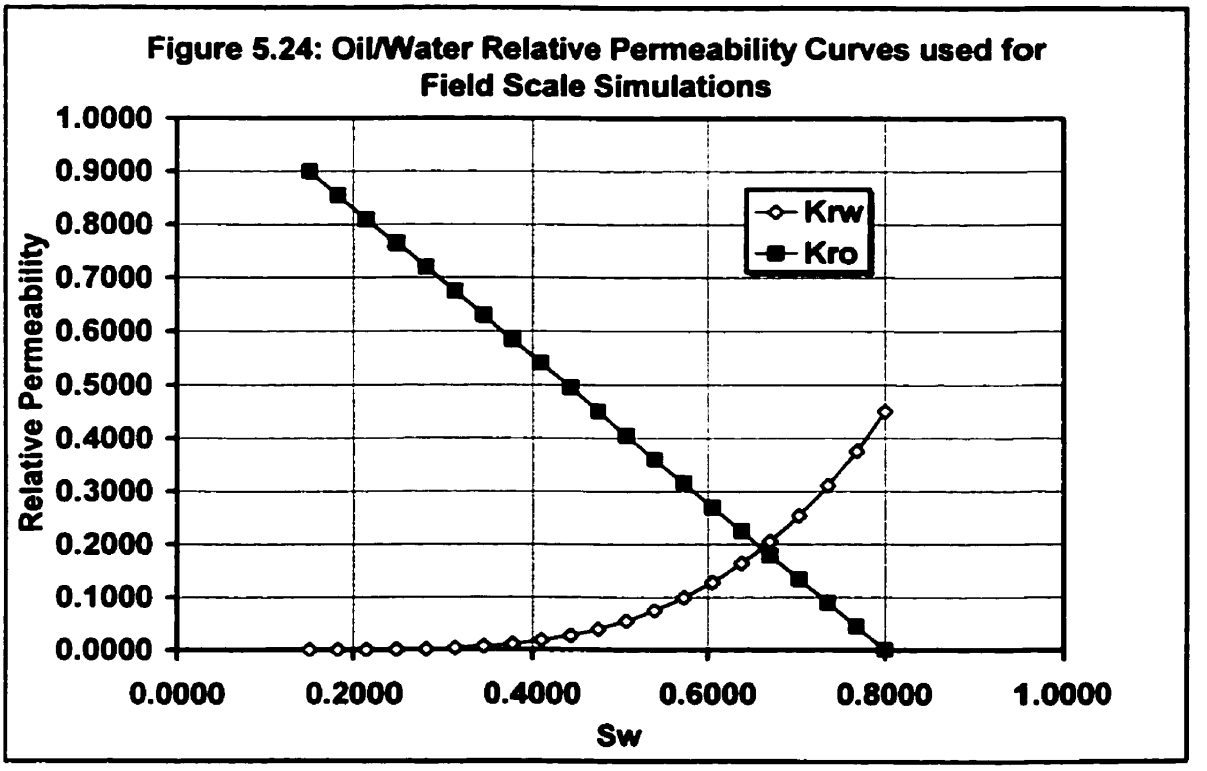

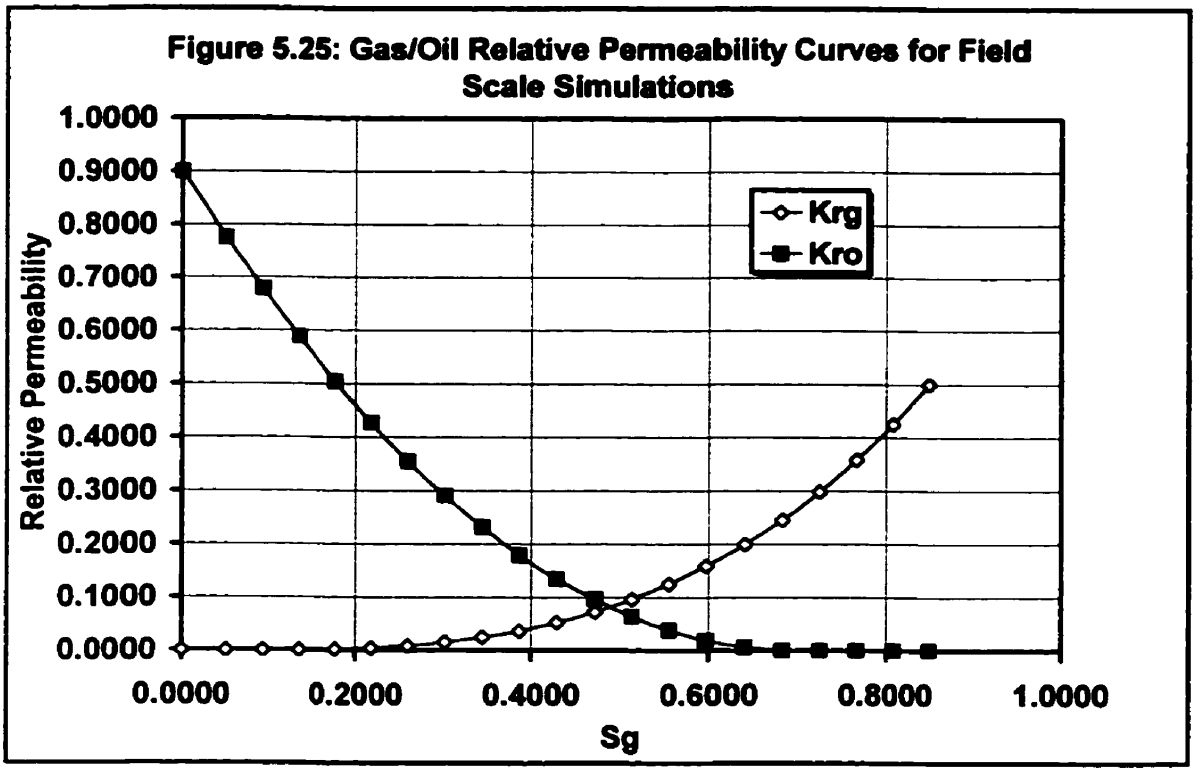
Figure 5.25: Gas/Oil Relative Permeability Curves for Field Scale Simulations
Relative Permeability
1.0000
0.9000
0.8000
0.7000
0.6000
0.5000
0.4000
0.3000
0.2000
0.1000
0.0000
Krg
Kro
0.0000
0.2000
0.4000
0.6000
0.8000
1.0000
Sg

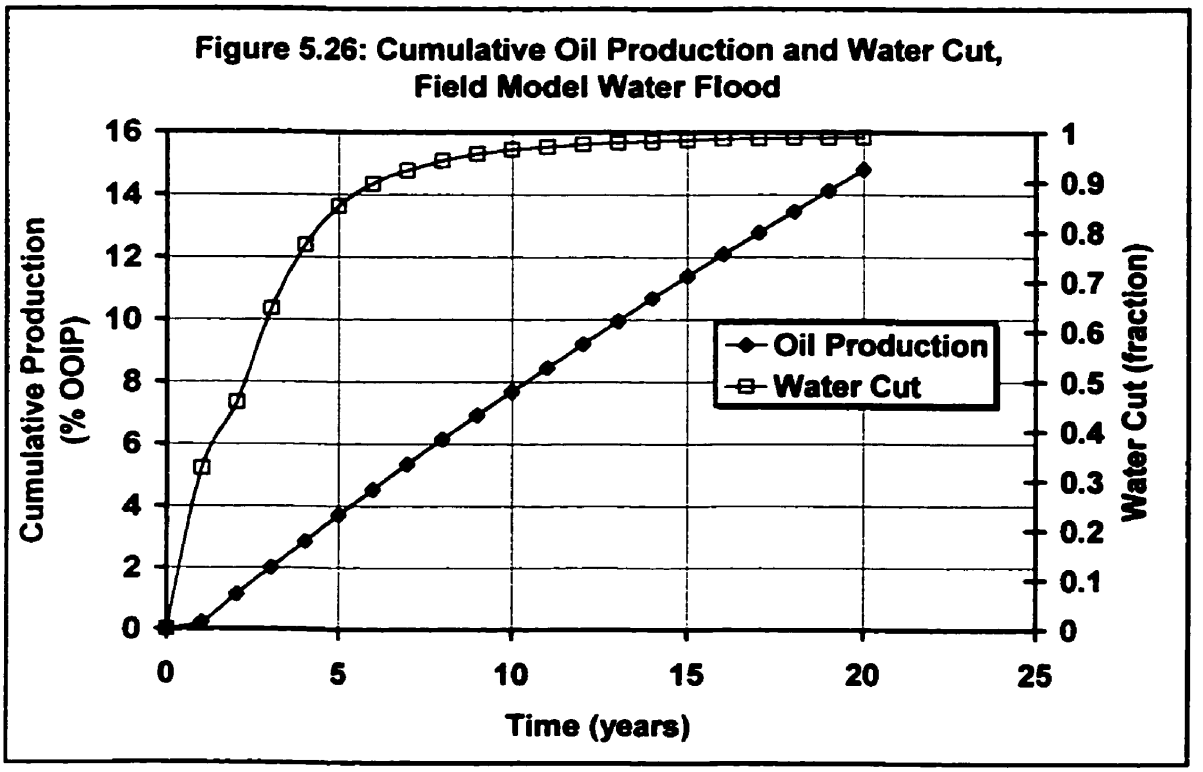
Figure 5.26: Cumulative Oil Production and Water Cut, Field Model Water Flood
Cumulative Production (% OOIP)
16
14
12
10
8
6
4
2
0
Oil Production
Water Cut
0
5
10
15
20
25
Time (years)
1
0.9
0.8
0.7
0.6
0.5
0.4
0.3
0.2
0.1
0
Water Cut (fraction)

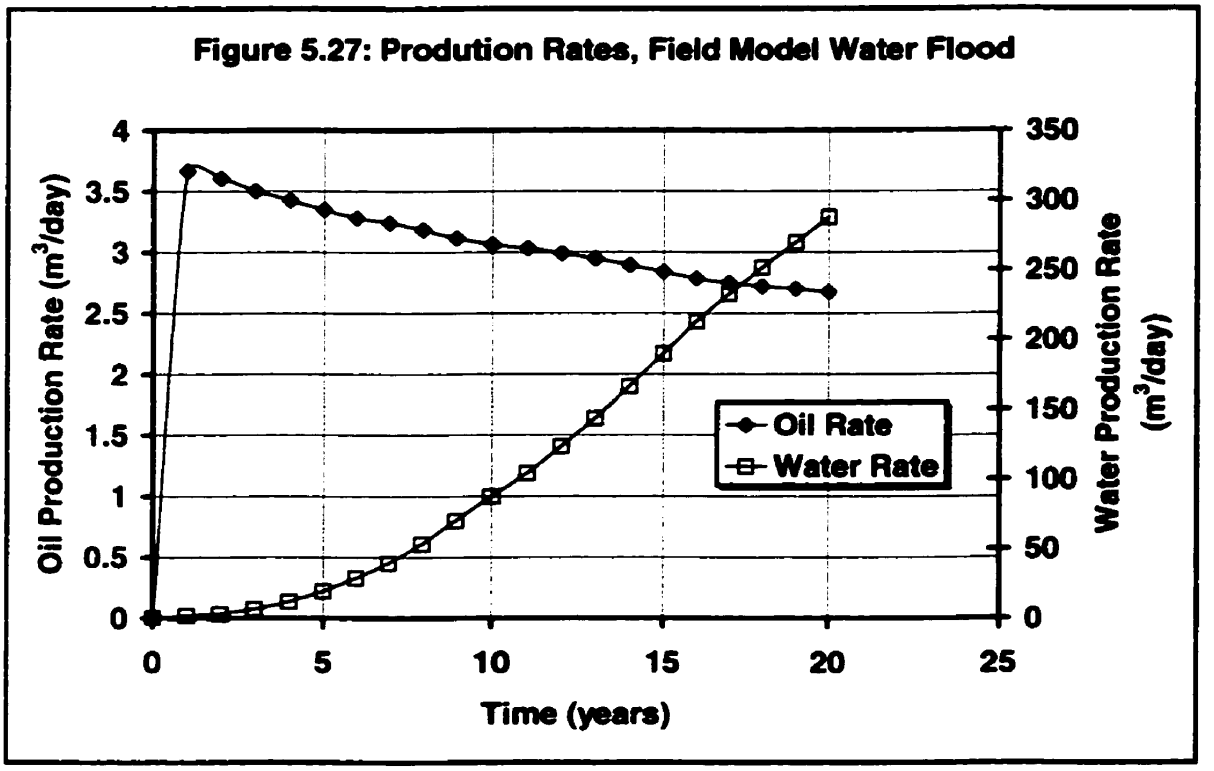

Figure 5.28: Water Saturations After Simulation Water Flood, Field Model, Profile View

Figure 5.29: Water Saturations After Simulation Water Flood, Field Model, Areal View Bottom Layer

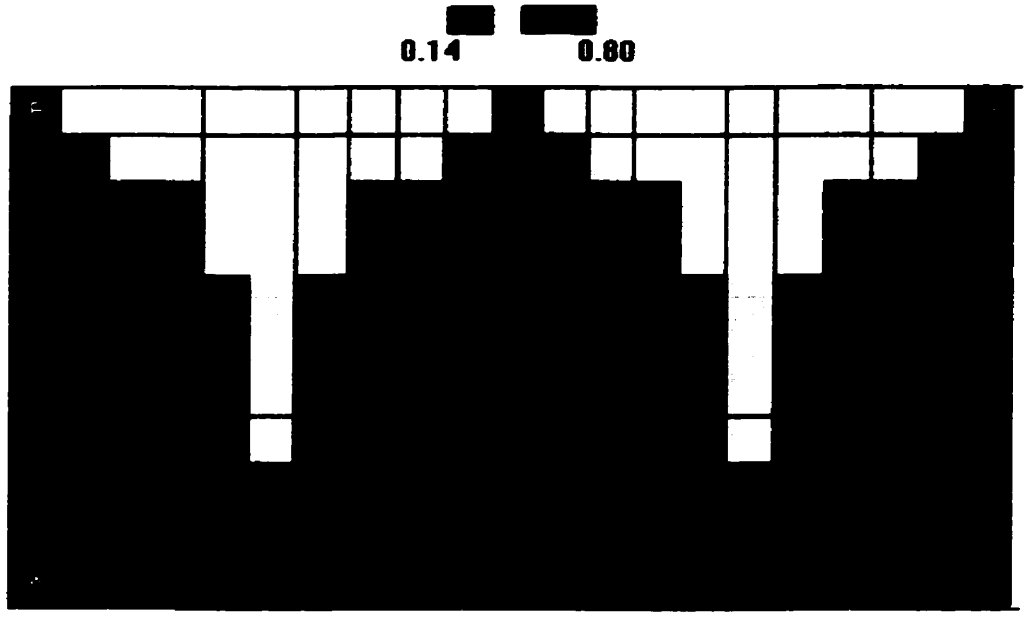

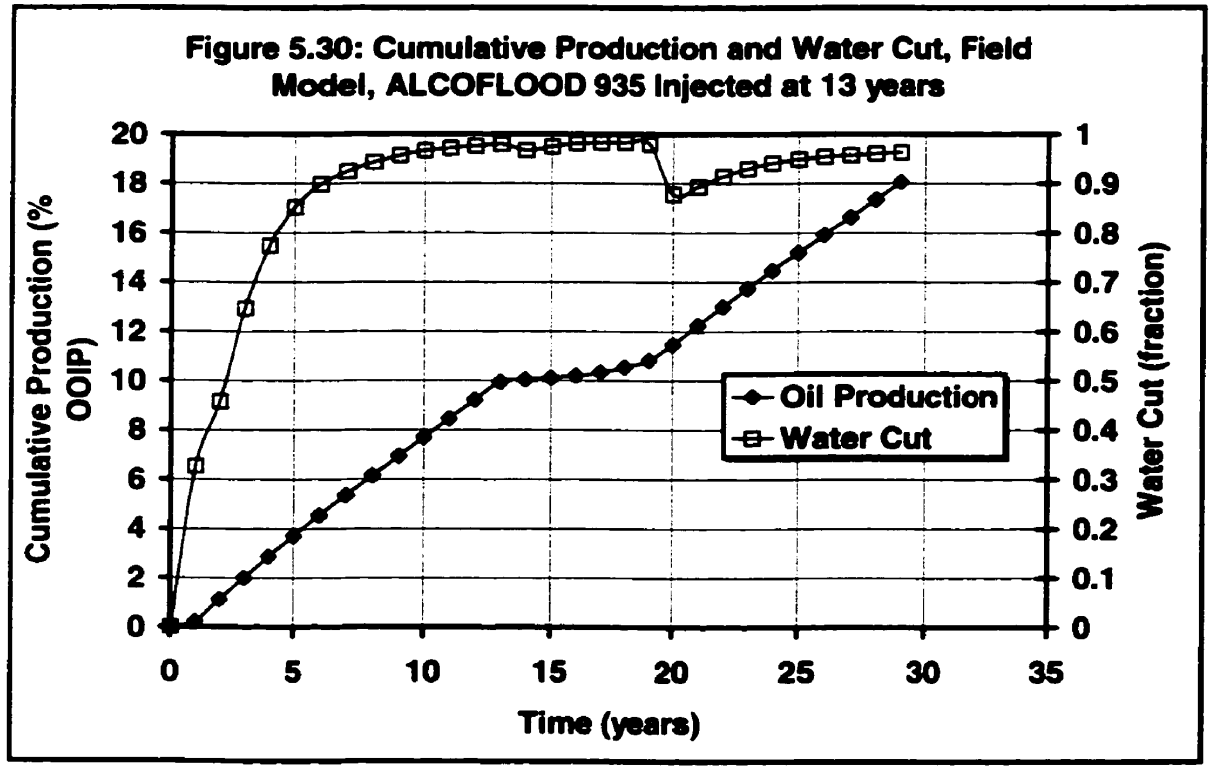

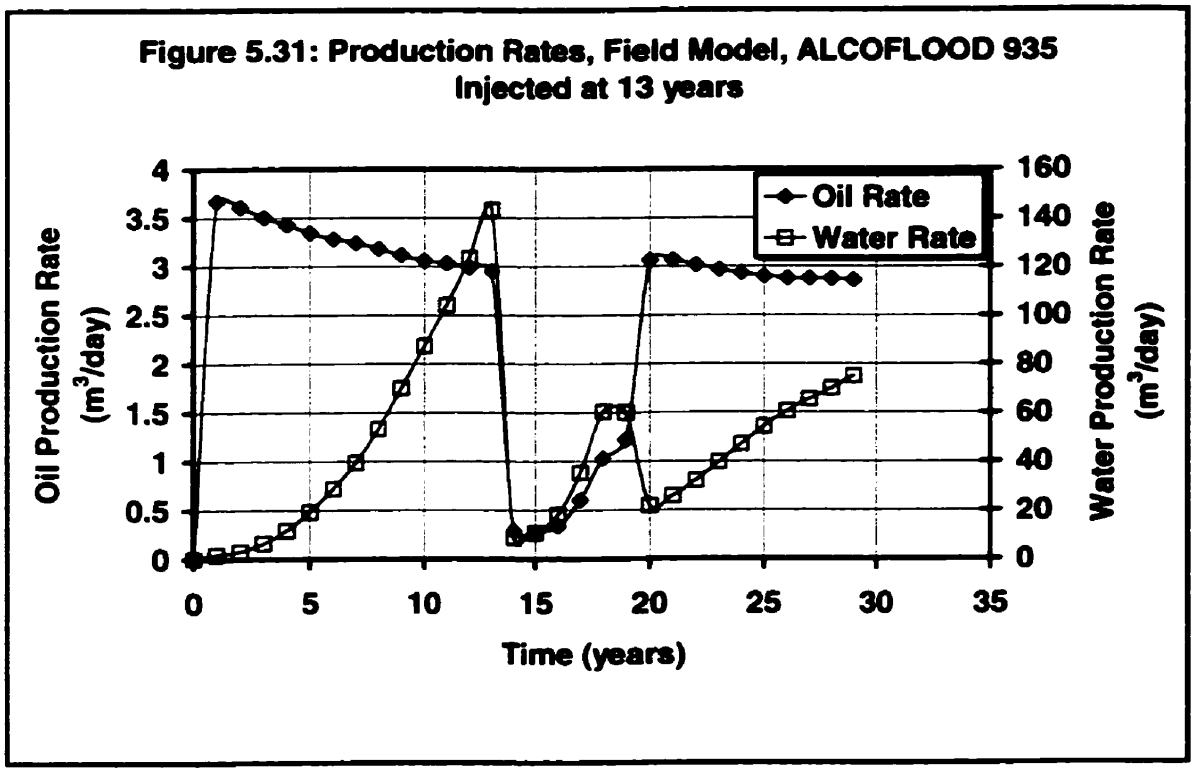

Figure 5.32: Water Saturations 19 years into Simulation of Polymer Flood, Field Model, Areal View

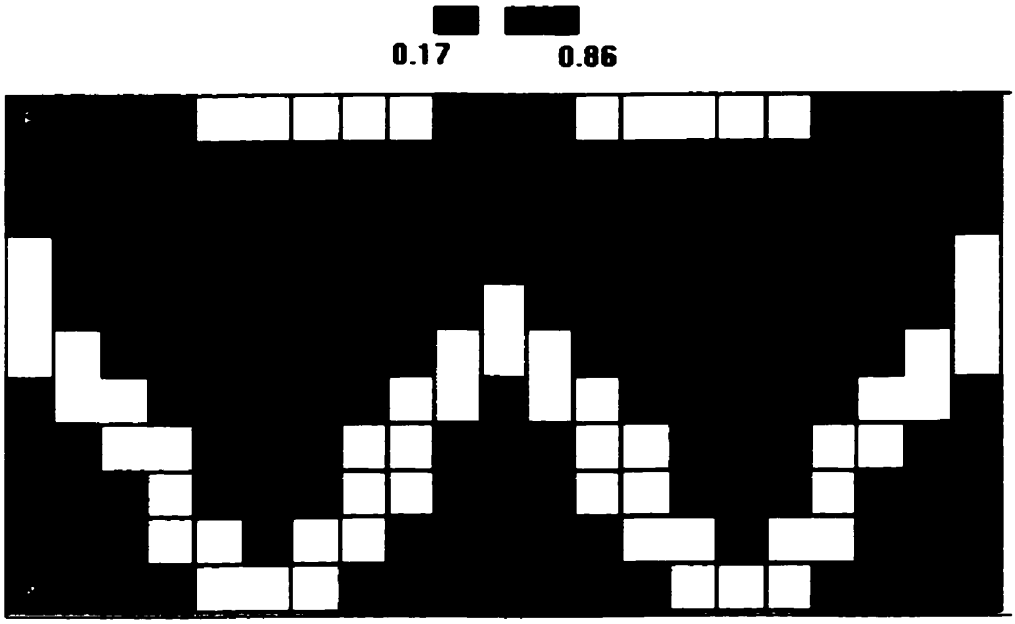

Figure 5.33: Water Saturations 19 years into Simulation of Polymer Flood, Field Model, Profile View

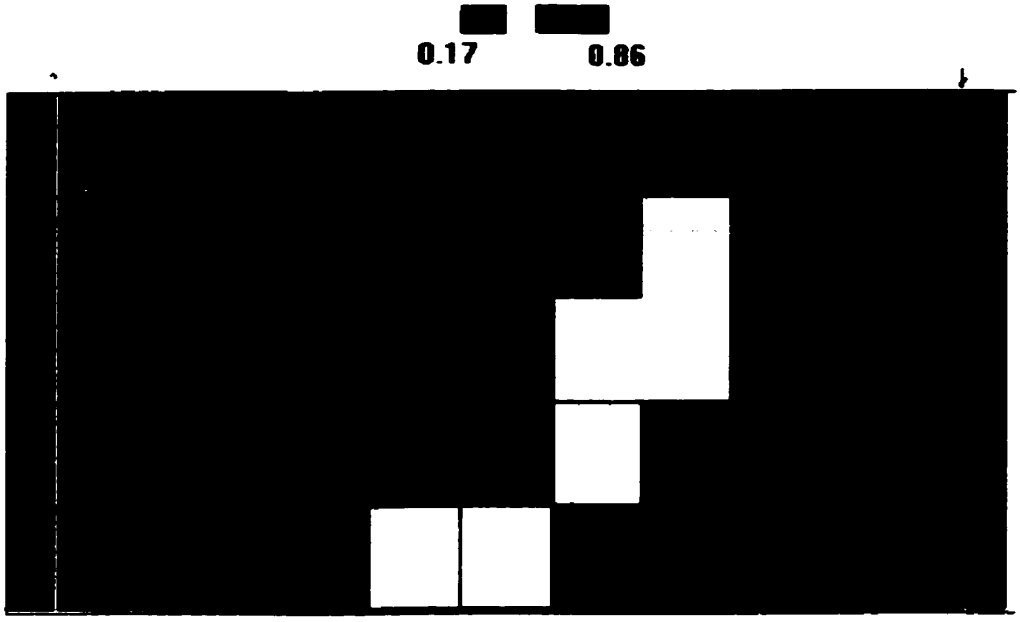

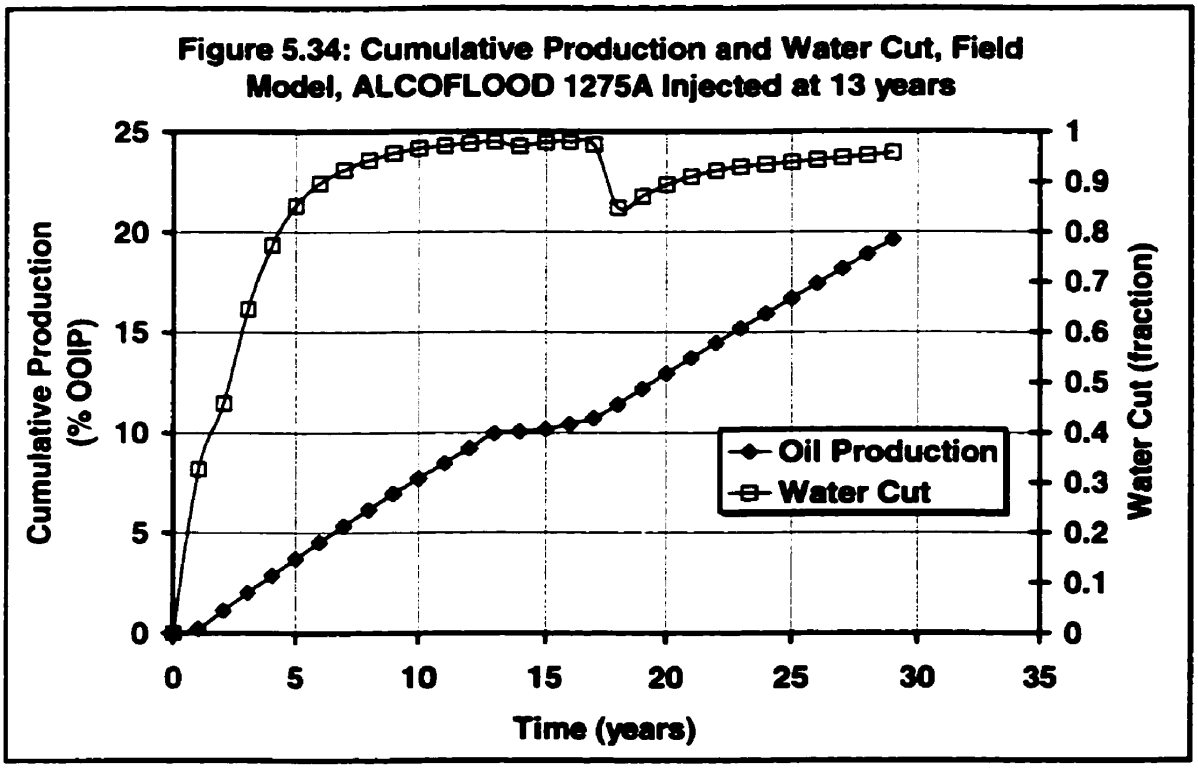

Figure 5.35: Production Rates, Field Model, ALCOFLOOD 1275A Injected at 13 years

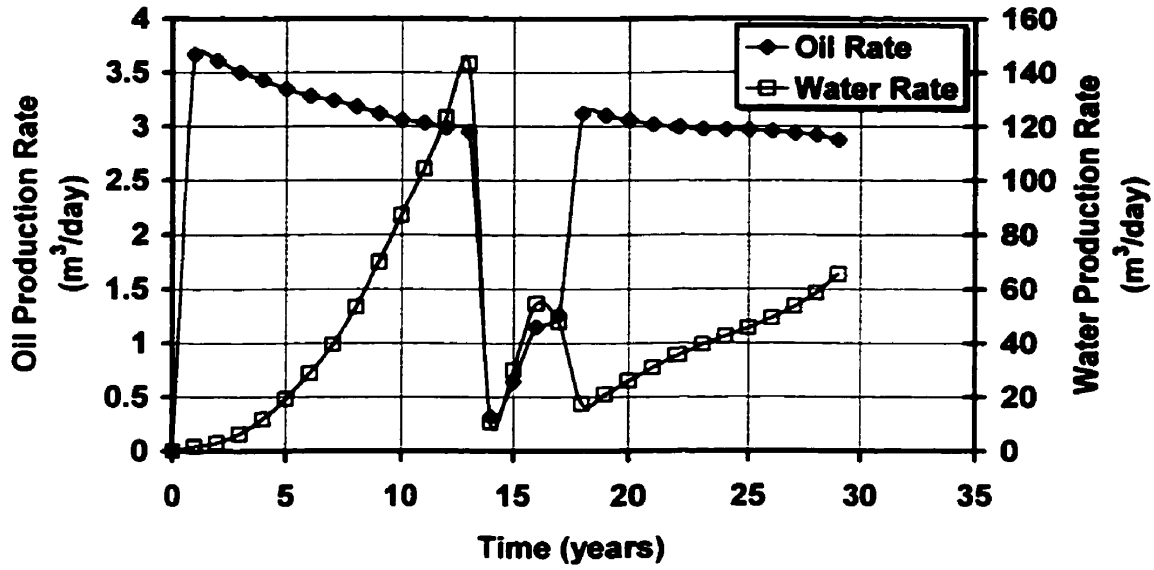

Figure 5.36: Cumulative Production and Water Cut, Field Model, ALCOFLOOD 1275A Injected at 6 years

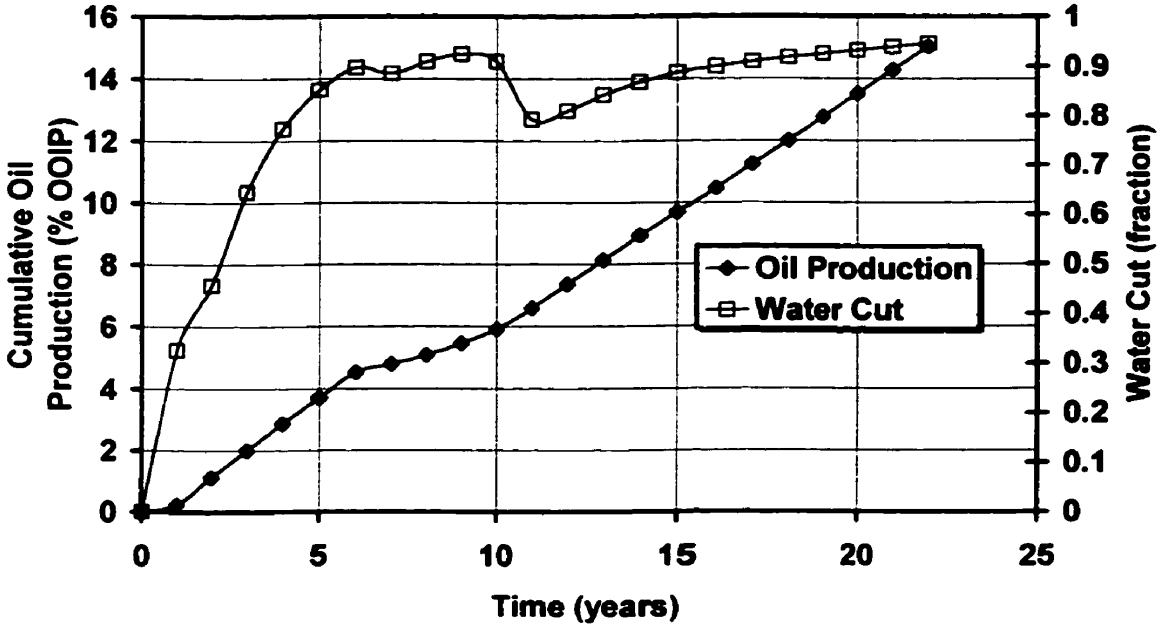

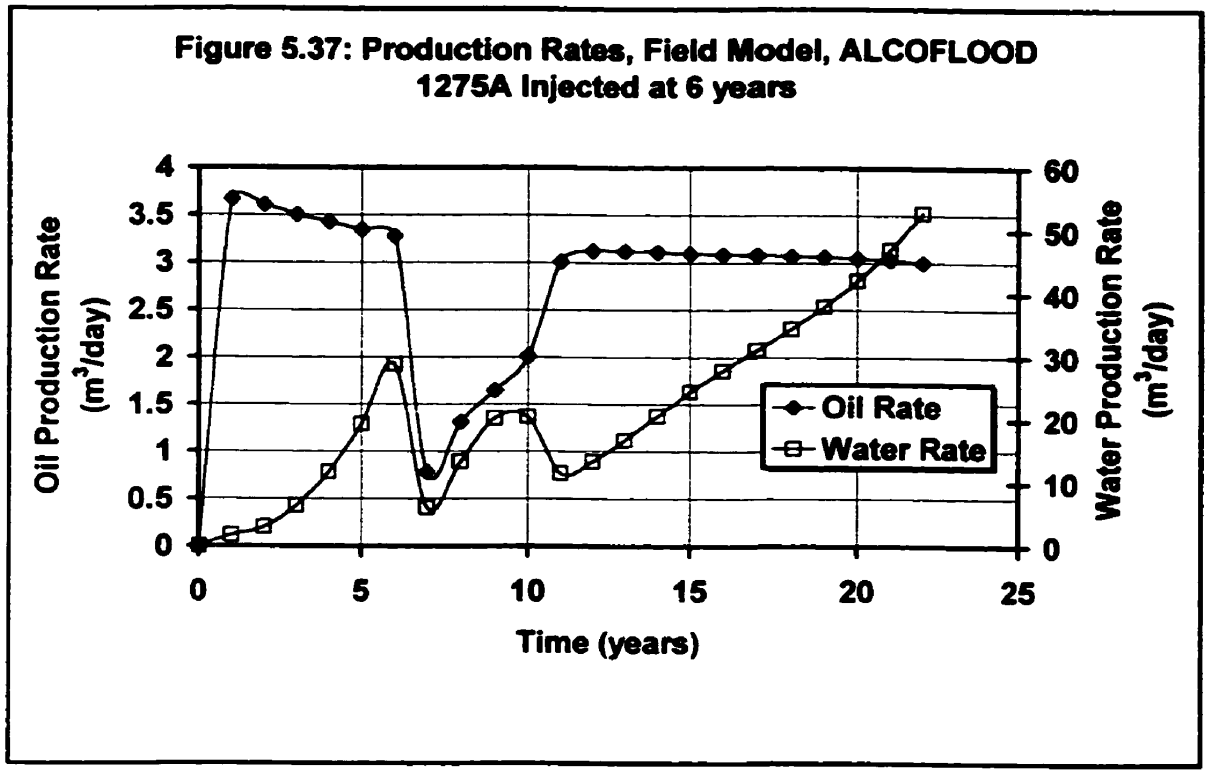

Figure 5.37: Production Rates, Field Model, ALCOFLOOD 1275A Injected at 6 years

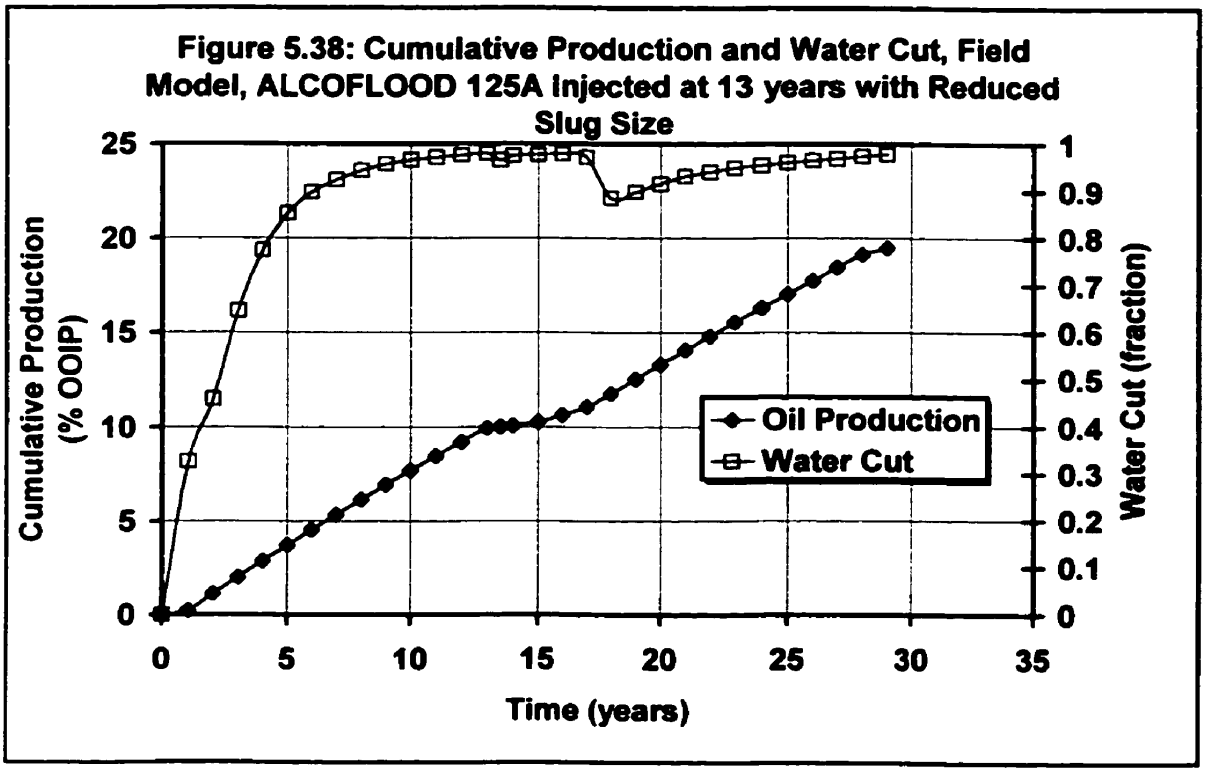

Figure 5.38: Cumulative Production and Water Cut, Field Model, ALCOFLOOD 125A Injected at 13 years with Reduced Slug Size

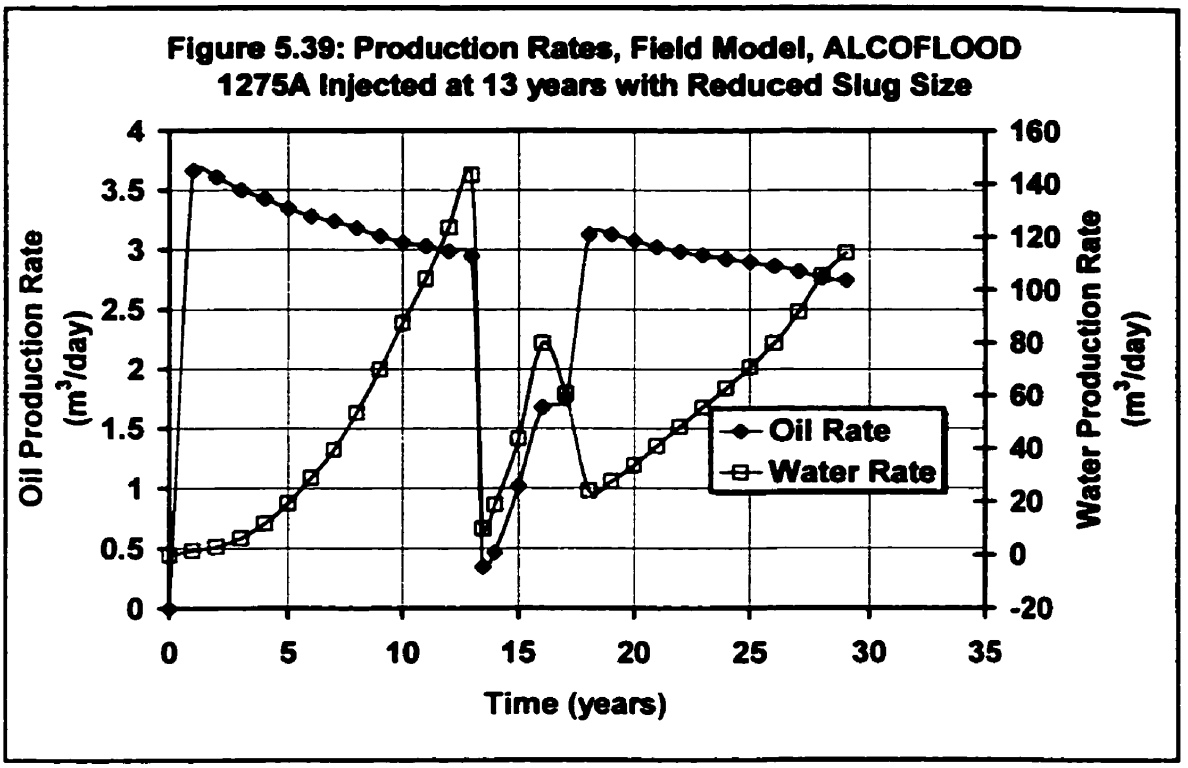
Figure 5.39: Production Rates, Field Model, ALCOFLOOD
1275A Injected at 13 years with Reduced Slug Size
Oil Production Rate (m³/day)
Water Production Rate (m³/day)
Time (years)
Oil Rate
Water Rate
0
0.5
1
1.5
2
2.5
3
3.5
4
-20
0
20
40
60
80
100
120
140
160
0
5
10
15
20
25
30
35

CHAPTER SIX: CONCLUSIONS AND RECOMMENDATIONS

As mentioned in the introduction, there exists a need for inexpensive non-thermal recovery techniques for heavy oil production. The aim of this study was to investigate possible non-thermal techniques and help develop an effective recovery strategy for heavy oil.

The experimental work and the simulation provided insight into the use of water flooding, gas flooding and polymer flooding for heavy oil recovery. From this work some conclusions can be drawn. As well, recommendations can be made for future research in this area.

For heavy oil that is mobile at reservoir conditions, water flooding can provide an effective method for secondary recovery. Imaging of the water floods with the Ambient Models indicated that the areal sweep was poor. However, some of the by-passed oil could be swept by altering the flood pattern. The same result could not be obtained with the field scale simulation. This was due to the fact that gravity under ride played a much more significant role in the field scale simulation than in the laboratory experiments. The vertical sweep could not be improved by altering the flood pattern. In reservoirs where gravity under ride is not an issue, pattern alteration may be an effective means of extending the life of the water flood.

The immiscible gas floods performed in the experiments were not effective in recovering additional oil after water flooding. The large difference between the viscosity of the gas the viscosity of the oil make effective displacement difficult. As well, the presence of high mobility channel of water, from previous water flooding, between the injection well and the production well seems to adversely affect the performance of the gas flood. The gas appears to have quickly moved through this channel, displacing the water and not contacting any of the unswept oil surrounding the channel.

Polymer flooding proved to very effective in the experiments, both with the Ambient Models and the Reservoir Models. The water cut declined drastically and large incremental recoveries were observed. This was a result of a reduction in the mobility ratio of the displacement as compared to the water flood. The reduction in the mobility ratio served to improve the fractional flow of oil behind the flood front, improve areal sweep efficiency and reduce viscous fingering. The polymer ALCOFLOOD 935 worked very well when mixed in fresh water, but was very sensitive to salinity. Another polymer product with a higher molecular weight, ALCOFLOOD 1275A, was not as sensitive to the presence of salt in the mixing water. The solution of ALCOFLOOD 1275A mixed in brine had a viscosity lower than that of ALCOFLOOD 935 mixed in fresh water but was shown to be quite effective in recovering oil.

The simulator was shown to be capable of matching the behaviour of the water floods and polymer floods performed in the Ambient Models quite effectively. Both the production history and the saturation profiles of the heavy oil displacements were matched with the simulator. However, the depletions performed with Reservoir Models, could not be matched. It was believed that this was due to both the rapid nature of the depletions as well as the uncertainties of the initial conditions with respect to the free gas in the model.

The field scale simulations of the polymer floods highlighted some of the potential issues associated with performing polymer flooding of heavy oil at the field level. The polymer was shown to reduce the water cut during field scale simulation. However, the loss of injectivity due to the high viscosity of the polymer solution resulted in a significant reduction in the production rate of both oil and water. The oil rate did recover after a few years, while water production took much longer to increase. The sustained reduction in water production rates may make polymer flooding economic for heavy oil recovery only if water handling costs are significant.

A field scale simulation where the less viscous polymer solution of ALCOFLOOD 1275A mixed in brine was used, showed that the polymer solution was just as effective as

the more viscous polymer solution in reducing the water production rates. However, the reduction of oil production rates was not as sustained as it was in the case of the more viscous polymer solution since the loss in injectivity was not as great. This led to the conclusion that a more viscous polymer solution is not necessarily better for recovering heavy oil. Field scale simulations showed that injecting the polymer solution earlier in the life of the water flood was not likely beneficial. Reducing the polymer slug size did not greatly affect the oil recovery but resulted in water production rates recovering quicker than in the case where the polymer slug was larger.

The water floods performed prior to polymer flooding in the experiments had poor areal sweep, while the water floods performed in the field scale simulations had poor vertical sweep. As a result the mechanism involved in recovering incremental oil by polymer flooding may be different for the two cases. Further experiments should be performed to determine if the polymer floods behave differently in the lab after water floods with poor vertical conformance have been performed as opposed to water floods with poor areal conformance. The results of these experiments could be scaled up with numerical simulation and compared to see how the results differ.

An experiment was performed where sand production was performed during primary production prior to any flooding. X-ray imaging indicated the formation of wormhole in the sand pack extending out from the production well. The presence of the wormhole did not appear to have adversely affected the performance of the water floods and polymer floods performed after the primary production when compared with an experiment run exactly the same except for the absence of any sand production. However, more experiments need to be run before any firm conclusion can be made.

A number of recommendations can be made for future work. The floods performed on the Ambient Models could be run at a constant rate instead of at constant pressure. They were run at constant pressure to ensure that the pressure would not increase in the model to the point where it might cause leaks. However, fairly high rates were observed when the floods were run at a low injection pressure, especially after water breakthrough.

Therefore, it would be possible to run the floods at a constant rate, as long as the rates were not very high (under 50 cm^3/hour), without causing any leaks in the model. This would result in more predictable liquid production rates. As a result better planning can be made in order to keep all the displacements running continuously.

It is also recommended that slower depletions be performed with the Reservoir Models so that they can be better simulated. As well, live oil samples should be drawn from the top of the piston cylinder prior to injecting oil into the models to ensure that there is no free gas being injected into the model. This should allow for possible history matching of the three phase Reservoir Model experiments with the simulator. These results could then be scaled up with field scale simulation.

Further work should be done to develop a technique to determine quantitative saturation from the gamma camera images. Previous authours have been successful in measuring saturations from gamma camera images in thin porous media. However, it appears from the work performed in this study that scatter and attenuation of gamma rays in a thicker porous media may cause complications. The quantitative information would be useful in the analysis of future experiments.

More experiments need to be performed where the oil saturations are monitored during polymer flooding. It would be preferable to do so with experiments performed on two dimensional models with radial flooding. It would then be possible to determine if banking of the oil occurs in these experiments.

As mentioned above, the field scale simulations indicated that significant injectivity was lost when the viscous polymer solution was injected. A less viscous polymer solution may be effective in reducing water cut but not result in such a large loss of injectivity. Further experiments should be performed using different polymer products and different polymer solution concentrations. The aim of the experiments should be to find the least viscous polymer solution that is still effective at recovering heavy oil, in order to minimize the loss in injectivity.

More experiments need to be performed to determine the effect of sand production and the presence of wormholes on subsequent recovery techniques. A single experiment was performed in this study as a preliminary investigation into the issue. More experiments need to be performed for any conclusions to be drawn. Some improvements can be made for future experiments. In order to prevent the nitrogen overburden from puncturing through to the sand pack, a stronger material should be used to separate the overburden cavity from the sand pack. A sheet of lead may be suitable. As well, it may not be necessary to perform the depletions as rapidly as was done in order to initiate sand production. If the depletion was performed slower in a more controlled manner, more accurate measurements of the gas production would be possible. It then may be possible to history match the results. However, the production of sand during the depletion would make simulation very complex.

It is believed that the conclusion obtained from this study have provided some useful insights into the potential use of water flooding and polymer flooding for heavy oil recovery. It is hoped that this work can be built upon in order to find an effective low cost alternative to thermal recovery techniques that will help develop the large amount of heavy oil deposits that exist in Western Canada.

REFERENCES:

Adams, D. M., "Experiences With Waterflooding Lloyminster Heavy-Oil Reservoirs", J. Pet. Tech., **34**(8), p. 1643-1650, 1982.

Baker, R., Private Correspondence, 1999.

Barrufet, M. A., Ali, L., "Modification of Relative Permeability Curves by Polymer Adsorption", SPE 27015, presented at the 3rd Latin American/Caribbean Petroleum Conference, Buenos Aires, Argentina, April 27-29, 1994.

Bora, R., Maini, B. B., Chakma, A., "Flow Visualization of Solution Gas Drive Process in Heavy Oil Reservoirs Using a Glass Micromodel", SPE 37519, presented at the International Thermal Operations and Heavy Oil Symposium, Bakersfield, California, February 10-12, 1997.

Briggs, P. J., Baron, R. P., Fulleylove, R. J., Wright, M. S., "Development of Heavy-Oil Reservoirs", SPE Res. Eng., **3**(1), p. 206-214, 1988.

Butler, R. M., Stephens, D. J., "The Gravity Drainage of Steam-heated Heavy Oil to Parallel Horizontal Wells", J. Can. Pet. Tech., **20**(3), p. 90-96, 1981.

Butler, R. M., "A New Approach to the Modelling of Steam-Assisted Gravity Drainage", J. Can. Pet. Tech., **24**(3), p. 42-51, 1985.

Butler, R. M., Thermal Recovery of Oil and Bitumen, Prentice Hall Inc., Englewood Cliffs, New Jersey, c. 1991.

Butler, R. M., Mokrys, I. J., "A New Process (VAPEX) for Recovering Heavy Oils Using Hot Water and Hydrocarbon Vapour", J. Can. Pet. Tech., **30**(1), p. 97-106, 1991.

Butler, R. M., Mokrys, I. J., "Recovery of Heavy Oils Using Vapourized Hydrocarbon Solvents: Development of the Vapex Process", J. Can. Pet. Tech., **32**(6), p. 56-62, 1993.

Castagno, R. E., Shupe, R. D., Gregory, M. D., Lescaboura, J. A., "Method for Laboratory and Field Evaluation of a Proposed Polymer Flood", SPE Res. Eng., **2**(4), p. 452-458, 1987.

Claridge, E. L., Prats, M., "A Proposed Model and Mechanism For Anomalous Foamy Heavy Oil, Behaviour", SPE 29243, presented at International Heavy Oil Symposium, Calgary, Alberta, Canada, June 19-21, 1995.

Craig, F. F., The Reservoir Engineering Aspects of Waterflooding, 2nd printing, Society of Petroleum Engineers of AIME, Dallas, TX, c. 1971.

de Mirabal, M., Gordillo, R., Rojas, G., Rodriguez, H., Huerta, M., "Impact of Foamy Oil Mechanism on the Hamaca Oil Reserves, Orinoco Belt-Venezuela", SPE 36140, presented at 4th Latin America and Caribbean Petroleum Engineering Conference, Port of Spain, Trinidad and Tobago, April 23-26, 1996.

Dusseault, M., "Cold Production and Enhanced Oil Recovery", J. Can. Pet. Tech., **32**(9), p. 16-18, 1993.

Farouq Ali, S. M., "Prospects of EOR techniques in Saskatchewan oil reservoirs", J. Can. Pet. Tech., **25**(2), p. 64-67, 1986.

Farouq Ali, S. M., Thomas, S., "The Promise and Problems of Enhanced Oil Recovery", J. Can. Pet. Tech., **35**(7), p.57-63, 1996.

Geilikman, M. B., Dusseault, M. B., Dullien, F. A. L., "Sand Production as a Viscoplastic Granular Flow", SPE 27343, presented at the International Symposium on Formation Damage Control, Lafayette, Louisiana, February 9-10, 1994a.

Geilikman, M. B., Dusseault, M. B., Dullien, F. A. L., "Fluid Production Enhancement by Exploiting Sand Production", SPE 27797, presented at the SPE/DOE 9th Symposium on Improved Oil Recovery, Tulsa, Oklahoma, USA, April 17-20, 1994b

Geilikman, M. B., Dusseault, M. B., Dullien, F. A. L., "Sand Production and Yield Propagation Around Wellbores", Paper 94-89, presented at the 45th Annual Technical Meeting of the Petroleum Society of the CIM, Calgary, Canada, June 12-15, 1994c.

Geilikman, M. B, Dusseault, M. B., Dullien, F. A. L., "Dynamic Effects of Foamy Fluid Flow in Sand Production Instabillity", SPE 30251, presented at International Heavy Oil Symposium, Calgary, Alberta, Canada, June 19-21, 1995.

Gogarty, W. B., "Mobility Control With Polymer Solutions", Trans AIME **240**, p. 161-169, 1967.

Jennings, H. Y., Johnson, C. E., McAuliffe, C. D., "A Caustic Waterflooding Process for Heavy Oils", J. Pet. Tech., **26**(12), p. 1344-1352, 1974.

Huang, W. S., Marcum, B. E., Chase, M. R., Yu, C. L., "Cold Production of Heavy Oil from Horizontal Wells in the Frog Lake Field", SPE 37545, presented at the International Thermal Operations and Heavy Oil Symposium, Bakersfield, California, February 10-12, 1997.

Huang, Y., Gryte, C. C., "Gamma-Camera Imaging of Oil Displacement in Thin Slabs of Porous Media", J. Pet. Tech., **40**(10), p. 1355-1360, 1988.

Huh, C., Lange, E. A., Cannella, W. J., "Polymer Retention in Porous Media", SPE 20235, presented at the SPE/DOE 7th Symposium of Enhanced Oil Recovery, Tulsa, Oklahoma, April 22-25, 1990.

Islam, M. R., Chakma, A., "Mechanisms of Bubble Flow in Heavy Oil Reservoirs", SPE 20070, presented at the 60th California Regional Meeting, Ventura, California, April 4-6, 1990.

Islam. M. R., Chakma, A., Jha, K. N., "Heavy Oil Recovery by Inert Gas Injection with Horizontal Wells", J. Pet. Sci. Eng., **11**, p. 213-226, 1994.

Jameson, C. E., "The Lloydminster Heavy Oil Area", J. Can. Pet. Tech., **12**(3), p. 17-19, 1973.

Kantzas, A., "Investigation of Physical Properties of Porous Rocks and Fluid Flow Phenomena in Porous Media Using Computer Assisted Tomography", In Situ, **14**(3), p. 77-132, 1990.

Kantzas, A., Marentette, D. F., Erno, B. P., Chatzis, I., "Recovery of Heavy Oil Using Horizontal Wells and Gravity Drainage with Pressure Maintenance", presented at the 4th Petroleum Conference of the South Saskatchewan Section, the Petroleum Society of CIM, held with CANMET, Regina, Saskatchewan, October 7-9, 1991.

Kraus, W. P., McCaffrey, W. J., Boyd, G. W., "Pseudo-Bubble Point Model for Foamy Oils", paper 93-45, presented at the 44th Annual Technical Meeting of the Petroleum Society of the CIM, Calgary, Alberta, May 9-12, 1993.

Lim, G. B., Kry, R. P., Harker, B. C., Jha, K. N., "Three-dimensional Scaled Physical Modelling of Solvent Vapour Extraction of Cold Lake Bitumen", J. Can. Pet. Tech., 35(4), p.32-40, 1996.

Littmann, W., Polymer Flooding, Elsevier Science Publishing Company Inc., New York, c. 1988.

Loughead, D. J., Slatuklaroglu, M., "Lloydminster Heavy Oil Production – Why So Unusual?", presented at the Ninth Annual Heavy Oil and Oil Sands Technology Symposium, Calgary, March 11, 1992.

Luhowy, V. M., Sametz, P. D., "Horizontal Wells Prove Effective in Canadian Heavy-Oil Field", Oil and Gas Journal, **91**(26), p. 47-52, 1993.

Maini, B., Sarma, H. K., George, A. E., "Significance of Foamy-oil Behaviour in Primary Production of Heavy Oils", J. Can. Pet. Tech., **32**(9), p. 50-54, 1993.

Mennella, A., Chiappa, L., Bryant, S. L., Burrafato, G., "Pore-scale mechanism for selective permeability reduction by polymer injection", SPE 39634, presented at the

1998 SPE/DOE Improved Oil Recovery Symposium, Tulsa, Oklahoma, April 19-22, 1998.

Metwally, M., Solanki, S. C., "Heavy Oil Reservoir Mechanisms, Lindbergh and Frog Lake Fields, Alberta Part I: Field Observations and Reservoir Simulation", Paper 95-63, presented at the 46th Annual Technical Meeting of The Petroleum Society of CIM, Banff, Alberta, May 14-17, 1995.

Mokrys, I. J., Butler, R. M., " The Rise of Interfering Solvent Chambers: Solvent Analog Model of Steam-Assisted Gravity Drainage", J. Can. Pet. Tech., **32**(3), p. 26-36, 1996.

Mungan, N., Smith, F. W., Thompson, J. L., "Some Aspects of Polymer Floods", Trans. AIME, **237**, p. 1143-1150, 1966.

Mungan, N., "Rheology and Adsorption of Aqueous Polymer Solutions", J. Can. Pet. Tech., **8**(2), p. 45-50, 1969.

Mungan, N., "Shear Viscosities of Ionic Polyarcylamide Solutions", SPE J., **12**(6), p. 469-473, 1972.

Mungan, N, "Enhanced oil recvery using water as a driving fluid: Part 4 – Fundamentals of alkaline flooding", World Oil, **192**(6), p.209-220, 1981.

O'Rourke, J. C., Begley, A. G., Boyle, H. A., Yee, C. T., Chambers, J. I., Luhning, R. W., "UTF Project Status Update May 1997", Paper 97-08, presented at the 48th Annual Technical Meeting of the Petroleum Society of the CIM, Calgary, Alberta, Canada, June 8-11, 1997.

Pooladi-Darvish, M., Firoozabadi, A., "Solution Gas Drive in Heavy Oil Reservoirs", Paper 97-113, presented at the 48th Annual Technical Meeting of the Petroleum Society of the CIM, Calgary, Canada, June 8-11, 1997.

Pye, D. J., "Improved Secondary Recovery by Control of Water Mobility", Trans. AIME **231**, p. 911-916, 1964.

Sandiford, B. B., "Laboratory and Field Studies of Water Floods Using Polymer Solutions to Increase Oil Recoveries", Trans. AIME **231**, p. 917-922, 1964.

Sarma, H., Bentsen, R. K., "An Experimental Verification of a Modified Instability Theory for Immiscible Displacements in Porous Media", J. Can. Pet. Tech, **26**(4), p. 88-99, 1987.

Sarma, H., Maini, B., "Role of Solution Gas In Primary Production of Heavy Oil", SPE 23631, presented at the 2nd Latin American Petroleum Engineering Conference of the Society of Petroleum Engineers, Caracas, Venezuela, March 8-11, 1992.

Selby, R., Alikhan, A. A., Farouq Ali, S. M., "Potential of Non-thermal Methods for Heavy Oil Recovery", J. Can. Pet. Tech., **28**(4), p. 45-59, 1989.

Shen, C., Batycky, J., "Some Observations of Mobility Enhancement of Heavy Oils Flowing Through Sand Packs Under Solution Gas Drive", Paper 96-27, presented at the 47th Annual Technical Meeting of the CIM, Calgary, Alberta, Canada, June 10-12, 1996.

Sheng, J. J., Maini, B. B., Hayes, R. E., Tortike, W. S., "A Non-Equilibrium Model to Calculate Foamy Oil Properties", Paper 95-19, presented at the 46th Annual Technical Meeting of The Petroleum Society of CIM, Banff, Alberta, May 14-17, 1995a.

Sheng, J. J., Hayes, R. E, Maini, B. B., Tortike, W. S, "A Proposed Dynamic Model for Foamy Oil Properties", SPE 30253, presented at the International Heavy Oil Symposium, Calgary, Alberta, Canada, June 19-21, 1995b.

Sheng, J. J., Maini, B. B., Hayes, R. E., "Experimental Study of Foamy Oil Stability", Paper 95-151, presented at the 6th Petroleum Conference of the South Saskatchewan Section of The Petroleum Society of the CIM, Regina, Saskatchewan, October 16-18, 1995c.

Smith, G. E., "Fluid Flow and Sand Production in Heavy Oil Reservoirs Under Solution-Gas Drive", SPE Prod. Eng., **3**(2), p. 169-180, 1988.

Smith, G. E., "Heavy Oil Waterflooding", 1990.

Smith, F. W., "The Behaviour of Partially Hydrolyzed Polyacrylamide Solutions in Porous Media", J. Pet. Tech., **22**(2), p. 148-156, 1970.

Sohn, W. O., Maltin, B. K., Volz, H., "Preconditioning Concepts in Polymer Flooding in High-Salinity Reservoirs: Laboratory Investigations and Case Histories", SPE Res. Eng., **5**(4), p. 503-507, 1990.

Sriviastava, R. K., Huang, S. S., Mourits, F. M., " A Laboratory Evaluation of Suitable Operating Strategies for Enhanced Heavy Oil Recovery by Gas Injection", J. Can. Pet. Tech., **36**(2), p. 33-41, 1997.

Szabo, M. T., "Some Aspects of Polymer Retention in Porous Media Using a C^{14}-Tagged Hydrolyzed Polyacrylamide", SPE J., **15**(4), p. 323-337, 1975a.

Szabo, M. T., "Laboratory Investigations of Factors Influencing Polymer Flood Performance", SPE J., August, **15**(4), p. 338-346, 1975b.

Taber, J. J., Martin, D., Seright, R. S., "EOR Screening Criteria Revisited", SPE 35385, presented at the SPE/DOE 10th Symposium on Improved Oil Recovery, Tulsa, Oklahoma, April 21-24, 1996.

Towson, D. E., "Canada's Heavy Oil Industry: A Technological Revolution", SPE 37972, presented at the International Thermal Operations and Heavy Oil Symposium, Bakersfield, California, February 10-12, 1997.

Treinen, R. J., Ring, W. W., Spence, A. P., de Mirabal, M., Corpoven, S. A., Huerta, M., "Hamaca: Solution Gas Drive Recovery in a Heavy Oil Reservoir, Experimental Results", SPE 39031, presented at the 5th Latin America and Caribbean Petroleum Engineering Conference and Exhibition, Rio de Janeiro, Brazil, August 30 – September 3, 1997.

Tremblay, B., Sedgewick, G., Forshner, K., "Imaging of Sand Production in a Horizontal Pack by X-ray Computed Tomography", SPE 30248, presented at the International Heavy Oil Symposium, Calgary, Albera, Canada, June 19-21, 1995.

Tremblay, B., Sedgewick, G., Forshner, K., "Simulation of Cold Production in Heavy Oil Reservoirs: Wormhole Dynamics", SPE 35387, presented at the SPE/DOE 10th Symposium on Improved Oil Recovery, Tulsa, Oklahoma, April 21-24, 1996.

Willhite, P. G., Waterflooding, Society of Petroleum Engineers, Richardson, TX, c. 1986.

Zaitoun, A., Kohler, N., "The Role of Adsorption in Polymer Propagation Through Reservoir Rocks", SPE 16274, presented at the SPE International Symposium on Oilfield Chemistry, San Antonio, Texas, February 4-6, 1987.

Zaitoun, A., Kohler, N., "Two-Phase Flow Through Porous Media: Effect of an Adsorbed Polymer Layer", SPE 18085, presented at the 63rd Annual Technical Conference and Exhibition of the Society of Petroleum Engineers, Houston, Texas, October 2-5, 1988.

Zaitoun, A., Bertin, H., Lasseux, D., "Two-Phase Flow Property Modifications by Polymer Adsorption", SPE 39631, presented at the 1998 SPE/DOE Improved Oil Recovery Symposium, Tulsa, Oklahoma, April 19-22, 1998.

Zheng, C. G., Gall, B. L., Gao, H. W., Miller, A. E., Bryant, R. S., "Effects of Polymer Adsorption and Flow Behaviour on Two-Phase Flow in Porous Media", SPE 39632, presented at the 1998 SPE/DOE Improved Oil Recovery Symposium, Tulsa, Oklahoma, April 19-22, 1998.